The Characterisation of the Organic Material in Ontong Java Plateau Tuff as an Analogue for the Search for Fossil Life on Earth and Mars

Graham William Henry Purvis

A thesis submitted in fulfilment of the requirements for the degree of Doctor of Philosophy, University of Newcastle upon Tyne.

School of Natural and Environmental Sciences,

University of Newcastle upon Tyne,

United Kingdom

September 2019

Dedication

For Jane, Emma and Kate.

I would like to dedicate this thesis to my wife Jane, without whose patience and support my long-held dream of studying for a PhD would not have been possible. I would like to thank Neil Gray, who was willing to take a chance on me, and who since then has been a dedicated and conscientious supervisor. I hope I have done enough to justify the chance he took.

Acknowledgements

ABSTRACT

Distinctive microtubules in glassy volcaniclastic shards can be observed within tuff from the Ontong Java Plateau (OJP_13), which have been suggested to be putative ichnofossils and could serve as analogues for the types of samples that may be encountered on Mars. Argon cluster ion beam etching and ultraviolet/ozone cleaning were evaluated as methods for decontaminating geological samples prior to analysis. X-ray photoelectron spectroscopy (XPS) and gas chromatography/mass spectrometry (GC/MS) were conducted on a sample of OJP_13 tuff. The comparative efficiency of conventional pyrolysis gas chromatography/mass spectrometry (py-GC/MS) and py-GC/MS with tetramethylammonium hydroxide, also called thermal hydrolysis and methylation-GC/MS (THM-GC/MS) to detect and identify the organic material in OJP_13 samples was assessed. Measurements of the carbon and nitrogen chemistry in OJP_13 were made using XPS, and this was compared to the data that was obtained by THM-GC/MS. The XPS analysis demonstrated that organic material was concentrated in the perimeter of the glass shards. Time of flight secondary ion mass spectrometry imaging demonstrated that the organic material was associated with micro-fractures in the surrounding matrix and in the devitrified glass textures in the perimeter of the shard. The analysis was conducted on OJP samples from different strata and basalts from other regions, which did not contain the tubular features. This demonstrated that nitrogenous organic material was not specific to the OJP_13 sample that contained the microtubules but appeared to occur throughout the OJP tuff. THM-GC/MS and XPS analyses were conducted on artificially decomposed plant biopolymers. The composition of the organic material in OJP tuff was similar to that of decomposed chitin. It was proposed that a component of the organic material in OJP could be the remnants of a chitinous organism. The presence of chitin implied that fungi could have produced the microtubular textures. Additionally, during this investigation, it was observed that carbonaceous films on the surfaces of minerals are thermally stable and are therefore undetectable by py-GC/MS. These films may be responsible for the non-biological synthesis of complex organic compounds.

Papers and Manuscripts Resulting from Investigations in this PhD Thesis

Chapter 3

Purvis, Graham, Neil Gray, Naoko Sano, Anders Barlow, Charles Cockell, Cees van der Land, Peter Cumpson. "Decontamination of Geological Samples by Gas Cluster Ion Beam Etching or Ultraviolet/Ozone., 2017. Decontamination of geological samples by gas cluster ion beam etching or ultraviolet/ozone. *Chemical Geology*, *466*, pp.256-262.

Name	Contribution	%
Graham Purvis	Writing, Py-GC/MS analysis and interpretation, geomicrobiology, organic geochemistry.	79
Neil Gray	Assistance with organic geochemistry	7
Naoko Sano,	XPS analysis	10
Anders Barlow,	Interpretation of XPS data	1
Charles Cockell,	Integration with astrobiology and planetary protection	1
Cees van der Land,	Geology, mineralogy	1
Peter Cumpson	Assistance with XPS analysis	1

Chapter 4

Purvis, Graham, Naoko Sano, Anders Barlow, Charles Cockell, Cees van der Land Peter Cumpson and Neil Gray. 'Combining Thermal Hydrolysis and Methylation-Gas Chromatography/Mass Spectrometry with X-ray Photoelectron Spectroscopy to Characterise Complex Organic Assemblages in Geological Material' *MethodsX. in Review.*

Purvis, Graham	Writing, Organic geochemistry Interpretation of XPS and py-GC/MS data	87
Naoko Sano	XPS analysis	3
Anders Barlow	Interpretation of XPS data	1
Charles Cockell	Integration with astrobiology	1
Cees van der Land	Assistance with background geology	3
Peter Cumpson	Assistance with XPS analysis	1

| Neil Gray | organic geochemistry; geology and geomicrobiology | 3 |
| Elisa Lopez Capel | Writing feedback, interpretation of data | 1 |

Chapter 5

Naoko Sano, Graham WH Purvis, Anders J. Barlow, Geoffrey D. Abbott, Neil ND Gray, and Peter J. Cumpson. 'Gas cluster ion beam for the characterization of organic materials in submarine basalts as Mars analogs.' *Journal of Vacuum Science & Technology A: Vacuum, Surfaces, and Films* 34, no. 4 (2016): 041405.

Name	Contribution	%
Naoko Sano	Writing PCA, XPS and ToF SIMS analysis and interpretation	25
Graham WH Purvis	Writing, Py-GC/MS analysis and interpretation, geomicrobiology, organic geochemistry.	71
Anders J. Barlow	Interpretation of XPS data	1
Geoffrey D. Abbott	Assistance with py-GC/MS	1
Neil Gray	Organic geochemistry geology and geomicrobiology	1
Peter Cumpson	PCA, XPS and ToF SIMS analysis	1

Chapter 6

Purvis, Graham, Naoko Sano, Anders Barlow, Charles Cockell, Cees van der Land, Elisa Lopez-Capel Peter Cumpson and Neil Gray. 'A stratigraphic comparison of the Organic Material in Submarine Basalts containing Microtubular Alteration Textures.' *Geobiology*, *17*(3), pp.281-293

Name	Contribution	%
Graham Purvis	Writing, organic geochemistry geology and geomicrobiology Interpretation of XPS and py-GC/MS data	85
Naoko Sano	Assistance with XPS analysis	3
Anders Barlow	Assistance with Interpretation of XPS data	1
Charles Cockell	Assistance with astrobiology	1
Cees van der Land	Assistance with sedimentology geology	3
Elisa Lopez-Capel	Assistance with interpretation of data pertaining to chars	1
Peter Cumpson	Assistance with XPS analysis	1
Neil Gray	Assistance with organic geochemistry and geomicrobiology	5

Table of Contents

List of Figures

List of Tables

<u>Acronyms and Abbreviations</u>

Ab.	Abundance
AC	Adventitious carbon
AR	As Received
at %	Atomic per cent
At-01	Atacama Desert Sample 1
CBR	Cosmic Background Radiation
CPS	Counts per second
CRB	Costa Rica Basalt
DCM	Dichloromethane
EDS	Electron Dispersive Spectroscopy
EM	Electron Microscopy
eV	electron volts
FSV	Fresh Shallow Valley
FTIR	Fourier Transform Infer-Red
FTT process	Fischer–Tropsch type process
Ga	Billion years
GC/MS	Gas Chromatography/Mass Spectrometry
GCIB	Gas Cluster Ion Beam
GEL	Global Equivalent Layer

HyPy	Hydrous Pyrolysis
IC	Intentionally contaminated
LHB	Late Heavy Bombardment
LOA	Limits of Analysis
LOD	Limits of Detection
m/z	mass to charge ratio
Ma	Million years
MARSIS	Mars Advanced Radar for Subsurface and Ionosphere Sounding
MAB	Mid-Atlantic Basalt
MER	Mars Exploration Rover (Spirit and Opportunity)
MISS	Microbially Induced Sedimentary Structures
MOMA	Mars Organic Molecule Analyser
MORB	Mid-ocean ridge Basalt
MSL	Mars Science Laboratory (Curiosity)
NIST	National Institute of Standards and Technology
ODP	Ocean Drilling Programme
OJP	Ontong Java plateau
PAH	Poly Aromatic Hydrocarbon
PCA	Principle Component Analysis
PD	Polar Desert
ppb	parts per billion
ppm	parts per million
Py	Conventional Flash Pyrolysis

RSL	Recurring Slope Linear
S/N	Signal to noise ratio
SAM	Surface Analysis at Mars
SEM	Scanning Electron Microscopy
T	temperature
THM	Thermal hydrolysis and methylation
TMAH	Tetramethylammonium hydroxide
TOC	Total Organic Carbon
ToF SIMS	Time of Flight Secondary Ion Mass Spectrometry
TV	Thermal volatilisation
u	Dalton (Atomic Mass Unit)
UV	Ultraviolet
UV/O_3	Ultraviolet/Ozone
WSD	Whin Sill Dolerite
WSD_AR	Whin Sill Dolerite As Received
WSD_IC	Whin Sill Dolerite-Intentionally Contaminated
XPS	X-ray Photoelectron Spectroscopy
µT	micro Tessla

Permissions

The images in the introduction that are credited to NASA/JPL-Caltech/MSSS refer to the National Aeronautics and Space admiration/Jet Propulsion Laboratory California Institute of Technology and Marlin Space Science Systems respectively. These are public domain because they were solely created by NASA. NASA copyright policy states that "NASA material is not protected by copyright unless noted" (See Template: PD-USGov, NASA copyright policy page or JPL Image Use Policy). NASA has no objection to their reproduction since they reproduced here for educational purposes and not for profit, thus do not fall under any restrictions described in www.nasa.gov/multimedia/guidelines/index.htm. The image credited to ESA (the European Space Agency) is reproduced under the ESA: standard licence. See www.esa.int/spaceinimages/ESA_Multimedia/Copyright_Notice_Images and www.dmlp.org/legal-guide/fair-use

The Figures in Chapter 3 are reproduced with the permission of Elsevier BV from:

Purvis, Graham, Neil Gray Naoko Sano, Anders Barlow, Charles Cockell, Cees van der Land, Peter Cumpson. 'Decontamination of Geological Samples by Gas Cluster Ion Beam Etching or Ultraviolet/Ozone., 2017. Decontamination of geological samples by gas cluster ion beam etching or ultraviolet/ozone. *Chemical Geology*, *466*, pp.256-262.'. Any third party material is expressly excluded from this permission. If any of the material you wish to use appears within our work with credit to another source, authorization from that source must be obtained.

The figures and tables in Chapter 6 are reproduced from 'Purvis, G., van der Land, C., Sano, N., Cockell, C., Barlow, A., Cumpson, P., Lopez-Capel, E. and Gray, N., (2018). The organic stratigraphy of Ontong Java Plateau Tuff correlated with the depth-related presence and absence of putative microbial alteration structures. *Geobiology'* and are the copyright of John Wiley & Sons Ltd 2018. Any third party material is expressly excluded from this permission. If any of the material you wish to use appears within our work with credit to another source, authorization from that source must be obtained.

The images in chapter 5 that are credited to AIP are reproduced from 'Sano, N., Purvis, G.W., Barlow, A.J., Abbott, G.D., Gray, N.N. and Cumpson, P.J., 2016. Gas cluster ion beam

for the characterization of organic materials in submarine basalts as Mars analogs. *Journal of Vacuum Science & Technology A: Vacuum, Surfaces, and Films*, *34*(4), p.041405', with the permission of AIP Publishing.

CHAPTER 1: INTRODUCTION

1.0.1 Overview

Given the abundance and diversity of life on Earth, it had long been assumed that life ought to exist on Mars. However, the first probes that were sent to study Mars found that the Martian climate was immiscible to life. Nevertheless, at the time, it was optimistically assumed that at least some sort of hardy complex life should exist, or at least a simple microbial biosphere should be present, on the near surface of Mars.

However, the Viking mission, which first attempted to search for life on the surface of Mars, in the 1970s, produced life detection results that were at best be considered ambiguous but were commonly considered negative. This lack of success was in part due to the lack of understanding of both the Martian surface's chemical and physical environment and a less than complete understanding of the physical boundaries of biology, along with the limitations in the technology available, at that time.

Since the Viking missions, strong evidence has emerged that at one time, Mars appears to have possessed all of the ingredients necessary for life. The climate history of Mars suggests that over 3.5 billion years ago, liquid water flowed across the surface. Liquid water may have been present on the surface of Mars for just sufficiently long enough to permit life to arise and support a microbially based biosphere. Then Mars became cooler and dryer, and the climate became too hostile to support life on the surface. Therefore, if life did arise on the surface of Mars, it is most likely to have been over 3.5 Ga ago. Thus, it is reasonable to focus the search for fossilised remnants of life, rather than extant life, on Mars. However, the search for fossilised life on Mars has comparable and greater challenges than the search fossilised microscopic life from 3.5 Ga, on Earth, although similar research approaches can be employed in both situations.

The approach that is often employed for the detection of microfossils on Earth is a visual identification of candidate fossil cellular structures or for the marks, imprinted in the geological record, which can provide an initial indication of biological activity. However,

morphology alone is an imprecise indicator of life, since many non-biological processes can produce biomorphic structures. Therefore, additional supporting evidence of biological activity is required to confirm the presence of biology. This can often be in the form of molecular biosignatures, which are the chemical, molecular or isotopic evidence of biological activity within organic material.

The molecular composition of organic material can be characterised using chromatography coupled to mass spectrometry (GC/MS) and this a mature technology that has been employed for the detection of molecular signatures. Accordingly, pyrolysis-gas chromatography/mass spectrometry has been employed, in the past for the detection and characterisation of organic material on Mars, such as the GC/MS on the Viking lander. This practice continues in the mission currently deployed on Mars, such as the SAM on the Curiosity rover. GC/MS is bulk analytical technique, which measures the contents of the entire volume of the sample, and therefore a drawback with this analytical approach is that the location of the organic material cannot be measured to a sufficiently high spatial resolution to allow any molecular biosignature to be attributed to any candidate microfossil structure. This drawback can be overcome by conducting direct measurements, which can be made on specific areas of a sample. This can be carried out using surface analysis technology. The purpose of the investigations described in this thesis is to combine the morphological with the chemical and molecular evidence of fossil life, by using a combination of proven bulk analytical technology with state-of-the-art surface analytical techniques.

The investigations described in this thesis, focused on a submarine basaltic tuff from the Ontong Java Plateau, which contains microscopic tubules that are implanted in the basaltic glass shards within this tuff. These tubules have been proposed to be morphological indicators of biological activity (Banerjee and Muehlenbachs, 2003). A biological provenance of these structures has remained controversial. However, the microtubular structures from the Ontong Java Plateau are both easily identified and localised and they are representative of a range of structures that are observed in several locations around the Earth and these structures are suggested to be some of the oldest morphological biosignatures available, which makes make them suitable as analogues for the types of structures that could

potentially be encountered on Mars. The purpose of this project was to characterise the organic material that was associated within the tuffs and map the organic material's spatial relationship with these structures to determine their provenance, and in this way, use them as an analogue for the types of Martian rock that may be studied in the future.

1.0.2 Scope, overall aim and objectives of this study

The scope of this thesis encompasses the development of novel surface analytical methods to chemically analyse and spatially map the organic material that was associated with the microtubular structures in glass shards in tuff from the Ontong Java plateau. The aim was to characterise the chemical and molecular composition and the spatial distribution of the organic material on µm and decametre scales, to connect morphological to the chemical evidence of biogenicity, in a putative microfossil. The overall objective was to advance the investigations into the biological and non-biological provenance of the structures in the glass shards of the Ontong Java Plateau. The approaches used in these investigations may assist in the identification of the most suitable samples on the surface of Mars, that could then be returned to the Earth to be investigated for the presence of Martian fossils.

This overall objective has been divided into following sub-objectives

1. To develop novel decontamination methods for fossil samples that are suitable for surface analysis.
2. To integrate proven GC/MS techniques with novel surface analytical techniques, for the analysis of fossil samples.
3. To use the techniques developed in (1) and (2), to determine any spatial relationship between the geological textures and the composition of the organic material, to provide synergistic evidence for biological activity at mm and sub-mm scales, in the OJP samples, containing putative microfossils.
4. To use the techniques developed in (1) and (2), to determine whether there is any relationship between the presence of putative microfossils and the composition of the organic material, at the Decimetre (stratigraphic) scale.

5. To use the techniques developed in (1) and (2), to characterise the organic material co-located with morphological textures to a sufficient level, to identify the presence of molecular biosignatures.

1.0.3 Chapter Summary

Chapter 1: Introduction

Chapter 1 served as both a literature review and described the line of reasoning that resulted in the development of the research hypothesises, and the rationale behind the approaches that were employed in this thesis. The introduction has been split into two primary sections to assist the reader.

Section I described the evidence for the climatic history of Mars to support the contention that biogenesis could have occurred on early Mars and that it could have sustained a microbial biosphere, before the surface of Mars became too hostile for life. This provided the rationale for the investigation of microfossils in this thesis.

Section II discussed evidence for the fossilised biological activity that can be obtained from rock morphology and from organic material. This provided the rationale behind the detection and analysis of organic material in Mars samples with surface analytical instruments. The concepts that are germane to chapters three to eight are described in the introduction of those chapters. This introductory material provided a more detailed consideration of the ideas and concepts explored in those chapters.

Chapter 2: Methods

This chapter provided the methods that were common to each of the following results chapters of this thesis. The methods that were exclusively found only in a particular chapter were placed with a supplementary methods section in those chapters.

Chapter 3: The Decontamination of Basalt Samples using Gas Cluster Ion Beam Etching and Ultraviolet Ozone Cleaning

The implementation of surface analysis was approached in an incremental manner since these analytical methods were novel approaches for the analysis of geological samples in general and fossil samples in particular, a novel approach to the challenge of removing contamination that is likely to result from sample acquisition, preparation and storage was required. Thus, the decontamination of the samples that were used in this project was

carried out using gas cluster ion beam and using ultraviolet ozone cleaning, etching for the surface analytical techniques and for the GC/MS analytical techniques respectively.

The overall contribution of organic contamination to geological samples containing high concentrations of organic material is comparatively trivial. However, the geological samples used in this study contained trace levels of organic material, and therefore, careful decontamination and handling were required to mitigate the effects of the deposition of exogenous organic material. One of the standard techniques used for the decontamination of geological samples is the removal of surface material using solvents. However, it was thought that the use of solvents, such as chromic acid, should be avoided for surface analysis, since this could conceivably add any dissolved organic material still present in the cleaning solvents onto the low organic content geological, and the effect that this additional material might have had on any results that were obtained by surface analysis, was unknown.

Consequently, this thesis used two novel approaches for the decontamination of geological samples prior to both pyrolysis-gas chromatography/mass spectrometry (GC/MS) and surface analysis. Chapter 3 described the evaluation of these decontamination protocols and discussed the rationale behind using them.

It was concluded that gas cluster ion beam etching was effective at removing carbonaceous contamination from the surface of the geological samples prior to XPS and time of flight secondary ion mass spectrometry (ToF SIMS) analysis. It was also concluded that ultraviolet/ozone cleaning was effective at removing organic contamination from geological samples prior to GC/MS analysis. These results provided greater confidence in later chapters and have been published (Purvis et al., 2017).

Chapter 4: The Detection and Analysis of Organic Material in Ontong Java Plateau Basalts using Thermally Assisted Hydrolysis and Methylation coupled to GC/MS and X-ray Photoelectron Spectroscopy

The efficiency of conventional flash pyrolysis gas chromatography/mass spectrometry (py-GC/MS) to detect and measure the organic material in samples from the Ontong Java

Plateau was compared to flash pyrolysis in the presence of tetra-methyl ammonium hydroxide, a technique that is also called thermal hydrolysis and methylation-gas chromatography/mass spectrometry (THM-GC/MS). The data that was acquired by using both of these GC/MS protocols were compared to the data that was obtained by X-ray photoelectron spectroscopy (XPS). Both GC/MS and XPS data indicated that a range of organic compounds could be detected. Intriguingly, nitrogenous organic material could be detected in the Ontong Java plateau samples, whereas the same nitrogen-rich material was undetected in the Whin Sill Dolerite control (Purvis et al., in review)

Chapter 5: The Characterisation of The Lateral Distribution of Organic Material in an Ontong Java Plateau Sample Containing Microtubule Structures

This chapter evaluated XPS and time of flight secondary ion mass spectrometry (ToF SIMS) to simultaneously map the distribution and characterise the organic material that was associated with the distinctive microtubular structures, embedded in the glassy shards within tuffs of the Ontong Java Plateau (OJP). X-ray Photoelectron Spectroscopy (XPS) was conducted sequentially in a grid array over glass shard, to a resolution of $35\mu m.pixel^{-1}$, this investigation indicated that the concentration of carbon and nitrogen was elevated in the perimeter of a glass shard. SIMS imaging was conducted on this region surrounding this area, at a spatial resolution of $2\mu m.pixel^{-1}$. This demonstrated that the organic material was present at elevated levels in micro-fractures and in the weathered perimeter of the glass shards. The molecular structure of the organic compounds in the OJP sample was identified using GC/MS, and this was used to obtain a molecular assignment for the ToF SIMS mass spectra. The molecular maps obtained with ToF SIMS suggested that specific organic compounds were located in the perimeter of glass shards and in the micro-fractures are different from the organic material in the surrounding matrix. This was published as Sano et al. (2017).

Chapter 6: The Organic Stratigraphy Of Ontong Java Plateau Tuff Correlated with the Depth Related Presence and Absence of Putative Microbial Alteration Structures

The presence of microtubular structures in the glass shards was correlated to decametre stratigraphic depth. Therefore, XPS and THM-GC/MS were used to compare the composition

of organic material in OJP samples from different stratigraphic horizons, to compare OJP samples with microtubules with those without microtubular structures, from the same region. The analysis also included a sample from the overlaying pelagic ooze, and from the charred woody material that is buried in the OJP tuff. These were further compared to basalt samples from locations, which were reported to possess fewer or different morphological alteration textures. In addition to these samples, dolerite that possessed no alteration textures was also analysed. These experiments demonstrated that the organic compounds detected in the OJP tuff were the same, irrespective of whether the glass shard exhibited alteration textures. However, the organic compounds in the OJP tuffs were different from the organic compounds detected in each of the other geological samples. The results of this chapter were published (Purvis et al., 2018)

Chapter 7: A Comparison Between Artificially Matured Plant Structural Biopolymers and the Organic Material in OJP

Previous chapters showed that pyridine and pyrrole compounds could be detected using THM-GC/MS and that organic nitrogen chemistry could be detected using XPS in the OJP tuff. The data from Chapter 5 and 6 indicated that the pyridines and pyrroles that were observed in the OJP might be equivalent to the diagenetic products of the fungal biomass reported by other authors (Smits 2006), which in turn also supported other investigators who have proposed that a marine fungi are present in the oceanic crust (Bengtson et al., 2014). The results obtained for this thesis suggested that the organic material in the OJP tuff may have been the diagenetic products of fungus. Therefore, plant structural biopolymers were artificially decomposed using hydrous pyrolysis, which is a procedure designed to mimic late diagenesis, to test this. The compounds that were produced in this way were compared to the compounds detected in the OJP using XPS and THM-GC/MS. The products of this hydrous pyrolysis were then compared to the composition of the organic material in the OJP tuff samples. This infers that the organic material in the OJP tuff could contain the diagenetic products of chitin, the structural biopolymer of fungus.

Chapter 8: The Detection of Carbonaceous Films on Mars Analogues and on Thermally Treated Geological Samples

Films of carbonaceous material can be detected on the surface of any material using nano-scale surface analysis. This includes both XPS and ToF SIMS techniques. Therefore, it was unsurprising that carbonaceous films were detected on the surfaces of the geological samples used in this thesis with these instruments. This chapter demonstrated that these carbonaceous films could be detected on the geological samples that were obtained from near-barren deserts. In earlier investigations, these served as analogues for the types of rock that are found on Mars and were reported to contain undetectable levels of organic material, using py-GC/MS. The results in this chapter demonstrated that organic material at very low concentrations was indeed undetectable with py-GC/MS and THM-GC/MS, although this material was detectable with XPS.

The XPS analysis indicated that the carbonaceous films on the mineral surfaces are comprised of aromatics or alkenes. It is speculated in this thesis that the carbonaceous film may undergo surface enhanced solid-state chemistry on mineral surfaces, resulting in the formation of complex high molecular weight compounds, such as polycyclic   aromatic hydrocarbons (PAHs), which may be the mechanism recently described as 'geopolymerisation'. Furthermore, this formation mechanism could be the source of non-biologically generated complex organic compounds.

Chapter 9: General Conclusions

This chapter considers the overall findings and conclusions of this thesis and future investigations.

Appendix A: Accompanying Investigation

In parallel to the investigations described in the main chapters, an additional investigation that was not part of the topic of the main thesis has been described. Here fossil samples from the lower Devonian period were characterised by employing the same THM-GC/MS and XPS analysis that was developed for the main topic of this thesis. The utility of these approaches to the analysis of fossil samples was demonstrated, and the characterisation of these samples indicated that the organic material in the lower Devonian was comparable to

the organic material in the OJP samples.

Appendix B: Control Experiments.

A number of experiments were conducted to demonstrate that the results obtained in this thesis were not the result of procedural artefacts.

1.1 Background

1.1.0 A Definition of Life

Whether life can be found elsewhere within the solar system is of huge academic and public interest (BBC, 2016; Drury, 2016). This is an existential question, because if it is possible to demonstrate that life can arise independently within the same solar system, then it implies that life be can be established readily and therefore may be widespread and common throughout the universe. If that is the case, then why have other extra-terrestrial technological civilisations never been detected? Does this suggest that some misfortune inevitably befalls technological civilisations before they have the opportunity to spread across the galaxy? This absence of any indication of advanced alien technological civilizations is called the Fermi Paradox. Therefore, by understanding the distribution of life in the solar system we can extrapolate its distribution throughout the universe, and therefore, it may be possible to predict likely outcomes of our own civilisation (Davies, 2010; McKay, 2010).

Before the search for extra-terrestrial life can begin, a definition of what life actually means should be made clear. However, defining what is meant by life is not easy. NASA has used "A self-sustaining chemical system capable of Darwinian evolution." (Cleland and Chyba, 2002; Benner et al., 2004; Benner, 2010) as a definition of life, which describes 'life' as a system or a system of systems. This definition is useful since it is agnostic, in other words, it makes no presumptions about the nature of what is being detected, and therefore, it can be applied to a broad range of possible forms of life, which may be operating at either a macroscopic scale or microscopic scale. However, this definition has drawbacks, because it does not provide an opportunity to detect life in situations where a limited set of observations might be available, for example, a snapshot of an individual entity, or a sub-component of the entity, such as an organ or a fruiting body. With this definition, the observation of an entity that is currently in stasis, such as a spore would be missed. Furthermore, it requires the living systems to be extant. Thus, the fossilised remnants of living systems would be overlooked.

A more practical definition is to consider 'life' as entities, rather than systems. In doing so, it may be possible to select a parameter that living entities possess that can distinguish them from purely abiotic processes. However, this approach has proved challenging (Lazcano, 2007), since it is not always possible to define specific processes or parameters that are exclusively biological. Frequently, for any given biological process, a similar abiotic counterpart process can usually be invoked that prevents this phenomenon from being used as a clear definition for life. This is certainly true for telluric organisms where biological processes are thought to be well understood, and therefore relatively easy to define. However, the problem becomes even more formidable in the search for extra-terrestrial life, where any number of unknown evolutionary trajectories and adaptations could have occurred (Irwin and Schulze-Makuch, 2002; Schulze-Makuch et al.,2005; Schulze-Makuch and Irwin, 2008; Cockell, 2014; Westall et al., 2015). This problem is exacerbated by the possibility that these evolutionary processes could have taken place in extra-terrestrial habitats that are not fully constrained and therefore the interaction and impact of the environmental context on life may not be fully understood (Jakosky and Shock, 1998). Therefore, the search for life would benefit from the investigation of one single feature that is common to all living system without making any prior assumptions about any potential organisms' physiology or metabolism (Irwin and Schulze-Makuch, 2002; Schulze-Makuch, 2008). In this approach, 'life' is thought of as an entity with a number of specific properties. Firstly, it must be able to create a barrier from its environment. Secondly, it must be capable of harvesting free energy from the environment to create structures that contain a localised decrease in entropy. Thirdly, the resulting entity must be self-sustaining, either by reacting to changes in its environment, by continually repairing itself, or by replicating itself (Botta et al., 2008).

However, this also has its pitfalls, because by using a definition of a living entity that is too broad risks the possibility of misidentifying an abiotic process as a feature of a living entity, and in contrast, using a definition that is too narrow risks not recognising a particular feature as the product of biological activity.

1.1.1 Life on Earth

The Earth's geosphere is dynamic. Atmospheric, hydrological and tectonic activity causes the alteration, surface redistribution and subduction of surface rocks, which are continually recycled with few examples of rock from the Earth's oldest periods remaining. Nevertheless, the appearance of biological activity can be dated to these earliest rocks, suggesting that life arose rapidly, and by implication relatively easily, once the environmental conditions on the Earth were suitable (Brasier et al., 2006; Brock and Banfield, 2007 Dodd et al., 2017).

Life appears to be everywhere on Earth, wherever the minimum set of physical and chemical conditions occur. These conditions need only occur intermittently, for short intervals in between extended periods where the conditions for life, are apparently impossible. Life as we currently understand it appears only to require three essential ingredients: liquid water, free energy, organic compounds and some minor but essential inorganic elements, such as phosphorus and sulphur and transition elements (Schulze-Makuch, and Irwin, 2008; Horneck and Baumstark-Khan 2012). These elements may occur in low concentrations, and therefore, organisms may need to extract them from the geosphere. This requirement for trace resources could potentially have resulted in the formation of the microstructures studied in this thesis (Cockell and Herrera, 2011). These ingredients are found on the Earth, and therefore, life flourishes. Thus, it is possible to imagine that wherever these conditions are met elsewhere in the Solar system, then there is a possibility that life could be detected. There are a number of candidate moons in the solar system where this might be possible. However, Mars is the only planet where life might currently be or have been present, and that can be accessed with the currently available technological and economic resources. Consequently, this planet has been the focus of a planned, ongoing campaign to discover evidence for extra-terrestrial life. Water, energy and organic chemistry appear to have existed at least for a fraction of Mars's history, and therefore, it is plausible that life could have arisen on Mars at some point in the past.

Section I

This section summarises what is known about the aerlogical history of Mars and the implications for its habitability. Aerology is the study of Mars, but for clarity, geology, geochemistry, geomorphology, which are terms applied to the study of the Earth are used. The term 'Telluric' refers to the 'Earth' are employed in this thesis rather than 'Terrestrial' which can refer to land.

1.2.0 The Hubris of Finding Life on Mars

Viewed from the Earth using the most powerful telescopes available, Mars appears to have many superficial similarities to our planet. It has broad topographical features, and it experiences seasonal changes in its climate. Therefore, up until the mid-1970s, the expectation of finding some sort of life form on Mars appeared to be entirely plausible. The expectation was that Martian life would be flourishing and very well-adapted to its environment. The absolute minimum expectation was that life on Mars would be found in the form of soil-dwelling microorganisms, although the possibility of macroscopic life was considered to be completely credible (Salisbury, 1962; Strughold, 1967). Consequently, once the spacecraft technology that permitted access the surface of Mars became available in the late 1960s and early 1970s, the detection of extant Martian life was considered to be a comparatively trivial process (Simmonds, 1969; Fedorova, 1972; Fedorova et al., 1973; Rubin, 1973). Therefore, a series of simple life detection experiments were designed and were deployed in 1976, by the two landers of the Viking missions.

However, after carrying out the experiments to detect life on Mars, it was generally accepted that the results should be interpreted as being negative for biology activity (Klein, 1978; Klein, 1991; Dick, 2006), and that the upper 10 centimetres of surface of Mars is currently devoid of life, with a few exceptions, e.g. (Levin, 2007). The lesson from the Viking lander's life experiments was that detecting life on Mars was far from a trivial process, and as of Summer 2019, no mission has successfully delivered an instrument suite to look for Martian biota specifically.

1.2.1 The Viking Life Experiments

The Viking mission consisted of two orbiters and two landers. Each of the Landers contained an organic molecular analysis experiment, also known as the Viking gas chromatograph–mass spectrometer (GC/MS; Anderson et al., 1972). The GC/MS was designed to heat soil (regolith) to pre-set temperatures of 200 ˚C, 350 ˚C, and 500 ˚C, and then analyse the gases that were released upon heating. In addition to semi-quantitatively obtaining atmospheric and water composition, qualitative and semi-quantitative measurements for any organic compounds present in the top 10 cm layer of the surface of Mars, were performed. Following pyrolysis, the gas chromatographic column-detector system would subsequently analyse the thermally desorbed organic material. Additionally, a mass spectrometer with a range of 12–200 u would operate in combination with the gas chromatograph. The detection limits of the GC/MS were in the ppbv range for compounds containing more than two carbon atoms and in the ppmv range for compounds containing one or two carbon atoms (Biemann, 1979). In addition to the direct measurements of the Martian environment, these instruments also served as the detector for the Viking life experiments (Levin, 1972).

Each of the landers carried a set of four experiments that had been designed in the 1960s to detect extant microbial life (Soffen, 1972). The experimental design was based upon the then existing knowledge of microbial physiology and metabolic processes. The experiments consisted of an adaption of the standard range of laboratory-based microbial nutrient enrichment protocols that were commonly used to culture microorganisms found in soil. The first two experiments were gas exchange (GEX) experiments that were designed to measure the gasses known to be produced by microbial respiration (Oyama, 1972). A further investigation consisted of radio-respirometry experiments that were designed to measure the release of CO or CO_2 by the metabolic breakdown of organic nutrients, (organotrophy) and this was called the labelled release (LR) experiment (Levin, 1972). The fourth experiment was designed to detect the pyrolysed products of biomass that would be formed from radiolabeled CO_2 by metabolic processes analogous to photosynthesis, called pyrolytic release (PR; Horowitz, 1972; These are described in Fig 1-1). The Viking mission acquired samples from the top 10 cm of the fine regolith at the Viking location. 0.5 g of

regolith was placed into inboard culture vessels. The samples were exposed to standard environmental conditions, which were considered to be the most conducive to microbial growth, as it was understood at the time. Consequently, investigations for phototrophic and organotrophic metabolisms in a humid and nutrient-rich environment were conducted, at the optimal temperatures for mesophilic organisms. Although the discovery of thermophilic bacteria around hydrothermal vents had been reported in the mid-1960s (Brock, 1967), which suggested micro-organisms could exist in a much wider range of conditions, but these were considered atypical for the 'soil-dwelling' micro-organisms that occur on Earth, which were thought to be analogous to the microorganisms that were predicted to exist in the regolith of Mars (Levin, 1972). The metabolic activity of the expected microorganisms would then be measured by either the evolution of waste gases or the consumption of various metabolites, using the onboard GC/MS.
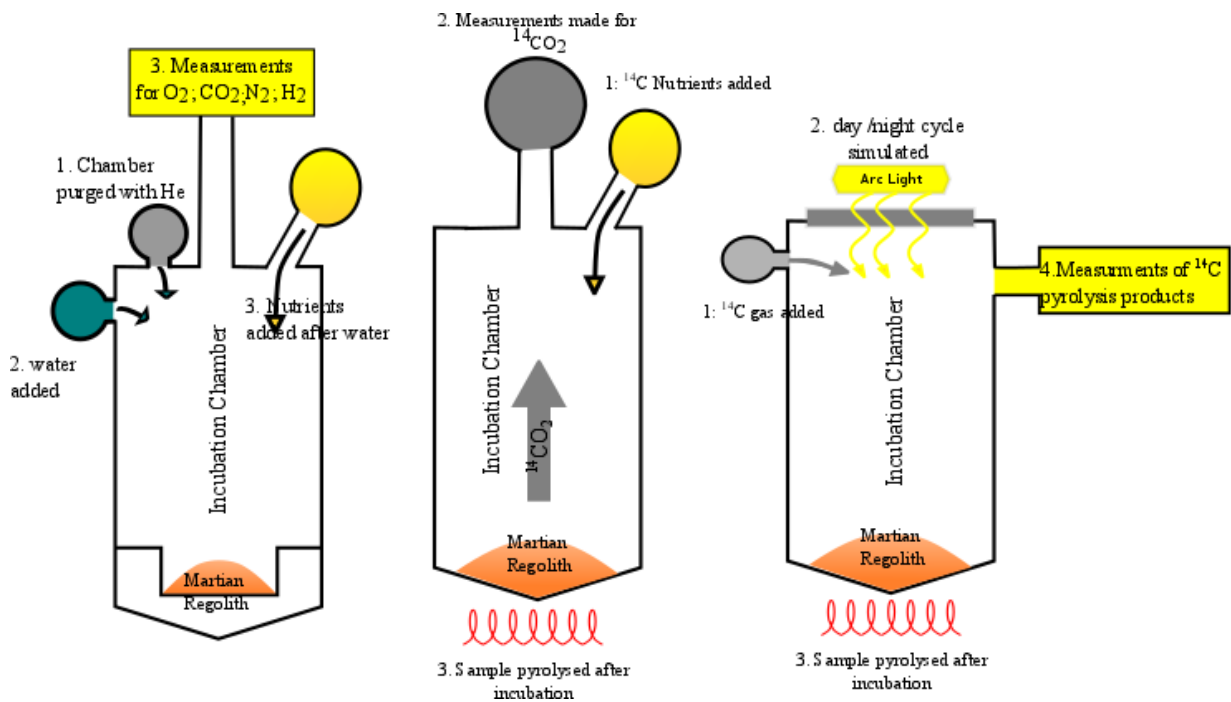
Fig 1-1. Diagrammatic representation of Viking life Experiments

A: Gas exchange Experiment:	B: Labeled release: experiment:	C: Pyrolytic release Experiment:
1: Inert gas added	1: ^{14}C- labelled nutrients added	1: $^{14}CO_2$ added
2: Water added	2: $^{14}CO_2$ measurements	2: Day/night cycle simulated
3: Nutrients added	3: Sample pyrolysed	3: Sample pyrolysed
4: Gas composition measurements	4: $^{14}CO_2$ measurements	4: Measurements for $^{14}CO_2$ evolved from pyrolysis products.

Table 1-1: Key to Fig 1-1 Viking life experiments

The intention of the gas exchange (GEX) experiment was to measure the metabolisation of nitrogen, oxygen, methane and carbon dioxide. The GEX was designed to test for life under two different conditions. First, (Fig 1-1, A), inert gas then water was added, on the assumption that dormant organisms could be revived and stimulated back into metabolic activity by the addition of moisture alone. The effect of these metabolic processes would alter the composition of the gases above the sample, which would then be measured by the

GC/MS. During a 10-sol (1 sol is 1 Martian day and is ca. 25 hours long) incubation period, the gas composition was measured five times. In the second wet nutrient experiment, a rich organic broth (called "chicken soup" by the investigators) that consisted of a solution of 19 amino acids, vitamins, a number of other organic compounds, and a few inorganic salts were introduced to the regolith to induce metabolic activity. Any change in the gas mixture might indicate metabolic activity, similar to the first investigation. The results from the gas exchange experiment indicated that although oxygen and CO_2 from humidified Martian soil, were generated, small changes were recorded in N_2 gas, which was attributed to abiotic processes (Oyama, 1977; Berdahl, 1977; Ballou et al., 1978).

The third labelled release (LR) investigation was designed to test for organotrophy. The regolith was incubated with water, and ^{14}C labelled nutrients (formate, D, L-lactate, glycolate, glycine, and D-L alanine). It was predicted that [14]CO_2 or [14]CO would be generated as a result of the metabolisation of these nutrients. At the time of the experiment design it was recognised that the atmospheric O_2 concentration on Mars, would be low (reported to be 0.1%) (Johnson, 1965; Carleton and Traub, 1972), and therefore the possibility of anaerobic organotrophy (fermentation) was considered a possibility (Levin, 1972), although, the labelled release experiment assumed oxygen was the terminal electron acceptor (Gilmore and Sephton,2004). Intriguingly, this investigation initially produced a positive result, where a steady stream of ^{14}C gases was produced by the regolith immediately following the first addition of nutrients and water, and following heating the sample to 1000°C, these were not produced (See Fig 1-2).
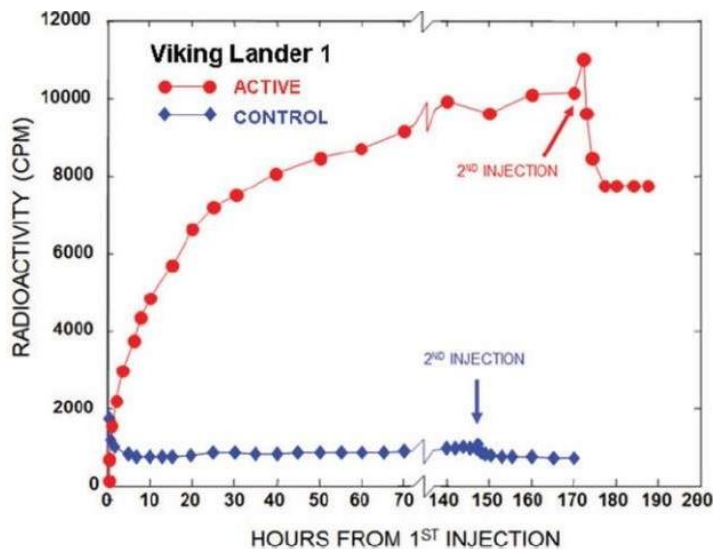
Fig. 1-2. *The Viking 1 Lander LR results showing that a sample of Martian regolith that $^{14}CO_2$ evolved following inoculation with ^{14}C labelled organic nutrients. This was repeated with a control sample that was produced by thermally treating the sample to 1000 ˚C.* Credit: Levin and Straat (1977)

The chart in Fig 1-2 showed that one or more of a set of radiolabeled organic nutrient compounds caused the release of $^{14}CO_2$, when placed in aqueous solution on the Martian surface, apparently via biologically mediated oxidative decomposition of the organic material. This observed production of $^{14}CO_2$, in the LR experiment, apparently implied a positive result for life. However, the further addition of organic nutrients a week later did not produce the same reaction, which would have been expected from a reaction that had been mediated by microbiological activity. Thus, the results produced by the Viking life experiments were considered ambiguous (Ballou et al., 1978; Klein, 1978).

The investigation designers and others continue to assert that the LR experiment was a positive result for life (Houtkooper and Schulze-Makuch, 2007; Levin, 2007). However, the observed reaction in the LR investigation is widely considered to be a false positive result (Klein, 1991), and this conclusion is based primarily upon the non-detection of organic material in the Martian regolith, by the Viking GC/MS. The false positive result was explained at the time, by an abiotic reaction caused by the presence of one or more inorganic super-oxides in the Martian regolith. The Viking Landers did not identify these compounds, but they were assumed to be either peroxides or peroxynitrates occurring in ppm concentrations in the Martian regolith (Levin and Straat, 1979; Houtkooper and Schulze-Makuch, 2007). These putative superoxides were also assumed to have thermally decomposed at 1000˚C, which was the temperature that was used to sterilise the reaction vessels. Subsequently, perchlorates were detected in the Martian regolith by the Phoenix

lander (Hecht et al., 2009), which provided the candidate compound for the super-oxide that produced this observation (see section 1.6.2).

The fourth experiment called pyrolytic release (PR) attempted to measure the fixation of CO_2 or CO into biomass, by photosynthesis or an analogous process. The PR experiment was carried out by incubating a soil sample in the presence of $^{14}CO_2$ and ^{14}CO, after which the soil was pyrolysed to release the $^{14}carbon$, from any of the hypothetical biomass that should have formed. Although trace amounts of CO_2 appear to have been assimilated into the regolith, the apparent absence of organic material and the negative results for the life experiments meant that the experiment was also considered to be negative for life (Horowitz, 1977; Ballou et al., 1978; Quinn and Orenberg, 1993).

The ambiguous life detection results that were obtained by the Viking Landers, and the widely accepted conclusion that extant life does not exist on the surface of Mars, resulted in a 20-year hiatus in the exploration of Mars. However, a renewed drive to find evidence of past or present life on Mars commenced in 1997. The campaign was initiated by the results obtained from the meteorite ALH84001 (McKay et al., 1996; see section 1.8.0). Furthermore, the possibility of life having arisen on the surface of Mars has now been reconsidered in the light of a deeper understanding of the much broader limits of where life can exist, along with a clearer indication of Mars's climatic history and whether that planet is - or could ever have been - capable of supporting life.

1.3.0 The Present Martian Environment

Mars is close to the outer perimeter of the Sun's 'Habitable Zone', which is defined as the circumstellar region of space where the energy from the star is at an intensity sufficient to generate a surface temperature that permits liquid water to persist for extended periods on rocky planets (Gilmore and Sephton, 2004). Therefore, the distance of Mars from the Sun results in an effective temperature of -57 °C. However, several different values for the observed average temperature on Mars are reported. Although temperatures between −55 °C and -63 °C, are frequently cited, e.g. (Gilmore and Sephton, 2004; space.com, 2017; NASA, 2018). The recorded maximum air temperature at midday in the Martian Summer in the equatorial regions is +35 °C, and a minimum temperature of -153 °C during the polar

winter has been recorded, e.g. (Gilmore and Sephton, 2004; space.com, 2017; NASA, 2018), these wide differences in temperature illustrate the inability of the Martian atmosphere to retain heat.

The Martian atmosphere is composed of 99% CO_2 with ca. 1% argon and some other trace gases that are at a mean pressure of ca. 600 Pa, which is ca. 0.6% that of the Earth's sea level pressure. The thermodynamic properties of water mean that it cannot exist as a liquid at these temperatures and pressures and water will rapidly sublime on the Martian surface. Consequently, the surface of Mars is extremely arid (see Fig. 1-3).

FIG 1-3. Mars Exploration Rover view south from Husband Hill, Mars. Credit: NASA, JPL, MSSS (see acknowledgments).

https://mars.nasa.gov/resources/5910/nasas-mars-rover-spirits-view-southward-from-husband-hill/?site=insight

In addition to the poor water retention, the thin Martian atmosphere is insufficiently thick to prevent cosmic background radiation reaching the surface and consequently most of the energy from incoming protons and neutrons from space are deposited on impact with the surface (Molina-Cuberos et al., 2001; Pavlov et al., 2002). Furthermore, the absence of significant levels of oxygen permits the transmission of ultraviolet (UV) radiation at wavelengths of <200 nm. Therefore, the Martian surface receives higher doses of the shorter, i.e. most biologically-damaging wavelengths of UV (UVB and UVC) in comparison to the Earth (Cockell, 2000). These high levels of UV radiation are capable of degrading biologically important organic molecules, such as DNA, amino acids and carboxylic acids (ten Kate et al., 2002; Stalport et al., 2008; ten Kate, 2010) and so the surface of Mars is extremely deleterious to life, as it is currently understood.

The Martian surface environment is, therefore, entirely hostile to life, and it is more extreme than the most extreme environment that can be currently encountered anywhere

on Earth. While there are many telluric taxa of extremophile microorganisms that are capable of at least tolerating one or two extreme environmental conditions on the surface of Mars, there are currently no known organisms that are capable of undergoing replication, under all of the surface conditions that are currently encountered on Mars (Schulze-Makuch et al., 2005; Cockell, 2014). This situation then argues against the possibility of life occurring on the surface of Mars presently, which is a conclusion supported by the evidence collected from the Viking Landers. However, several lines of evidence strongly indicate that the current surface environment is substantially different from the paleoenvironment of the Martian surface.

1.3.1 The Martian Paleoenvironment

Fig 1-4 presents the timeline for the geological history of Mars. The Martian stratochronological period boundaries can be organised using the fluvial and volcanic activity that was occurring at that time, although periods based on the dominant mineralogical processes that occurred at a particular time are also commonly used. However, there are strong caveats to the Martian dating process. The ageing of surface regions on Mars is based on both crater numbers and extent of their erosion (Craddock and Maxwell, 1990; Craddock, 1997; Cabrol and Grin, 1999; Hartmann and Neukum, 2001; McBride and Gilmour, 2004; Werner, 2008). This dating method is similar to the approach applied to other bodies in the solar system, such as the Moon, where radiometric dating has also been used to calibrate the crater density/time parameter. Thus, more craters indicate a greater age. However, the dating method is equivocal because calibrations made for the Moon is now questioned. Indeed, the crater density dating method that was extrapolated to Mars must make some assumptions, such as the effect of meteor bombardment frequency in that part of the solar system and the unconstrained density of the early Martian atmosphere (Melosh and Vickery, 1989; McBride and Gilmour, 2004).

Mars has undergone several types of geological process. However, other than impact basins, which mark instantaneous formation events, the boundaries between these processes are not sharply punctuated (Carr, 2006; Tanaka 1986; Werner, and Tanaka 2011 Irwin et al., 2013). Therefore, the age boundaries presented below and in Fig 1-4 are approximate, and no longer strictly apply to the region they were originally named after. Nevertheless, they

are used to provide a convenient method to describe the chronology of the Martian climate broadly.

The Martian chronology is divided into three periods

- **Noachian period:** This period was named after Noachis Terra region. It has the highest density of craters, indicating that these are the oldest surviving surfaces and are approximately dated to 4.5-3.5Ga.± 0.5Ga (Werner, and Tanaka 2011). During this period, Mars appears to have been sufficiently warm to possess an active hydrological cycle, a thick atmosphere and open water (see section 1.4.3 and 1.4.4).

- **Hesperian period:** This period was named after Hesperia Planum region. It was a period of declining rates of impact cratering and has consequently was dated to 3.5-2.9 Ga (Carr, 2006). The period appears to be characterised by intense and widespread volcanic activity. During this period, the Martian surface became progressively drier and fluvial activity consisted of massive but intermittent flood events, rather than hydrological cycling (Carr 2006; Head and Wilson, 2011).

- **Amazonian period:** This period was named after Amazonis Planitia region, which has the lowest density of meteorite impact craters and is dated to 2.9 Ga to present (Carr, 2006). It is characterised by cold, hyper-arid surface conditions that are dominated by aeolian activity, similar to those observed on Mars at present.

The history and evolution of the Martian climate have been a product of its size as well as its position in the solar system. The young Mars began with a large hot Ni-Fe core that was probably capable of powering a global dynamo, which generated a magnetosphere. The evidence from the strong crustal magnetisation implies that this magnetosphere is all but certain to have existed in the planet's early history (Acuna et al., 1998) and was comparable in strength to the magnetosphere at the Earth's surface (i.e., ca. 10s of μT; Williams and Nimmo, 2004; Nimmo, 2005). However, Mars is approximately 30% of the mass of the Earth, resulting in a higher surface area to volume ratio. This difference means that the planet's internal heat was lost more rapidly in comparison to the Earth. Therefore, Mars' liquid Fe-Ni core is much smaller than the Earth's and is now ineffective as a dynamo required to generate a strong magnetic field. Consequently, Mars' magnetic field is now ca. 40 times weaker and it is heterogeneously distributed, due to asteroid impact-induced crustal

magnetisation, which is observed across the entire surface (Rüdiger, 2006; Roberts et al., 2009). This heterogeneity suggests that the strong magnetosphere has been lost for a considerable time (Stevenson, 2001; Solomon et al., 2005; Arkani-Hamed and Ghods, 2011; Lillis et al., 2013).

After the loss of the dynamo-driven global magnetic field, the Martian atmosphere would have been exposed directly to the solar wind, which was stronger than it is at present (Wood et al., 2005; Jakosky et al., 2015), this would have increased the rate of atmospheric erosion (Lundin et al., 2007; Lammer et al., 2008). This erosion resulted in the loss of ca. 90% of the original Martian atmosphere and as discussed above, had significant consequences for the evolution of the Martian climate. Most importantly, the loss of the atmosphere with its insulating greenhouse effect resulted in global cooling and pressure loss, causing liquid water loss from the surface and a thick sub-surface global cryosphere to develop (Pepin, 1994; Carr, 1999; Valeille et al., 2010).
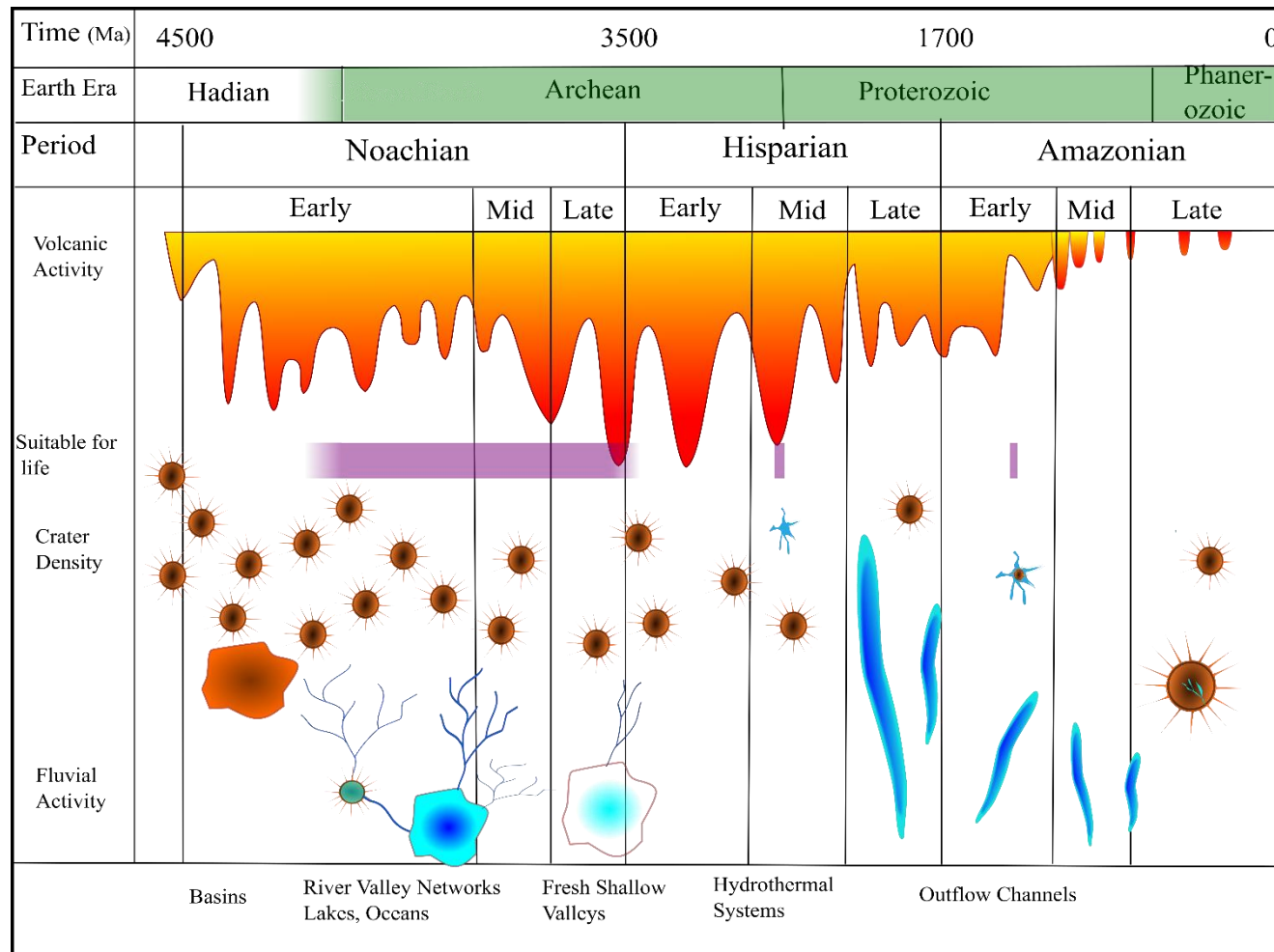
Fig 1-4. *Diagrammatic representation of the Geological and Fluvial History of Mars. The green bar shows where life arose on the Earth, and the purple bar indicates the periods when a localised or the global climate may have been suitable for life on Mars. Based on the diagram by Lakdawalla, Planetary Society.* www.planetary.org/blogs/emily-lakdawalla/2013/10251246-noachian-hesperian-amazonian.html*. Retrieved: 1 December 2018*

25

1.4.0 Water and Life

Water is essential for life, and on Earth, life can be detected in every location where liquid water is present. Water is essential for life because it provides a polar solvent in which the necessary chemical reactions needed for life can take place. Although liquid ammonia has been suggested as a hypothetical alternative medium that could potentially be utilised by any putative extra-terrestrial life (Botta et al., 2008; Schulze-Makuch, 2008). The temperature at which water is a liquid will permit chemical reactions to take place at energies that are not detrimental to biological molecules and structures but are still sufficiently energetic enough to permit the chemical reactions that are required for the synthesis of the polymeric molecules utilised by life (Horneck and Baumstark-Khan 2012). Additionally, polar solvents permit the formation of the phospholipid bilayer membranes that serve as the barrier between the internal chemistry and the environment. Therefore, the detection of fluvial activity on Mars, in the past, or at present, has been considered the principal objective in determining whether Mars is, or has ever been, inhabited (Hubbard et al., 2002).

1.4.1 The Evidence for Water on Mars at Present

Water is common throughout the solar system and was delivered to Mars via the same mechanisms that are shared by all other planets: either by out-gassing from the nascent planet and/or by cometary delivery (Carr and Wanke, 1992; Drake, 2005). Thus, the water inventory, on the newly formed Mars would likely have been similar to all of the other inner planets. Thus theoretically, early Mars should have been supplied with water, and therefore, its detection and quantification is the subject of continued investigation.

The orbital observations made by the Mars Odyssey neutron spectrometer indicated that a significant amount of hydrogen could be detected in the upper 1 metre of the surface of Mars (Boynton et al., 2007), which was interpreted as the presence of water ice. These observations suggest that water ice is widely distributed on contemporary Mars, although the ice has a covering of regolith. The presence of water is supported by the increasing numbers of observed topographical features that have been interpreted as glacier-like surface creep features (see Fig 1.5a) (Milliken et al., 2003) and ice domes (Brothers and Holt,

2016), chaos terrain and patterned ground (Soare et al., 2016). Chaos terrain is characterised by irregular assemblages of large blocks, and each block is in the order of tens of kilometres wide and up to one hundred metres high. These tilted and flat-topped blocks create depressions in the Martian surface that are hundreds of metres deep (See Fig 1.5b).
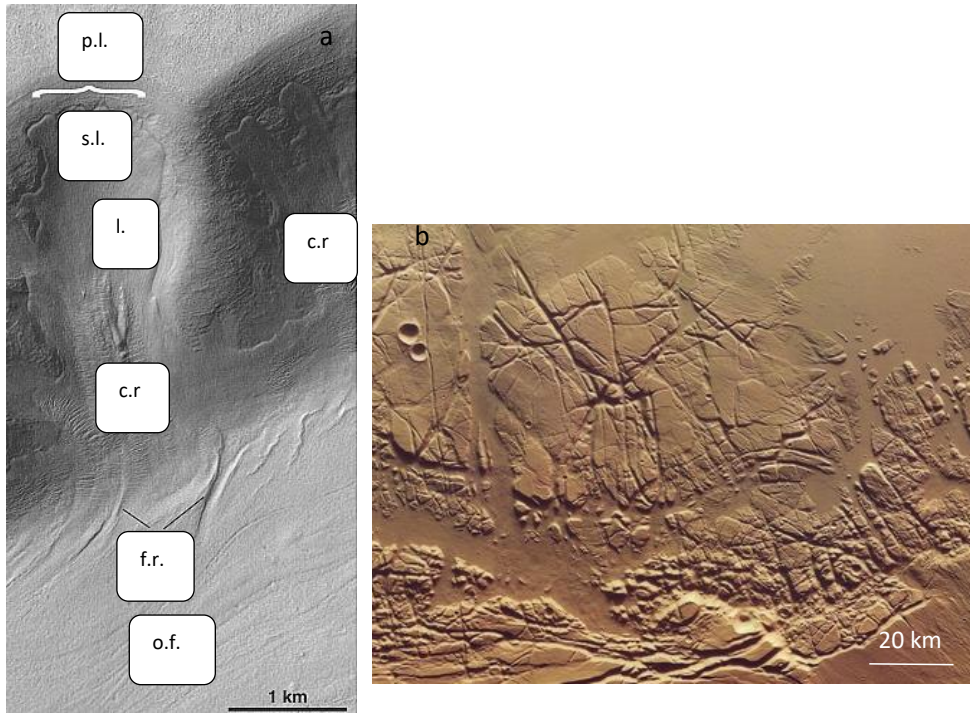
FIG 1-5 Left. *Examples of viscous flow feature characteristics, including primary lobes (p.l.), secondary lobes (s.l.), surface lineations (l), compression/extension ridges (c.r.), flow front ridges (f.r.), and older flow (o.f.)*. Credit: Millican et al*. (2003).* **Right.** *Example of Chaotic terrain*. Copyright NASA, phys.org/news/2009-11-mars-chaotic-terrain-kasei-valles.html

These geomorphological observations suggest that the water, which is present on Mars today exists almost entirely as ground ice ca. 90–95% in a region within the crust called the cryosphere, where the temperature remains continuously below the freezing point of water (Carr and Head, 2010; Carr, 1986; Squyres and Carr, 1986). The measurements of this ice were made by the Mars Advanced Radar for Subsurface and Ionosphere Sounding (MARSIS) that has measured the global distribution of the ice. While ca. 18% of the subsurface volume consists of ice, overall, the distribution varies, with 99.5% of subsurface ice being detected in

the polar regions, whereas ice is found in patches in the mid-latitudes to equatorial regions (Feldman, 2004). The cryosphere thickness ranges from ca. 2.3–4.7 km at the equator to ca. 6.5–12.5 kilometres at the pole. It has been suggested that if the ice that is currently locked in Martian subsurface were spread over the entire planet it would hypothetically be ca. 30 metres deep (Orosei et al., 2015), this is designated as the 'global equivalent layer' (GEL) and is used to describe the amount of water on Mars (Carr and Head, 2003).

It had been speculated that groundwater aquifers are trapped beneath this cryosphere, in a part of the crust where radiogenic heating from long-lived radioisotopes may have increased rock temperature to above the freezing point of water (Fanale, 1976; Clifford et al., 2010). Additionally, there may be transient situations where the production of groundwater could be caused by thermal disruption of the crust resulting from meteor impacts or volcanic activity, e.g. (Osinski et al., 2012).

The amount of this ice may have altered since the late Hesperian period. The amount of water that has been lost to space is equivalent to a GEL of ca. 15 metres (Valeille et al., 2010) and an unknown quantity have been incorporated into hydrated minerals. But in contrast, inputs from exsolution and outgassing from Martian magmas may also have increased the water volume equivalent to a GEL of ca. 5 m (Craddock and Greeley, 2009).

The extent of the cryosphere and the existence of any deep groundwater has implications for the survival of any putative life within deep subsurface habitats, which are isolated and protected from the surface environment (Onstott et al., 1998; Onstott et al., 2006; McMahon, 2013). The estimates of crustal porosity at cryosphere depths suggest the total pore volume of the Martian cryosphere is sufficient to cold trap ca. 0.5 kilometres GEL of H_2O, which is equivalent to the lower estimates of the initial planetary water inventory that was proposed by Carr (1986).

However, if the planetary water inventory is as great as Carr's maximum estimate of a ca. 1-kilometre GEL, then it is possible that large aquifers, up to several hundreds of meters thick, may be present beneath the cryosphere (Clifford et al. 2010). Until very recently, little evidence had been obtained to indicate that sub-cryosphere groundwater is present, and the reasons for this lack of detection may have been due to the thickness of the cryosphere. Therefore, most of the groundwater is assumed to be at depths are greater than the

estimated ca. 3–5 kilometres maximum penetration depth of the MARSIS instrument. However, in July 2018 the first reports of the detection of a subsurface lake by the MARSIS instrument was announced (Orosei et al., 2018)

In addition to trapped ice, the Curiosity rover and Phoenix lander both have detected trivial quantities of water vapour in the Martian atmosphere (Tamppari et al., 2014). Hypothetically, if this water condensed, it would result in a GEL of no more than 10 micrometres (Feldman, 2004). Recently, observations of the relative humidity, the air temperature and ground temperature by the Curiosity rover at Gale crater supported the formation of night-time transient liquid brines in the uppermost 5 centimetres of the subsurface that then evaporates after Sunrise (Martin-Torres et al., 2015). Therefore, the current atmospheric reservoir of water provides a conduit for the gradual migration of ice from one part of the surface to another on both seasonal and geological timescales.

The paucity of liquid water appears to negate the possibility of detecting extant life near the surface of Mars. However, there are strong geomorphological and geochemical observations made from orbit, and by the surface landers and rovers showing that this was not always the case, and there are many visibly identifiable features on the surface of Mars that can provide several lines of evidence for large and persistent volumes of liquid water on Mars, in the past.

1.4.2 Features That Have Fluvial-Like Processes that are Currently Forming on Mars

There have been several reports presenting evidence to suggest that modest amounts of fluvial processes are occurring at present on the surface of Mars, which have raised hopes that extant life could be detected on the near surface of Mars (Ojha et al., 2015); however, this evidence is equivocal (Edwards and Piqueux, 2016).

For instance, gullies can be observed on a range of slopes, including dunes and crater walls. Prolonged observation of these features has shown a progressive change in their morphologies. On the dune slopes, newly formed channels or existing channels can be observed, these feature changes in channel sinuosity, the alcoves in crater walls appear to expand, and the deposition of extensive new aprons. On rockier slopes, new channel segments and small terraces, empty channels, and boulder-strewn lobate features are

observed. It was proposed that these features are indicative of contemporary fluvial activity on Mars. However, the timing of this activity is normally correlated with the presence of seasonal frosts. Furthermore, the distribution of seasonal frost on slopes is similar to the orientation distribution of gullies. Since most of the seasonal frost on Mars consists of CO_2, then CO_2 sublimation may be the prevailing process in gully formation (Diniega et al., 2010; Dundas et al., 2010; Dundas et al., 2012).
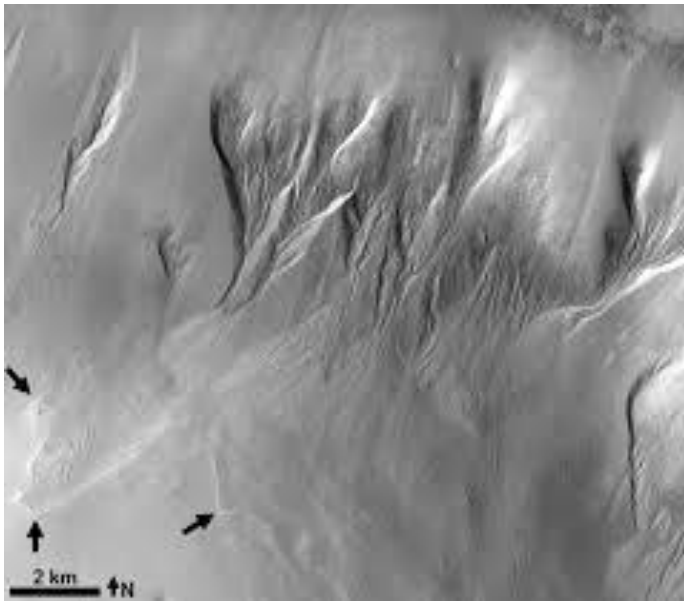
Fig 1-6. *Shows that the general topography of the gully features can be divided into three regions: an alcove – any area where the flow would be confined, the different branches come together into a down-slope channel that leads into a debris apron where there was evidence of deposition.* Credit: McEwen et al. (2013).

Other active features that appear on the Martian terrain are the recurring slope lineae (RSL) (see Fig 1-7). These are annually recurring dark streaks that grow slowly down steep slopes that are warmed by insolation during the Martian Summer. These then fade as the weather cools, and then reform during the following summer as the insolation intensifies. RSL extend down-slope from bedrock outcrops often following small gullies that are ca. 0.5 to 5 metres wide, with lengths up to hundreds of metres, and some of the locations display more than 1,000 individual flows. Their behaviour and morphology suggest the activity of a volatile liquid. However, remote sensing studies have not detected evidence of recent water (Edwards and Piqueux, 2016). Thus, several different hypotheses for RSL formation are proposed, such as rapid heating of nocturnal frost, the flow of CO_2 or dry or lubricated granular flows (Hugenholtz, 2008). However, the leading hypothesis for fluvial activity is liquid water in the form of brines, since they were observed at temperatures below the freezing point of water. Recently the presence of hydrated minerals has been found in the

same region as the RSL suggesting that the formation of these features is the result of deliquescence, a process by which water is absorbed from the atmosphere by salts (Ojha, 2015). However, since RSLs are found at many latitudes, with various topographical parameters and geologic environments on Mars, it is feasible that the formation of these features is the result of more than one mechanism.
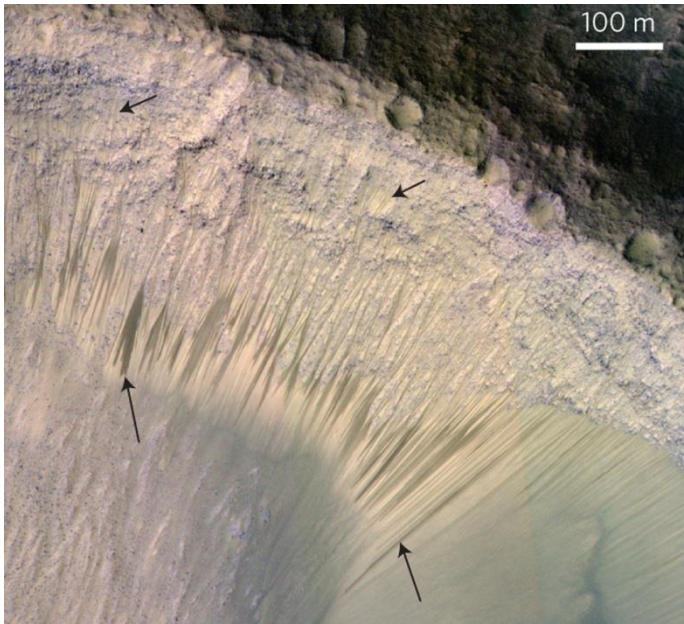
Fig 1-7. *Example of Recurring Slope Linear (examples indicated by black arrows). The transiently forming dark streaks are formed by hydrated mineral deposits. These are commonly observed in the Martian equatorial regions. However, there is little evidence to suggest these are the result of fluvial activity*. Credit: Ojha (2015).

There are two hypothetical scenarios that could permit the intermittent presence of liquid water briefly on the surface of Mars. Firstly, Mars has no large moon to stabilise its procession. Therefore, the variation in the planet's axial tilt (or obliquity) is far greater than that of the Earth (Ward, 1973; Touma and Wisdom, 1993; Jakosky et al., 1995). Consequently, the northern hemisphere can be inclined toward the Sun by much as 70°, and it has been proposed that on several occasions the increased insolation could have raised the surface temperature on Mars sufficiently to permit the presence of liquid water for 10^5-year intervals (Ward and Rudy, 1991). Another warming mechanism is impact-induced hydrothermal systems, where the intermittent meteor strikes on the surface of Mars can result in the formation of localised hydrothermal systems that could also potentially last for 10^5-year intervals. The detection of silica sinter-like structures along with geomorphological evidence on Mars, which suggest that extinct hydrothermal systems can be observed on Mars (Cockell et al., 2002a; Osinski et al., 2013; Ruff and Farmer, 2016), and an example of these systems is the impact-generated hydrothermal environment has been discovered in

the rim of Endeavour Crater by the Mars exploration rover 'Opportunity' (Squyres et al., 2012; Arvidson et al., 2014; Fox et al., 2016).

1.4.3 Evidence for Water on Mars in the Past

The history of water on Mars is summarised in Figure 1-4.

In the past, the surface of Mars temperature appears to have regularly exceeded that required for sustained fluvial activity (Pollack et al., 1987; Squyres and Kasting, 1994; Wordsworth et al., 2015; Wordsworth et al., 2016). This milder climate is hard to reconcile, given the distance of Mars from the Sun, since without an atmosphere the average global temperature would be particularly low, particularly as the luminosity of the Sun 4.5 Ga ago was potentially 30% lower than it is at present. Therefore, to permit the temperatures greater than the melting point of water, Mars would have required a CO_2 atmosphere that was >10.0 kpa (Kasting, 1993). A thick CO_2 atmosphere should have resulted in the formation of carbonate minerals. However, no such deposits have been detected, to support this thick CO_2 atmosphere hypothesis, to date (Wray et al., 2016). Although, other gases such as SO_2 and CH_4, from volcanic activity, could theoretically serve as the greenhouse gases required to raise the surface temperature of Mars.

These gases can be released from water ice-like solids, in which small non-polar molecules, such as methane, are trapped inside 'cages' of ice, called clathrates. Clathrates are chemical substances that consist of lattice 'cages' that are able to trap or contain other molecules that formed from water ice that has "self-associated" through numerous hydrogen-bonding interactions (Chastain and Chevrier, 2007).
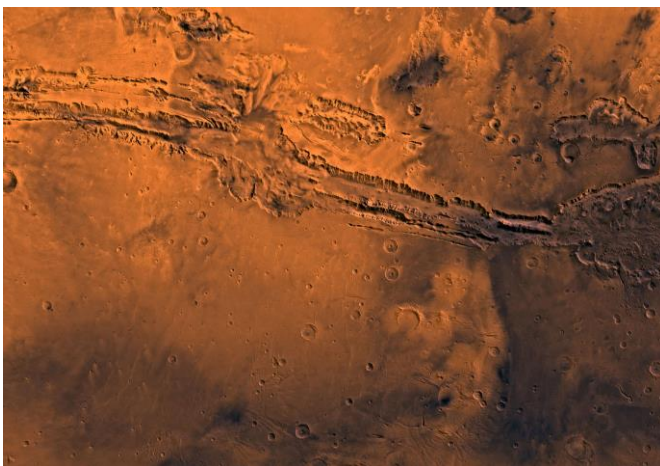
Fig 1-8. *Example of an Outflow channel image taken by Viking 1 Orbiter.* Credit: NASA, JPL,MSSS (see acknowledgments)

https://www.jpl.nasa.gov/spaceimages/details.php?id=PIA00178

Fig 1-8 shows the most salient structures that demonstrate the flow of water on Mars. These are the outflow channels that were formed by huge episodic flood events (Baker and Milton, 1974). These channels are typically tens of km across and hundreds of km long. They are thought to have been carved during the Hesperian age (Carr, 1979) with a time of peak outflow channel activity occurring towards the end of that age ca. 3 Ga (Tanaka, 1986), and the evidence indicates that these catastrophic outflows persisted for timescales of 10^5–10^7 years (Carr and Head, 2010; Hoke et al., 2011; Keske et al., 2015; Rodriguez et al., 2015). These features have no identifiable headwater or collection source and appear to originate in the chaos terrains. (See Fig 1-9). Consequently, they are thought to have been carved by fluvial activity from sporadic outbursts of large volumes of subsurface water. (Harrison and Grimm, 2004; Harrison and Chapman, 2008). The exceptional flow rates and the inferred volumes would have required the release of the water from some form of long-term stores, such as subsurface aquifers, that were in sealed by ice, which were then breached by meteorite impact or by geological activity, rather than a slow continuous formation that would be caused by a hydrological cycle. The volume of water that is required to erode the Martian outflow channels, and the likely subsurface extent of their original source regions, suggests that at the time of their formation, Mars possessed a planetary inventory of water equal to a global equivalent layer (GEL) ca. 0.5–1 km deep. It is proposed by Rodriguez et al. (2015) that the bulk of water from this era still persists today, trapped in the cryosphere and within sub-cryosphere aquifers.

In addition to these massive channels, a set of well-preserved mid-latitude and equatorial fluvial valleys have been identified. These are smaller, but they are less worn and are therefore considered to be younger than the outflow channels; these are described as 'fresh shallow valleys' (FSVs; See Fig 1-9) (Howard et al., 2005; Irwin et al., 2005; Adeli et al., 2016; Salese et al., 2016; Kite, 2017). These are widely distributed in the mid-latitudes in both hemispheres. They typically start abruptly as alcoves on steeper slopes leading to V-shaped channels and terminate in depositional aprons in topographic depressions at elevations corresponding to model-predicted paleolake levels. The morphology of FSVs are consistent with an active hydrological system that would have existed near the boundary of the Hesperian-Amazonian periods. However, this is a time-period on Mars that has been

considered to be less favourable for precipitation (possibly in the form of snow) and its runoff. This implies a substantial depth of water on the landscape, which would possibly extend habitable conditions well into the Amazonian period (Wilson et al., 2016).

Several mechanisms have been proposed for the formation of FSVs. Initially, it was proposed that gully formation was caused by aquifer-fed groundwater flow through layers of porous bedrock. Although this theory has since been questioned by the discovery of gullies at random elevations (Schon and Head, 2011) and on isolated crater hilltops (Costard et al., 2002) that have flow directions that appear to go up the local topographic gradients. Therefore, the formation of FSVs may not be the result of post-formation modification of the landscape, but rather they may be the result of pressurised flow beneath an overlying cap of ice and snow, which was subsequently removed from the landscape. The water flow produced tunnels, which then subsequently collapsed (Hobley et al., 2014). However, the formation mechanism is presently not understood and although non-fluvial activity such as debris flows and periodic CO_2-lubricated grain flows have been proposed (Pilorget, 2015), the possibility of liquid water, as a formation mechanism, is still being investigated (Dundas and Keszthelyi, 2014; Conway et al., 2015; Vincendon, 2015; Conway et al, 2016).

In addition to the outflow channels, older and smaller channels that form interconnected branching fluvial networks, typically less than 200 km long, <0.5-4 km wide and 50–200 m deep, which drain into local topographic lows, these are described as river valley networks. However, more recent imagery has also emphasised that the term "valley network" can incorporate a variety of different valley forms, which can be observed across several different spatial scales, in different Martian geological settings (See Fig 1-9). These features which usually terminate in river deltas and resemble telluric river drainage basins. These typically date from the late Noachian age (ca. 4 Ga ago). However, the characteristically small size of individual catchments and the relative narrowness of the valleys means that dating this process cannot be conducted precisely, using crater counting.
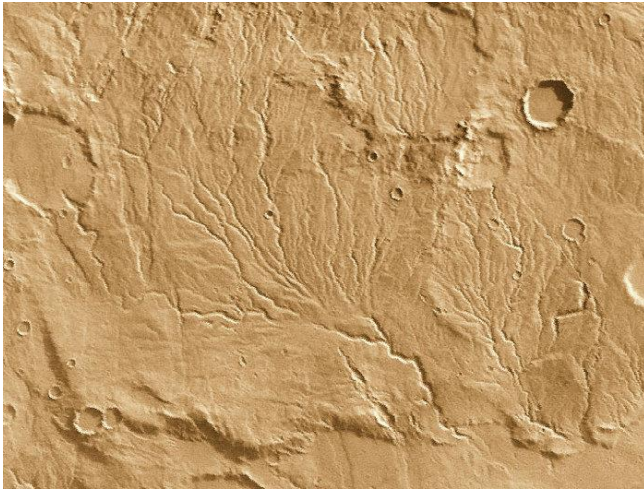
Fig 1-9. *An example of fresh valley network draining into a basin in the bottom right of the picture. The basin topography suggests the presence of a paleolake or paleoocean. credit: ESA (see acknowledgments)*
http://www.esa.int/spaceinimages/Images/2003/04/Valley_networks_suggest_that_rivers_once_flowed_on_Mars

Other convincing geomorphological features, which are indicative of fluvial activity on Mars include the detection of the perimeters of ancient lakebeds, (Cabrol and Grin, 1999) and a shoreline that is indicative of a paleoocean that may have covered 30% of the planet, with water up to 1 km deep (Di Achille and Hynek, 2010). The evidence for such ancient paleolakes and an ocean is growing, indicating that standing bodies of liquid water that may have persisted on the Martian surface from the early-Noachian to the late-Noachian/early-Hesperian periods (Goudge et al., 2012; Hynek et al., 2015). Recently, mudstones and sedimentary rock formations have been observed by the NASA Curiosity rover (Fig 1-10a). Additionally, pebbles with a rounded morphology demonstrated that water flowed between from several cms to a m deep along on a former streambed, at the base of an alluvial fan system that descended from a crater wall showing that fluvial activity must have persisted for a time sufficiently long enough for these pebbles to form (see Fig 1-10b; Jerolmack, 2013; Szabo et al., 2015). These formations demonstrate that fluvial activity was widely distributed on Mars for sustained periods.

Fig 1-10. (Top): Mudstone sediments adapted from
https://www.nasa.gov/feature/jpl/nasas-curiosity-rover-team-confirms-ancient-lakes-on-mars

(**Bottom**) *Pebbles. Both observed at the base of Mount Sharp, Gale Crater by the Curiosity rover.* Adapted from *https://mars.nasa.gov/resources/4721/rock-outcrops-on-mars-and-earth/?site=insight*

Credit: NASA, JPL,MSSS (see acknowledgments)

1.4.4 The Geochemical Evidence for Water on Mars

Mars is predominantly composed of igneous rock, consisting of magnesium and iron-rich (mafic) minerals that have crystallised from magma. Basalt is common through the Solar System, and therefore, unsurprisingly, it is the primary rock type on Mars. Several minerals occur in basalt, which includes feldspar, pyroxenes and olivine, and these have all been detected by the CheMin instrument on the Curiosity rover (Downs et al.,2015), suggesting that Martian basalt is compositionally analogous to the telluric palogonised basalt (basalt altered by water) and has been labelled as JSC-1 by NASA (Brown, 2012). Much the primary and secondary rocks on Mars are now in the form of a granulated rock, which is described as 'regolith'. This material has been distributed planet-wide by aeolian action, which has created a globally homogenous mineral composition (Chevrier and Mathé, 2007).

This homogeneity has made the detection and the analysis of secondary minerals from Mars's deep past more difficult. In particular, carbonates appear not to be well represented in the geological record. Carbonates are of interest because they would provide supporting evidence of a thicker CO_2 rich atmosphere that may have been necessary for the active hydrosphere in Mars's past. However, other secondary minerals, which have been produced through hydrothermal alteration and weathering of primary basaltic minerals, have left a mineralogical record of the first billion years of Mars climatic history. This is most evident in the characteristic red colour of the Martian landscape, which is a result of widespread distribution of ferric oxides, particularly hematite (Fe_2O_3) and ferric oxide ($Fe(OH)_3$) and these minerals demonstrate the interaction of iron-rich minerals with liquid water (Banin et al., 1993). For instance, haematite will typically form in standing bodies of liquid water and may have been deposited as the water evaporated. The presence of hematite, therefore, implies the presence of open bodies of water for sustained periods on the surface of Mars (Bell et al., 1990; Rubie et al., 2004; Tosca, 2005; Murchie et al., 2009).

Other geochemical evidence for the presence of water on Mars includes phyllosilicates (clay minerals) that have been identified in units dating from the Noachian period (McKeown et al., 2009; Ehlmann et al., 2011; Grotzinger et al., 2014). These minerals indicate that a neutral/alkaline aqueous environment existed for an extended period on Mars, which resulted in a process or a set of processes that weathered the mostly basaltic bedrock, during the Noachian period. The detection of iron sulphate minerals such as jarosite and opaline silica, and gypsum in Hesperian period units imply that there was an increased release of sulphur that was probably released either during volcanic activity or from gases trapped in clathrates (For a definition, see section 1.4.3) in the cryosphere (Chassefiere et al., 2013). This release would have increased the acidity of the hydrosphere and produced the observed sulphate minerals (Farquhar et al., 2000; Poulet et al., 2005; Halevy et al., 2007; Lammer et al., 2008; Gaillard and Scaillet, 2009).

In conclusion, the Martian geomorphological evidence suggests that there was a transition from a high-erosion environment that involved principally fluvial activity in the past, to a low-erosion environment that was dominated by the aeolian processes that are observed at present. This transition is supported by geochemical evidence of a transition in the

hydration state of crustal minerals early in Martian history that produced phyllosilicates under alkaline conditions to the more acidic environment, forming sulphates, followed by the eradication of liquid water altogether that was contemporaneous with the geomorphological transition. These events were synchronised with the growth of a thick global cryosphere. This evidence strongly indicates that a substantial global climatic change occurred on Mars, from a relatively warm and wet to a cold and dry environment (Pollack et al., 1987; Squyres and Kasting, 1994; Grotzinger et al., 2014; Wordsworth et al., 2015). This process appears to have started approximately at the end of the Noachian period, and ended in the Early Amazonian period, although the magnitude and duration of this transition remains poorly constrained (Mangold et al., 2012).

1.3.1 The chaotic obliquity of Mars and the implications for the climate

The climate on Mars changed from a comparatively warm and wet environment to the cooler and drier environment that is observed today. However, this climate may not necessarily be stable, the Earth's climate has undergone many cyclic changes due to minor changes in distance from the Sun and in obliquity, which is the angle between an object's rotational axis and its orbital axis or inclination. The absence of a comparatively large stabilising moon around Mars means that the changes in obliquity on Mars is more chaotic in comparison to that of the Earth's, such that the Mars's inclination could have been greater than 60˚ and lower than 10˚ and for much of the Solar System's history, the obliquity of Mars was greater than 25˚ meaning a Sunward facing hemisphere in the summer this would result in warmer summers and colder winters than on present-day Mars (Christensen, 2003; Lewis et al., 2008;). The increased insolation during the Martian summer, therefore, could have increased temperatures in that hemisphere above the freezing point of water for periods longer than 10^5 years (Costard et al., 2002; Ward 1992). The implication for life is that this 'punctuated' habitability could permit life to persist on Mars during these relatively benign periods and then enter some form of stasis, such as spore formation, during the periods when the climate was too hostile for active biology, such those observed at present on Mars (Grotzinger et al., 2014; Jakosky et al 2003).

1.5.0 The Free Energy Available to life on Mars

From a biophysical perspective, all known living things obey the 2nd Law of Thermodynamics and therefore require an external source of energy to create an ordered system, which results in a net decrease in entropy that is bounded by the structure of the organism. Any organism's energy harvesting system is based upon the type of free energy that is available. On Earth, 90% of the free energy that is available is obtained from the radiant energy of the Sun. As a result, most of the organisms on modern Earth, either directly or indirectly obtain their energy from the process of oxygenic photosynthesis. The remaining 10% of the free energy available is in the form of differences in redox potential that occur as a result of geothermal activity and other sources, such as the radiolysis of water, which generates hydrogen. There are other sources of free energy that are hypothetically available, e.g. gravity or osmotic gradients (Schulze-Makuch, 2008). However, the abundant energy from the Sun and the available geothermal energy, below ground means that these unusual, relatively low energy gradient sources are, so far, unknown on Earth and they are unlikely to be utilised by any hypothetical Martian biota (Hoehler et al., 2007).

The solar flux to the Earth's sunward-facing disc is equal to 1370 $W.m^{-2}$ and represents the most abundant source of free energy available to life (McBride and Gilmore, 2004; Gilmore and Sephton, 2004) and, therefore, it is the ultimate source of energy for >99% of the life on Earth. Despite being further away from the Sun, the solar flux on Mars is 593 $W.m^{-2}$, this is still a substantial 43% of the solar flux of the Earth, and therefore sunlight represents the largest available source of free energy, on Mars (McBride and Gilmour, 2004; Horneck and Baumstark-Khan, 2012). The harsh conditions on the surface of Mars (see section 1.3.0) are very likely to limit any organism's ability to survive in places where light energy harvesting regimes could be utilised.

There is strong evidence for the Earth's biosphere extending deep below the surface, where energy sources that are independent of the surface-based light energy harvesting metabolisms (Lovley and Chapelle, 1995; Stevens and Mckinley, 1995; Stevens, 1997; Amend and Teske, 2005; Lever, 2013; Lever et al., 2013). Therefore, using the Telluric subsurface biology as a model, it has been suggested that biospheres could exist where geothermal, radiological and chemical energy could provide sources for biological activity (Schulze-Makuch and Irwin, 2008).

The free energy from the sources described in the previous paragraph is acquired by organisms via stepped transportation of electrons. Organisms can shuttle electrons between redox couples (acceptors and donors) with various redox potentials. Therefore, given a thermodynamically favourable redox reaction, electrons are obtained from donors, and then the acquired electrons are passed through their redox gradient via enzymatically directed redox reactions along an electron transport chain that terminates at an electron acceptor (Lubert, 2015). On Earth, there is a wide range of readily available redox couples that are found throughout the environment, and nearly all available redox transitions are utilised by at least one type of organism. For example, NH_4^+, hydrocarbon molecules, reduced and oxidized metals and atmospheric gases (CO_2, CH_4, H_2, H_2S, CO, and O_2) are only just a few of the many available sources (Madigan, 2008).

On Mars, there are a few plausible candidate redox couples present that could be harnessed for energy, by any life in the subsurface. For example, hydrogen can serve as an electron donor. Sources of hydrogen that could be generated in trace amounts through photochemical reactions in the Martian atmosphere that could then diffuse down through the regolith (Weiss et al., 2000). Additionally, molecular hydrogen can be produced from the reduction of water by the abundant ferrous-iron crust on Mars, in a process called serpentinisation (See section 1.6.4). Alternatively, hydrogen could be released either by radiolysis or photochemistry making hydrogen potentially available to life on Mars. (Kelley et al., 2005; Lin et al., 2005; Russell, 2009; Ohara et al., 2012; Michalski et al., 2013 and see section 1.6.4.).

Hydrogen can be redox coupled to CO_2 as the electron acceptor to produce energy for microorganisms, with methane as the by-product (Chassefiere and Leblanc, 2011). Interestingly, such methanogenic bacteria are able to exist in some of the harshest environments on Earth, including acidic environments and inside Greenland glacial ice 3-kilometres deep, which is an environment considered as analogous to Martian subsurface ice environments (Stevens and Mckinley, 1995; Chapelle et al., 2002; Tung et al., 2005). Telluric methanogenic microorganisms have been suggested as plausible models for Martian life forms (Boston et al., 1992; Weiss et al., 2000; Schulze-Makuch et al., 2008; Mickol and Kral 2016) and methane has possibly been detected on the surface of Mars which could be

attributed to methanogenic bacteria (Krasnopolsky et al., 2004). Although, there are many plausible abiotic sources of methane, and the presence of methane in the Martian atmosphere, is still contended (see section 1.6.3).

Many telluric microorganisms are capable of harnessing the chemical energy yielded from reduction-oxidation (redox) reactions in the environment. Iron and sulphur mineral species can function both as electron donors and acceptors and given the prevalence iron, in particular, the redox cycle of iron drives the metabolisms of a substantial number of Telluric microbial populations Earth (Bach and Edwards, 2003; Weber, 2006).

The top surface of the Martian regolith is widely covered by reddish-brown iron oxides. However, darker reduced iron (Fe^{2+}) occurs a few centimetres below the surface (Vaniman et al., 2013; See Fig 1-11). Indeed, Fe^{2+}-bearing minerals such as olivine, $(Mg, Fe^{2+})_2SiO^4$ have been detected in many locations of the Martian surface (Hoefen et al., 2003). Furthermore, large amounts of basaltic glass (amorphous Fe^{2+}-containing materials) are contained within Martian crustal rocks (Morris et al., 2006a; Morris et al., 2006b; McSween et al., 2009). The iron is present principally as Fe^{2+} on Mars, and this is widely available electron donor, that could potentially be exploited by any extant Martian microorganisms. On Earth, oxygen acts as the electron acceptor, and in anaerobic conditions on Earth, many microorganisms can use nitrate (NO_3^{-0}) as the electron acceptor (Straub et al., 2004). However, nitrates have yet to be detected on Mars.

Fig 1-11. *The dark Fe^{3+} in the shallow subsurface exposed by the tracks of the Mars exploration rover 'Spirit'.* https://mars.nasa.gov/resources/5821/rover-tracks-near-husband-hill/ Credit: NASA, JPL,MSSS (see acknowledgments)

On Earth, the microorganisms oxidise ferrous (Fe^{2+}) to ferric (Fe^{3+}) iron, which is coupled to the reduction of oxygen, or nitrate in the case of anoxic environments (Straub et al., 1996). Iron is an abundant electron donor on Mars. However, the absence of free oxygen, nitrate or any other suitable electron acceptor, implies that the oxidation of iron, to drive metabolic

activity is unlikely to be encountered (Cockell et al., 2011). Conversely, Microorganisms that reduce ferrous (Fe^{3+}) to ferric (Fe^{2+}) iron are also are found on Earth. In this case, iron oxides and oxyhydroxides, are practical terminal electron acceptors (Lovely, 2006) and on Earth ferrihydrite is commonly reduced by telluric microorganisms (Roden and Zachara 1996, Cutting et al. 2009). On Mars, hematite and goethite are minerals that are widely distributed across the Martian surface and are therefore available to serve as electron acceptors (Nealson and Cox, 2002; Nixon et al., 2012; Nealson, 1999).

It has been proposed that the perchlorate (ClO^- ; $_4$), which appears to be widely distributed through the Martian regolith could serve as an electron acceptor (Coates and Achenbach, 2004; see section 1.6.2). However, the ΔG for Fe/ClO_3 redox couples of -14.86 kJ/mol may not be adequate to permit growth, and to date, no organisms capable of being cultured with perchlorate as the electron acceptor, have been reported.

Until July 2018, only traces of carbon had been detected on the surface of Mars (Miller et al., 2016), suggesting that there was an apparent paucity of organic electron donors on Mars (Nixon et al., 2016). However, the detection of organic material by the Curiosity rover (Eigenbrode et al., 2018) permits a full redox couple to exist, which could support microbial iron reduction. Alternatively, magmatic carbon detected in Martian meteorites (Steele, 2012) could provide an endogenous source of carbon that, if released into the subsurface environment, as it is on Earth (Tingle and Hochella, 1993; Holm and Charlou, 2001; McCollom, 2013) could potentially be utilised by Martian life. Therefore, the presence of organic material on Mars may be essential for the generation of energy, as well as providing the molecules that are the scaffolding for life.

1.6.0 Organic Chemicals on Mars

Carbon is the element that is used to construct living systems on Earth. Carbon's position in period two (group 14) means it has a relatively small atomic radius, and therefore it both readily forms covalent bonds and has tetrameric valence meaning that it is capable of forming single, double and triple covalent bonds, both with other carbon atoms and with hydrogen, oxygen, nitrogen, phosphorous and sulphur (Hiscox, 1999). Together, these

elements are able to form an essentially infinite number of organic molecular structures that could be potentially used by life.

Complex organic compounds are ubiquitous throughout the Galaxy (Meinert et al., 2011), and it is reasonable to assume that they are common throughout the Cosmos. Organic molecules can be identified in the interstellar medium (Millar, 2004; Ehrenfreund and Cami, 2010; Dolomatov and Zhuravleva, 2014), in comets (Crovisier, 2004), and in meteorites where the concentration of carbonaceous material can be up to 2 % $^w/_w$ (Botta and Bada, 2002; Sephton, 2002; Pizzarello, 2006) making it an abundant resource for any life in the solar system.

During the planning of the Viking missions to Mars, it had been anticipated that even without life, an accretion of detectable levels abiotic organic material should have occurred in the Martian regolith, from the exogenous delivery of material to the Martian surface from the interstellar medium for over 3.5 Ga (Flynn, 1996). Given the low levels of surface geological activity on Mars throughout this time, it was imagined that this material should have accumulated in the upper few metres of the surface. This theory was based on the assumption that there was no mechanism for the removal of such organic material from the Martian geosphere (Simmonds, 1969).

The inventory of organic molecules delivered to the surface via meteorites, comets and interplanetary dust in-fall is thought to be an order-of-magnitude higher on Mars than it is for Earth, due to its lower surface gravity that results in a lower atmospheric meteorite entry velocity and hence a lower impact temperature. On this basis, relatively more of the organic fraction of the meteoritic material survives in its original state, during surface accretion on Mars (Flynn, 1996). Furthermore, the lack of tectonic activity and the lack of any plausible carbon sinks in the Martian geology, along with the lower geological weathering rates on Mars, in comparison to the Earth should have, theoretically, permitted meteorites to persist for considerably longer periods on Mars, compared to Earth (Bland and Smith, 2000 and references therein). This should have resulted in an estimated yearly accumulation rate of 5×10^2 to 5×10^5 meteorites, and this is equivalent to >10 grams in mass per square kilometre (Bland and Smith, 2000). In addition to the meteorites, it was calculated that ca. 25% of the infalling micro-meteoritic dust reaches the Martian surface.

The total mass accretion rate by comets, meteorites, and dust particles is estimated between $1.8x10^{-5}$ and $4x10^{-4}$ g.m^{-2} per year (Flynn and McKay, 1990), which corresponds to the deposition to the Martian surface on the order of 10^6 kg organic material per year. Assuming a constant deposition rate, the total deposition over 4 Ga should be 1 x10^{15} kg (Flynn, 1996), in comparison to the estimated total biomass of the Earth, which is 6 x 10^{16} kg (Chyba, 1990). The surface area of Mars is 1.44 x 10^6 km^2 and assuming that the organic material would be evenly distributed across the planet in the upper 10 metres of regolith this equates to a hypothetical value of carbonaceous material of 2.0 kg.m^{-2} of regolith. Based on the complex organic material detected in carbonaceous chondritic meteorites (Sephton, 2002). The carbonaceous material that is derived from meteorite accretion and still close to its original condition on the surface of Mars should similarly be composed of complex organic molecules, i.e. mainly in the form of kerogen-like organic material.

In addition to the exogenous delivery, other potential mechanisms of organic material have been proposed, which includes lightning discharge, coronal discharge, UV radiation, and atmospheric shocks. Since these have been proposed as mechanisms for the accumulation of complex organic compounds on early Earth, it has been reasoned that they may also have occurred on early Mars (Chyba and Sagan, 1992). Additionally, the serpentinisation and fischer-tropsch type (FTT) processes are all capable of producing the abiotic accumulation of organic material (see section 1.6.4) and Chapter 8.

1.6.1 Previous and Current Attempts to detect organic material on Mars

Given that the exogenous delivery of organic material to the surface of Mars was understood by the Viking mission designers (Ringwood and Clark, 1971; Anderson, 1972) and the detection of Martian life seemed highly likely, it had seemed reasonable to assume that the concentrations of organic material on the surface of Mars would be comfortably within detection limits of organics by the py-GC/MS instrument on board the Viking Landers (Simmonds, 1969; Simmonds, 1970). However, contrary to these expectations, this instrument failed to conclusively detect organic material in the fine Martian regolith collected from the upper 10 cm of the surface. These results were met with great surprise at the time (Biemann, 1977; Biemann, 2007) and these results were used to support the general conclusion that the Martian surface was devoid of life.

Two possible explanations for this surprising non-detection were posited. Either the organic material has radiolytically, photolitically and chemolitically decomposed in the Martian environment (see ten Kate et al., 2002; ten Kate 2010, and references therein), or the instrument techniques to detect organic matter on the Martian regolith, are ineffective, which was a result of the interaction between environmental conditions and/or mineralogy with any organic matter present (Benner, 2000; Navarro-Gonzalez et al., 2006).

The absence of a magnetosphere and the thin Martian atmosphere (see section 1.3.0) means that the surface of Mars is not protected from high U.V. flux, able to penetrate a few cms into the surface, or from the cosmic background radiation that is thought to penetrate metres into the surface. Both of these types of radiation are capable of degrading complex organic compounds. In addition to radiation, other physically destructive agents are also proposed, such as glow discharge plasmas that are electrostatically generated during Martian dust storms (ten Kate, 2010).

In addition, or alternatively to, the physical breakdown of organics, it has been suggested that the non-detection of organic material within the Martian regolith was due to the UV mediated oxidation of organic material to form a thermally metastable organic salt, such as benzoate (Fig. 1-12) (Benner, 2000). The formation of this thermally stable compound would have prevented the volitisation of organic species, at the temperatures applied by the Viking experiments, since only volatile organic molecules are able to pass through a gas chromatograph prior to entering the mass spectrometer (Benner, 2000).
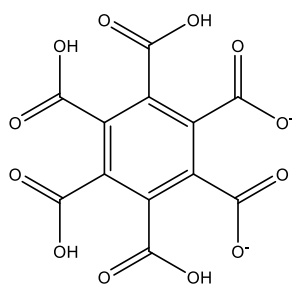
3,4,5,6-tetracarboxyphthalate
Boiling Point: 1258.96 [K]
Melting Point: 1132.98 [K]

Fig. 1-12. *A hypothetical metastable organic compound that could potentially be produced in the Martian environment that would be unamiable to detection by py-GC/MS.* Credit: Benner, (2000)

A further alternative explanation was that the Viking py-GC/MS protocols were inadequate for the detection of organic material in the Martian regolith. The efficiency of thermal extraction at lower volitisation temperatures is reduced in geological samples with low organic content (Navarro-Gonzalez et al., 2006; Chapter 8), whereas higher pyrolytic temperatures do permit extraction but conversely cause the concurrent thermal decomposition of complex organic macromolecules. This phenomenon would require the presence of an oxidising agent in the Martian regolith, that would be capable of decomposing organic material during pyrolysis. While a hypothetical oxidant such as H_2O_2 was proposed soon after the Viking missions (Klein, 1991), it was the subsequent detection of perchlorate by the Phoenix lander that eventually provided the required oxidising properties to explain the Viking results (Hetcht et al., 2009) (See section 1.6.2).

The limitations of GC/MS to detect organic material that results from the inefficiency of the pyrolysis process used to extract organic compounds thermally has also been considered and Navarro-Gonzalez et al., (2006) reported that the key limiting factor with pyrolysis coupled to GC/MS is that iron-containing soils attenuate the detection of low levels of organics. Iron within the sample material, such as the iron-rich soils that are found on Mars and Mars soil analogues on Earth, causes the oxidation of organic material to CO_2 and this problem would be exacerbated by the presence of perchlorate (Navarro-Gonzalez, 2010).

A further limitation in detecting organics, using pyrolysis for thermal extraction is in situations where the geological samples possess very low concentrations of organic material. Examples of organic-poor soils are telluric desert regolith, where the organic content is below 1500 parts per million (ppm) (0.15 %). However, when the concentration of organic material is <150 ppm (<0.015%), then organic material is undetected (see section 8.2.3). This was attributed to the decomposition of the organic material to CO_2 caused by a thermally induced oxidation, which is mediated by any oxidising minerals in the sample, such as Fe^{2+} (Lewis et al., 2015). The inference is that this decomposition could potentially occur during the py-GC/MS analysis of the Martian regolith by the Viking landers because the Martian regolith possesses both trace levels of organic material, and an iron-rich geology (Navarro-González, 2009).

Contrary to the conclusions made following the Viking experiments, organic material has indeed been detected at trace levels in the Martian surface. For instance, in the four samples taken from surface and subsurface material from both landing sites, water (0.1–1.0 wt.%), carbon dioxide (0.05–0.6 ppm), and some organics were detected, including benzene and toluene (Bieman et al., 1976; Biemann et al., 1977). Furthermore, both the Viking 1 and Viking 2 landers detected chloromethane at concentrations of 15-40 ppbv. However, these chlorohydrocarbons were all dismissed as contamination that had originated from the dichloromethane that was used to clean the Viking instruments during their fabrication. This was despite the fact that these compounds were undetected at those levels in the in-flight test runs, which were conducted during the journey to Mars (Biemann, 1976; Biemann,1977). The conclusion that was reached was that organic compounds of Martian origin were absent in the Martian Regolith (Biemann et al., 1977). Twenty-two years later the Phoenix Lander Thermal and Evolved Gas Analyser instrument designed to analyse dissolved materials that had been recovered from the Martian polar desert also failed to detect dissolved organics at >ppb levels (Ming, 2009; Sutter, 2009).

In July 2018, it was reported that thiophenic, aromatic, and aliphatic compounds had been detected on Mars, by the Curiosity rover (Eigenbrode et al., 2018). The samples were obtained from the drill spalling extracted from a hole drilled in mudstones at Gale Crater. This demonstrated, firstly, that organic material is able to survive on Mars by being protected from the Martian environment in the internal volume of rock. Secondly, that the pyrolysis-gas chromatography/mass spectrometry, such as the one on the SAM instrument package on Curiosity rover is capable of detecting and identifying organic material on Mars.

1.6.2 Perchlorates in the Martian Environment

Although chlorine had been detected in the Martian regolith during the Viking missions (Clark, 1976; Clark and Vanhart, 1981), the detection of perchlorates (ClO_4^-), which is a highly oxidised form of chlorine, was made in the Martian polar ice, by the Phoenix lander (Hecht et al., 2009). Subsequently, other oxychloride phases have been detected at similar levels by the Sample Analysis at Mars (SAM) instrument on the Curiosity rover (Glavin et al., 2013) and both ClO_4^- and ClO_3^- have been detected in Martian meteorite EETA79001 (Kounaves et al., 2014). These species are present in the form of magnesium perchlorate,

($Mg(ClO_4)_2$), or calcium perchlorate, ($Ca(ClO_4)_2$) 0.4 to 0.6 wt. % with chloride present as only a minor constituent: 0.01 to 0.04 wt. %, based upon the further detection of perchlorate at the Gale crater site in the equatorial region (Glavin et al., 2013).

A perchlorate formation process has been proposed by Carrier and Kounaves (2015) who demonstrated that highly reactive oxychlorides and radicals are produced both from oxidation of mineral chlorides such as halite to perchlorate by the action of UV irradiation and from the radiolysis of perchlorates by the action of cosmic gamma and X-rays (Quinn et al., 2013). The highly reactive intermediates produced from these pathways are capable of decomposing organics by oxidizing and/or chlorinating them. This reaction pathway is illustrated in Fig 1-13.
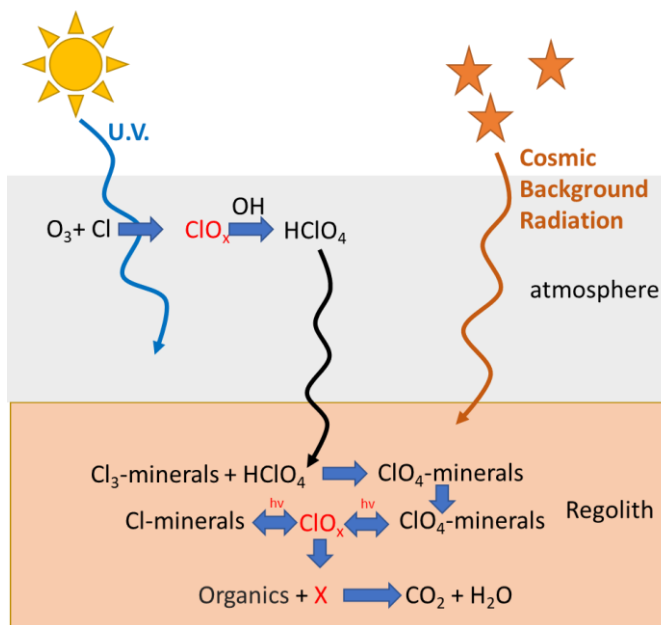
Fig 1-13. *The proposed pathway for perchlorate production on Mars. Adapted from: Planetary Chemical Analysis Group*, Tufts University.

X=oxidant

The detection of perchlorate widely distributed throughout the Martian regolith has important implications for the detection of organics for past, and future missions to Mars since perchlorates are capable of oxidising organics into carbon dioxide upon heating to the pyrolysis temperatures used in both GC/MS analysis of Martian regolith. The complete decomposition and oxidation of organic material would negate thermal extraction as the ideal method of obtaining organic material for the subsequent detection in the GC/MS analytical phase (Ming et al., 2009).

1.6.3 Methane

Methane was originally detected in the Martian atmosphere both from orbit (Formisano et al., 2004) and by using ground-based observations (Krasnopolsky et al., 2004) with measurements of the global average concentrations of 10^{-5} ppb $^v/_v$ and 10^{-3} ppb $^v/_v$ respectively. Both observation methods suggested that there was a geographical and seasonal variation in the concentrations with the highest concentrations being observed in the Martian Summer (Geminale et al., 2008). Methane has a hypothetical residence time in the atmosphere of ca. 300–600 years before it photolytically degrades (Nair et al., 1994; Summers et al., 2002). Although the observed residence time of methane in the Martian atmosphere appears to be in the order of a few years (Mumma et al., 2009; Lefevre and Forget, 2009). Consequently, it has been suggested that this methane may be undergoing adsorption onto the charged surfaces of minerals that have been chemically activated by aeolian driven mechanicochemical processes (Jensen et al., 2014; See section 8.4.1). This short-term change implied a cyclical, seasonal cycle, with production from equinox to summer and then loss from summer to equinox, where rates of methane production are in the order of 0.5 kg.s^{-1} (Mumma et al., 2009).

These results were initially considered contentious. However, methane and chlorinated methane compounds subsequently have been detected *in situ* in the Gale crater, on the surface of Mars where ten-fold spikes in methane concentrations from 0.7 ppb to spikes of 7 ppb were observed during the Martian day (Webster et al., 2015).

It is possible to explain this methane production by geological processes such as volcanism (Neukum et al., 2004). However, there is little evidence for significant amounts of this type of activity currently on Mars (Christensen et al., 2004; Richardson et al., 2013). Therefore, other geochemical processes have been invoked, such as serpentinisation (see section 1.6.4). Other potential sources of methane could include outgassing of trapped methane from clathrate hydrates that could hypothetically exist in the cryosphere (see section 1.4.3; Chastain and Chevrier, 2007). Exogenous sources of methane could be obtained from the outgassing of volatile organic material from carbonaceous comets and meteorites (Keppler et al., 2012; Fries et al., 2015). One intriguing possibility is that methanogenic bacteria are

responsible for this methane-producing process (Krasnopolsky et al., 2004; Reid et al., 2006).

1.6.4 The Possible Sources of Organic Compounds on Mars

On Earth, the biosphere is responsible for the bulk of the observed organic material. However, this can be synthesised through some non-biological processes, and the most well-known of these is serpentinization. This is a process where rock (normally ultramafic) is altered by the addition of water that acts as a catalyst to form one of the serpentine groups. A common reaction is the conversion of anhydrous ferromagnesian silicate minerals such as pyroxene or olivine ((Mg^{2+}, Fe^{2+})$_2$ SiO_4), into hydrous silicate minerals (Fe_2SiO_4 and Mg_2SiO_4) plus other possible minerals like brucite $Mg(OH)_2$) or magnetite (Fe_3O_4; e.g. eq. 1).

$$3\ Fe_2SiO_4 + 2\ H_2O \rightarrow 2\ Fe_3O_4 + 3\ SiO_2 + 2\ H_2 \qquad\qquad (1)$$
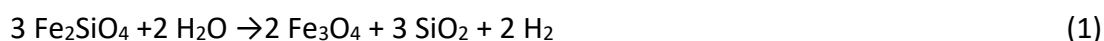
When this reaction occurs in the presence of CO_2 (eq. 2), for example, in the CO_2 rich environment of the Martian atmosphere then the hydrogen can combine with the CO_2 to form methane (eq.2):

$$(Fe,Mg)_2SiO_4 + n{\cdot}H_2O + CO_2 \rightarrow Mg_3Si_2O_5(OH)_4 + Fe_3O_4 + CH_4 \qquad\qquad (2)$$

The non-detection of significant amounts of organic material on Mars by the Viking py-GC/MS instruments had been surprising (see section 1.6.1) since it had been thought by the Viking mission planners that even in the absence of a biosphere present on Mars, organic material should have been encountered in the upper 10 cm of the surface regolith and a "good picture" of Martian organic geochemistry would be obtained (Anderson et al., 1972). It had been known at that time that carbonaceous chondritic meteorites contain approximately 1.3% complex "kerogen-like" organic material (Hayes, 1967; Sephton and Gilmore, 2001) including water-soluble amino acids (Cronin and Moore, 1971) later it was calculated that the average organic content of interplanetary dust is in the order of 10% (Anders, 1989). Thus, given the absence of tectonic activity that this organic material would accrete in the Martian regolith and given the organic concentration and the estimated flux it was estimated that in excess of 1×10^{15} kg organic material should have accumulated in the upper 1 m of the surface (Flynn, 1996), an amount comparable to the 6×10^{14} present on the surface of the Earth (Chyba et al., 1990). The composition of the organic matter is

complex and contains amino acids, hydrocarbons, carboxylic acids, carbohydrates and nucleobases (Cooper et al., 2001; Sephton, 2002; Martins et al., 2008). Some amino acids demonstrate L-enantiomeric excesses, implying that possibility they may have contributed to terrestrial homochirality observed in contemporary proteins and therefore the early Earth and indeed early Mars with both enantiomeric excesses (Pizzarello, 2004). Consequently, it has been speculated that the organic material from meteorites could have provided the precursor molecules for prebiotic chemistry on the Earth (Ehrenfreund and Charnley, 2000) and it is plausible that a similar deposition of pre-organic chemistry may also have occurred on Mars.

In addition to the predicted exogenous delivery of complex organic material to the surface of Mars, by carbonaceous meteorite in-fall, it is possible to endogenously synthesise pre-biological organic chemistry. This was demonstrated by the Millat-Uray experiment where amino acids were synthesised in a reaction vessel with conditions that are thought to mimic the highly reduced environment of the early Earth (Millar, 1953). Given that the atmospheres of the two planets were comparable during their early history (Kasting, 1993; Owen et al., 1993). Therefore, it is possible to presume that a similar abiotic synthesis of complex organic compounds may have occurred on Mars (Anders et al., 1972). Furthermore, the geochemical synthesis of hydrocarbons through Fischer-Tropsch-type (FFT) reactions, which are considered to be geological processes that are analogous to the industrial Fischer-Tropsch reactions, which are used to synthesise commercially important organic compounds (Holm and Charlou, 2001; Russell, 2007; Zolotov, 2003) have also been demonstrated to generate C_2 and C_3 hydrocarbons from methane (McCollum, 2013). These process could potentially occur in the hydrothermal vents, and there could also be an endogenous source of pre-biotic chemistry. Recently a mechanism for manganese oxide interactions with low molecular weight hydrocarbons that resulted in the formation of high molecular weight polyaromatic hydrocarbons described as geopolymerisation has been reported (Johnson et al., 2015) and this is the subject of further investigation (see Chapter 8). Crucially, due to its complexity and insolubility, the diagenetic products of biological material called kerogen (see section 1.10.1) is difficult to characterise at a molecular level, consequently distinguishing between biologically derived kerogen and non-biologically synthesised

kerogen-like material is considered to be a subject requiring further investigation (De Gregorio et al., 2012).

1.6.5 The Role of Trace Elements for Life

Carbon is the central supporting element for life, not only as the scaffolding, but also as an electron donor or acceptor for in Redox couples with other elements or compounds that can drive an electron transport chain (Banerjee et al., 2000; Lovely and Philips, 1988; Madigan et al., 2008). In addition to carbon, the presence of a range of other elements is a minimum requirement for life to emerge, particularly hydrogen, oxygen, nitrogen, phosphorus, and sulphur (HONPS). Fortunately, since the inner solar system formed from a comparatively homogenous distribution of materials, the organic element (C, H, O, N, P and S) inventory on the early rocky planets were comparable (McBride and Gilmore, 2004). The importance of phosphate is illustrated where apatite (a Calcium Phosphate mineral) is the first mineral to be dissolved. This is essential for the microorganisms given that phosphorous is essential, and availability is a limiting factor in the microbial activity. In addition, biological activity also requires soluble e.g. cations (sodium, calcium, magnesium, ammonium, and ferrous and ferric iron), base metals (chromium, nickel, copper, cobalt, zinc, lead, and mercury), and soluble anions (chloride, nitrite, nitrate, hydrogen sulphide, sulphite, sulphate, phosphate, selenite, and arsenate) (Southam and Westall, 2007).

The transition metals iron, zinc, copper, molybdenum, cobalt, chromium, vanadium, and nickel are important to biology relative to their abundance in living organisms. It is noted that although zinc is not strictly a transition metal, it does share many bioinorganic properties with transition metals. Further, the levels of these elements in the environment are relative to their importance to biological activity, implying that early life appropriated transition metal based on both their chemical properties and their comparative availability (Kobayashi and Ponnamperuma, 1985). These elements are generally found either bound directly to proteins or in cofactors such as porphyrins or cobalamins, or in clusters that are in tum bound by the protein; the ligands are usually O, N, S, or C. The functions of the proteins with which transition metals and zinc are most commonly associated with is catalysis. They are particularly associated with intramolecular or intermolecular rearrangement of electrons, depending on nutrient requirements of the organism. These

compounds can be used in anabolic reactions, such as the generation of new biomass or in catabolic processes used to generate the energy (Theil and Raymond, 1994).

The transition elements also serve as the electron acceptors or donors in a range of redox couples that are suitable drive metabolic processes in lithotrophic microorganisms (Madigan et al., 1997; see Section 1.9.1). The microbially facilitated weathering of permits access to elements that may be limited in their environment, for example, micronutrients, such as Fe, P, Co, Zn, Mo, Cu, and Ni, which are represented in trace amounts in most terrestrial materials (Bennett et al., 1996; Brantley et al., 2001; Hiebert and Bennett, 1992; Rogers et al., 1998).

1.7.0 Implications for Life on Mars: The Lessons from Earth and the History of Mars

To summarise the preceding sections, it is possible to conclude that the observations obtained from the Viking life experiments (see section 1.2.1) and the non-detection of organic material on Mars had led to a rather pessimistic conclusion for the prospects of detecting life on Mars. However, the evidence subsequently collected during the geochemical and geomorphological exploration of Mars since 1997 has demonstrated that a variety of paleoenvironments have existed on Mars that has persisted on timescales of several hundreds of thousands to a few million years, some of these environments may have been conducive to the formation and assemblage of prebiotic molecules from water and carbon into primitive cells (Martin and Russell, 2007), and these environments may have been adequate for life to subsist on the surface of Mars, particularly during the Noachian period. However, whether the conditions were ever capable of sustaining a flourishing biosphere is not clear (Westall et al., 2013; Cockell, 2014).

Using the Earth as an example, it may be possible to make some deductions regarding the environmental, spatial, and chronological parameters that are required for the appearance of life and extrapolate those to the emergence of life Mars. For instance, on Earth there is evidence of the remains of complex stromatolites that are reported to be microbial colonies, in rock formations that are approximately 3.7 billion years old (Mojzsis et al., 1996). This fossil evidence implies that complex life on Earth was already sophisticated and robust at the time of the host rock formation, which suggests that the earliest life on Earth

likely evolved over 4 Ga ago (Abramov and Mojzsis, 2009). Isotopic measurements of ^{12}C: ^{13}C ratios suggest that carbon in the oldest surviving rocks on Earth have undergone biological processing and these observations have been used to support the morphological evidence that cell-like structures already present on Earth 3.77 to 4.27 Ga were indeed microorganisms (Bell et al., 2015; Dodd, 2017). These observations potentially push the presence of life into the Hadean period, when the late heavy bombardment (LHB) is considered to be still active. This again, implies that life evolved early and prolifically in Earth's history, which also infers life can arise rapidly anywhere once the suitable conditions are met (See section 1.1.1; Marshall et al., 2007; Allwood, 2016; Nutman et al., 2016).

The dates of the earliest life on Earth from Dodd et al. (2017) and dates of the cooling and drying of the Martian climate around the Noachian/Hesperian boundary at 3.5 Ga, provide a window of opportunity for prolific life on Mars between 0.27 to 0.77 Ga, when the climate was relatively benign (see Fig 1-4). Since the time span between the end of the LHB and the evidence for the first life on Earth is less than 0.5 Ga, then there is cautious optimism that the Martian paleoclimate may have been suitably benign for a sufficiently long enough time for life to arise, before the climate became too hostile. Again, using the Earth as an example, the chronological window that was favourable for the appearance of life between the pre-Noachian to Noachian Periods imply that any life that may have appeared on Mars would have likely to have been, at best, in the form of simple single cellular organisms, since while microorganisms can exist as colonies such as stromatolites, multicellular organisms did not arise until ca. 2.0 Ga after the first Archean cellular life had appeared on Earth (Hedges et al., 2004; Brasier et al., 2015).

Given the changes in the Martian climate, and assuming life had arisen on Mars during the pre/early-Noachian period, then it is possible to make a few speculations regarding the trajectories that any life that might have followed (Irwin and Schulze-Makuch, 2002; Schulze-Makuch et al., 2005). The first possibility is that any life on the surface of Mars would have subsequently perished, as the planet became cooler and drier, potentially leaving only fossilised remnants on the Martian surface as the only measurable phenomenon that can be accessed with current and near-future technology. A second possibility is that Martian organisms could have retreated into the subsurface and the

interiors of surface rocks in much the same way as microorganisms have in the polar deserts (Cary et al., 2010; Cockell, 2011; McMahon, 2013). Since solar radiation is the most abundant and available energy source on the surface of a planet and given the early evolution of phototrophic organisms on Earth, then the probability of phototrophic organisms evolving on Mars, superficially, seems logical (See section 1.5.0). To support this theory, there are Telluric examples where the photosynthetic cyanobacteria that are usually found in aquatic and marine environments, which can be observed in the interior spaces of rock as endoliths or chasmoendoliths in polar and temperate desert environments (Cockell et al., 2002b; Lim, 2002). However, the possibility that lithotrophic organisms would be able to persist in the Martian sub-surface also seems entirely plausible (Schulze-Makuch et al., 2005; Jepsen et al., 2007).

Such lithotrophic organisms could have survived on Mars by retreating into protected places such as subterranean voids, such as lava tubes, fractures, fissures, or caverns. This evolutionary scenario is analogous to the Earth's deep biosphere, where organisms can live in highly saline conditions in a range of temperatures from 115°C to −20°C. Further evolutionary possibilities are Martian analogues of the chemoautotrophic psychrophiles that are found under glaciers in Earth, which could survive in the aquifers under the Martian cryosphere. Lastly, there are a small number of sites known on Earth where chemotrophic organisms are supported by chemical energy, for example, within deep basalt aquifers (Stevens and McKinley, 1995), hydrothermal vents, and anoxic sediments (Stevens and Mckinley, 1995; Stevens, 1997; McKinley et al., 2000).

When liquid water is intermittently available, then any life must adapt to these cyclical conditions by alternating between active and dormant conditions. Therefore, life could be found in two different modes on Mars, either existing as chemolithotrophs or possessing some mechanism such as sporation that allows the organism to survive the unfavourable conditions for extended periods (Cockell, 2014). Given the variation in the Martian climate caused by the large changes in obliquity at time scales of 10^5-10^7 ,then survival of sporating organisms might be possible, where potentially Mars's cold, dry and thus uninhabitable environment can be punctuated by shorter-lived habitable conditions. A further scenario that would permit the survival of sporating organisms would be where areas at the surface

are intermittently warmed by impact-induced hydrothermal systems creating short-lived 'oases' (Cockell et al., 2002a; Osinski et al., 2013).

1.8.1 The approaches to locating paleobiological activity on Mars

If life did indeed arise on Mars, only to expire on the surface as the environment became increasingly uninhabitable, then potentially fossilised remnants may be the only evidence that the surface of Mars once hosted life (Schulze-Makuch et al., 2005; Westall et al., 2013; Cockell, 2014). Since the presence of extant life or dormant life on Mars does not exclude the possibility of fossilised biology, then the methods for detecting fossilised Martian life are the principal focus of this thesis. Here, the development of analytical methods to interpret the geobiological record for the presence of fossilised microbial life and understanding of what can be considered as the signals for life on Earth are applied to the astrobiological exploration of Mars (Cady et al., 2003; Cady and Noffke, 2009). However, the interpretation of the tenuous information left by fossilised microbial life on Earth and the remnants of life on Mars has proved to be challenging, and therefore more than one method is required for the detection of fossilised life on Mars (Cady et al., 2003; Brasier et al., 2006; Cady and Noffke, 2009; Brasier et al., 2015; Westall et al., 2015).

Section II

The following section considers the types of Telluric fossil evidence that could be encountered Mars, the state that this evidence would be in and how this could serve as potential evidence for life on Mars. Finally, this section introduces the instruments that could be used to detect and correlate these two lines of evidence.

1.8.0 Microscopic Scale Structures on Martian Meteorites and Their Past and Present Interpretation

The detection of fossils on Mars is derived from the approaches that have been already used for telluric paleobiology (Cady et al., 2003). The approach is to locate regions that are conducive to the formation of fossils, which are then visually inspected for features that have sizes, shapes and distribution that might imply fossilised biology (Botta et al., 2008; Westall, 2008; Cady and Noffke, 2009). The structures may be formed from either the remnants of the cells themselves or the fossilised traces of biological activity imprinted in the rock. Precambrian cellular structures have been reported as coccoidal microbial fossils, which are considered to be a common cellular morphology for that period (Westall et al., 2001). Fossilised assemblages of these organisms might be expected to contain a set of microscopic characteristics indicating a biogenic origin, for example, objects that are irregular spheroids in shape. A determinable cell wall would bound this shape, and the object would have a diameter that is constrained by the sizes typical of modern bacteria. Other visual indicators of biology that may be examples of fused pairs of spheroids, indicating they had undergone binary fission, before fossilisation. Furthermore, their distribution in the geological record ought to reflect their organisation and interaction in the environment. For example, a fossilised benthic microorganism would exhibit a relatively flat lower surface where the colony propagated across a substrate and a more globular upper surface where extension of the colony was less physically inhibited (Schopf, 2006).

Mars is tectonically inactive, and other types of geological activity are significantly diminished, in comparison to the Earth. The assumption is that any fossil evidence from the Noachian period will not be as geologically reworked, to the same extent, as Telluric

Archean fossils. Any such fossil evidence that presently exists on the surface of Mars would have potentially undergone 3.5 Ga of mechanical weathering, principally through aeolian activity (Thomas et al., 2005), which would result in the significant degradation of any morphological evidence.

The morphology of candidate fossilised microorganisms is not completely reliable evidence, on its own (Ruiz et al., 2002; Cady et al., 2003). An example of this was the apparent detection of the fossilised life that had originated on Mars. This was observed on a Martian meteorite called Allan Hills 84001 (ALH 84001) and was reported widely in the media in 1996 (McKay et al., 1996). Following its collection in the Antarctic in 1984, the ALH 84001 meteorite was stored for ten years before several analyses were conducted on the sample. In terms of its provenance, this material was thought to have crystallised from molten rock 4.091 billion years ago, i.e. during the Noachian Period. Radiometric dating suggested that the ALH84001 sample was ejected from the surface of Eos Chasma on Mars by a meteor strike ca. 17 Ma ago and landed in the ca. Antarctic 13,000 years ago (McKay et al., 1996). Several features were observed on the surface of the sample, using scanning electron microscopy (SEM). These features resembled some modern terrestrial bacteria and their appendages that were 10-100 µm long, and also appeared in formations that resembled colonies and biofilms (see Fig 1-14, Left).

Initially, structures attributed to fossilised nano (or nanno) bacteria were observed. Nanobacteria are putative cell-walled microorganisms that were smaller than the accepted ca. 200 nm lower size limit for life (McKay et al., 1996; Folk and Lynch, 1997). The detection of PAHs in the region of these structures was used to support the conclusion that these were biogenic. Furthermore, the presence of magnetite in the samples also led to the suggestion that these structures were biogenic (Thomas-Keprta et al., 1998). However, the existence of biogenic structures on ALH 84001 is not now widely accepted, since the internal volume of the putative fossilised nano-organisms is considered too small to sufficiently host all of the metabolic apparatus required for a living organism. Subsequent investigations suggest that these features can be attributed to an artefact of the sample preparation needed for electron microscopy (Thomas-Keprta et al., 1998; Gibson et al., 2001; Martel et al., 2012).

Furthermore, both carbonate crystals (Folk, 1999; Folk and Lynch, 2001) and PAHs can form abiotically (see section1.6.4). In conclusion, the ALH84001 sample appears not to provide any evidence of a fossilised biological activity (Bradley et al., 1997; Scott et al., 1998; Zolotov and Shock, 2000; Brearley, 2003).

In addition to ALH84001, indigenous ovoid structures have been observed on the Nakhla Martian meteorite (Fig. 1-14, Right). These structures are formed from iron-rich clay and amorphous material. While these structures have a spherical biogenic-like appearance, their morphology and distribution have been attributed to the purely abiotic processes through the action of liquid water despite the evidence that this meteorite formed about 1.3 billion years ago, during the mid-Amazonian period when the surface of Mars is considered to have been dry. Clays form in the presence of water, which suggests that at the time the Meteorite was ejected, liquid water was available on Mars. Therefore, potentially conducive to life (Chatzitheodoridis et al., 2014).
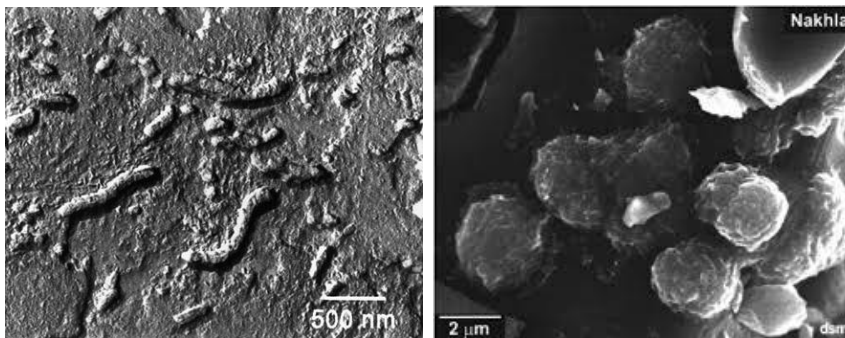
Fig. 1-14. *Nano-scale structures on the surface of (Left) ALH84001. Credit: NASA. and (Right) clay ovoids on the surface of the Nakhla meteorite.* Credit: Chatzitheodoridis (2014)

1.8.1 Macroscopic Scale Structures as Candidates for Locating Fossils on Mars

In addition to microscopic scale structures such as fossilised cells, morphological evidence in the form of visible microscopic and macroscopic scale structures are formed through biological activity in the geological record (ichnofossils), which can provide evidence of biological activity. Such structures can be the result of a range of biological activities, including tracks caused by locomotion or by burrowing.

Examples of macroscopic scale ichnofossils on Earth are the microbialites. These are a range of organo-sedimentary structures, which form from the interaction between benthic microbial communities and the sediments in their surrounding environment. Their formation occurs in response to the physical perturbations of their marine environment to

stabilise the sediments in the organism's locality (Riding, 2011; Noffke and Awramik 2013a; see Fig 1-15). This interaction occurs through the production of an adhesive mucilaginous matrix of extracellular polymeric substances (Decho, 1990; Noffke et al., 2013b) that is used to trap and bind inorganic particles in an organic mesh. Examples of colonies of Precambrian microorganisms that have the potential to form visible fossilised structures are the stromatolites. These structures differ from the microbially induced sedimentary structures (MISS), in that they consist of layered biochemical accretionary structures that are formed in shallow water by the trapping, binding and cementation of sedimentary grains in the biofilms (microbial mats) of microorganisms, especially cyanobacteria (Riding 2011; Riding, 2012; Noffke, 2013; Davies et al., 2016). Many contemporary examples of these structures can be observed (Castenholz, 2013), and there are also good examples of these structures preserved in the fossil record. The structures that form from the colonies of filamentous microorganisms that lived in shallow marine environments that resulted in MISS provide some of the oldest evidence for life on Earth (see Fig 1-15 a-d; Walter et al., 1980; Noffke et al., 2013b).
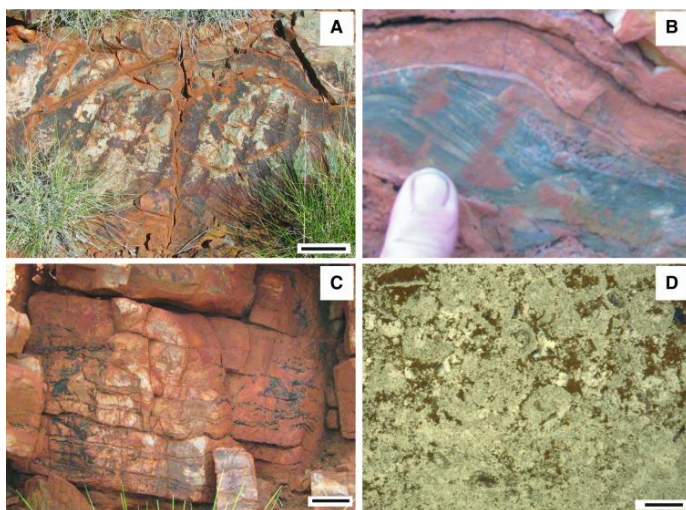
Fig 1-15. *Microbially Induced Sedimentary Structures Recording an Ancient Ecosystem in the ca. 3.48 Billion-Year-Old Dresser Formation, Pilbara, Western Australia. (A) Wave ripple marks Scale: 10 cm. (B) Ripple cross stratification (C) Tidalites Scale: 0.5 cm. (D) Oncoids in thin section. Scale: 0.25 mm.* Credit: Noffke et al (2013a)

The visibly identifiable remains of fossilised MISS and microbialites originate from some of the earliest organisms to have arisen and constitute a form of fossil biota that has the

potential to be visibly identified. Therefore, the discovery of comparable structures such as these, on Mars, could potentially provide the initial location of Martian biota. As such, the detection of these structures is a prime target for the astrobiological exploration of Mars.

Recently, several candidate structures, on Mars, have been reported. Indeed, the detection of visible formations that could be attributed to a biogenic origin have already been detected on Mars and had they occurred on Earth they would have been attributed to MISS (Noffke, 2015). Furthermore, visible evidence from the Opportunity rover's Athena instrument showed microstructures organised in intertwined filaments of microspherules, which are comparable to observable features in fossilised telluric stromatolites and other types of microbialites (see Fig 1-16; Bianciardi, 2015).
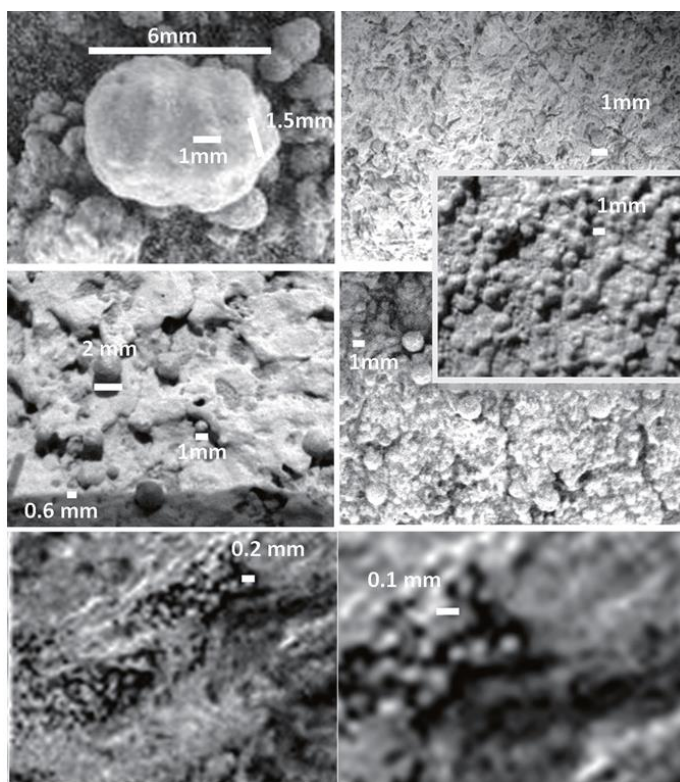
Fig 1-16. *An example of potentially macroscopic biogenic structures on a Martian Meteorite.* Credit: Bianciardi et al.(2015).

In addition to the microscopic structures observed on Martian meteorites, macroscopic structures, such as the nodular and digitate features, have been detected within silica deposits around the location of an ancient volcanic hydrothermal setting on Mars. These have a comparable morphology to structures that are produced on Earth by a combination of biotic and abiotic processes, which occur in comparable discharge channels of active hot

61

springs and geysers (see Fig 1-17; Ruff and Farmer, 2016). Therefore, there is mounting evidence for macroscopic scale structure that are candidates for fossilised life on Mars.

Fig 1-17. *A comparison between the morphology of geological structures at different scales at El Tatio hot spring, Chile and a paleo-hot spring at Gustav Crater, Mars.* Credit: Ruff and Farmer, (2016)
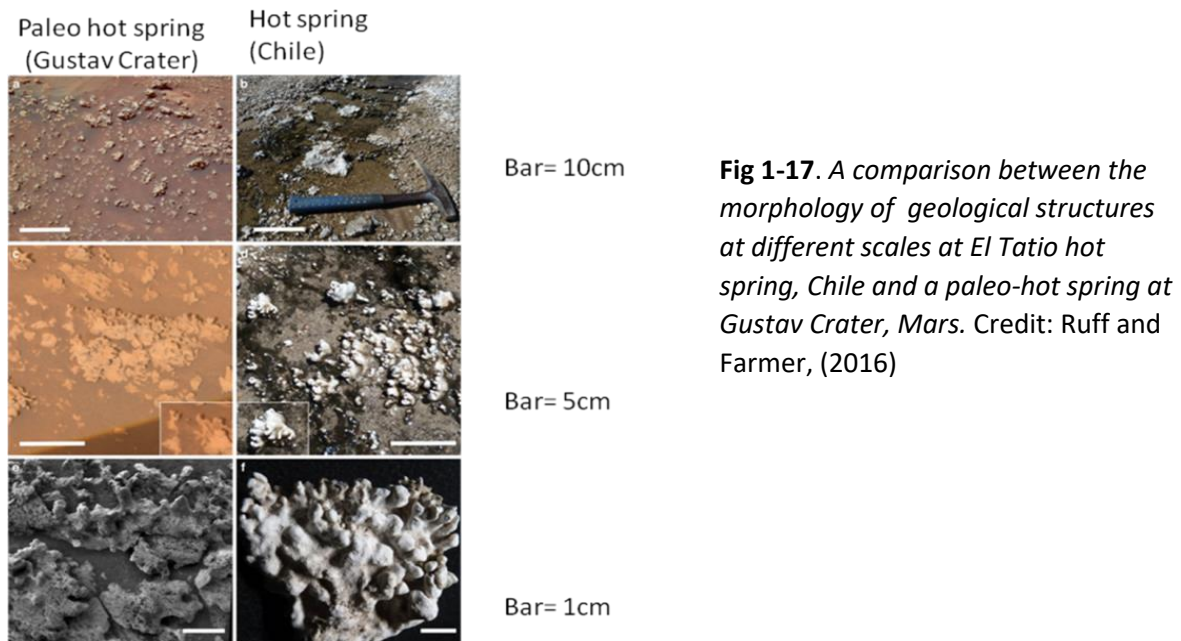
1.9.0 The Relevance and Importance of Studying Mars Analogues

The ejection of geological material from the surface by large meteorites striking Mars results in fragments of the Martian crust to travel through space, then fall to the Earth as meteorites (Nyquist, 2001). Thus, there are no pristine Martian meteorite samples that exist. Although these specimens have been a repository of information regarding the condition of the composition of Martian crust, they remain rare. Furthermore, the conditions they experienced during their journey to Earth and the potential for contamination during their time on the ground is great, which therefore adds unknown parameters to any experimental data from such samples.

The presence of an extant biosphere beneath the Martian cryosphere is plausible (see section 1.4.1). However, the *in-situ* access to the deep subsurface of other planets is not possible presently, and the expense, complexity and technical challenges in the forthcoming astrobiological exploration of Mars, are faced. These challenges require careful long-term planning decades before the mission's successful outcome. During the planning stage, the optimal analytical approaches for the detection of fossil Martian life needs to be considered, without the benefit of genuine Martian samples. Therefore, materials that are analogous to

those that may be found on Mars have been used to test experimental and analytical approaches. For instance, this current study has utilised sub-oceanic basalt to mimic the composition of the basalt, which is the ubiquitous primary rock type on Mars (Marlow et al., 2008).

Seventy per cent of the Earth's crust is comprised of basalt, and it is a common rock throughout the solar system (McBride and Gilmour, 2004). Consequently, it represents an abundant rock type that endolithic life might exploit (Allen et al., 1981). Thus, analysis of organic material for molecular biosignatures in telluric geological samples represents an analogue for the extra-terrestrial rocks that may be encountered in planetary exploration (Sephton and Botta, 2007; Cady and Noffke, 2009).

1.9.1 Endolithic Microorganisms

In addition to macroscopic and cell-like fossil structures, the ichnofossils that are produced by endolithic microorganisms are also thought to be potential targets for detecting fossilised Martian life (Allen et al., 1981; Izawa et al., 2010). Rocks are weathered by interactions with the environment, through the action of chemical, thermal or mechanical processes, which can result in textural changes and features within the rock. However, rock weathering can also have a microbial component (Berthelin,1988). Endolithic organisms are those that colonise the interiors of rock, and these are candidates for the types of organisms that retreated into the geosphere as the Martian surface climate became progressively hostile to life. There are three sub-classes of these organisms: 1. Chasmoendoliths that colonise fissures and cracks; 2. Cryptoendoliths that colonise cavities and fissures within porous rocks and 3. Endoliths that actively bore into the interior of rocks forming cavities and tunnels, which may often result in characteristic textural features in the rock. These features, therefore, are considered to be indicative of microbial activity (McLoughlin et al., 2007; McLoughlin et al., 2010; Wacey et al., 2014).

1.9.2 Structures in Rock Glasses That May Be Indicative of Biological Activity

Microbially induced weathering can occur in any rock, however, microbially induced weathering (or alteration) textures are most readily observed in the relatively transparent vitric shards in basalts of the oceanic plates, ophiolites and greenstones, which are found in

many locations across the Earth (Staudigel, 2006; Staudigel et al., 2008; Staudigel and Clague, 2010; Staudigel et al., 2014). Furthermore, vitric shards have also been suggested to be present on the surface of Mars as tektites, which form from the rapid cooling of debris ejected during meteorite impacts (Cannon and Mustard, 2015).

The alteration texture morphology occurs either as a granular form or as a scarcer micro-tubular form (Fisk et al., 1998; Alt and Mata, 2000; Etienne and Dupont, 2002; Banerjee and Muehlenbachs, 2003; Smits 2006b; Cockell et al., 2009; Smits, 2013). These structures are described as 'bioalteration' textures or ichnofossils in the literature, due to the proposed biological origin. (Fisk et al., 1998; Alt and Mata, 2000; Etienne and Dupont, 2002; Banerjee and Muehlenbachs, 2003). However, these are referred to as alteration textures in this thesis, as no presumption is made here regarding the biological or the non-biological origin of these features.

Alteration textures with a granular morphology, are typically formed from clusters of ca.2 μm diameter spheres, which have been suggested as being the result of an etching by bacteria (Staudigel et al., 2008). These features principally consist of 1 μm diameter spheres, that are suggestive of fossil coccoid and rod-shaped structures (2.0–3.8 μm, in length) and structures that are equivalent to the size of *Bacillus* bacteria in 3.3–3.5 Ga cherts from the Onverwacht Group, South Africa, have been observed. Therefore, these structures potentially provide the earliest morphological evidence for life in the Archean period on Earth (Westall et al., 2001), making these structures contemporaneous with the late Noachian period on Mars. In contrast, the group that are described as having a microtubular morphological texture, vary from 1.0–5.0 μm in diameter and 20.0 μm to 200.0 μm in length and may be twisted, coiled, and/or branched sometimes with segmentation or crenulations, which have been proposed to be locations where cell division may have occurred.

These structures are contrasted with indisputably abiotic ambient inclusion trails, which have a different morphology. These are usually mechanically formed, when mineral grains are driven through the rock by high-pressure fluids, leaving a hollow tubular trail that may remain empty or be in-filled by a secondary mineral phase or by an opportunistic chasmoendolithic organism. This process results in tubes that are smooth sided and crosscut

or branch with angular cross-sections and curved or twisted paths often with a mineral grain at the end and longitudinal striations (Barghoorn, 1965; McLoughlin et al., 2007).

1.9.3 The Ontong Java Plateau

A particularly distinctive example of tubular alteration textures can be seen in glass shards found in specific horizons in tuff from the Ontong Java Plateau (Fig. 1-18). The main phase of the Ontong Java Plateau was produced 125–120 Ma ago by a flood-basalt eruption of a large mantle plume and was one of the largest lava eruptions on Earth during the past 300 Ma. A secondary phase of lava eruptions occurred 20-40 Ma later (100-80 Ma ago). Most of the plateau was formed underwater and is currently submerged, but the size of the plateau means that it is unable to be subducted. Therefore, a tectonic collision with the Solomon Island Block has caused the uplift of parts of the Ontong Java Plateau (Fitton et al., 2001; Chambers et al., 2002). The exploration of this region by Leg 192 of the Ocean Drilling Program in 2000 (Ocean Drilling Programme, 2005), was conducted. However, the region of the OJP sampled by ODP Leg192 1184A hole formed through a hydroshardic eruption 43 Ma, thus 80-90 Ma after the main phase of OJP construction. This region consists of basaltic tuff containing basaltic glass shards formed from the rapid sub-aerial quenching of basalt. These shards are embedded in a volcanishardic matrix of lapilli sized grains, which accreted on the sea floor (Thordarson, 2004; Ocean Drilling programme, 2005).

Fig 1-18. *Position of the Ontong Java Plateau.* **Credit:** *www.volcanodiscovery.com/ontong-java-plateau.html*

The eastern sea lobe of the OJP is constructed from tuff, rather than the flood basalt that is typical of the main sequence (Tarduno et al., 1991; Fitton et al., 2004). The basement unit consists of at least six subunits, five of which are delineated by horizons containing the

visible remnants of woody higher plant material (see Fig 5-1). This observation suggests that a succession of 6-10 sub-aerial volcanishardic events formed this region (Thordarson, 2004). This volcanishardic basement has subsequently been covered by ca. 201 metres of calcareous pelagic ooze, a sedimentary material consisting of diatom shells. It has been suggested this ooze is a repository and source of nutrients for the putative organisms that produced the microtubular features (Banerjee and Muehlenbachs, 2003).

1.9.4 The Ambiguity of The Morphological Evidence for Life

Any morphological evidence alone is rarely sufficient to unequivocally identify life (Ruiz et al., 2002; Cady and Noffke, 2009). The function of the microbial excavation is not clearly understood. While it has been possible to invoke protection from predation or the environment, or the acquisition of essential nutrients, for example, phosphorus. Such behaviour would be energetically expensive, particularly when no known evolutionary advantage can be ascertained (Cockell and Herrera, 2008). Microorganisms have never been directly observed actively excavating these features, either *in vitro* or in the microcosms that have been placed on the seafloor (Einen et al., 2006). Indeed, laboratory experiments have shown that it is possible to etch vitric basalts to produce similar structures using acids, (Fisk et al., 2013) or to physically form tubular structures by the process of alpha-recoil using an alpha particle source (French and Blake, 2016).

Most microfossils are not easily distinguished from many types of geological structures, which can form by abiotic means, so usually cannot be unequivocally said to be biogenic in origin (Ruiz et al., 2002). Thus, both Grotzinger and Rothman (1996) and Hofmann et al. (2007) have suggested that any structures that are older than 3.0×10^9 years are not accepted as biological in origin until the possibility of an abiogenic origin can be eliminated.

1.10.0 The Characterisation of Molecular Biomarkers for The Detection of Extra-Terrestrial Life

Assigning putative morphological micro-structures to a biological origin is challenging, and therefore, other lines of evidence are needed to support the assertion that any particular microscopic or macroscopic structure is the result of biological activity. Thus, detection of molecular biomarkers resulting from geochemically altered chemical remnants that are

unequivocally biological in origin can provide evidence of life (Eglington, 1964; Brocks and Banfield, 2007; Summons et al. 2007) and can be used to support the morphological evidence, particularly if they are spatially associated with the putative fossil structures (Cady et al., 2003; Cady and Noffke, 2009).

The detection of life dating from Earth's Archean period poses a significant challenge (Lowe and Tice, 2007). On Mars, this difficulty is exacerbated, since the possible existence of unknown biochemistry confounds the search for extra-terrestrial molecular biomarkers. These compounds could potentially be confused with complex organic compounds that are formed through unknown biochemistry or by purely abiotic processes (see Chapter 8).

For example, the carbonaceous chondritic meteorites that were produced 4.5 Ga ago, during the formation of the Solar System, possess a range of complex organic compounds such lipids, amino acids and nucleotides that are the basis of Telluric biochemistry (Pizzarello et al., 2006; Pizzarello and Shock, 2010. Sephton, 2002; Sephton and Botta, 2007). These meteorites will have introduced complex organic compounds onto the surface of all the rocky planets of the solar system, including Mars. Indeed, these complex compounds may have provided the basic building blocks for nascent life on Earth (Shock, 2002) and thus potentially on Mars as well.

Summons et al. (2007) catalogues some of the key attributes of molecular biomarkers, which include:

• An excess of a particular enantiomer, e.g. L amino acids and D carbohydrates

• Diastereoisomeric preference

• Structural isomer preference

• Repeating constitutional sub-units or atomic ratios

• Systematic isotopic ordering at molecular and intramolecular levels

• Uneven distribution patterns or clusters (e.g. C-number, concentration, $\delta^{13}C$) of structurally related compounds.

Abiotic reactions involving organic compounds can occur an essentially infinite number of configurations. In contrast, life is bounded by constraints imposed by enzymatic catalysis (Schulze-Makuch, 2008). Enzymes, the catalysts of living systems are highly efficient, but at

the cost of being highly specific, to the extent of being specific to one type of stereoisomer (Berg et al., 2015) or isotope (Schidlowski, 1988; Gilmore and Sephton, 2004). This specificity results in life utilising a restricted set of molecular and isotopic precursors to construct the enormous array of macromolecules that are necessary to construct and maintain themselves. The limited number of monomers that are used to construct the polymeric macromolecules has resulted in a biosignature composed of a highly conservative set of molecular patterns.

The climatic conditions during the Archean period on Earth can provide good analogues for the types of environments that potentially existed during the contemporaneous "warmer and wetter" Noachian Period Mars (Westall et al., 2005). At that time, the Earth's environment was considerably different to the one we observe now, implying that both planets could have hosted comparable habitats for early life forms (Westall et al., 2007). The early-mid Achaean rocks and sediments of Earth have been reported to host molecular biosignatures (Alleon et al., 2016). Tectonic activity did not rework the surface of Mars (see sections 1.3.0 and 1.4.0), so it is at least hypothetically possible for molecular biosignatures to have survived on Mars for 3.5 Ga. However, the previous and contemporary climatic conditions and the geological parameters of Mars are likely to have or had a significant impact on the preservation of these signals. Thus, candidate Martian molecular biosignatures have potentially shared the same destructive fate as other organic compounds on the surface of Mars (see section 1.6.0). Conversely, the cold anoxic and abiotic Martian environment may have provided more suitable conditions for the preservation of organic material, in comparison to the Earth (Kanavarioti and Mancinelli 1990).

However, evaporites and phyllosilicates on Mars have been detected, and these minerals have been demonstrated to be capable of preserving organic material in telluric geological samples (Sephton and Botta, 2007; Griffith et al., 2008). This preservation is accomplished through physical entrapment, in either fluid inclusions within evaporates or within the interlayers of the phyllosilicate sheets through interactions with the electrostatic charges on the mineral surfaces. While this supports the preservation of organic material, this makes

the thermal extraction of organic material from phyllosilicates more challenging (Eigenbrode, personal communication).

1.10.1 The Loss or Alteration of Molecular Biosignatures in the Telluric Environment

Most molecular biosignatures usually provide ambiguous interpretations of an early biosphere, since they originate from unfamiliar biogeochemistry and history. Therefore, given the level of understanding about the climatic history of Mars, it would not be unreasonable to suppose that the detection of life on Mars will present comparable or even greater challenges (Eigenbrode et al., 2007).

Biomolecules are transformed, and information is eroded, first through both biological and then through geochemical processes. This is described as diagenesis, which commences immediately following the demise of the organism. Early diagenesis is the initial process, and it is principally biologically mediated, whereas late diagenesis is a physical and chemical process (Kilops , 2013; Buseck and Beyssac, 2014)

Early diagenesis begins with the rapid re-assimilation of the biomolecules by saprophytic heterotrophs to scavenge both the energy and the nutrients contained within these compounds. In this way, most of the organic compounds, from the organisms are ultimately converted to carbon dioxide (Engel, 2013). Most bio-matter is highly labile, and therefore susceptible to this fate. However, several conditions may confer resistance against degradation, on some of the fractions of the organic material. For example, although interactions with oxidising minerals can have an impact, the main factors controlling the initial decay are a function of the amount of biological activity in the milieu, which in turn is controlled by environmental factors. Such that in areas that are unfavourable to biological activity, the initial rate of degradation is slow (Kilops, 2013). Some compounds, such as lipids, are resistant to microbial degradation and can be preserved (Eigenbrode, 2007). The residue of early diagenesis is composed of molecularly uncharacterised organic matter, consisting of chemically complex compounds relatively resistant to biological degradation (Schnitzer, 1991; Schmidt et al., 2011).

Late diagenesis takes place as the burial depth increases with the associated increase in temperature and pressure. The sedimentary organic substances become dehydrated,

compacted and consolidated as a function of the increasing maturity and depth within the geological strata, which restricts biological activity (Kilops, 2013; Tissot, 1984). Therefore, although thermophilic bacteria can have a modest effect on the composition of the organic material, it is the physically mediated chemical alteration that becomes the dominant factor at depth.

As the thermal energy becomes high enough to break chemical bonds, the organic material undergoes increasing levels of polycondensation and becomes increasingly condensed and insoluble in both organic solvents and acids. Usually, this is due to the loss of superficial hydrophilic functional groups (e.g. OH and COOH) and dehydrogenation reactions. These processes are essentially low-temperature combustion reactions. This loss is a process of thermal maturation called catagenesis, which results in the formation of a complex organic material called kerogen (Tissot and Velt, 1984). This process can result in the formation of molecular fossils, which are characterised by the loss of superficial hydrophilic functional groups, such as –OH and –COOH from the core molecule, e.g. Fig 1-19.
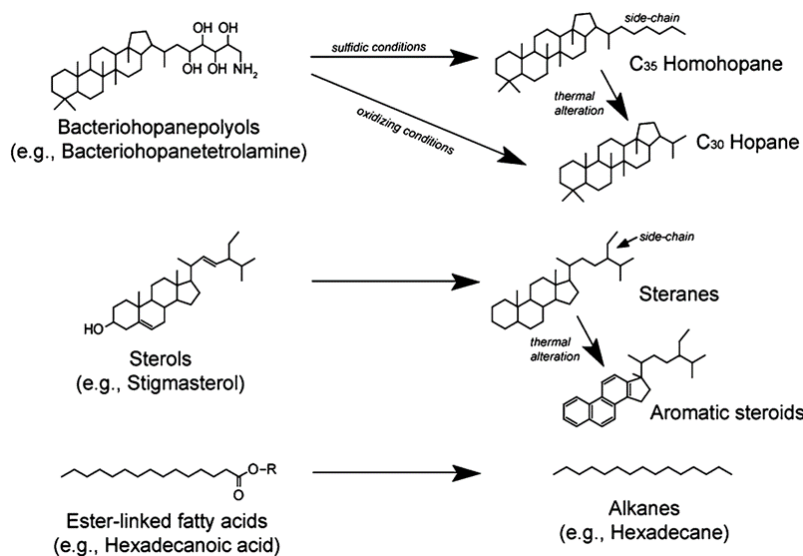
Fig 1-19. *Biolipids commonly found in organisms and their geochemical derivatives (molecular fossils) after diagenesis and thermal alteration. R denotes various polar head groups.* Credit: Eigenbrode (2007).

The chemical composition of kerogen is dependent on both the origin of the initial organic matter and its degree of thermal alteration. Such material is essentially an amorphous carbon skeleton, and due to its resistance to standard analytical approaches the process is

characterised poorly, and the heterogeneous structure of kerogens (See Fig 1-19) reflect their assorted environmental sources as well as post-depositional processing.

The van Krevelen diagram (See Fig 1-20) illustrates that throughout the geochemical processing stage, there is an increase in the C:O ratio. In contrast, the hydrogen levels remain constant for most of the early geochemical stage, but then the C:H begins to increase in the later stages of diagenesis. This loss of hydrogen is the result of the increasing aromatisation of the organic compounds. A progressive increase in the C:H and C:O ratio resulting from increases in aromaticity, characterises the continued maturation process. As the maturation process continues, the aromatic rings cluster and fuse to form multi-ring polyaromatic structures. Ultimately, this reprocessing yields amorphous carbon that is partly towards the structure of graphite which is the most thermodynamically stable form of carbon under surface conditions (Bernard and Papineau, 2014; Buseck and Beyssac, 2014).
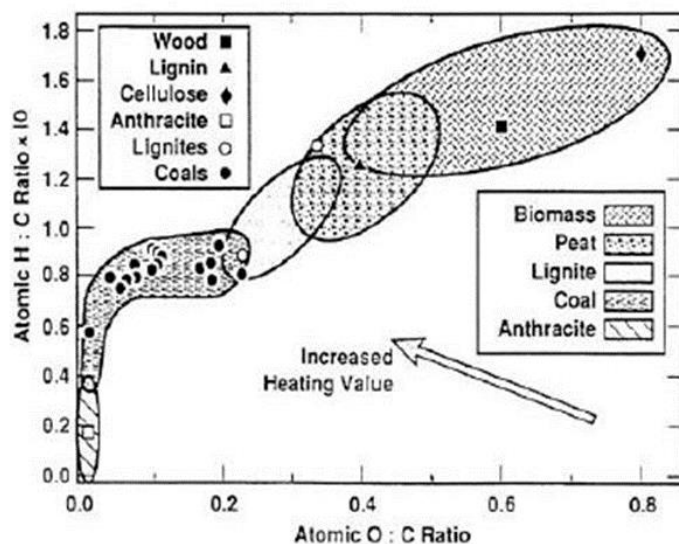
Fig: 1-20. *A Van Krevelen diagram, showing the generic geological processing of biological material indicating the three main types of organic matter (type I for hydrogen-rich kerogen deposited in lacustrine anoxic environments, type II for oil-prone kerogen of marine shales, type IIIC for kerogen derived from higher plants in tertiary and quaternary coals and related shales).* Credit: Killops (2013).

It is this reprocessing of organic material, as described above, leads to the progressive destruction of organic compounds, and the subsequent loss of the entrained information

within the molecular biosignatures over time (Bernard, 2014). Therefore, the great antiquity of the earliest fossils, on Earth, confound the identification of genuine molecular fossils. A further confounding effect of increasing fossil age is the greater potential for partially preserved biosignatures from younger strata to be carried into the location of the fossil. For example, by fluid migration in high permeability sediments, e.g. (French et al., 2015). Over time the molecular information in organic material is progressively degraded, differences in carbon stable isotopic ratios, which would be resistant to the extensive biological degradation and geophysical (e.g. thermal and baric) repossessing can preserve evidence of biological processing.

1.10.2 The Fate of Molecular Biosignatures in the Geosphere

The preservation of isotopic, elemental, and molecular biosignatures is possible when molecular fossils are chemically bound or occluded in the kerogen matrix and where the biomolecules are resistant to the remineralisation process, and this can occur at the monomer, polymer or supramolecular scales. Consequently, some compounds are more resistant to microbial and thermal degradation and have the potential to be selectively preserved (Mayer, 2004).

While it is possible in some specific circumstances for fragments of biopolymers to be preserved, e.g. Griffith et al. (2008), the majority of the degradation-resistant molecules is derived from lipids of cell membranes (Peters, 2005), where the hydrocarbon backbone of lipids, potentially permits a high level of preservation. Thus, the lipids that constitute the cell membranes and the multi-ring compounds, such as sterols and hopanols can be preserved in the fossil record, and indeed can be used to provide taxonomic information regarding the organisms that produced them (Farrimond et al., 2004; Cook et al., 2008).

One of the most chemically and thermally stable structural biopolymers is chitin, which is a chain of N-acetyl-D-glucosamine $(C_8H_{13}O_5N)_n$. Where n is the number of monomers. Chitin is the key component of many structural polymers and is utilised by a diverse range of organisms, transcending kingdom boundaries. For instance, the cell walls of fungi, the exoskeletons of insects and arthropods (e.g. scorpions, crabs, and shrimps), the radulae of molluscs, and the beaks of cephalopods, such as squid and octopuses, as well as freshwater

and marine sponges consist of chitin. The preservation of this material in the geological record is good. The detection of molecular signatures of chitin has been reported in a (310 Ma) scorpion cuticle (417 Ma) and a Silurian *Eurypterid* (Cody et al., 2011). Oldest of all, the presence of preserved chitin has been reported in 505 Ma fossil sponges (*Vauxia gracilenta*) from the Burgess Shale (Ehrlich et al., 2013), suggesting that given the correct preservation conditions, fossils may retain some of their molecular as well as structural, and isotopic, information for at least 505 Ma.

1.11.0 Methods for Detecting Organic Compounds in Geological Samples

A major advantage in the detection of candidate morphological biosignatures, on both Earth and Mars, is that the procedure does not require highly complex apparatus. Detection can be carried out rapidly, by simple visual inspection either by eye or using cameras, which are instruments that are easily re-purposed for this application, from other tasks. In contrast, the instruments used for the detection of molecular biosignatures are relatively complex and bulky.

1.11.1 Gas Chromatography/Mass Spectrometry

To date, the detection and elucidation of organic compounds in the robotic exploration of the solar system have relied mainly on gas chromatography (GC) coupled with a mass spectrometer (MS). The development of gas chromatography, coupled to mass spectroscopy, took place in the 1950s (James and Martin, 1952). However, increased computing power, concurrent with a decrease in the cost of electronics, permitted improvements that have resulted in the widespread deployment of these instruments in analytical laboratories.

During the operation of GC/MS, organic compounds pass through a capillary column driven by an inert carrier gas, typically helium and individual compounds are separated by the interactions with the column's stationary phase, according to the selected properties of the stationary phase material and the properties of the organic compounds. For example, chromatography based on the interactions between ions, or based on the path length through the stationary phase, which is dependent on the size of the organic compound. The eluted compounds pass through an electron beam that ionises the molecules. The energy

73

imparted to the molecular ion, usually fragments it, producing further smaller ions with characteristic masses and relative abundances. Four charged rods called quadrupoles accelerate the ions to separate them. In this way, the ions with different mass-to-charge ratios will reach the detector at different times, permitting the selection of ions with a specific mass to charge ratios (*m/z*). A range of *m/z* values can then be obtained by continuously varying the applied voltage to the quadrupoles. The masses detected can then be compared to a library of m/z ratios to identify the molecular structure. Conventionally, a single ionisation event occurs. Therefore, the charge equals -1 and therefore, usually the mass to charge ratio (m/z) equals the mass of the fragment, and this thesis uses this convention. Furthermore, the intensity on the y-axis is a representation of numbers of ions that are detected, and this intensity is proportional to the amount of analyte, and therefore GC/MS is a quantitative technique based on an integration of the peak area. Relative response to ionisation for a given compound (relative response factor) is factored into this calculation, and a calibration using an internal standard with a known concentration is required, to account for slight variations in experimental conditions.

GC/MS instruments are highly sensitive, with quoted limits of detection of organic compounds of a few ppb, depending on the compounds (Anderson, 1972; Navarro-Gonzalez, 2006 also see section 8.1.3). GC/MS can provide diagnostic mass spectral fractionation patterns of organic matter components and can distinguish isotopes, enantiomers and stereoisomers. Since this is a mature technology, with instruments that can detect and elucidate a wide range of organic compounds, and accurately differentiate isotopic information, and are amenable to miniaturisation. Therefore, they are considered the ideal instrument for a wide range of analytical applications.

GC/MS has been the preferred instrument on earlier planetary exploration missions (Johnson, 2011). Importantly, GC/MS meets the requirements of robustness and simplicity of handling necessary for planetary exploration missions. For example, GC/MS was on the 1976 Viking landers (Anderson, 1972; Klein, 1978) and both the Venera 11 and 12 and Pioneer Venus used GC/MS to analyse the atmosphere of Venus (Krasnopolsky and Parshev, 1981). The Huygens probe of the Cassini-Huygens mission landed a GC/MS on Titan in 2006 (Niemann et al., 2005) and the Rosetta mission analysed material in the comet

67P/Churyumov-Gerasimenko in 2014 (Thiemann and Meierhenrich, 2001). The Curiosity rover that landed on Mars in 2012 also has on board a sophisticated GC/MS, as a part of the Surface Analysis on Mars (SAM) instrument package that can be used to analyse both soil and atmospheric samples (Cabane et al., 2004; Mahaffy, 2008).

1.11.2 Pyrolysis and Thermal Volatilisation

The maximum molecular weight that can be analysed by GC/MS is limited to less than 1200 u and is usually limited a maximum of ca. 700 u, depending on the instrument used. Additionally, before analysis, organic compounds must be mobilised to separate the organic material from the host matrix and to be carried to the mobile phase of the chromatograph (Kitson et al., 1996). This mobilisation can be achieved by using either a solvent or by conducting thermal extraction. The literature occasionally uses thermal volatilisation interchangeably with the term pyrolysis, to refer to this thermal extraction. However, thermal volatilisation (TV) is the process where organic matter is moved from the solid to the gaseous phase and is desorbed from the host rock. In contrast, pyrolysis is a process in which bond cleavage or a molecular scission mechanism is induced by thermal energy in a non-oxidizing environment, such as vacuum, or in the presence of an inert gas such as helium (Hartgers et al.,1991; Moldoveanu, 1998). Generally, when dealing with organic geochemistry, thermal desorption occurs at temperatures <450 ˚C and pyrolysis occurs at temperatures > 450 ˚C (Marbot, 1998; Donahoe, personal communication).

The level of pyrolysis is dependent on the strength of specific bonds within the molecule and the thermal energy input. Thus, higher temperatures yield greater levels of bond cleavage for a given exposure time. Therefore, there is an optimum temperature that is sufficient to desorb and fragment compounds of interest, but without achieving the same levels of bond cleavage that would degrade the molecular information (Marbot, 1998). The robust simplicity and ease of handling means that pyrolysis and thermal volatility (TV), has been, and may continue to be, used to extract the organic component from the inorganic source material for GC/MS analysis, in planetary exploration.

1.11.3 Thermal Hydrolysis and Methylation

The presence of chemical reagents during pyrolysis can increase the efficiency of detecting organic compounds, using GC/MS (Kitson et al., 1996). Many of the organic compounds that are candidate biomarkers are often thermally labile, and they will consequently decompose at temperatures lower than those that permit them to be successfully thermally extracted. Several chemical derivatisation pre-treatments can be used to mitigate this (Cabane, 2001). However, most derivatisation processes require resources that are not available for *in situ* planetary exploration. Consequently, two simple single-step reactions that are suitable for space-based experiments have been selected to be carried on SAM instrument package on board the Curiosity rover to determine the presence of amino acids and carboxylic acids on the surface of Mars.

Two of the 72 SAM sample cuvettes contain tetramethylammonium hydroxide (TMAH) (Salport et al., 2012). This compound is a chemolytic reagent which assists thermal hydrolysis and induces methylation. It allows both an efficient thermal cleavage of polar bonds, which results in increased volatility, which permits lower temperatures to be used to desorb thermally labile compounds from an inorganic matrix. This desorption allows greater access to larger biomolecules that conventional py-GC/MS might otherwise miss. The reagent also methylates COOH, OH and NH_2 groups (Geffroy-Rodier et al., 2009). The reaction which shows the conversion of polar compounds into non-polar compounds that permit their transit through the GC column, for detection by MS (Fig.1-21).

This technique was applied to the analysis of two Martian analogues to validate the technique. Here the molecular biosignatures of microbial and higher plants origin such as lipids (n-alkenes, fatty acids) and carbohydrates were detected in Atacama Desert samples (Buch et al., 2006)
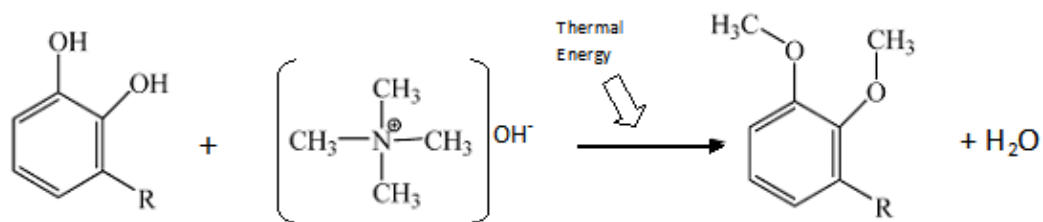
Fig. 1-21: *The reaction pathway for TMAH with a hydroxyl-group bearing organic compounds, e.g. catechol Credit: Kitson* et al.*, (1998)*

1.11.4 X-ray Photoelectron Spectroscopy

GC/MS is described as a 'bulk' analytical technique, since it measures all of the material that is capable of being extracted, in a given volume of the sample. In contrast, in surface analytical techniques, the analysis can be conducted on specific regions, and therefore spatial as well as compositional information may be acquired. Since this direct measurement does not require an extraction step, surface analytical techniques can be used to analyse the insoluble and refractory polymeric, high molecular weight organic materials usually described as 'kerogen', which is the product of diagenetic processes (see 1.8.7).

One such surface analytical technique is X-ray Photoelectron Spectroscopy (XPS) (Beamson and Briggs, 1992; Chastain and King, 1995; Watts and Wolstenholme, 2003; Fairley, 2009). XPS irradiates the surface of a sample with a monochromatic X-ray, which can penetrate several μm into the sample surface, the X-rays cause electrons to be emitted from the surface (1-10 nm) of the sample, depending upon its elemental composition. The numbers and kinetic energies of the emitted electrons are dependent on the configuration of the core electrons of the parent atoms (see Fig 1-22). The energy of the photons with a known wavelength can be calculated using plank's equation:

$E = h\nu$

Where

E= energy

h= Planck constant

v= frequency
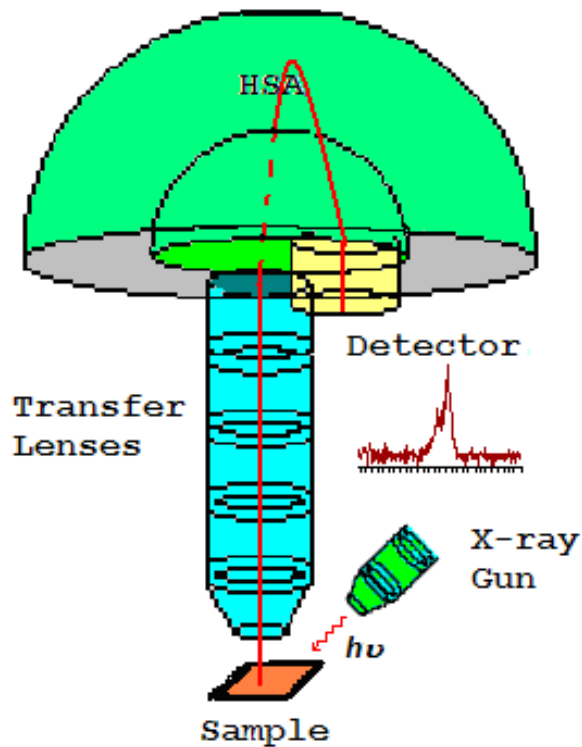
Fig 1-22. *diagrammatic representation of XPS analysis with schematic of XPS operation. Adapted from Fairley, 2009*
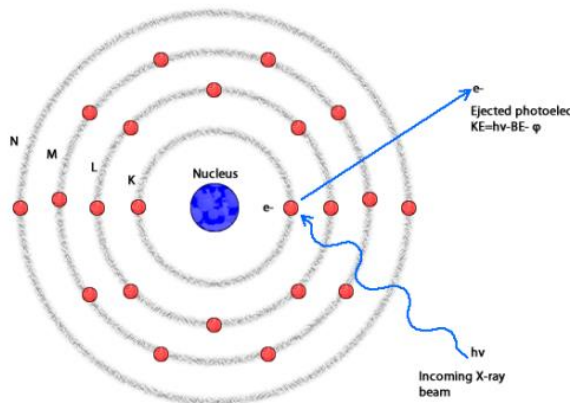
XPS uses the photon energy (E_{photon}) of the X-rays emitted from the K alpha shell of aluminium which is = 1486.7 eV., i.e. the X-ray emission resulting from an electron transition to the innermost "K" shell from a 2p orbital of the second or "L" shell of aluminium. The photonic energy causes the emission of core electrons from the target surface. The energy required to immediately emit an electron to a point above a solid state surface in a vacuum is called the photoelectric work function. Since the kinetic energies of the emitted electrons are measured by a detector ($E_{kinetic}$), the electron binding energy ($E_{binding}$), which can be

thought of as analogous to the ionisation energy and can be calculated by using equation (1).

$$E_{binding} = E_{photon} - (E_{kinetic} + \varphi) \tag{1}$$

Where

E = Energy

φ = work function

The core level electrons in solid-state atoms are quantised. Therefore, the resulting binding energy spectra produce peaks that are characteristic of the electronic structure for those atoms, which are dependent upon the electronic configuration of the original element. The electrons from all elements can be detected (except for hydrogen, which does not have core electrons) with the proviso that they are in a solid state (Fairley, 2009) since XPS requires an ultra-high vacuum to allow the free movement of the photoelectrons. However, in practice, a single core electron has an overriding emission energy, that produces a dominant peak, referred to as the 'major' peaks (Fairley, 2009). The major peak for carbon is the electron in the 1s position, which is detected at 285 eV, and for nitrogen, it is the 1s position, which is detected at 400.4 eV. Therefore, the measurements of carbon and nitrogen using XPS in this thesis, refer to these major peaks.

The work function term (φ) is an adjustable instrumental correction factor (also called a Schofield correction factor) that accounts for the few eV of kinetic energy given up by the photoelectron as it becomes absorbed by the instrument's detector. In practice, this constant is consistent, and so adjustments to are rarely needed to be carried out.

A typical XPS spectrum can be plotted based on both the number of electrons detected as counts per unit time (this thesis used counts per second; Y-axis, ordinate) versus the binding energy of the electrons detected (X-axis, abscissa). The number of detected electrons for each of the characteristic peaks is directly related to the surface concentration of the element within the XPS sampling volume, and in this way, it can provide quantitative information. Each raw XPS signal must be corrected by dividing its signal intensity (number of electrons detected) by a "relative sensitivity factor" (RSF) and normalised over all of the

elements detected, to generate atomic percentage values. Since hydrogen is not detected, these atomic percentages exclude hydrogen.

The peak position provides an unambiguous measurement of the elements, in the surface of the sample, but additional information can be obtained regarding the bonding environment of the parent atom, resulting from a shift in the position of the peak. The binding energies of electrons alter if they are shared by another atom, in a covalent or ionic bond. These shifts can provide information about such things as the chemistry of the sample or its oxidation state (Chastain and King, 1995; Fairley, 2009). The shifts are illustrated in Fig 1-23, showing the peak positions of different carbon compounds in an XPS high-resolution carbon spectrum.
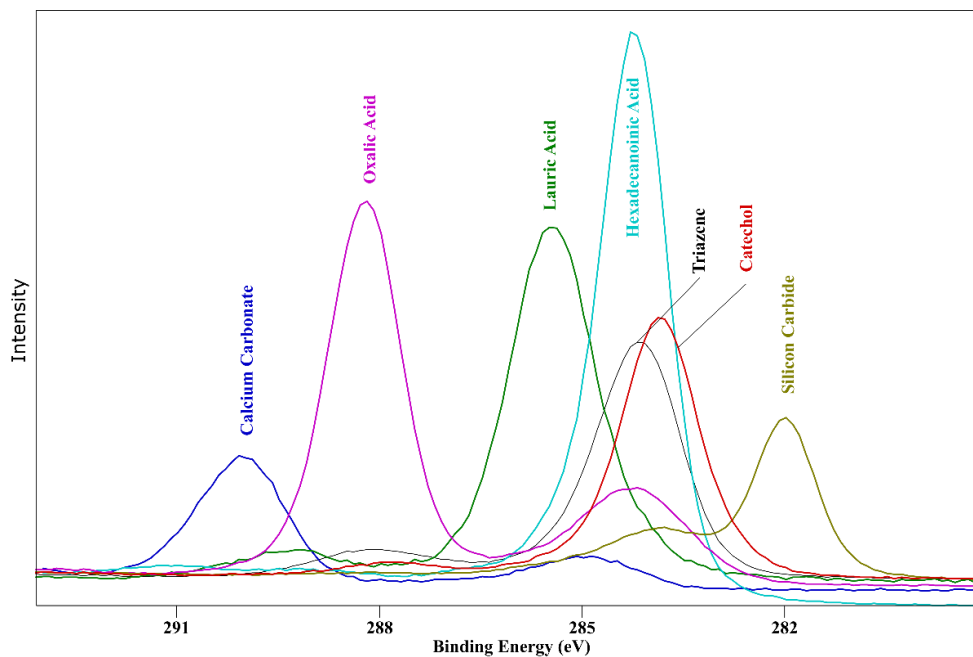
Fig 1-23. *High-resolution XPS spectra of different carbon compounds these values are consistent with online databases (srdata.nist.gov/xps/; www.lasurface.com) Fig 1-23 represented from* Purvis et al., in press. *CPS= counts per second.*

1.11.5 Time-of-Flight Secondary Ion Mass Spectrometry (TOF-SIMS)

Time-of-flight secondary ion mass spectrometry (ToF-SIMS) is also a surface analysis technique, that is designed to analyse the composition and spatial distribution of molecules and chemical structures (Vickerman and Briggs, 2013; Sjovall et al., 2008; Thiel and Sjovall, 2011; Fearn, 2015). This technique has detection limits that are comparable to GC/MS

analysis, with elemental detection limits ranging from ppm to ppb. The surface of samples is bombarded with ions (primary beam), causing the removal of particles from atomic monolayers on the surface (secondary ions) (Beamson and Briggs, 2004; Fairley 2009). These particles are accelerated into a "flight tube", and by measuring the time of flight required to reach the detector, the mass can be determined (see Fig 1-24).
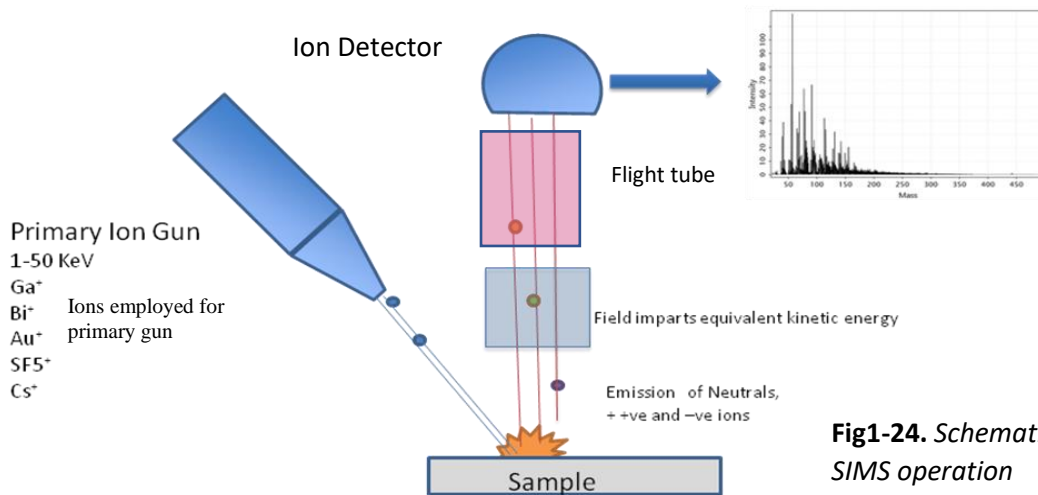
Fig1-24. *Schematic of ToF SIMS operation*

The primary ions are a focused into a 0.1–20 keV primary beam, which is rastered over an analysis spot, the primary ions collide with surfaces transferring some of the energy (Stephan, 2001; Stephan 2005; Vickerman and Briggs 2013; Fearn, 2015).

The impact energy induces the ejection of secondary particles from the target. This is a process called sputtering. Sputtering produces an assortment of monatomic and polyatomic particles along with electrons and photons, importantly ca. 1% of the secondary particles carry either a negative or a positive charge. These ionised particles can be collimated and accelerated to appropriately high energy in an electromagnetic field.

This acceleration imparts a nearly identical kinetic energy to the ions, and therefore the velocity attained by ions with differing mass must also differ, using the formula (2)

Kinetic energy= ½mass.velocity²   (2)

Thus, the time taken for an ion with a given charge to travel a given distance permits the discrimination of ions of different mass. Therefore, the mass of an ion is proportional to the square of the time taken to travel a fixed distance. So, by measuring the travel time down the flight tube to the ion detector, the mass of the ions can be obtained. The secondary ions are separated according to their mass to charge ratio (m/z) to record the mass spectrum.

In addition to time of flight, there are several other commonly used mass analysers available such as quadrupole, magnetic sector, ion trap and orbitrap, each of which provides different detection ranges in terms of mass and spectral resolution. The measurement creates a mass spectrum that provides information about the molecular and elemental species that are present on the surface. All the elements in the periodic table, including H, can generally be detected, and theoretically, there is no upper limit to the size of the mass that can be detected, although in practice ToF SIMS has a mass range of 0-10,000 u. ToF SIMS detects the positive or negative ions of isotopes, and molecular compounds, which include the biopolymers, organic compounds, and amino acids (Stephan, 2001; Stephan 2005; Vickerman and Briggs 2013; Fearn, 2015).

Three types of ion gun produce the primary beams. The choice of the ion species and ion gun respectively depends on the current required (pulsed or continuous), the required beam dimensions of the primary ion beam and on the dimension of the sample. The original liquid metal ion gun (LMIG), uses metals such as gallium which is liquid at 29.2 °C (Vickerman and Briggs, 2013) and this has been further developed by using other metals, where the metal alloys of bismuth or gold were used to reduce the melting point to room temperature, or slightly above.

The LMIG provides a tightly focused ion beam (<50 nm), with moderate intensity and it can generate short pulsed ion beams, which is suitable for dynamic SIMS. It is therefore commonly restricted to static SIMS instruments. A second source type generates $^{133}Cs^+$ primary ions (Fearn, 2015). Here, depending on the gun design, a fine beam dimension or high current can be obtained, and to date, these are used as the primary sources for 'nano-SIMS'.

A further development of primary ion sources are the ionised gas cluster ion beam (GCIB) guns, which can generate the primary beam (Rabbani et al., 2011). The sources for these

clusters can be oxygen and sulphur hexafluoride, fullerenes or the ions of noble gases such as argon and xenon. The advantage of gas clusters is that equivalent amounts of energy are distributed across multiple ions. Although beam focus is more difficult to achieve, GCIBs have twin advantages: firstly, by inducing less bond scission, which is less damaging to high molecular weight compounds; secondly, there is less intermixing between the surface layers of material and the underlying material. The beam focus in earlier systems has been more difficult with gases, but the high current ion beams have at the time of writing, permitted larger molecular compounds to be detected (Rabbani et al., 2011; Vickerman and Briggs 2013 Angerer et al., 2015).

Secondary ion mass spectrometry is nominally a destructive technique. The two types of SIMS available are static SIMS and dynamic SIMS (Vickerman and Briggs, 2001). These techniques are differentiated by their sputtering intensity, which is a function of the ion dosage delivered to the surface of the sample by the primary ion beam. Static SIMS analysis uses a primary ion dose density of below 10^{12}–10^{13} ions cm^{-2} called the static limit. This concentration minimises the interaction of the primary ion beam with the top layer of atoms or molecules, resulting in the removal of <1% of the surface material. Thus, information is obtained from the top atomic monolayer (or the top surface molecular layer), using the primary beam, in a pulsed mode (Rabbani et al., 2011; Garrison, 2013).

A ToF-SIMS mass spectrum contains a wide range of molecularly specific ion peaks, which, as explained below, permits detailed chemical analysis, and the identification of the specific empirical formula of organic compounds. Hypothetically, the numbers of ions detected with a particular mass should be proportional to the surface concentration of those elements or compounds, in the surface of the sample. However, in practice quantisation is not possible, due to the large variation in ionisation probabilities among different materials (Stephan 2005; Sjovall et al. 2008; Vickerman and Briggs; 2013; Fearn, 2015). Thus, SIMS is generally considered to be a qualitative technique, although quantisation is possible with the use of standards.

The ToF-SIMS technique analyses a sample that is in its solid state. Consequently, the chemical distribution within the sample remains unchanged. The advantage of analysing samples in their solid native state means that along with the chemical information, the

location of the chemistry is measured. Therefore, it is possible to produce ion/chemical maps of the sample in the XY dimension (www.ionoptika.com/products/j105-sims). The advantage of this analytical method is utilised in the investigations in this thesis, since it permits the analysis of specific structural features in the geological samples, of particular interest, to relate the mass spectral information from organic molecules to morphological features that are indicative of fossilised biological activity (Ivarsson et al., 2013a).

ToF SIMS has some drawbacks, for example, the hyphenated analytical instruments, such as gas chromatography/mass spectrometry has a chromatographic pre-step that can separate a mixture of compounds, based upon their retention time (see section1.11.1). This chromatography is capable not only of separating individual compounds, but it also provides an additional means of chromatographically separating particles before analysis.

The chromatographic pre-step is not available for ToF SIMS (Spool, 2004; Theil and Sjovall, 2011). Therefore, two species can have the same nominal mass (for example both Si and C_2H_4 each have an atomic mass unit of 28 u), which would theoretically appear in a single peak. However, in practice they can be distinguished from one another because there is a slight mass shift as atoms enter a bound state because of the relationship between mass and energy (e=mc^2) and the spectral resolution or mass resolving power is described using the formula (3):

M/ΔM   (3)

Where

M = the mass of the species that produces the peak

Δ = the peak width, which is obtained from the full width of the peak at half of the maximum height of the peak (f.w.h.m.)

ToF SIMS has a high spectral resolution with a M/ΔM of 10^3 or 0.001 u. Therefore, it is possible to detect shifts from the nominal masses that are the result of small changes in the ion flight-time, due to their composition (Vickerman and Briggs 2013). For example, organic compounds with different molecular formula may have the same nominal mass, but

fortunately, these are readily distinguished since each additional hydrogen-atom shifts the peak 7.98×10^{-3} u to the right of the nominal mass (towards higher masses) See Figure 1-25
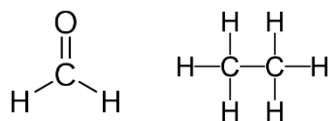
Figure 1-25. *Formaldehyde and propane each have a nominal mass of 30 u but have different flight times, due to the different number of hydrogen atoms in the molecule.*

SIMS spectra are highly complex and contain information about sample composition, isotopic ratios, molecular orientation surface order, chemical bonding and structural information *etc*. High-resolution ToF SIMS imaging can acquire up to 10^6 individual spectra; therefore, the amount of data acquired can be 500 Gb. Consequently, de-convolution to extract any useful information, is a highly intricate process, particularly, given the large sizes of the datasets. However, the spectra are amenable to chemometric analysis. The most frequently used process is principal component analysis (PCA) to extract the variables that contrite the most variation (Vickerman and Briggs, 2013; Spool, 2004).

The ability of SIMS to acquire chemical and isotopic information at high lateral spatial resolutions has made it useful for the analysis of geological and geochemical specimens (Orphan and House 2009). It has been used to localise biomarkers and metabolites within microbial cells, consortia of microorganisms such as biofilms, microbial mats. Additionally, SIMS has been used to map the distribution and function of microbial extracellular polymeric substances in both contemporary and fossilised specimens (Siljestrom et al., 2017).

1.11.6 Argon Gas Cluster Ion Beams

Argon gas clusters ion beams (GCIB) as a primary ion source for ToF SIMS are discussed in section 1.11.5. However, GCIB can serve other roles in surface analysis. XPS and SIMS are capable of obtaining chemical and molecular information, based upon the distributions at high spatial resolutions, laterally across a sample (in the x and y-axes). But the depth of analysis of XPS and ToF SIMS instruments is comparably shallow, in comparison to other analytical techniques. Other instruments, for example, X-ray diffraction measures the

average composition and/or quantity of material throughout a greater depth of analysis. In some investigations, it is advantageous to acquire data that is specific to the surface, however, in many instances, it is essential to obtain data through the depth of the sample, i.e. in the z-axis. The measurement is acquired using an ion gun to remove the surface layer of material by sputter etching. In this process, craters form in the surface material that exposes the layer beneath, which can then undergo analysis. A profile of the composition of the material in the z-axis is produced by repeating this process.

Depth profiling can be carried out using single ions or gas clusters (Barlow et al., 2014; Counsell et al., 2014; Mahoney, 2010; Miyayama et al., 2010; Shard et al. 2012; Shard et al. 2015; Winograd, 2013; Yamada et al., 2001). Conducting depth profile analysis in a single ion mode results in the rapid removal of material. However, all of the energy is contained in a single ion. The high energy results in ion beam induced atomic mixing, by either cascade mixing and/or the recoil implantation of the surface material deeper into the sample. Furthermore, the energy in a single beam splits chemical bonds, and this is a significant problem in the analysis of the high molecular weight organic compounds that comprise molecular biosignatures. In comparison, conducting depth profile analysis using gas cluster ion beams mitigates the problems with using single ion beams, by spreading energy through many ions. The impact crater created by the gas cluster ion beams is shallower than those created by a single ion beam sputter, resulting in a lower the sputter rates and a slower etching process. However, the intermixing of material and bond scission is also significantly reduced (Purvis et al., 2017 and references therein).

CHAPTER 2: METHODS COMMON TO CHAPTERS 3 TO 8

2.1.1 Sample Descriptions and Handling

The samples from the mid-Atlantic ridge, the Costa Rica Flank and Ontong Java Plateau, used in this study (see Table 2-1) were obtained from the Texas repository of the Ocean Drilling Programme (ODP) International Ocean Discovery Program (Texas A&M University, TX, USA, www-odp.tamu.edu/). Solid sections of rock sample were cut from the internal volume of parent samples to remove the outer 5-10 mm of the sample. All sample cutting was carried out on a Buehler Isomet 1000, cutting wheel (Buehler AG, Uzwil, Switzerland), nitrile gloves were worn at all times during sample handling.

Solid rock samples for XPS were trimmed into billets that were ca. 10 mm^2 × 5 mm. These were either placed directly on to the instrument where they were held in place by clips or were immobilised on to a ½ sized microscope slide with 3M double-sided tape, depending on the fragility of the rock sample.

Solid samples were prepared for pyrolysis-GC/MS analysis trimming to remove the exposed surfaces and cut into ca. 100 gram pieces. The large pieces of dolerite from the Whin Sill were powdered in a Tema ring rock pulveriser (Tema Machinery Ltd, Northants. UK), for 30 seconds. Small samples obtained from the Ocean drilling programme (ODP) were powdered by hand using a stainless steel pestle and mortar that had been dry heated to 1000°C in a muffle furnace for 8 hours to remove adventitious carbon. Fragments of powdered samples, with a size of between 50 μm and 150 μm were obtained by initially passing through a 150 μm sieve, then passing through a 50 μm sieve, and reserving the unpassed material. Grinding, sieving and storing in a glass vial were conducted under a fume hood.

All solid samples were held with flamed forceps and stored in glass vials with Al foil cleaned by sonication in dichloromethane under a screw top lid. Trimmed pieces were handled with flamed forceps, before storage in glass vials sealed with Al foil cleaned by sonication for 30 minutes in dichloromethane and allowed to dry and closed under screw top lids. Vials were orientated upright during storage and transport, to prevent these samples inadvertently contacting the foil seals.

Powdered samples were immobilised for XPS analysis by compaction onto an aluminium foil disk using a manual hydraulic press (Specac Ltd. Orpington, London, UK), using 1.5 t.m^2 of pressure. The compaction was necessary because fine rock particles can cause damage to the XPS by being drawn into the vacuum pump. Furthermore, the Al foil helped to mitigate the effects of surface charging on the insulating rock surfaces during XPS analysis.

Identifier	Description	Exp.	Site	Core	Sect.	interval(cm) *	Depth (m.b.s.f.)	Depth into basement (m.)	Glass Shards	Alteration Textures	Location	Ref
OJP_8	Pelagic Ooze	192	1184 A	008 R	04 W	49-51	201.10	-	N/A	N/A	5°0.6653' S 164°13.9771'E	[1,2]
OJP_13	Oceanic tuff	192	1184 A	013 R	03 W	145-148	224.55	23.45	Y	Y	5°0.6653' S 164°13.9771'E	[2,3]
OJP_22	Oceanic tuff	192	1184 A	022 R	03 W	86.5-89	299.99	98.89	Y	N	5°0.6653' S 164°13.9771'E	[1,2,4]
OJP_43	Oceanic tuff	192	1184 A	043 R	03 W	120-122	495.18	294.08	Y	N	5°0.6653' S 164°13.9771'E	[4]
OJP_45	Wood Fragment	192	1184 A	045 R	7	48-65	527.61	326.51	N	N	5°0.6653' S 164°13.9771'E	[4]
CRB	Oceanic Basalt	148	896A	011 R	01 W	111-115	287.10	91.9	Y	Y	1°13.0062'N 83°43.3920'W	[5]
MAB	Oceanic Basalt	46	396B	020 R	4W	36-40	291.36	140.86	Y	Y	22°59.1420'N 43°30.9000'W	[6]
WSD	Terrestrial Dolerite	-	-	-	-	-	0	-	N	N	N55° 28.427' 001 35. 577' W	[7]

Table 2-1. *The geological samples used in the investigation in chapters 3-7, The codes and descriptions of samples from the Ontong Java Plateau and submarine and terrestrial basalts.*

OJP=Ontong Java Plateau; CRB=Costa Rica Basalt; MAB Mid-Atlantic ridge Basalt; WSD Whin Sill Dolerite

Code	Description	Acquired from
At_ 01	Atacama Desert	23° 24' 27.38"S 69° 31' 3.78" W
PD_01	Polar Desert	Ref: 845/240
PD_02	Polar Desert	Ref: 856/123

Table 2-2(a). *The geological samples used in Chapter 8. The codes and descriptions of the near-barren, organic poor, desert samples equivalent to those samples used as Mars Analogues.*

Code	Description	Acquired from
JSC-1	Volcanic palagonite	Orbitec, Inc
Sand	Soxhlet extracted Sand	Sigma Aldrich
Bent	Bentonite clay	Sigma Aldrich

Table 2-2(b). *The codes and descriptions of the samples that served as expendable analogues for the desert samples in table 8-1(a).*

2.3.1 Protocol for Decontamination by Gas Cluster Ion Beam Etching

To decontaminate the samples for XPS and ToF SIMS analysis, argon gas cluster ion beam (GCIB) etching was conducted for 90 seconds at 4 keV over a 1.5 mm x 1.5 mm raster area, within the XPS instrument, according to (Purvis et al, 2017), using the protocol adapted from Barlow et al (2014).

The GCIB source was a Thermo Scientific[tm] MAGCIS[tm] gun (Thermo-Fisher Scientific Inc., Waltham, MA, United States) mounted within the XPS instrument. The GCIB was operated at 4 keV generating a broad, semi-log distribution of argon cluster sizes centred on 1000 atoms per cluster at an input pressure of 4 bar. Neutral atoms are not expected to escape from the MAGCIS[tm] due to a 2° bend in the ion optics. Furthermore, argon clusters with multiple charges were not expected to be stable enough to emerge from the source. The beam current was stable around 20 nA ±2 nA (as measured at the sample plate within the instrument). An ion beam raster of 1 mm x 2 mm was used, and an X-ray spot size of 200 x 400 μm, providing a gap of 0.4 mm and 0.8 mm between the perimeter of the GCIB etch area and the perimeter of the XPS analysis, i.e. within the area of the sputter crater. The samples were immediately analysed without removal from the XPS instrument.

2.3.2 Protocol for Decontamination using Ultra-violet Ozone Cleaning

The samples required for bulk analysis, e.g. gas chromatography/mass spectrometry, were decontaminated using UV/O_3. Three trimmed pieces of the samples were cleaned using UV/O_3 using a Jelight-144AX UV/O cleaner[tm] (Jelight Co Inc., Irvine, CA, United States) for 20 minutes; adapted from the UV/O_3 cleaning protocol reported by Cumpson and Sano (2013). Decontamination was evaluated with XPS, carbon combustion and py-GC/MS.

2.4.1 Protocol for the analysis of geological samples using X-ray photoelectron spectroscopy

XPS analysis was conducted using a Thermo Scientific K-alpha X-ray photoelectron spectrometer[tm] (Thermo Scientific, East Grinstead, UK). Two types of scans are used, survey and high-resolution scans. Survey spectra (broad energy, multiple elements), sometimes called wide scans were used to obtain the elemental data obtained with scans between -5.0

eV and 1350.0 eV; a dwell time of 50 milliseconds, a step size of 1.0 eV and a pass energy of 200.0 eV. In contrast, chemical state information on a single element was obtained with a high-resolution (narrow energy) scan. The spectra were collected at 40 eV pass energy with a 0.1 eV step size. Spectra were acquired using a monochromatic Al Kα X-ray source with an output energy of 1486.6 eV with a maximum X-ray beam spot size of 40 μm. A low energy dual-beam electron/ion flood gun operated at 40 eV was used for surface charge compensation on both survey and high-resolution scans. Any necessary charge correction was carried out for each new data acquisition using the Na1s binding energy peak position at 1070.5 eV in the survey spectra as the reference standard.

Spectral analysis was carried out using CasaXPS software (Teignmouth, UK), with major peaks selected for element identification using the Handbook of X-ray Photoelectron Spectroscopy (Chastain and King, 1995). Scofield atomic sensitivity factors and Shirley background deduction were used to measure the relative concentrations of elements and were expressed as an atomic per cent (at %).

The high-resolution spectra resulting from analysis spots were normalised and summed, then synthetic component fitting was conducted. The fitting was conducted using best-fit envelopes, and the chemical states were identified using CasaXPS software. The chemical state identities of the components were obtained using the NIST databases (www.srdata.nist.gov/xps), La surface (www.lasurface.com) and Beamson and Briggs, (1992). The relative concentrations of the chemical bonds expressed as per cent values were obtained from the areas of the synthetic components.

2.4.2 Protocol for the Operation of Gas Chromatography/Mass Spectrometry Instrument

Samples were weighed (ca. 10 mg) into clean quartz pyrolysis tubes then plugged with extracted silica wool. Conventional flash pyrolysis gas chromatography/mass spectrometry (py-GC/MS) was conducted using a pulsed-mode open pyrolysis system, using a CDS 1000 pyroprobe unit (CDS Analytical, USA) fitted with a platinum coil and a CDS 1500 valved interface operated at 320 °C. This apparatus was connected to a Hewlett-Packard 6890GC split injector (320°C) linked to a Hewlett-Packard 5973MSD (electron voltage 70eV, filament current 220uA, source temperature 230 °C, quadrupole temperature 150 °C, multiplier

voltage 2200 V., interface temperature 320 °C).THM was carried out at the experiment temperatures described in the results section for 10 s (20 °C.ms^{-1} temperature ramp). The pyroprobe interface was maintained at 320 °C with the products passing into an HP6890 gas chromatograph (GC) with a 60 m HP-5MS column (0.25 mm internal diameter, 0.25 um film thickness; J and W Scientific, USA). A helium carrier gas at a flow rate of 1 mL.min^{-1}. The GC was held at 50 °C for 1 minute, was used, and then the temperature was ramped from 50°C to310 °C at 5 °C min^{-1} and held at final temperature for 15 minutes, for a total time of 65 minutes. Product detection was carried out using an HP5972 series mass selective detector in full scan mode (50-650 u). The data acquisition was controlled by an HP kayak xa ChemStation computer. Peak identification and analysis of mass spectra were conducted using OpenChrom® (www.openchrom.net) open source software, using first derivative peak detection set to a 'high' threshold and a signal/noise ratio of 5.0.

The most intense ions were obtained from the mass spectrum ion list, and the compounds were identified using the National Institute of Standards and Technology 2005 (NIST05) mass spectra library (Stein, 1994; Stein, 2008), from each of the peaks that were identified with Openchrom® peak detector. However, it was found that the most intense ions were sufficient to obtain an accurate peak assignment from the NIST05 library. The Openchrom package provided a match of 0 to 1.0, between the compounds that were detected and the compounds in the library, with 1.0 equalling a complete match. All matches less than fair (<0.65) were discarded.

The thermal hydrolysis and methylation (THM) experimental protocol was identical in all respects to the py-GC/MS protocol, described above, and was adapted from Robertson et al. (2008), with the following exception: 2μl of 25%^{v}/v TMAH (Sigma-Aldrich) in distilled water, was added immediately prior to pyrolysis. Any internal standards used 2μl of 1uM androstane, which was added to immediately before the analysis.

2.4.3 Measurement of Total Organic Carbon using Dry Combustion

Total organic carbon (TOC) measurements were obtained by carbon combustion, using a CS230 Carbon/Sulphur Determinator (Leco Corporation, Michigan, u.S.A.) and were conducted in triplicate.

The thermal treatment was used to remove organic material from the geological samples and laboratory hardware, in a muffle furnace set to 1000 ˚C ±50 °C for 8 hours, using the protocol adapted from Eigenbrode (2011). Samples for GC/MS were then milled by hand in either a thermally decontaminated stainless-steel pestle, and mortar or a UV/O$_3$ cleaned agate pestle and mortar.

2.5.1 Protocol for the Visual Identification of Geological Textures using Optical Petrography

Thin sections for optical petrography were prepared by Durham University, Thin Section Services. Optical petrography was used to confirm the presence or absence of tubule alteration textures in each of the samples using a Leica DM2700M microscope in transmitted light mode. Images were captured using a co-axially mounted Leica DFC450C camera.

2.5.2 Protocol for Scanning Electron Microscopy and Energy (X-ray) Dispersive Spectroscopy

Scanning electron microscope (SEM) images of solid samples were obtained using a Hitachi TM3030 (Hitachi UK, Maidenhead, UK). This instrument was co-axially mounded with Bruker Quantax WDS energy (sometimes called X-ray) dispersive spectroscopy (EDS or XDS) instrument, to obtain the distribution of the elemental composition. The geological sample fragments used for SEM were not prepared.

CHAPTER 3: DECONTAMINATION OF GEOLOGICAL SAMPLES BY GAS CLUSTER ION BEAM ETCHING OR ULTRAVIOLET/OZONE.

Abstract

The organic matter within rocks contains chemical and isotopic evidence of its provenance, including information on past and extant life. Such information could further the understanding of life on the early Earth and yield evidence of the existence of past life on Mars. However, the collection of geological samples and its subsequent transfer to analytical facilities possibly via long-term storage provides ample opportunity for organic contamination from a variety of sources before analysis. Erroneous assignment of organic contamination as authentic indigenous organic material is a significant issue in any geological specimen but is exacerbated in rocks containing trace levels. This investigation evaluated two decontamination methods for geological samples, namely, the recently developed gas cluster ion beam etching, which supersedes monoatomic sputter etching, and ultraviolet/ozone cleaning. Decontamination evaluation involved removal of intentionally applied organic contamination applied to basalt, which initially possessed only trace levels of indigenous organic material. Flash pyrolysis-gas chromatography/mass spectrometry and X-ray photoelectron spectroscopy were used to measure contaminant removal. Both techniques are suitable for removing organic contamination during the preparation of geological samples.

3.1.0 Introduction

Analysis of organic matter embedded in rocks can provide information regarding its origins. It is essential that any molecular biosignatures (see section 1.10.1) that are detected in geological samples, are actually indigenous to the host rock in question, and are distinguished from those that were subsequently introduced from non-indigenous natural processes or during sample removal, storage, and preparation for analysis (Brocks and Banfield, 2007; Sherman et al., 2007).

95

Decontamination of acquisition equipment is vital (Eigenbrode et al. 2009), as is the scrupulous decontamination of geological samples, after removal from the environment, for example, during the sampling of sectioned drill cores. Chemicals such as chromic acid or organic solvents are frequently employed to clean geological samples, but these can be hazardous and risk the deposition of adventitious carbonaceous material. When rocks contain only trace levels of indigenous organic matter (<100 ppb), the unintentional addition of organic matter makes a significant contribution to the net organic inventory, which may be erroneously identified as indigenous. Often indigenous organic matter is found in small and precious fossils and meteorites, which require minimally destructive decontamination protocols.

For example, the detection of a trace amount of a hopane lipid biomarker in an investigation of Precambrian rocks was originally thought to be indigenous (Brocks et al., 1999). Although, a subsequent investigation (French et al., 2015), using a more rigorous cleaning protocol for the coring and sectioning equipment, was unable to detect hopanes. It was suggested that the rock cutting equipment, in the original investigation had deposited lubricants containing hopanes on to the surface of the rock sections during the coring and cutting process. This example of contamination illustrates that attempts to avoid the exogenous organic material on rocks by sampling the internal volume can result in the introduction of organic material from the sampling equipment.

Furthermore, a human presence on Mars will inevitably lead to the risk of the forward contamination (i.e. from Earth to Mars) by terrestrial organic material (Rummel, 2001; Mancinelli, 2003; Board, 2006; Rummel, 2006), potentially compromising samples obtained during these missions. Hence, decontamination of Martian rock samples, immediately before *in situ* analysis, should be addressed before a human mission to Mars. Furthermore, solvent or acid-based decontamination protocols may inadvertently add exogenous organic material to the sample or alter the chemical and molecular structure of the organic compounds of interest (McDonnell and Russell, 1999; Penna et al., 2001).

In this chapter, two surface cleaning methods used for the analysis of semiconductors in materials science were tested. Specifically, the recently developed argon gas cluster ion

beam (GCIB) etching, which removes surface contamination more gently than earlier monoatomic etching, and ultraviolet ozone (UV/O$_3$), to decontaminate the surface layers of geological samples contaminated during acquisition and storage.

3.1.1 Whin Sill Dolerite

Whin Sill Dolerite (WSD) contains no vitric shards or identifiable weathering within its internal volume, and since it was readily available. WSD was used extensively in these investigations as a negative control since it contains trace amounts of indigenous organic carbon readily distinguishable from the increased carbon concentrations resulting from intentional contamination.

The Whin Sill is a 295 Ma tholeiitic quartz dolerite intrusion in northern England, (Fitch, 1967; Liss et al., 2004) The WSD is emplaced in Carboniferous strata and was exposed by glacial erosion approximately 17×10^3 years ago (Bateman et al., 2015; Goulty, 2005).

The petrography of the WSD used in this study was described as containing '*fresh labradorite feldspar and purplish brown augite which occurs as broken patches, interstitial grains and long blades. Ilmenite in black, often rectangular grains and quartz in small grains often intergrown with the feldspar are present together with apatite and brownish-green chlorite*' Evens et al., (1962) and this conforms to the standard petrographic description of the average Whin Sill dolerite Thomas (1927). This demonstrated that the mineralogy of the WSD was heterogeneous. Consequently, to obtain a whole rock mineral composition of the WSD, wet-chemistry methods were used (Randall, 1989). This is in contrast to the XPS analysis volume that measured 50µm^2 × 1-10 nm(see section 1.11.3). Therefore, to mimic the whole rock analysis using XPS, 5 × 100-gram pieces of WSD were milled (see section 7.2.1) to homogenise the minerals within the WSD, to create an average composition, and this was measured by XPS. Table 3-1 (over page) compared mineralogy of the whole rock (Randall, 1989) with the elemental analysis of the milled WSD using XPS by using the formula in section 3.3.2.

Mineral	SiO$_2$	TiO$_2$	Al$_2$O$_3$	Fe$_2$O$_3$	FeO	MnO	MgO	CaO	Na$_2$O	K$_2$O
mineral composition (%)[1]	50.5	2.16	13.8	3.46	8.96	0.17	9.55	2.55	2.55	0.77
element:oxygen ratio	1:2	1:2	2:3	2:3	1:1	1:1	1:1	1:1	2:1	2:1
Element	Si	Ti	Al	Fe	Fe	Mn	Mg	Ca	Na	K
Wet chemistry O deducted	16.8	0.7	5.5	1.384	4.48	0.1	4.8	1.3	1.7	0.5
[2]XPS analysis milled	20.1	0.1	5.3	3.8		0.1	5	3.5	0.36	0.1
[2]XPS analysis solid	21.2	0.1	7.9	1.8		0.1	4.2	2.4	1.8	0.1

Table 3-1: *A comparison of the whole rock mineral analysis using wet chemistry (Randall, 1989) with the elemental analysis of milled (homogenised) WSD. Element:oxygen ratio permitted the comparison of mineral composition from [1]Randall (1989) to the elemental composition measured using XPS in this thesis.* surface concertation (at %)

3.1.2 Decontamination with Gas cluster ion beam etching

Monatomic ion beam sputter etching has previously been employed to remove surface contamination from semiconductors physically (e.g. Czanderna, 2012; Taborelli, 2007), and has been applied to a sample of OJP_13, before analysis (Preston 2011). For the monoatomic etching technique, individual high energy ions are propelled up to 20 nm into surfaces, which may force surface material deeper into the sample, thus mixing any adventitious surface contamination with any underlying indigenous organic material of interest. Furthermore, the concentrated energy will break chemical bonds, destroying chemical and molecular information. The damage is problematic for the 1-10 nm and 1 nm analysis depths, encompassed by surface analytical techniques such as X-ray Photoelectron Spectroscopy (XPS) and Time of Flight Secondary Ion Spectroscopy (ToF SIMS) respectively.

The drawbacks with monatomic sputtering have been mitigated by the recently developed argon gas cluster ion beam (GCIB), which creates a beam consisting of clusters of 1000 argon atoms with a single charge, rather than individual argon ions. The energy is thus distributed across all atoms in the cluster, therefore greatly reducing the damage depth created by the atoms in the cluster. Consequently, a crater only a few nm deep in the surface of the sample is created. The depth of the crater is dependent upon several factors such as the cluster size, the impact energy and the composition of the target sample. This process removes material in the predefined area exposed to the gas clusters (Cheng and Winograd, 2006; Cheng et al., 2006; Yamada et al., 2001). Damage to chemical bonds in organic compounds caused by GCIB is minimal, and therefore, the chemical states of the target material are available for analysis (Barlow et al., 2014; Counsell et al., 2014;

Mahoney, 2010; Miyayama et al., 2010; Shard et al. 2012; Shard et al. 2015; Winograd, 2013; Yamada et al., 2001).

3.1.3 Ultraviolet light and ozone (UV/O₃) cleaning

Ultraviolet-ozone (UV/O₃) cleaning, utilises a combination of UV light to photolytically breakdown organic material, and ozone that fully oxidises the breakdown products (Vig, 1985) to decontaminate the entire surface of a sample. UV/O₃ has been used for many cleaning applications (Vig, 1985, Cumpson and Seah 1996) including olivine and feldspar geological samples, albeit without rigorous evaluation (Nugent et al., 1998; Hausrath et al., 2007). In this chapter UV/O₃ decontamination of basalt was evaluated using XPS and pyrolysis-gas chromatography/mass spectrometry (py-GC/MS), an analytical technique, which identifies molecular information in organic compounds from a bulk sample, e.g. (Mason et al., 2009).

3.1.4 Intentional Contamination for Evaluating Decontamination Methods

The strategy adopted in this study was to use WD40, to deliberately contaminate a low indigenous organic carbon geological sample, such as the Whin Sill dolerite. WD40 is a commercially available silicone lubricant, commonly used to clean and lubricate cutting tools, and has previously been employed to evaluate the decontamination of silicon wafers by UV/O cleaning (Cumpson and Sano, 2013). The organic components in WD40 that evaporate at temperatures <100 °C, at atmospheric pressure, will evaporate when they are exposed to the ultra-high vacuum of the XPS instrument analysis chamber, leaving a residue of low volatility high molecular weight organic compounds. So, although WD40 is not a contaminant encountered in standard geological investigations, in chemical terms, its residue represents a particularly difficult contaminant to remove compared to, for example, a pure low molecular weight hydrocarbon. Additionally, the levels of intentional contamination used in this study were more than might be encountered during geological sample preparation and storage. This intentional contamination, therefore, provided a greater challenge for both GCIB etching and UV/O cleaning than would be anticipated in typical investigations acting as a 'worst case scenario'. The decrease in the carbon

concentration, relative to those of the other elements which constitute the parent rock was used to measure the decontamination efficiency.

3.2.0 Methods

3.2.1.Sample Handling and XPS Analysis

Loose ca. 2 x 1 kg pieces of Whin Sill Dolerite (WSD) were obtained from the shoreline at Craster, Northumberland. Grid reference N55° 28.427' 001 35. 577' W (See Table 2-1). These were solid samples and were prepared and stored according to the protocol described in section 2.1.1.

Only XPS survey spectral analysis was conducted on these samples, according to the protocol described in section 2.4.1. High-resolution analysis of the carbon spectra was not required for this chapter. Py-GC/MS analysis was then conducted, using the parameters described in section 2.4.2. The evaluation of the gas cluster ion beam etching decontamination protocol was conducted using the MAGIS® gas cluster gun (see section 2.2.1) and the UV/O_3 cleaning was carried out according to section 2.3.2.

3.2.2 Deliberate Contamination

The geological samples used in this thesis were exposed to the environment for several thousand years, in this case, giving ample opportunity for water and dissolved organic contaminants to penetrate into the surface of rocks (Lassen et al., 1997; Becker et al., 1999). Sectioned rock cores were prepared to mitigate this problem. Accordingly, the outer 5-10 mm environment exposed surface was trimmed from the parent sample, revealing un-weathered internal surfaces of basalt, which were then trimmed to ca. 10 mm x 10 mm x 5 mm pieces, mimicking the acquisition of rock from sectioned core samples.

The faces of Whin Sill Dolerite that were untreated designated Whin Sill Dolerite 'as received' (WSD_AR) were photographed to record which face of the dolerite piece had been intentionally contaminated. A section of absorbent paper was sprayed with WD40, saturating the paper, then a piece of trimmed basalt was lightly pressed onto the paper for 10 seconds. These 'intentionally contaminated' pieces (designated as WSD_IC) were then air dried (10 minutes) and stored in the same way as WSD_AR.

3.3.0 Results

3.3.1 Example of the XPS Survey Spectra used in this Thesis
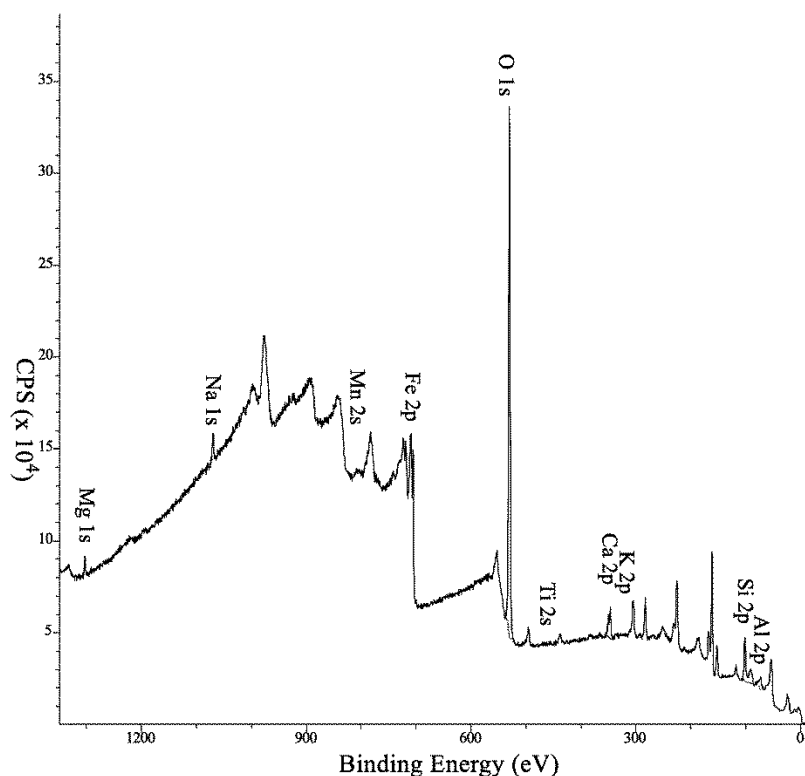
Fig.3-1. *An example of an XPS Survey spectrum of Whin Sill Dolerite with major element peak assignments labelled. Credit: Purvis* et al. *(2017).*

The XPS survey spectra of the Whin Sill Dolerite as received (WSD_AR) and Whin Sill Dolerite deliberately contaminated (WSD_IC) samples consistently showed a series of clearly defined major peaks for O 1s, Si 2p, Al 2p, Mg 2s, Ca 2p, Fe 2p, Mn 2s and Ti 2s, which demonstrated that the XPS measurements were reliable, and the Fig.3-2 provides an example. The specific binding energies for the different electron orbitals of the major elements present in all basalts were identified, e.g. (McBride and Gilmore, 2004) and were consistent with published data for those elements (Chastain and King, 1995) using the CasaXPS software (Fairey, 2009).

3.3.2 XPS Quantitative Analysis Of WSD Inorganic Elemental Composition

Elemental concentrations are derived from XPS spectral intensities. However, experimental setup, such as X-ray beam focus, size of analysis area or any variations in the sample

topography, can cause variations in these intensities. Therefore, spectral intensities must be expressed as relative, rather than absolute values, and are expressed as a proportion of the total element composition in units of atomic percentage (at%; Watts and Wolstenholme, 2003). The CasaXPS software was used to calculate the relative surface concentrations of inorganic elements occurring at concentrations >0.1% in the dolerite samples used in this study.

The comparison between the values measured in this study and the reported values are within one order of magnitude of each other with a Pearson correlation coefficient of 0.96. These were compared to the previously reported elemental concentrations for mid-ocean ridge (MORB), which are normally obtained by electron microprobe and X-ray fluorescence (XRF), and are reported in the literature (Randall, 1989, Mahoney, 1993; McBride and Gilmour, 2004; Fig 3-2). It should be noted that unlike XPS, XRF is unable to obtain carbon and nitrogen measurements.

The analysis described by Randall (1989) provided a quantitative analysis of the mean mineral composition. The data was compared to the XPS data by deducting the contribution made by O_2 to the mineral fraction reported.

e.g. SiO_2 = ⅓ Si and is ⅔ O_2

The reported percentage of SiO_2 in a rock= 50%.

Thus, the elemental fraction was calculated as follows:

Si fraction is ⅓ of 50%, Therefore Si = 16.6 %

This calculation permitted a comparison between the reported mineralogical data, obtained by electron microprobe and elemental data obtained by XPS. The results indicated that the elemental composition of the Whin Sill dolerite, measured by XPS, was comparable to the mean composition measured by electron microprobe and reported by Randall (1989).

While quantitative measurements made by XPS are considered to be precise (Briggs and Seah, 1983), we suggest that the measurements are also accurate. This implies that the surface concentration measurements of carbon and nitrogen are also precise and accurate.

It was essential that changes in the metallic element concentrations, as a result of GCIB sputter etching was assessed, to measure relative changes in the carbon concentration (shown in Fig.3-3a). Accordingly, the metallic element concentrations were measured during sputter etching, and the concentrations of WSD_IC were plotted as a function of etch time (Fig 3-3b inset). This indicated that there was minimal concentration variation of the metallic elements as a function of GCIB etch time, and the sum of the elements occurring at concentrations >1.0 at% (Al, Ca, Fe, Mg Na, and Si) was used as an unvarying standard to evaluate the relative changes in the carbon concentration.
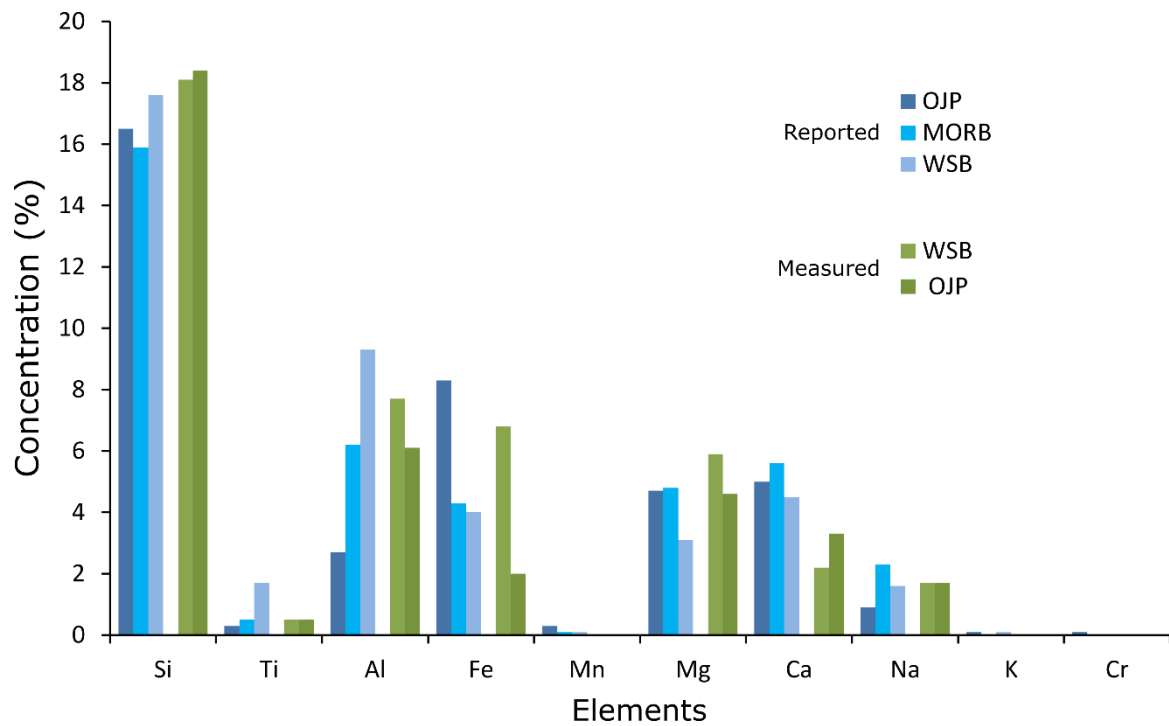
Fig 3-2. *A comparison between the reported concentrations using XRF (Mahoney et al., 1993; McBride and Gilmore, 2004) and the concentration measured in this study using XPS of the elemental used as an unchanging standards reference. OJP=Ontong Java Plateau MORB= mid-ocean ridge basalt WSD = Whin Sill Dolerite. Reported values: OJP (Mahoney et al., 1993; McBride and Gilmore, 2004; Randall, 1989). See Table 2-1 for location details. Credit Purvis et al. (2017). © 2017 Elsevier B.V. All rights reserved.*

3.3.3 Depth Profile Analysis to Evaluate Decontamination of WSD_AR and WSD_IC Using Gas Cluster Ion Beam Etching

Fig 3-3a presents the proportional change in the carbon concentration in the WSD_IC, and the mean carbon concentration of WSD_AR samples relative to the sum of the concentrations of the metallic elements as a function of GCIB sputter etch time. The plot showed that carbon concentrations decreased as a result of GCIB sputtering, relative to the unvarying concentrations of those elements. The WSD_IC carbon concentration exhibited an initial large decrease in the first 10 seconds of etching, followed by a decline in carbon reduction between 20 and 90 seconds, then reaching a stable concentration with minimal variation. The carbon concentration of the WSD prior to contamination, (WSD_AR) was added to Fig 3-3a, to illustrate carbon reduction to pre-contamination levels.
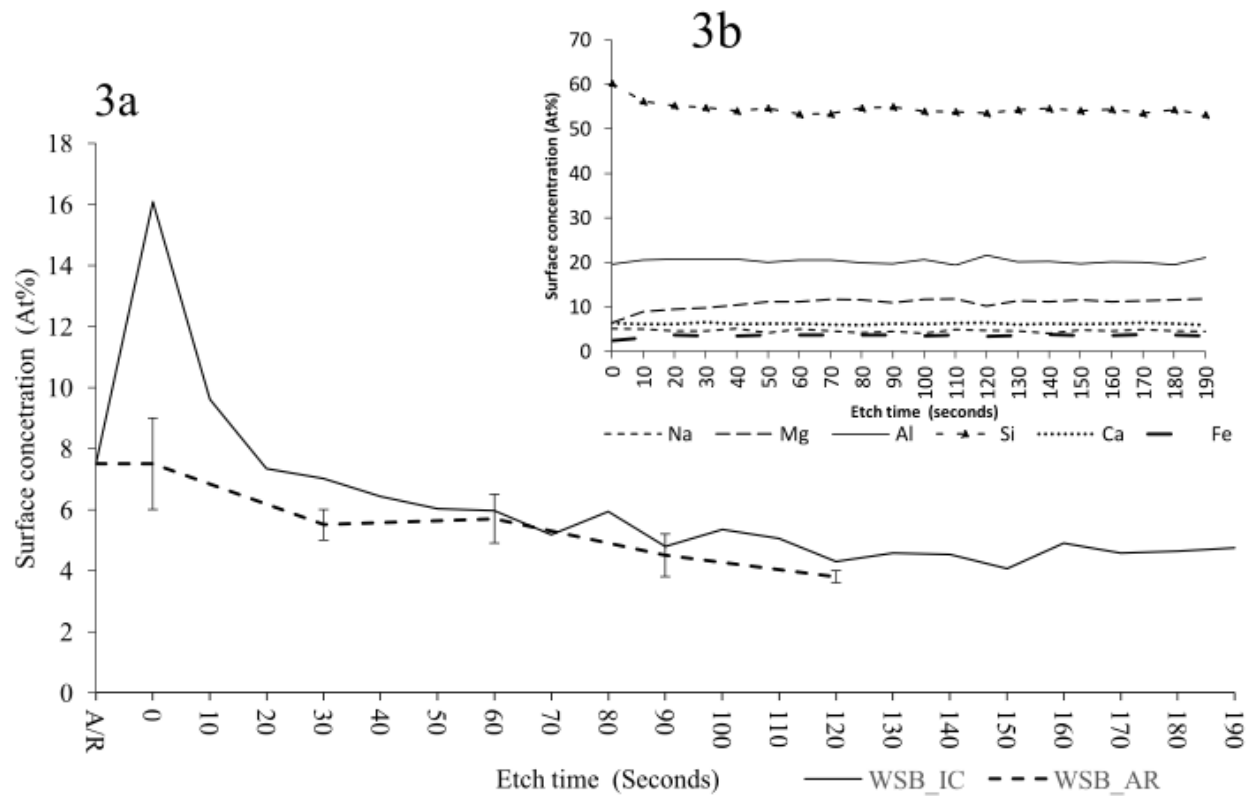
FIG 3-3a. *XPS measurements to obtain the surface concentration of carbon as a function of GCIB sputter etch time on WSD_IC (n=1) and WSD_AR (n=3).* **3-3b.** *The surface concentration of non-carbon elements as a function of GCIB sputter etch time. Credit Purvis et al. (2017). © 2017 Elsevier B.V. All rights reserved.*

3.3.4 Decontamination using UV/ozone

Surface analysis only requires decontamination in the region where the analysis is being conducted. However, decontamination of the entire surface of a material is required for bulk analysis by, for example, py-GC/MS, for which rock samples must be powderised prior to analysis. Here, the purpose of the py-GC/MS was to measure the effectiveness of UV/O_3 decontamination rather than for detection of specific compounds as it is used. Trace levels of organic compounds comparable to the TOC values measured by carbon combustion (0.041% ±0.05%), were not observed in the py-GC/MS analysis of the WSD_AR internal volume (Fig 3-4a) indicating that adventitious carbon was not introduced during the preparative grinding and sieving. However, the WSD_AR XPS measurements were 3.5 at%

Fig 4a. WSB_AR

Fig 4b. WSB_ICprior to cleaning

Fig 4c. WSB_IC following UV/O cleaning
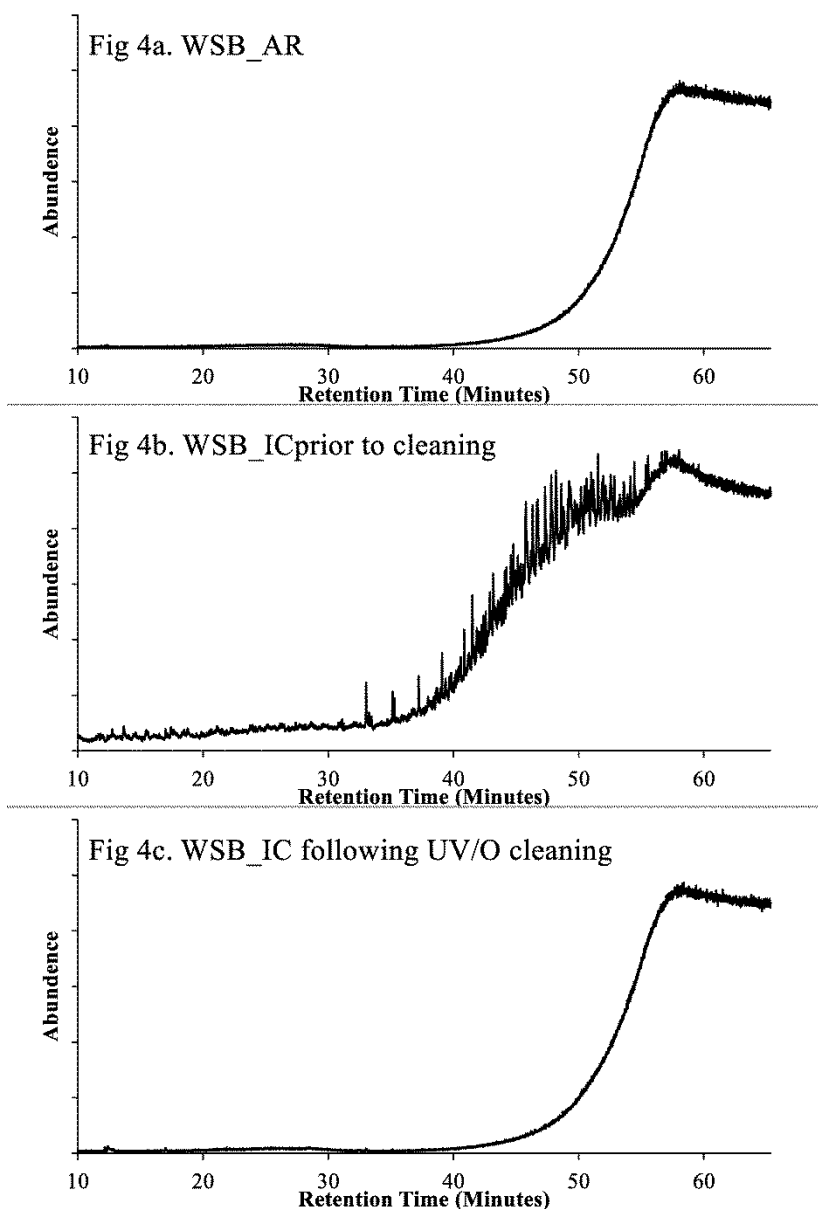
FIG.3-4 a-c. Py-GC/MS Chromatograms of (**a**) WSD_AR showing trace levels of contamination followed by (**b**) WSD_IC, prior to cleaning demonstrating the presence of a range of organic compounds consistent with those found in WD40 followed by (**c**) WSD_IC, which was cleaned using UV ozone (UV/O) for 20 m, showing that trace levels of organic compounds are observed. This is a non-quantitative study, and the composition of WD40 is understood; therefore, the assignment of peaks to specific compounds is not germane. Credit Purvis et al. (2017). © 2017 Elsevier B.V. All rights reserved.

A range of high molecular weight hydrocarbon compounds consistent with those found in WD40 residue was identified in WSD_IC using py-GC/MS (Fig 4b) consistent with TOC values of 1.74% ±0.05%. Following decontamination using UV/O treatment, the WD40 compounds were undetected by py-GC/MS analysis (Fig 3-4c). Furthermore, the TOC values were reduced to 0.04% ±0.05%, indicating that 20 minutes UV/O treatment removed WD40 hydrocarbons from the WSD samples.

Corroborative XPS analysis indicated the carbon concentration of WSD_AR changes from 4.8 at% to 3.5 ±1.0 at%, following UV/O cleaning. The intentional contamination increased carbon concentration to 22.3 ±3.0 at%, then after cleaning with 20 minutes UV/O to 3.0 ±2.7 at%. These carbon concentrations were comparable to those of the intentionally contaminated sample, after decontamination by 90 seconds of GCIB etching.

A comparison of the spectra of WSD_AR spiked with aromatics and aliphatic compounds indicated that UV/O_3 caused no detectable attenuating effects on either the peak intensities, or peak shape (see Appendix A2.0), specifically, between those elements detected in the low binding energy part of the spectrum, with those that are detected at the higher binding energies of the spectrum (see Fig 1-23). Therefore, during XPS analysis, the passage of the electrons, emitted from the sample surface, through the intentionally added carbon, did not produce a detectable attenuation of their energy and by extension attenuation of the signal strength. Furthermore, a comparison of the WSD_AR and WSD_IC spectra indicated no attenuating effects on either the peak intensities or peak shape of high-resolution spectra, specifically, between those elements detected at the low and higher binding energies. Thus, there were no observed changes in electron emission energies in any part of the XPS spectra that resulted from the intentional addition of carbon.

3.4.0 Discussion

To date, monatomic sputter etching has been used to remove carbonaceous materials from geological samples (Preston, 2011), as has UV/O_3 cleaning (Nugent et al., 1998; Hausrath et al., 2007). However, GCIB sputter etching, most commonly used for surface analyses of semiconductors, and has been applied to the Earth Sciences, recently. Sano et al. (2016)

applied GCIB and UV/O$_3$ decontamination prior to XPS, ToF SIMS and py-GC/MS analysis, and detected organic compounds that were consistent with remnant biological material. This chapter provided a rigorous and complete evaluation of the efficiency of decontamination procedures when coupled to XPS and bulk chemical analysis techniques. This chapter showed that these decontamination approaches could be considered useful as part of the application of surface analysis to different situations, in Earth sciences and planetary exploration.

3.4.1 An evaluation of decontamination by GCIB

Before evaluation of decontamination the accuracy of XPS, when applied to the dolerite, several considerations were addressed:

1. A comparison of measured elemental composition with those typically reported for basalts (Fig 3-2, McBride and Gilmour 2004) was made, and by implication, the close correlation observed implies that the carbon concentration measured to assess decontamination are similarly accurate.

2. Since the GCIB gun used in this investigation was mounted within the XPS instrument, and analysis commenced immediately following GCIB etching, the possibility of re-contamination or accumulation of carbon on the sample was eliminated.

3. The ultra-high vacuum drew the sputtered material away from the raster area, assuring that the high molecular weight organic compounds in the WD40 residue on the WSD_IC could not migrate from the raster perimeter to the analysis spot, between the repeated cycles of GCIB sputter etching.

4. During XPS analysis, the passage of the electrons emitted from the sample surface, through the intentionally added carbon, did not produce a detectable attenuation of their energy and by extension attenuation of the signal strength.

5. Observed changes in carbon concentrations with GCIB etching were not the result of relative changes in the metallic element concentrations (Fig 3-3b) since no significant preferential sputter yields were detected, for these elements. However, a 5.0 at% decrease in the Si concentration was observed. The decrease may have been due to the removal of the Si in WD40 that was deposited during its application or may have

been due to minor differences in sputter yields for Si, in comparison to the other elements. However, this had no significant impact on the measurements.

6. UV/O$_3$ cleaning had no impact on the chemical composition of the samples.

With regards to the actual evaluation of decontamination, the carbon concentration after intentional contamination (WSD_IC) at t= 0 seconds must be considered the sum of both the initial indigenous and the adventitious carbon as observed in the WSD_AR, plus the intentional contamination. Consistent with this assumption, the carbon concentration of WSD_IC was reduced to a value less than the WSD_AR, following >90 seconds GCIB (Fig 3a). This net decrease plausibly resulted from the removal of both the adventitious carbon already present on WSD_AR, in addition to removal of the intentionally applied WD40 carbon. The carbon concentrations, observed at t> 90 seconds GCIB etching remained unchanged, regardless of etching time and are, therefore, is considered indicative of the indigenous carbon. Corroboratively, the WSD_AR demonstrated an initial, albeit smaller decrease in the mean carbon concentration as a function of GCIB etch time here just indicating the removal of adventurous carbon associated with this sample. These results demonstrated the ability of by XPS operating in conjunction with GCIB, to discriminate between adventitious and indigenous carbon,

In terms of the mechanism of carbon removal, GCIB can be regarded as a selective ion etching process. The sputter yield, which is the rate at which sputtering occurs for organic material, is many times that for inorganic material (Cumpson et al., 2013a). Therefore, although the decrease observed in carbon concentration in this study may be the result of the complete removal of the surface material, in the raster area, including inorganic material and the attendant carbon, it is more likely due to preferential sputtering of carbon, with the removal of minimal amounts of non-carbon material. Regardless of the mechanism, this study was able to evaluate the removal of surface carbon from geological samples allowing the analysis of the underlying indigenous carbon.

The physical impact of GCIB etching and the depth distribution of adventitious and intentionally applied carbon is of interest, but, because the dolerite surface was uneven, it was not possible to measure surface topography by interferometry or atomic force

microscopy and thereby measure sputter yields. Sputter yields could, however, be approximated using other data. Cumpson et al. (2013a) examined the etch rates of different materials and found that 1000 atom argon clusters with a total energy of 4 keV produce sputter yields of 0.056 nm.min^{-1} in a Si wafer target and higher sputter yields of 23.86 nm.min^{-1} for styrene targets. Since basalts are typically composed of 45% to 52% SiO$_2$ and styrene is an organic polymer, we anticipate that results obtained by Cumpson et al. (2013a) are an indicative framework for dolerite (and basalt) sputter yields generally. This sputter rate would produce an estimated final etch depth in the GCIB raster area of 0.084 nm after the minimum of 90 seconds needed to decontaminate the sample, which implies that intentional and adventitious carbon were restricted to that depth range. The depth of analysis of XPS is up to 10 nm depending on the elemental composition (Briggs and Grant 2003).

3.4.2 The disparity between indigenous organic matter detected by XPS and trace carbon detected by GC/MS after decontamination

Although GC/MS is sensitive to ppb concentrations of organic matter, it was not detected in the WSD_AR by this approach (Fig 4a). Additionally, WSD_AR bulk TOC measurements were at the limits of detection. However, basalts typically contain trace levels of organic carbon (Fristad, 2015) and carbonaceous material has been detected in basalt using XPS (Tingle et al., 1991) which is consistent with the carbon observed in low concentrations in both the WSD_AR and WSD_IC by XPS analysis after etching times >90 seconds.

Interestingly, carbon was detected in WSD by XPS with a peak position consistent with the presence of unsaturated or aromatic compounds, although this material did not yield detectable organic matter by py-GC/MS or THM-GC/MS. This discrepancy can be explained by the presence of nm thick films of carbonaceous material that are detected using surface analytical techniques (e.g. De Gregorio et al, 2011) and by a previous report, which showed that basalts contain a reduced, thermally stable carbonaceous component in some basaltic samples (Tingle and Hochella, 1993). These aromatics are demonstrably detectable by XPS, but their thermal stability could make this material resistant to thermal extraction and consequently undetectable by either py-GC/MS or THM-GC/MS analysis (see Chapter 8).

This trace material not detected by py-GC/MS can likely be ascribable to the presence of carbonaceous films formed on cracks on reactive mineral surfaces such as fused quartz (Jensen et al., 2014). Such carbonaceous material is considered thermally stabilised by olivine and other minerals and glasses and has been previously detected using XPS (Tingle and Hochella,1993; Johnson et al., 2015). Therefore, thermally stable carbon may explain the discrepancy between the XPS and py-GC/MS or TOC results for the WSD, since the latter two rely upon thermal processes such as pyrolysis extraction (Py-GC/MS) or dry combustion (see Chapter 8).

2.5.0 Conclusion

This study used GCIB sputter etching on a dolerite core sample, to remove organic contamination that may have diffused into top 5-10 mm of the surfaces exposed to the environment. WSD was a practical analogue for testing these decontamination protocols. In situations where the possibility of organic contamination ingression into the surface of the rock is impossible, we suggest that these protocols could be used for the decontamination of any geological samples without necessarily cutting and sectioning to remove contaminated material.

The non-contact methods evaluated here successfully removed organic material intentionally applied to basalt. The implication is that these processes will be proficient at the removal of the relatively trivial amounts of contamination caused by the sectioning of geological samples or any subsequent storage and handling. These techniques do not require contact with samples. Therefore, they can be considered effective at decontaminating samples without the risk of introducing additional contamination. These results increased the confidence that that basalt, and by implication, other geological samples can be decontaminated effectively.

CHAPTER 4: THE DETECTION AND ANALYSIS OF ORGANIC MATERIAL IN ONTONG JAVA PLATEAU BASALTS USING THERMALLY ASSISTED HYDROLYSIS AND METHYLATION COUPLED TO GC/MS AND X-RAY PHOTOELECTRON SPECTROSCOPY

Abstract

Tuff from the Ontong Java Plateau (OJP) contains distinctive microtubular features that are thought to be evidence of a lithosphere-biosphere interaction. A sample of this OJP tuff was characterised using gas chromatography/mass spectrometry (GC/MS) and X-ray photoelectron spectroscopy (XPS). Thermal extraction and pyrolysis were used to separate the organic material from the rock. The addition of a thermochemolytic agent increased the efficiency of the thermal extraction and permitted the detection of aliphatic and functionalised aromatic compounds, several of which contained a nitrogen substitution in their ring. This thermal extraction was carried out at different temperatures to obtain the maximum amount of information from the organic compounds. The compounds detected by GC/MS were in turn compared to XPS analysis, which was used to measure the chemical states of the carbon in the OJP tuffs. This analysis indicated that chemical states of the carbon were consistent with the compounds that were identified by GC/MS. The results suggested that XPS analysis, in combination with THM-GC/MS analysis provided a synergistic set of data, which indicated that XPS contributed to the detection of organic material in Telluric (Earth) rocks and by extension other types of geological and extra-terrestrial material.

4.1 Introduction

The methods of removing adventitious material from a geological sample using both gas cluster ion beam etching and ultraviolet ozone cleaning were evaluated in Chapter 3, and it was demonstrated that it was possible to distinguish between the endogenous and the indigenous material, using X-ray photoelectron spectroscopy (XPS). The ability of XPS and gas chromatography/mass spectrometry (GC/MS) to characterise organic material in the OJP samples (see section 1.9.3) was then evaluated, and this was compared to Whin Sill Dolerite (WSD) (see section 3.1.1), which served as a procedural blank.

Samples from the OJP were selected for three reasons. Firstly, because Ocean Drilling Programme, core 13R from Leg 192 hole 1184A (see Table 2-1 and hereafter referred to as OJP_13) contains a distinctive example of tubular alteration textures within glass shards that have been suggested to be ichnofossils (see section 1.9.2). Secondly, Cannon and Mustard, (2015), reported the presence of tektitic glass shards on Mars and these could potentially contain the same types of alteration textures seen in the Telluric samples (Allen, 1981). Therefore, the investigation of Telluric glass shards may assist in the selection of samples that will be returned to the Earth, from Mars, in the future. Thirdly, the carbonaceous material in these samples was previously characterised and correlated with the textures in this rock using FTIR microscopy (Preston et al., 2011). This earlier FTIR microscopy study measured the organic material in 400 μm^2 regions on the surface of the OJP_13 that were considered to be 'rich' in microtubules and in areas that were 'poor' in microtubules, and this indicated that aliphatic hydrocarbons, carboxylic acids and amides appeared to be co-localised to areas of the sample where the microtubule textures were most dense. This observation implied that there was a correlation between the composition of the organic material in the regions rich in microtubule structures.

The purpose of this chapter was to evaluate the methods that could be used to characterise the indigenous organic material in the OJP_13 sample, by conventional pyrolysis (py) and by thermally assisted hydrolysis and methylation (THM) coupled to gas chromatography mass spectrometry (GC/MS; see section 1.11.2 and 1.11.3). Pyrolysis is the fragmentation of molecules through the thermally induced cleavage of chemical bonds. Therefore, higher pyrolysis temperatures will break stronger chemical bonds, which could potentially result in higher levels of molecule fragmentation that can lead to the loss of molecular information. Conversely, lower pyrolysis temperatures may result in too little fragmentation, resulting in the failure to detect higher molecular weight organic compounds. Therefore, different compounds can be detected depending on the thermal desorption/pyrolysis temperatures used (Marbot, 1997). This phenomenon was exploited in this investigation to obtain the maximum range of compounds that could be present in the OJP_13.

The data that was obtained using GC/MS were compared to the data that was obtained with surface analysis, in this instance XPS, to assess how these two types of data can be

associated to characterise the OJP_13 sample synergistically. X-ray photoelectron spectroscopy (XPS) is capable of unambiguously identifying and simultaneously measuring the relative surface concentrations of elements (Watts and Wolstenholme, 2003; Fairley 2009; see chart in section 3.3.3, Chapter 3). However, synthetic peak component fitting of the spectra, which is analogous to the processes that are described as deconvolution in the analysis of GC/MS peaks can also be used to quantitatively assess the individual chemical states of the parent element (Beamson and Briggs, 1992; Chastain and King, 1995). By using two analytical approaches, this investigation was able to assess the relative effectiveness of the two types of instruments to analyse the organic material in the OJP_13.

4.2 Methods

4.2.1 OJP_13 and WSD Sample preparation and Optical Petrography

The Leg 192, Hole 1184A, Core 013R, Section 03W, Interval 145-148 cm (hereafter OJP_13) (see table 2-1) sample from the Ocean Drilling Programme. The Whin Sill Dolerite (WSD) from the shoreline at Craster, Northumberland (N55° 28.427' 001 35. 577' W) (see Table 2-1) was obtained and was prepared according to the methods described in section 2.1.1.

Standard thin sections of OJP_13 sample for optical petrography were prepared by Durham Thin Section Services, according to the description in section 2.5.1. The sample was prepared without polishing or without the inclusion of a bonded coverslip permitting surface analysis of a thin section of the OJP_13. Additionally, WSD was prepared, according to the methods described in sections 2.1.1.

4.2.2 Decontamination of the WSD and OJP_13 Samples with GC/MS and XPS

The decontamination of the OJP_13 and the WSD samples intended for XPS analysis was carried out with GCIB sputter etching at 4 keV for 120 seconds, according to chapter 3, and used the survey and the C1s high-resolution XPS analysis (see section 2.4.1). Preparation of the samples for both py-GC/MS and THM-GC/MS was carried out according to section 2.1.1; these were decontaminated using UV/O_3 for 20 minutes according to methods described in Chapter 3.

4.2.3 Analysis of the WSD and OJP_13 Samples with GC/MS and XPS

The XPS analysis was conducted according to the protocol in section 2.4.1. The py-GC/MS and THM-GC/MS analysis was conducted according to the protocol in section 2.4.2. For simplicity, the results section presented the identities of the major peaks, and this provided an overview of the compounds that were detected as an illustrative sample of the compounds detected in the minor peaks. The top 10 most intense m/z ions used by the NIST05 mass spectra library were used to obtain the molecular identities of the major peaks, were also presented. The optimal pyrolysis temperature for the analysis of the organic material in the OJP_13 was investigated by adjusting the maximum flash pyrolysis temperature to 120 ˚C, 240 °C, 450° C, (thermal desorption) and 610 °C and 1000 °C (pyrolysis).

4.3 Results

4.3.1 Optical Petrography of OJP_13

Visual inspection verified the presence of the microtubule textures (Fig.4-2a-b). The microtubules observed in this thesis were similar in appearance and distribution to those previously reported, e.g. (Banergee et al., 2003; Preston et al., 2011; Staudigel et al., 2014). Fig 4-2a, shows a typical basaltic glass shard obtained from the OJP sample used in this study. The shards from this region are typically <1500 μm along their longest axis. A brown perimeter of the glass shard resulting from the weathered and devitrified palagonite rind. The ingression of microtubules caused the glass darker area in the samples (Banerjee and Muehlenbachs, 2003). This observation demonstrated that the basaltic glass shards in the OJP sample obtained for this study contained the tubular alteration textures that putatively indicated biological activity and was therefore comparable to those already studied.

No salient surface textures in the WSD sample were observed (see Fig 6-3f). Therefore, no specific regions were selected. Consequently, nine 40 μm^2 spots on the surface of the WSD were selected randomly for XPS analysis.
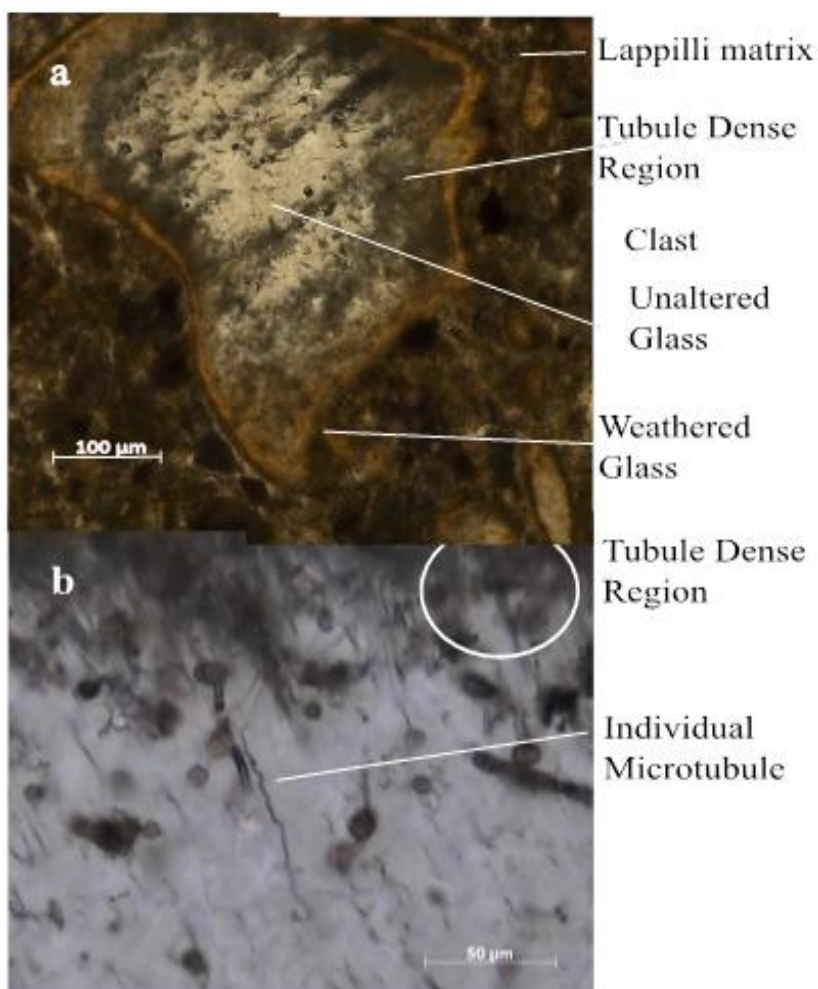
Fig. 4-1(a and b). *The optical petrographic image of the OJP sample showing (a) location and morphology of the alteration textures within the glass shards of the OJP used in this study, ×20. (b) Detail of a microtubule structure, ×40.*

4.3.2 A comparison of conventional pyrolysis with Thermally Assisted Methylation (THM) of OJP tuff and WSD.

Following cleaning with UV/O_3, the amount of organic material detected in the OJP tuff using conventional py-GC/MS was compared to the amount that was detected using THM-GC/MS, in both the OJP and WSD samples (Fig. 4-2a-d). No identifiable peaks could be observed in WSD using conventional pyrolysis py-GC/MS (FIG. 4-2a), The THM-GC/MS of WSD at a pyrolysis temperature of 610 °C (hereafter, T=610 °C) resulted in a single peak corresponding to azulene, (Fig 4-2b), this is a pyrolysite of TMAH (Morisson et al., 2017).

In contrast, the py-GC/MS (T= 610 °C) of the OJP material resulted in the detection of a range of organic compounds that could be identified using the NIST05 (Stein, 2008; Fig. 4-2c) including a number of functionalised aromatic compounds, some of which possessed a nitrogen substitution within the ring. The addition of TMAH prior to pyrolysis then GC/MS analysis (THM-GC/MS) (T= 610 °C) of the OJP sample increased the number of peaks with

two orders of magnitude increase in the numbers of ions detected (intensity), compared to the conventional py-GC/MS ion intensity (Fig. 4-3d). This increase in the response facilitated the identification of several alkylated aromatic compounds, some of which possessed nitrogen substitutions (Table 1). The complexity of compounds detected confounded the identification of specific compounds. The relative response factors of the different compounds could not be obtained, which prevented the application of peak integrations to acquire the concentrations of the detected compounds.

Table 4-1 provides the key to the major peaks identified in the chromatograms shown in Fig 4-2a-d and presents the 10 most abundant mass/charge (m/z) values for the major peaks that were obtained from the OJP samples using py-GC/MS and THM-GC/MS. The possible peak assignments obtained using NIST05 and the corresponding quantification of the match to the m/z values in the NIST05 mass spectra library (Stein, 2008). This resulted in a reverse match factor compound identification that ranged from 0.7 to 0.9, implying fair to good matches (Stein, 1994; Ausloos et al., 1999; Stein, 2008). Precise assignments of peaks to specific organic compounds using THM-GC/MS was not possible, due to their complexity. This complexity also prevented the use of standard compound additions to provide definitive evidence of the presence of specific compounds and resulted in many compounds that were unknown to the NIST mass spectra library.
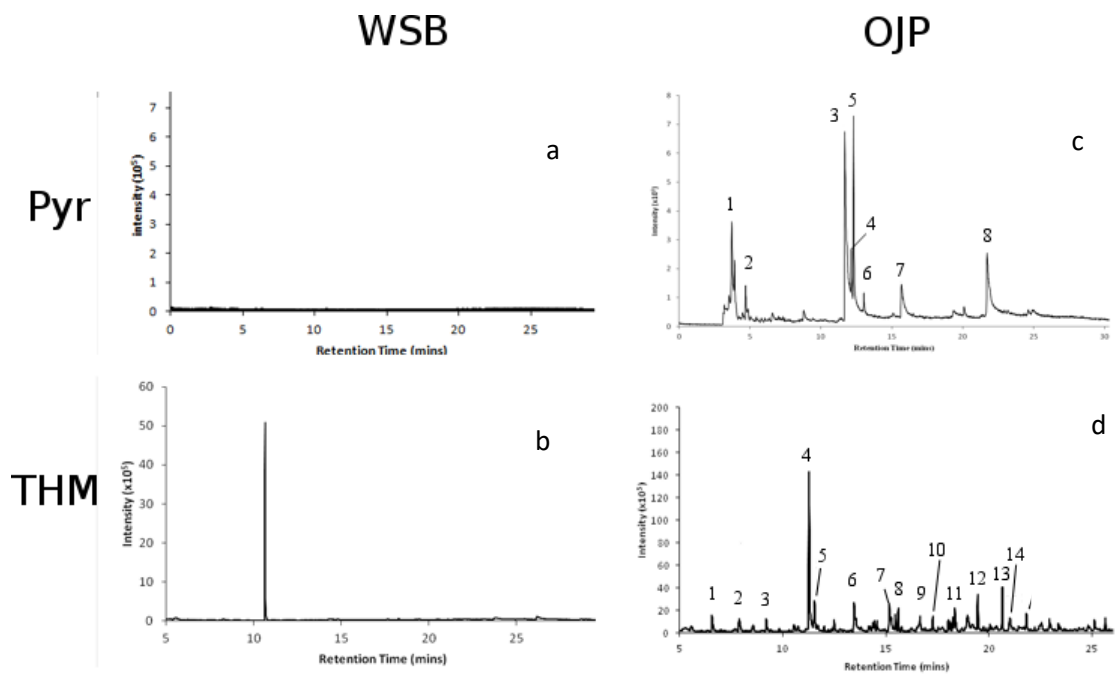
Fig 4-2 a-d. *Partial total ion chromatograms comparing the organic material obtained from WSD and OJP, using conventional pyrolysis and pyrolysis in the presence of TMAH (THM with TMAH-GC/MS. See Table 1 for the peak identification key.*

title																						

Table 4-1 Values for the THM -GC/MS of OJP and Key to Chromatogram 4-1d

Peak	m/z	Ab.	m/z	Ab.	m/z	Ab.	m/z	Ab.	m/z	Ab.	m/z	Ab.	m/z	Ab.	m/z	Ab.	m/z	Ab.	m/z	Ab.	peak assignment	match
1	54	1	55	1	56	2	57	4	58	100	59	4	61	5	73	1	89	1	105	1	*Butylamine*	0.8
2	51	11	63	9	65	11	77	14	78	8	91	100	92	13	93	17	105	23	106	51	*3-Ethylpyridine*	0.9
3	51	13	58	36	59	25	77	15	89	24	91	100	102	11	103	9	105	20	106	44	Ethylbenzene	0.85
4	50	12	51	16	63	13	65	69	77	21	78	61	79	18	93	16	108	100	109	8	Methoxybenzene	0.94
5	77	13	86	9	91	12	94	11	103	10	105	100	106	9	119	12	120	47	128	10	Isopropylbenzene	0.88
6	55	11	57	32	77	16	79	11	91	23	105	100	117	11	119	62	120	54	134	15	*Butylpyridine*	0.86
7	51	17	53	12	77	41	78	11	79	40	80	14	89	15	90	22	107	89	108	100	4-Methylphenol	0.94
8	51	11	63	16	65	14	89	15	91	100	92	17	107	15	108	12	119	29	120	71	Meta Tolualdehyde	0.9
9	51	12	65	15	77	12	91	42	92	16	115	58	116	16	117	100	131	18	132	96	1-Propenyl-Toluene	0.85
10	51	15	77	40	78	18	79	23	91	34	103	15	107	98	119	20	121	42	122	100	2,3-Dimethylphenol	0.9
11	65	5	77	8	91	16	115	9	117	9	119	100	120	10	133	9	134	47	135	5	1-Isopropyl-4-Methylbenzene	0.93
12	77	13	91	22	107	10	115	11	117	11	119	100	120	10	122	8	133	7	134	47	1-Isopropyl-4-Methylbenzene	0.86
13	77	12	91	19	103	10	105	14	107	11	119	19	120	8	135	100	136	10	150	26	Ortho-Methoxyacetophenone	0.9
14	77	6	91	12	105	8	115	10	117	8	119	9	131	4	133	100	134	12	148	30	Pentamethylbenzene	0.85

Table 4-2 Key to and Values for Chromatogram 4-1c

Peak	m/z	Ab.	m/z	Ab.	m/z	Ab.	m/z	Ab.	m/z	Ab.	m/z	Ab.	m/z	Ab.	m/z	Ab.	m/z	Ab.	m/z	Ab.	assignment	match
1	50	37	51	30	52	11	53	47	54	45	55	46	56	100	57	6	58	5	79	4	2-Propenal	0.71
2	51	3	53	3	55	3	67	2	69	3	71	100	72	99	73	4	77	2	78	4	Propylamine	0.83
3	50	8	51	6	55	7	61	4	62	6	63	11	65	32	66	44	94	100	95	7	Phenol	0.93
4	51	11	63	11	65	22	66	24	77	14	91	11	94	56	105	100	119	10	120	45	Isopropylbenzene	0.82
5	50	7	61	6	62	14	63	29	64	7	89	53	90	41	94	13	118	100	119	9	Benzofuran	0.9
6	63	13	65	20	66	24	77	15	91	17	94	53	103	12	105	100	119	25	120	49	Ethyltoluene	0.86
7	50	9	51	15	63	10	77	18	78	11	94	8	103	20	131	100	132	70	133	8	3-Phenyl-2-Propenal	0.79
8	50	54	51	96	62	72	64	59	77	97	91	57	127	84	131	76	134	88	157	100	5-Chloro-2-Dimethylaminopyrimidine	0.63

Tables 4-1 and 4-2 (previous page): *presented the relative abundances (Ab), that had been normalised to the most intense mass fragment of the mass to charge values (m/z) obtained from the thermochemolytically assisted pyrolysis coupled to GC/MS of WSD and OJP tuffs. Tables 4-1 and 4-2 also include the possible peak assignments and match factor (where 1 = a complete match and 0 = no match) of those assignments to the compounds NIST05 library spectra. Organic compounds were not identified in the WSD other than the TMAH residue. Therefore, the table is not presented. Peak numbers correspond to the annotations in the relevant chromatogram.*

4.3.3 Comparison of THM-GC/MS analysis of the OJP tuff at different pyrolysis temperatures

In addition to conducting THM-GC/MS at 610 °C (pyrolysis), THM-GC/MS analysis was also conducted on the OJP samples at temperatures of 120 °C, 240 °C 450 °C (thermal desorption), and 1000 °C (pyrolysis). The results presented in Figs 4-3 a-d and Table 4-1 and 4-2 suggested that aliphatic compounds with carboxyl and hydroxyl groups were detected at THM-GC/MS T=450 °C, but were undetected using THM-GC/MS T=610 °C and T=1000 °C. Functionalised double ring compounds were detected THM (T=1000 °C), in addition to the single ring compounds already identified in the THM-GC/MS (T=610°C). Critically, some of the compounds in the OJP_13 sample possessed nitrogen substitutions within the aromatic rings, at each of these pyrolysis temperatures. However, no organic compounds could be identified at pyrolysis temperatures of 120 °C, and 240 °C.
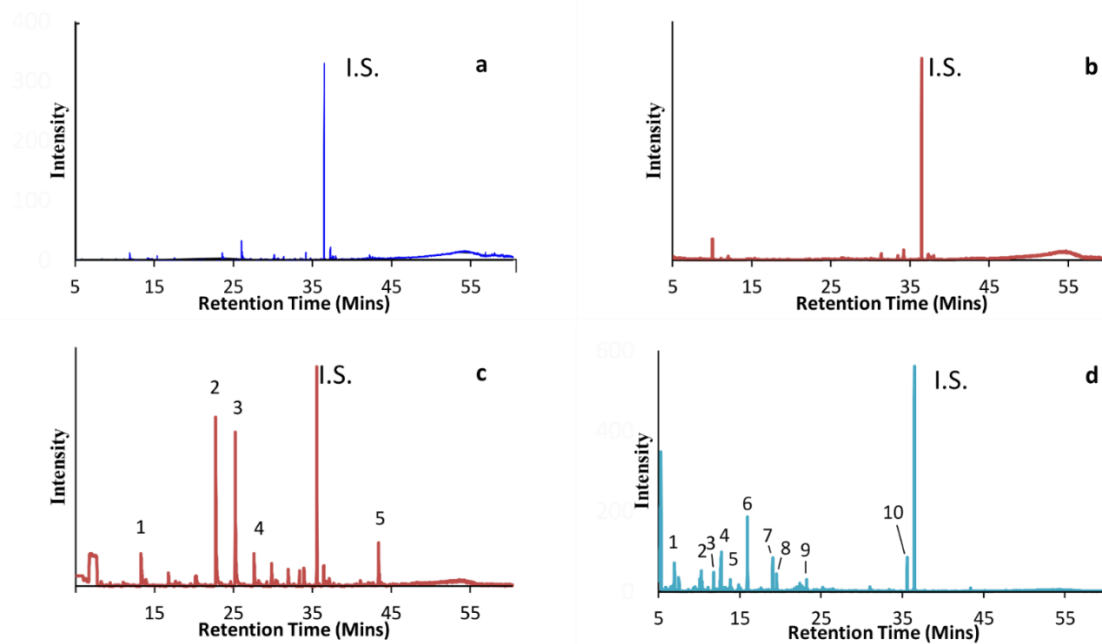
Fig 4-3 (a-d). *Comparison of organic material obtained from OJP using THM-GC/MS at different pyrolysis temperatures. (a) T= 120°C (b) T =240°C (c) T=450°C. (d) T= 1000°C Unidentified peaks were unlabelled. I.S. = 2pmol androstane internal standard. See Table 4-2 for the peak identification key.* **Note**: *The peaks that were detected in T=120˚C and 240˚C had matches <0.65 and were, therefore, could not be reliably identified and were not annotated.*

Table 4-2. Key to Chromatogram 4-3 (c) m/z values and Identified Peaks with match factors, for GC/MS using Thermal hydrolysis and methylation of OJP_13. With flash pyrolysis temperature set to 450˚C. Match= match factor with NIST05 mass spectra library

.

peak#	m/z	Ab.	m/z	Ab	m/z	Ab	m/z	Ab	m/z	Ab	m/z	Ab	m/z	Ab	m/z	Ab	m/z	Ab	assignment	match
1	50	16	51	33	74	8	75	4	76	5	77	65	78	5	105	100	106	8	methyl benzoic acid	0.95
2	55	31	57	12	59	21	69	11	74	100	87	49	101	9	129	12	141	14	nonanoic acid	0.88
3	55	100	59	88	69	87	74	86	83	48	87	43	97	64	129	98	138	94	Octanedioic Acid Dimethyl Ester	0.84
4	55	100	59	70	69	36	74	72	83	59	87	30	111	43	143	39	152	92	Nonanedioic acid dimethyl ester	0.82
5	55	100	59	66	74	73	83	32	84	32	97	44	98	45	125	43	138	33	Dodecanedioic acid, dimethyl ester	0.77

124

Table 4-3. Key to and Values chromatogram 4-3(d) *m/z values and Identified Peaks with match factors, for GC/MS using Thermal hydrolysis and methylation of OJP_13. With flash pyrolysis temperature set to 1000˚C. Match= match factor with NIST05 mass spectra library.*

peak#	m/z	Ab.	m/z	Int	m/z	Ab.	m/z	Ab.	m/z	Ab.	m/z	Ab.	m/z	Ab.	m/z	Ab.	m/z	Ab.	Assignment	match
1	51	13	63	13	65	13	77	15	78	11	91	100	92	14	93	16	105	23	Ethylbenzene	0.9
2	50	22	51	27	63	12	74	12	77	20	78	48	102	10	103	48	104	100	3-Cyanopyridine	0.9
3	50	26	51	19	62	11	63	18	65	35	66	53	75	15	76	28	94	100	Phenylethyl 2-Furoate	0.82
4	50	7	51	6	62	8	63	16	74	5	87	5	89	14	115	100	116	94	1-Methyl-3-Cyanobenzene	0.82
5	52	3	53	3	66	7	67	38	69	9	82	23	83	53	108	100	109	53	Propylcyclohexane-1-Ol	0.93
6	108	100	67	18	119	17	123	13	134	9	56	8	109	8	97	7	54	7	4-Methoxyaniline	0.74
7	50	5	51	5	63	5	74	6	75	5	102	9	126	7	127	13	128	100	Naphthalene	0.89
8	51	4	63	8	74	4	89	5	115	36	116	4	139	10	141	88	142	100	a-Methylnaphthalene	0.94
9	50	4	62	5	63	8	74	5	89	6	115	39	139	10	141	90	142	100	1,2-Dihydroacenaphthylene	0.85
10	63	3	74	5	75	4	76	5	86	3	126	3	150	14	151	19	152	100	Acenaphthene	0.86

.

4.3.5 XPS Analysis of Ontong Java Plateau Organic Chemistry

For this study, the OJP samples were divided into three descriptive geological textures. These were the fine-grained lapilli that surrounded the glass, and described as the *'matrix'* (areas 1, 4 and 5), the centre of the glass shards where fewer microtubules described as '*tubule-poor'* regions (areas 3,6 and 7), and the perimeter of the glass shards where the density of microtubules was highest described as the *'tubule-rich'* regions (areas 2, 8 and 9) (See Fig 4-4).

Fig 4-4. *The XPS beam area targeting camera image of the analysis region on the OJP sample. For clarity, the perimeters of the glass shards are highlighted in white. The GCIB raster area used to decontaminate the sample is indicated by the orange rectangle. Each of the XPS analysis spots are indicated by numbered red target symbol. Areas 1, 4 and 5= the lapilli matrix; 3, 6 and 7= the centre (microtubule-poor) and the 2, 8 and 9= perimeter (microtubule-rich).*

| Surface concentration | | | | |
Position	C 1s	N 1s	N:C	Area
1	17.85	0.68	0.038095	Matrix
2	12.07	0.47	0.03894	Perimeter
3	8.47	0.11	0.012987	Centre
4	8.47	0.38	0.044864	Matrix
5	11.00	0.27	0.024545	Matrix
6	8.08	0.14	0.017327	Centre
7	9.35	0.20	0.02139	Centre
8	8.38	0.31	0.036993	Perimeter
9	8.70	0.19	0.021839	Perimeter

Table 4-6. *The surface concentration of carbon and nitrogen in the different textures of the OJP_13 sample. The position corresponds to the photomicrograph in Fig 4-2. The carbon and nitrogen surface concentrations were measured relative to the element concentrations described in section 3.2.2 (Fig 3-2).*

The results presented in Table 4-6 demonstrated that there was variation in the surface concentrations of both carbon and nitrogen, which resulted in the variation in the N:C ratio. However, contrary to Preston et al. (2011), there appeared to be no correlation between the carbon and nitrogen concentrations and the C:N ratio and the matrix and centre, both of which were microtubule-poor areas and the perimeter, which was a microtubule-rich area.

Furthermore, the XPS targeting camera could not provide images of the surface textures of the geological samples at sufficiently high-resolution. Therefore, it was not possible to precisely identify the position of perimeter region of glass shard in the OJP. Since the organic material was heterogeneously distributed in the OJP samples, nine 50 μm spots were selected over the surface to obtain a mean carbon spectrum shown in Fig 4-5a. This failure to localise specific types of organic material to particular rock textures provided the incentive to conduct the sequential XPS and ToF SIMS analysis described in Chapter 5.

The relative carbon and nitrogen concentrations were measured relative to the inorganic element concentrations (see section 3.2.1). The XPS survey spectra indicated that the surface concentration of carbon on the WSD was 3.5 at %, and that the nitrogen surface concentration was below the limits of detection, whereas the OJP carbon concentration was

12.5 at % and the nitrogen concentration was 0.5 at %, suggesting that the OJP carbon concentration is ca. 4 times greater than WSD. This measurement is inconsistent with the py-GC/MS and the THM-GC/MS analysis of WSD, which indicated that organic material in WSD was not detected by this bulk analytical approach. The possible reasons for this disparity were considered in Chapter 8.

The spectral profile of WSD carbon high-resolution spectra indicated a single dominant component, equivalent to OJP component (i) at 284.6 eV, which equates to 96% of the WSD carbon spectrum (Fig 4-5b). In contrast, the OJP produced a more complex peak shape (Fig. 3-5a), which resulted from carbon with a more diverse consortium of chemical states, and by extension a more complex range of organic compounds. Five synthetic components were fitted to the spectra, to produce the best fit. The binding energy positions of the components were used to determine chemical state assignment candidates, according to Beamson and Briggs (1992) and the component areas, expressed as a percentage of the peak area of the spectra area are presented in chapter 6, Table 6-1.

Table 4-2 shows that component (i) was assigned to aromatic or alkene hydrocarbons and supports the detection of n-alkylated aromatics using THM-GC/MS. Component (ii) was consistent with the presence of aliphatic alkanes. These compounds potentially corresponded to the chain moieties of the fatty acids that were detected in the THM-GC/MS (T=450 °C). Components (iv) (v) and (iv) were consistent with a combination of C-N C-O, and C=O chemical states. The nitrogen peak observed in the high-resolution spectra at 400.5eV (Fig. 4-5a inset) was indicative of an N-C supporting the nitrogen contribution to components (iv) and (v). C-O and C=O compounds were potentially the product of the carboxylic acids moieties of the fatty acid detected in THM-GC/MS (T=450 °C). Component (vii) was indicative of CO_3 and was therefore assigned to inorganic carbon, possibly in the form of calcium carbonate.

The peak at the position of ca. 400 eV indicated the presence of nitrogen in OJP but not in WSD (Fig. 4-5 a and b inset). However, this low nitrogen concentration produced a spectrum with a weak signal to noise ratio. Therefore, any fine structure in the nitrogen spectrum could not be identified. The smoothed peak at position ca. 400.5 eV was consistent with the

presence of N-C bonds, the reciprocal of component (iv), which represented the C-N of the carbon spectrum.

To obtain the carbon and nitrogen high-resolution spectra that were shown in Fig 4-6a, the nine areas shown in Fig 4-5 above were normalised and summed, then synthetic component fitting was conducted using CasaXPS. The minimum number of synthetic components were fitted automatically, using a best fit envelope using a Marquart least squares linear regression analysis within the CasaXPS software. The chemical state identities of the synthetic components were obtained using the National Institute of Standards and Technology (NIST) (www.srdata.nist.gov/xps), La Surface (www.lasurface.com), and Beamson and Briggs (1992) databases.
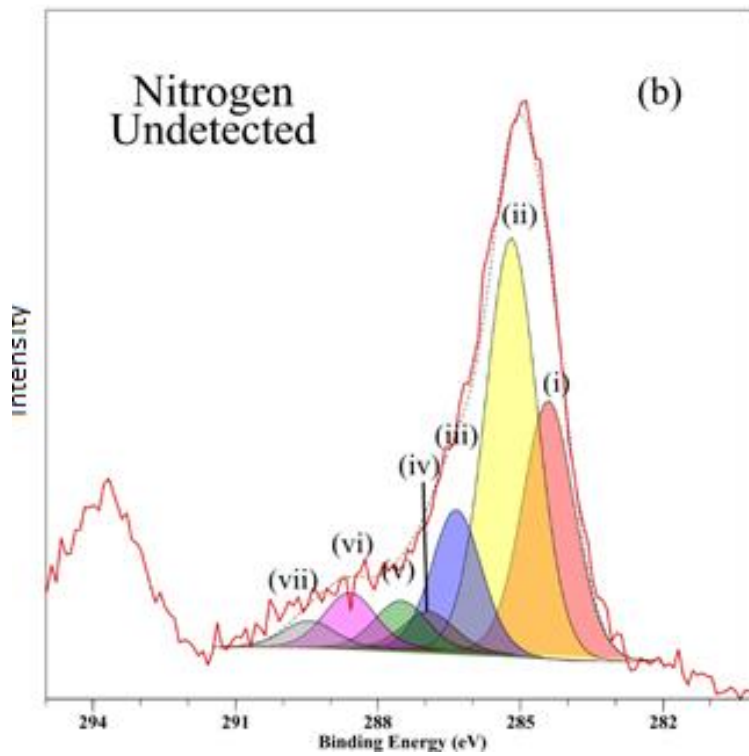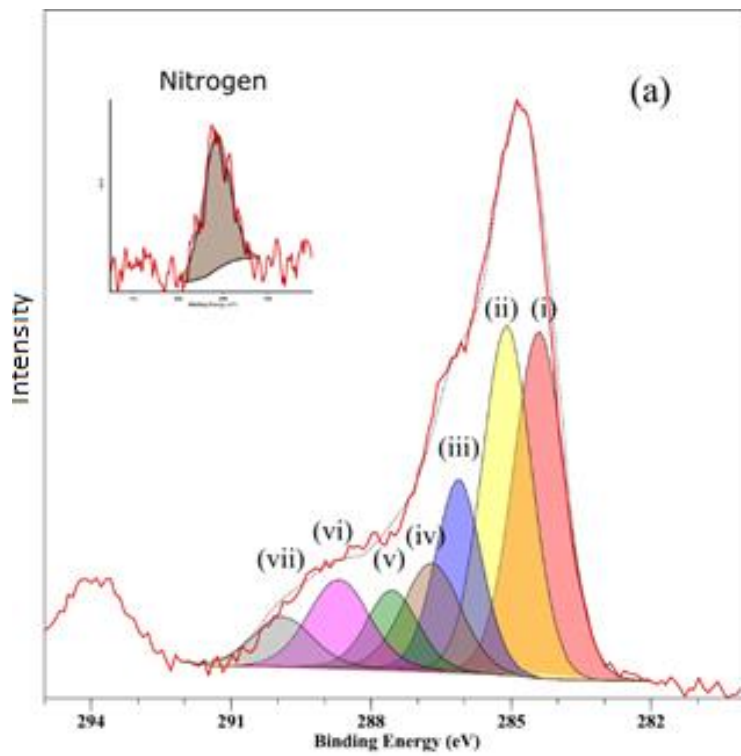
Fig. 4-5 (a and b). *High-resolution XPS spectra with peak component fitting, providing an indication of the chemical states of the carbon. (a) WSD C1s spectrum, nitrogen was undetected (b) OJP_13 C1s spectrum with nitrogen inset spectrum inset.*

Component	Binding Energy (eV)	Assignment	Moiety
(i)	284.6	C=C	aromatic
(ii)	285.0	C-C	aliphatic
(iii)	286.4	C-OH	hydroxyl
(iv)	287.0	C-N	amide
(v)	287.6	C=O	Carbonyl
(vi)	288.6	O-C=O	Carboxyl
(vii)	290	CO_3	Carbonate

Table 4-6. *Presents the key to Fig 4-5a and b, which shows the identities of the synthetic peak components and the areas of these components, indicating the relative concentrations of the different chemical states of carbon in OJP_13 and WSD.*

4.4 Discussion

4.4.1 Optical Petrography

The microtubules observed in The OJP_13 sample were similar in appearance and distribution to those in other OJP_13 samples, which had been previously reported (e.g. Preston et al., 2011; Staudigel et al., 2014). Fig. 4-1a shows a typical basaltic glass shard obtained from the OJP sample used in this study. The surface of the glasses become devitrified (weathered), and this can be observed as the brown perimeter (sometimes described as a rind) of the glass shard a process that is typically attributed to physical and chemical weathering. This result is consistent with the observations made by Banergee and Muehlenbachs (2003) and Staudigel et al. (2006).

4.4.2 Contamination mitigation.

No organic material could be detected in the WSD using py-GC/MS, and trace amounts of material could be detected using THM-GC/MS (for a definition of the term 'trace' see section 8.1.3). This result implied that the UV/O_3 decontamination methods were effective on the WSD, implying that the decontamination was equally effective on the OJP sample. The OJP and WSD core samples were prepared in an identical way suggesting that the organic material detected in the OJP by GC/MS and XPS was indigenous and that the contamination mitigation procedures described in Chapter 3 and in Purvis et al. (2017) had been effective.

4.4.3 Comparison of conventional pyrolysis with Thermally Assisted Methylation (THM)

The THM-GC/MS analysis of WSD detected a single peak identified as azulene, the pyrolysite of TMAH (Morisson, 2017), regardless of the pyrolysis temperature. This indicated that the addition of TMAH did not promote the erroneous detection of organic compounds in either of the rocks that were analysed (see appendix 2). This excluded the possibility that the nitrogen-bearing aromatic compounds detected in the OJP_13 sample using THM-GC/MS analysis, conducted at 610 °C, were the result of procedural artefacts (see appendix 2).

In contrast to the WSD, a range of peaks could be detected and then identified in the OJP samples using both py-GC/MS and THM-GC/MS. This demonstrated the increased effectiveness of THM-GC/MS to detect and identify the organic compounds in the OJP_13 tuff. Therefore, THM-GC/MS analysis of organic material in other types of geological material was considered optimal.

4.4.4 Comparison of Thermally Assisted Methylation (THM) Conducted at different temperatures

Concerning THM-GC/MS and pyrolysis temperature, it is interesting to note that a different set of compounds were identified at the THM conducted at 450 °C, which appeared to contain carboxyl and hydroxyl groups. This finding is perhaps unsurprising when it is considered that these groups are thermally labile and may decompose at elevated pyrolysis temperatures (e.g. Eigenbrode et al., 2011; Stalport et al., 2012). Their detection at the lower temperature (450 °C) is important because the presence of these compounds is entirely consistent with the carboxylic acids that were detected by FTIR microscopy analysis of the OJP_13 sample (Preston, 2011). THM conducted at 1000 °C identified a different set of organic compounds, indicating the presence of higher molecular weight (multi-ring) aromatic compounds.

The THM conducted at 610 °C produced the greatest number of identifiable peaks, and therefore was the most efficient temperature to carry out THM for the analysis of organic material in the geological samples used in the study, and this was unsurprising since 610 ̊C is the Curie point for geopolymers (Stankiewicz et al., 1998). The precise identity of the organic compounds in OJP_13 could not be obtained unequivocally from the current GC/MS data,

132

using the NIST05 database. However, the peak assignments strongly indicated the general class of organic compounds that had been detected with the compounds occurring in the OJP were predominantly composed of functionalised aromatic compounds (see Table 4-1).

4.4.5 Measurement of Organic Material Using XPS

The THM-GC/MS analysis of OJP tuff suggested that functionalised of aromatic compounds were present, some of which were nitrogen heteroaromatic compounds. However, these observations were limited by the confidence that could be placed in the efficient thermal extraction of the entire range of organic compounds during pyrolysis, and their correct identification using the comparison with the NIST mass spectrum library. Therefore, XPS was used to independently corroborate the GC/MS data by measuring the chemical states of the organic material.

XPS analysis directly measures organic material in the sample without a pre-extraction step. Thus, the correlation between the class of organic compound detected using THM-GC/MS, and the carbon chemical states data obtained by XPS provided further corroborative evidence that nitrogen bearing aromatic compounds identified by THM-GC/MS was not the misidentification of organic material by the mass spectra library algorithms or artefacts of the thermal extraction process. The comparison to the published values for basalt composition demonstrated the XPS data was consistent with the data reported in the literature implying that carbon and nitrogen measurements were also accurate to the same extent (Purvis et al., 2017).

4.4.6 Heterogeneous Distribution of Carbon and Nitrogen in OJP_13

Due to the analysis of the OJP_13 sample using FTIR microscopy that was reported by Preston et al. (2011), it had been anticipated that XPS measurements would have resulted in the highest concentration of nitrogen and carbon in the perimeter (tubule-rich region) in the perimeter of the glass shards. However, while there was variation in the carbon and nitrogen surface concentration, this did not correlate to any specific type of texture. There were two potential reasons for this observation. Either the low-resolution images that can be obtained by the XPS targeting camera resulted in imprecise targeting of the XPS's beam spot. Alternatively, there was no correlation between the three different textures of the OJP_13

(matrix, centre and perimeter). This anomaly is addressed by the research described in Chapter 5.

4.4.8 The Carbon Chemistry of OJP_13

The XPS analysis of the OJP_13 tuff suggested the presence of C=C, C-C and C-N chemistry (Table 4-2) and these chemical states were consistent with the alkylated nitrogen heteroatomic aromatics identified by THM-GC/MS. Likewise, the C=O and C-O, along with detection of C-C chemistry, were consistent with aliphatic and fatty acids, which were also identified by THM-GC/MS. Therefore, the carbon chemical state data obtained using XPS provided further evidence that the identities of the compound classes obtained by THM-GC/MS were correct. Significantly, the assignments of these synthetic components to the chemical states presented in Table 4-3 correspond with the chemical bonds found in the organic compounds that were detected in the THM-GC/MS.

Also, the chemical states consistent with aliphatic compounds and fatty acids were detected by XPS, which supports the detection of these compounds using THM-GC/MS (T= 450 °C), providing further evidence that the compounds that were identified by the THM-GC/MS were not an artefact of the thermal extraction process. The presence of aliphatic hydrocarbons, amides and fatty acids observed in this study also supported the earlier FTIR microscopy investigation of OJP (Preston et al., 2011). However, in contrast to the FTIR microscopy investigation. The investigation here also detected aromatic compounds using THM-GC/MS, and this was supported by the identification of a C=C component in the XPS data. This observation concurs with the carbonaceous material detected in desert regoliths and their analogues using XPS (see Chapter 8). The reasons for this are not clearly understood presently, and the mechanism for this selective non-detection by FTIR may be a function of the depth of analysis (see Chapter 8, Fig. 8-6).

4.5 Conclusions

This chapter showed that the OJP_13 sample selected for this thesis did indeed possess the microtubular features that were comparable to those that had previously reported. Therefore, THM-GC/MS and XPS were both able to measure the organic material in the OJP and by implication, the other geological samples studied in this thesis. This chapter

demonstrated that surface analytical techniques, such as XPS, can accurately measure and quantify the chemical states of organic material in geological samples without an extraction step before analysis. Flash pyrolysis before GC/MS was conducted at different temperatures, and this indicated that the optimal temperature for this was 610 ℃ and that the addition of TMAH increased the efficiency of detection. Therefore, the THM at 610 ℃ was used as the standard technique for the remainder of this instigation. The compounds identified by the THM-GC/MS could be utilised to identify the mass fragments in Chapter 5. A comparison of the OJP_13 (containing alteration textures) and the WSD showed the organic material was compositionally different and critically the OJP appears to possess nitrogen compounds and the THM-GC/MS analysis indicated as substitutions within aromatic rings (i.e. pyrroles and pyridines). The results in this chapter showed that GC/MS data could be used to support the analysis of organic material in geological samples using XPS. Reciprocally, XPS was also able to detect a component of the organic material in WSD that was undetectable by THM-GC/MS. The composition of the organic material implied that it was the product of diagenesis, rather than the types of compounds that would be produced by an extant organism. However, the presence of nitrogen substituted aromatic compounds in the OJP_13 sample was unanticipated, and these conclusions were investigated in Chapter 7. The detection with XPS of aromatic carbon in WSD was also not anticipated and was investigated in Chapter 8.

The implications for this chapter are that XPS could be used to support the characterisation of organic material in rock in both telluric paleobiology and planetary exploration for the detection of molecular biomarkers.

CHAPTER 5: THE CHARACTERISATION OF THE LATERAL DISTRIBUTION OF ORGANIC MATERIAL IN AN ONTONG JAVA PLATEAU SAMPLE CONTAINING MICROTUBULE STRUCTURES

Abstract

This chapter focuses on the analysis of organic matter and how it is distributed in relation to features and petrographic textures in the Ontong Java Plateau tuff. This investigation was carried out by elaborating upon the XPS analysis that was described in Chapter 4 and by using a J105 time of flight secondary ion mass spectrometer (ToF-SIMS). The data obtained using THM-GC/MS from Chapter 3 was used to obtain the molecular assignments for some of the mass fragments that were obtained using ToF SIMS. The XPS analysis described in Chapter 4 had indicated that the organic material was heterogeneously distributed, but no specific correlation with the microtubular features could be ascertained. However, in this chapter, the data obtained from the J105 indicated that a correlation between the different parts of the OJP_13 could be observed. Specifically, those regions in the sample that were either rich or poor in microtubule textures and the composition of the organic compounds detected in those microtubule-rich and microtubule-poor regions. These results demonstrated that the J105 ToF-SIMS, using an Ar GCIB primary beam, was effective at detecting organic materials in geological samples. Furthermore, the J105 ToF-SIMS, combined with XPS and THM-GC/MS, can be used to match morphological features with their organic and inorganic composition at the μm scale. It is possible to conclude that the J105 may be a useful instrument for the study of organic material in paleobiological, geochemical, cosmochemical and astrobiological relevant samples.

5.1 Introduction

The results presented in Chapter 3 demonstrated that adventitious carbon could be removed from the surface of geological samples, using GCIB etching. In Chapter 4, it was shown that organic material in the OJP tuff from Hole 1184A, core 13R (OJP_13; for the location of this sample, see Table 2-1) could be detected. The analysis in Chapter 3 was conducted using both XPS and THM-GC/MS, which indicated that the identities of the organic compounds that were detected using GC/MS, were comparable chemical state data was obtained using XPS. The investigation in chapter 4 demonstrated that the GC/MS bulk analytical and the XPS surface analytical approaches, used in combination, could be an effective method for the analysis of the OJP_13 sample. Chapter 4 described how the XPS analysis was conducted on three different textures within the OJP_13 sample, on the centre of the shards, where the density of the microtubules is low, in the perimeter of the shard where the microtubule density is highest and in the surrounding lapilli matrix. However, contrary to expectation, no correlation between the tubule-rich perimeter and the nitrogen concentration was observed (see section 4.2.5). The weathered microtubule-rich perimeter, the microtubule-poor, vitric centre, and the surrounding matrix are collectively described as the petrographic textures. Since no correlation at the µm scale could be discerned, mapping of an entire OJP_13 shard along with the surrounding material was required. This mapping was achieved using XPS, nanoSIMS and the J105 time of flight secondary ion mass spectrometer (ToF SIMS).

5.1.1 Surface Analysis for Imaging

Surface analysis techniques can measure a specific spot on the surface sample directly. Many discrete measurements can then be conducted sequentially over the surface of the sample which can generate a mass spectral 'pixel'. These arrays of 'pixels' can then be used to generate an image based on spectral data. Each of the pixels is composed of many mass fragments, which represent data with high numbers of dimensions, which cannot be plotted into a single two-dimensional chart, that can be readily interpreted. Therefore, Principle Component Analysis (PCA) is frequently used to interpret the complex mass spectra data that are generated by ToF SIMS, by reducing the multidimensional mass spectral data, into a

single dimension containing the maximum amount of variation and disregarding the variables with the least amount of effect on the data set.

5.1.2 Principle Component Analysis

Principal component analysis (PCA) can condense the mass spectral data obtained from ToF SIMS (see section 1.12.5). PCA is a statistical procedure that converts a set of observed variables that are possibly correlated into a set of values of variables called principal components. The transformation is conducted in such a way that the first principal component is a vector that passes through the data points that produce the largest possible variance in the data, i.e. the data values that account for as much of the variability in the data as possible, which can be thought of as a line of best fit through the maximum variation.

The weight of each standardised original value can then be multiplied to get the component score. These are thought of as the 'variance' between the data point and the line of best fit. In PCA these variances are called the 'loadings'. The weight of the loadings (i.e. the amount of variance) can then be assigned a colour and then plotted as a pixel corresponding to the position on the sample where the data was acquired. This plot can be used to generate an image that can highlight regions of differences or similarities that can allow the ready identification of patterns in the distribution of the mass spectra. In the application of PCA to ToF SIMS analysis, the data points are the masses of the ions. Once ion masses can be assigned to a molecule, using THM-GC/MS analysis, then the distribution of molecules across the sample surface can be mapped.

5.1.3 Electron Microscopy

Scanning electron microscopy (SEM) coupled to energy dispersive spectroscopy (EDS), which is sometimes called X-ray dispersive spectroscopy (XDS) was conducted upon two samples of OJP that had been cleaned using UV/O$_3$ (see chapter 3). The samples used for SEM/EDS were not cut or trimmed. This analysis was carried out to ascertain whether the observations that had been made using the ToF SIMS were unique to the sample that was used in that particular analysis and the whether any observed organic material was the result of the sample preparation process.

5.2.0 Methods

5.2.1 Sample Preparation

The OJP_13 sample (see table 2-1) is described in Section 4.2.1 and was used in chapter 4 and was re-used for this investigation. Optical microscopy was used to identify a suitable glass shard using an Olympus CR32 Microscope, and the region of the shard was photomicrographed using an in-line mounted Olympus OM-D Mark II camera. A mosaic image was produced. The target shard region was marked on the glass slide below the target shard region. A suitably sized target shard was selected, which would be bounded by the grid array footprint, and therefore, regions of the OJP_13 that were tubule-poor, tubule-rich and lapilli matrix material could be measured.

5.2.2 X-ray Photoelectron Spectroscopy of OJP_13

The limitation in beam targeting precision was caused by the low-resolution images that were obtained by the XPS K-alpha targeting camera, which did not permit the accurate identification of the tubules-rich regions. Therefore, the precise targeting on the perimeter region of the glass shard with any attendant microtubules needed to be approximately estimated in the investigations described in Chapter 4 (see Fig. 4-5). To overcome this drawback, XPS analysis was carried out sequentially over an area of the OJP_13 sample that contained an entire shard. This was done by producing a grid composed of a 30 x30 array of cells with each cell in the grid being $50\mu m^2$, this grid covered a 1.6 mm^2 area on the sample (See Fig. 5-1). Carbon, nitrogen and silicon high-resolution XPS scans were conducted in each of the cells in a raster pattern. The area for each scan was $35\mu m^2$ on the shard that was designated as 'snail'. In this way, the XPS spectra containing chemical state information was co-localised to the different textural regions.
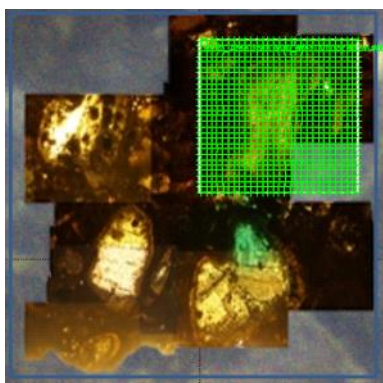
Fig. 5-1. *Showing the analysis grid array using for the XPS analysis, superimposed over the target shard called 'snail', each cell of the array was analysed to produce a map of the carbon and nitrogen chemical state and concentration associated with this shard.*

An XPS heat map of the snail shard (See Fig. 5-2) was produced to visualise the surface concentrations of the carbon and the nitrogen using the Advantage software package (Thermo-Fisher Scientific, East Grinstead, UK) that was installed on the Theta probe XPS instrument. The concentrations were assigned a colour from the 'heatmap' colour palette according to their surface concentration. The black colour was low concentration, and the bright yellow was high concentration. These colours were then plotted to their coordinates on the grid to produce a 'heatmap' image with the scaling adjusted to obtain the maximum contrast.

5.2.3 Time of Flight Secondary Ion Mass Spectrometry Analysis of OJP_13

The 50µm^2 spatial resolution of the XPS analysis grid (Fig. 5-1) was insufficient to resolve specific regions within the shard. Therefore, ToF SIMS analysis was conducted on an OJP_13 shard to determine the lateral distribution of the mass spectra across the surface of the sample at a 2µm^2 spatial resolution.

Two sets of ToF SIMS data were obtained. Firstly, high-resolution maps were obtained from a PHI TRIFT V nanoTOF (Ulvac, Inc. Kanagawa, Japan), using bismuth as the primary ions. Secondly, from a J105 (Ionoptika, Southhampton, UK) using its argon gas cluster ion beam (GCIB) as the primary ion source. The argon gas clusters sizes were centred around an average of 4000 atoms per cluster.

The data for the PHI TRIFT V was unprocessed, and the J105 data was processed using PCA using a MATLAB programme (uk.mathworks.com) that was written for this purpose. This mass spectral information was correlated to the THM-GC/MS molecular identity data that was described in Section 4.2.3, to obtain candidate molecular identities of the mass fragments that were obtained by the ToF SIMS analysis.

5.3 Results

5.3.1 Optical Petrography

Fig. 5-2 shows the background image obtained using the K-alpha XPS targeting camera. This demonstrated that a sufficiently high-resolution image could not be acquired from the XPS targeting camera to accurately discern the tubule-rich regions of the glass shards (Fig. 5-1). Therefore, accurate targeting of a glass shard was not possible. The targeting problem was resolved by using a high contrast photomicrograph image (bounded by a red box in Fig. 5-2) that was superimposed over the XPS targeting camera image. This image shows three labelled glass shards that were called 'snail', fish and 'Australia'. In the 'Queensland' part of the 'Australia' shard is the location marker on the underside of the mount. The area of the red box is ca. 3.2 mm x 3.2 mm. This image demonstrated that optical microscopy could resolve the rind of the weathered perimeter of the glass shard and that a dark region within this perimeter was a result of the microtubules (see Section 3.3.1). However, since the samples were required for surface analysis, no coverslip was used. Therefore, these images were not as clear as those shown in Fig. 4-1. The XPS analysis area was superimposed over the 'snail' shard, (bounded by the blue box in Fig. 5-2), and the area was 1.4 mm × 1.4 mm bounding the target shard.
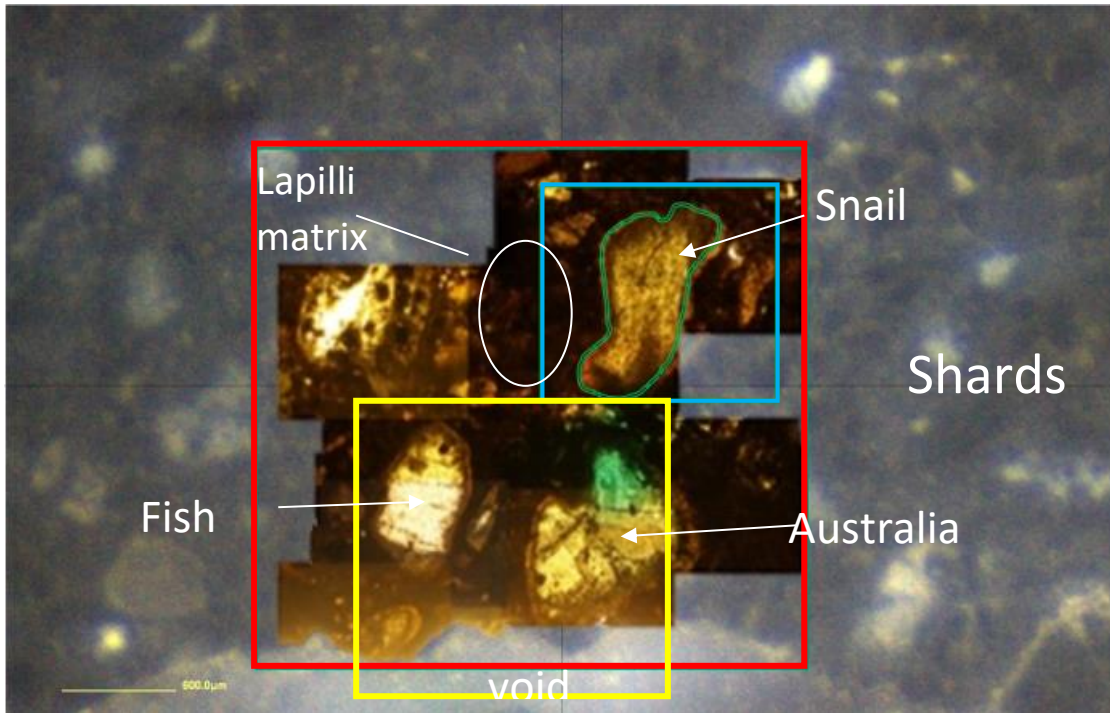
Fig. 5-2. *The background image is the XPS targeting camera image. The optical microscope image (red box). The XPS PHI TRIFT V analysis area (blue box). The J105 ToF SIMS analysis area (yellow box). The perimeter of the snail shard (outlined with two green lines). Note the orange/brown devitrified rind in the 'Fish' and 'Australia' shard and the void region at the bottom of the image. Note: The area below the edge is preparation artefact resulting in a void caused by the unintentional removal of material during the sample sectioning.*
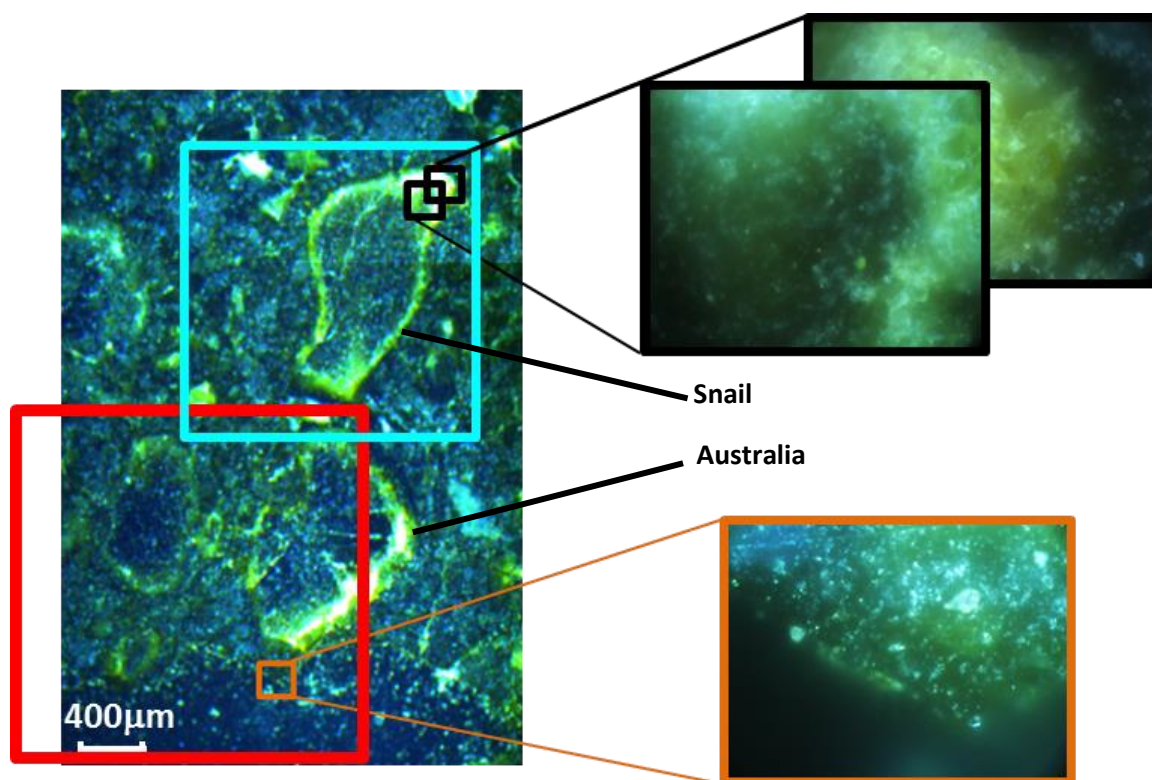
Fig. 5-3. Shows *the optical microscope images of Snail and Australia, using the Leica DFC450C microscope at x20 magnification with corresponding detailed x40 images (black and orange boxes). This image is the same region of the OJP_13 observed using the Olympus microscope in transmitted light mode (Fig. 5-2). The blue box bounds the snail shard that was analysed using the XPS PHI TRIFT V. The red box bounds the J105 ToF-SIMS analysis area. Credit: AIP, see permissions (page ii).*

Fig. 5-3 demonstrated that in contrast to the images obtained by transmitted light, the images obtained using top lit green filtered light were able to highlight the perimeter of the shards. This highlighting was caused by the back-scattering of light, which was the result of the basaltic glass being amorphous (i.e. weathered or devitrified) glass, rather than being crystalline. The region of the image bounded by the black rectangles and shown at x40 magnification show that the devitrified glass area corresponding to the carbon and nitrogen-rich region that was observed in the XPS analysis (see Fig. 5-4).

5.3.2 The Distribution of Carbon and Nitrogen in the Region of a Glass Shard Using Sequential XPS Analysis
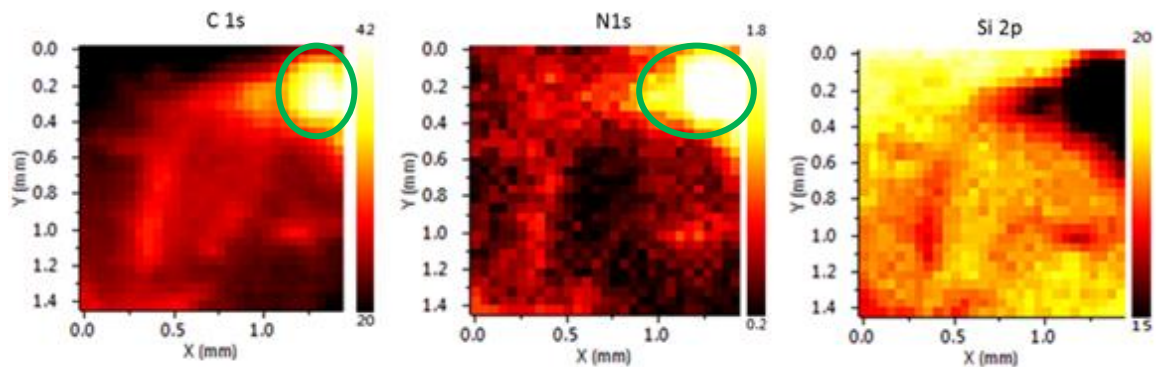
Fig. 5-4. *Showing the heat map image of the high-resolution carbon, nitrogen and silicon XPS scans of the snail shard (Blue boxes in Figs 5-3 and 5-3). The vertical bar on the left-hand side of each of the images shows the colour scale used, the numerals at the top and the bottom of the sample are the bounding values for the scale in at%. The green box bounds the 'hot spot' the area of the analysis that contained a high concentration of organic carbon and nitrogen. Credit: AIP, see permissions (page ii).*

Fig. 5-4 show the distribution maps of carbon, nitrogen and silicon obtained by XPS. A comparison of these maps showed that carbon and nitrogen are co-located in the perimeter of the shard and the area of the high concentration hot spot, bounded by the green ellipse. While the nitrogen appears to be distributed through the lapilli matrix and is depleted in the centre of the shard, whereas the carbon concentration appears to be more elevated, in the region of the snail shard. The surface concentrations plotted here, are presented as the percentage values. Consequently, the distribution of the silicon shows an anti-correlation with the carbon distribution, since the carbon increases the relative silicon concentration is decreased. The maximum concentration of nitrogen is 1.8 at% and therefore has little impact on the overall relative surface concentrations.
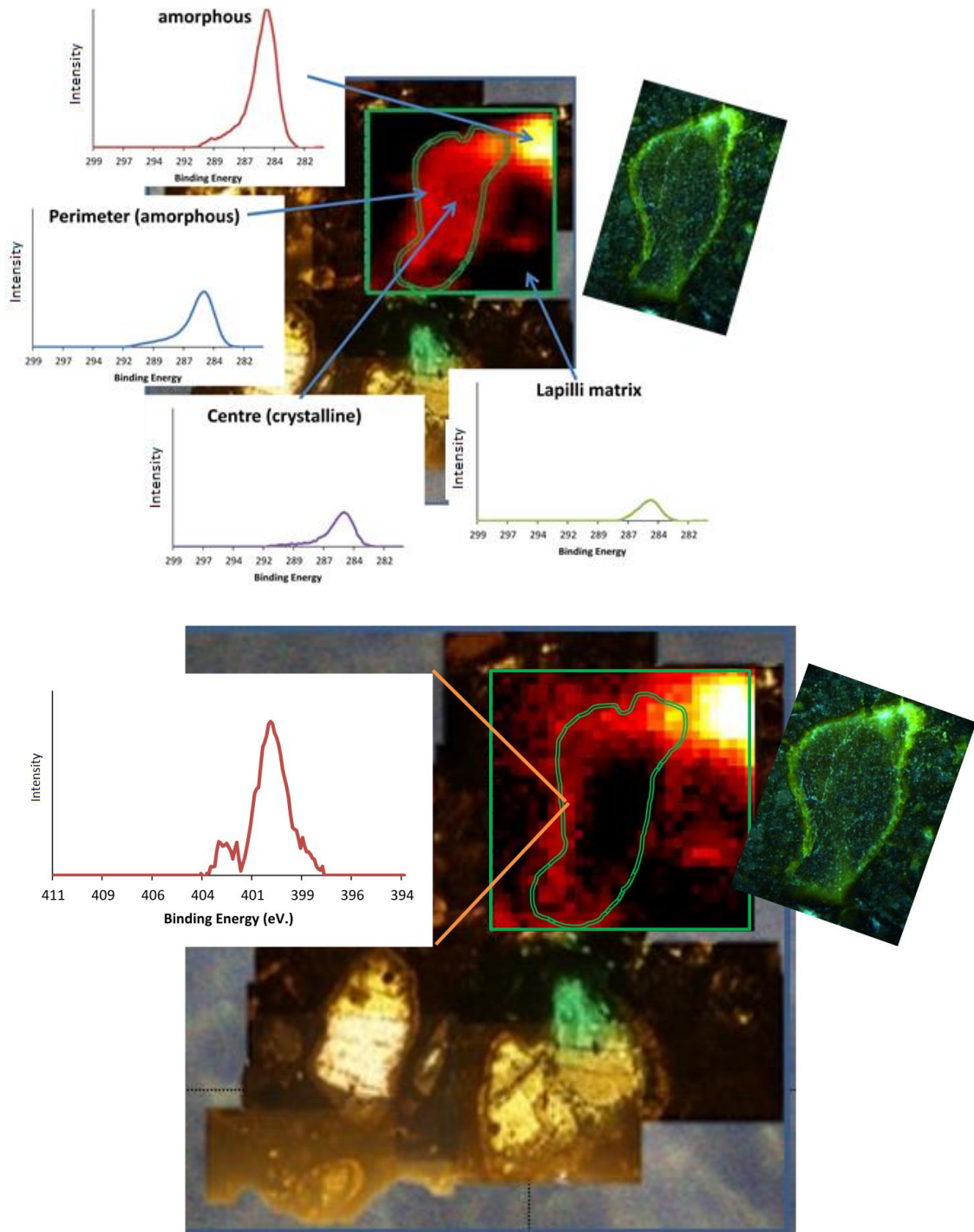
Fig. 5-5. *Examples of the high-resolution spectra, carbon (top) and nitrogen (bottom) from different regions of the snail shard in the XPS analysis area that were acquired. The image adjacent highlights the regions of devitrified (weathered glass).*

145

Fig. 5-5 (top) showed the chemical states of the carbon within the 'snail' shard and the surrounding lapilli matrix, within the XPS analysis area, and examples of the spectra that were obtained from the different regions were presented. The carbon concentration was elevated in the region of the shard. However, in addition to this, a region of high carbon concentration was measured in outside the shard (in the upper right of the analysis area) this concentration was higher than the carbon concentration in the region of the shard. The peak shift demonstrated that the chemical states of the carbon were different in different regions of the sample. The Table 4-3, in section 4.3.5, showed the chemical state assignments of the synthetic peak components, which provided an indication of the types of carbon compounds in the different regions of the glass shard and the surrounding matrix.

Fig. 5-5 (bottom) showed the distribution of the organic nitrogen within the 'snail' shard and the surrounding lapilli matrix, which is bounded by the area of the XPS analysis. This figure showed that nitrogen with a chemical state of N-C was present, at an elevated concentration, in the region of the shard perimeter. A high nitrogen concentration in the upper right corner of the analysis area was co-localised to the high carbon surface concentration was also observed, indicating that this devitrified glass region was rich in C-N compounds.

5.3.3 Time of Flight Secondary Ion Mass spectrometer Analysis of the OJP_13 Glass Shards

ToF-SIMS analysis was required to investigate the lateral distribution molecules in the OJP_13 specimen at a greater spatial resolution than the XPS sequential analysis described in the previous section. This analysis was carried out by two different instruments. First, the PHI TRIFT V S-SIMS, and second, an Ionoptika J105 ToF SIMS.

The PHI TRIFT V nanoTOF instrument used a Bi_3^{++} primary ion beam that was able to obtain a relatively high spatial resolution. However, it was not able to confidently detect mass fragments that were greater than 100 u. The positive ion images are shown in Fig. 5-6 and were obtained by the mosaic mapping mode over a 1.6 mm × 1.6 mm analysis area, covering the 'snail' shard used in the XPS analysis. Unsurprisingly, the centres of the shards contain inorganic elements such as Si, Al and Fe. These elements are consistent with the values of typical sub-oceanic basalts (McBride and Gilmore, 2004) that are measured using

146

X-ray fluorescence and are consistent with the elements detected by the XPS survey analysis of basalts (see section 3.2.1).

In addition to the inorganic elements, a 30 u mass fragment was assigned to the CH_4N^+ ion. The distribution of this ion showed an anti-correlation to that of the inorganic fragments other than the region of the glass shard. This anti-correlation is consistent with the XPS mapping of carbon and nitrogen, as shown in Fig. 5-4. These results suggested that organic material could be located in the glass shard area ,and also in crack-like textures, that is hereafter described as microfractures. However, since higher molecular weight organic compounds could not be detected using the PHI TRIFT V, a fuller characterisation of the molecular identities of the organic compounds was required.
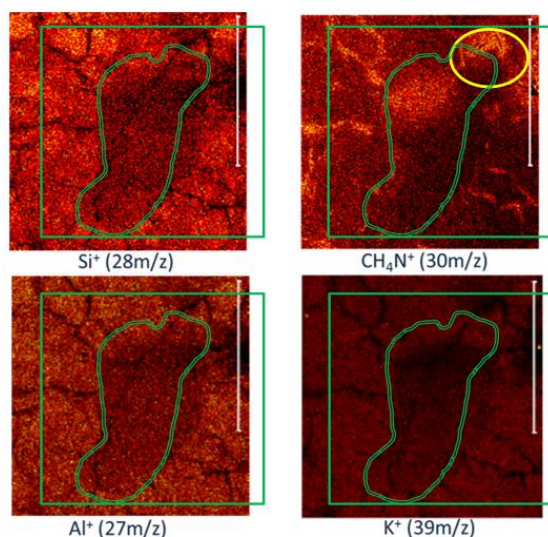
FIG 5-6. *Si^+, Al^+, K^+ and CH_4N^+ PHI TRIFT V ToF SIMS (positive ion) images of snail shard (1.6 mm × 1.6 mm) using Bi_3^{++} source. The green outline is the perimeter of the shard. The yellow ellipse is the 'hot spot' area observed in the XPS analysis shown in Fig. 4-4. All scale bars are 1mm. Credit: AIP, see permissions (page ii).*

An additional analysis was conducted on a second area, utilising an Ionoptika J105 instrument with an Ar GCIB as the primary ion beam. The argon cluster primary ion source in the J105 was used for the additional analysis because the energy spread in the Ar GCIB permitted the detection of higher mass fragments than the Bi_3^{++} ion source of the PHI TRIFT

V and therefore was able to obtain additional organic molecular information from the sample. A different area of the sample was selected to avoid the region that may have been damaged by the X-ray and the Bi^{++} ion beam during the previous XPS and ToF-SIMS analyses. A region was identified that contained glass shards using optical microscopy (Figs. 5-2 and 5-3) and selected for analysis with the J105. The red square in Fig. 5-3 highlighted the area of analysis. Unlike the positive ion, images were taken using the Bi^{++} ion source, as shown in Fig. 5-4. A greater range of higher molecular weight fragment peaks between 40 u and 400 u were detect using the argon GCIB source. However, the positive ion images using the argon GCIB source did not provide good contrast between inorganic fragments and organic fragments for the tubule-poor centre of the shard and the tubule-rich perimeter of the shard and the surrounding lapilli matrix.
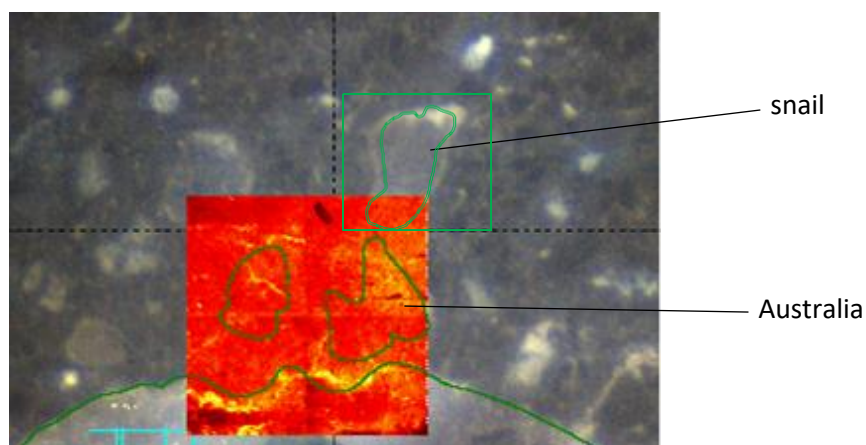
Fig. 5-7. *Optical microscope image showing the positions of GCIB ToF SIMS total ion image. 'Fish' and 'Australia' shards and the void perimeter outlined in green. 'Snail' is outlined for orientation. Credit: AIP, see permissions on page ii.*

PCA was carried out on the J105 data, to characterise the lateral distribution of the molecules in the OJP_13 sample. It had been anticipated that the first principal component, i.e. the one with the greatest variation (PC1: 24.9%) representing the total ion image of the analysis area would highlight the greatest differences in the organic chemistry in the target area. Surprisingly, as Fig. 5-8 (next page) illustrates the loading plot of PC1 did not produce any significant contrast between the textures.
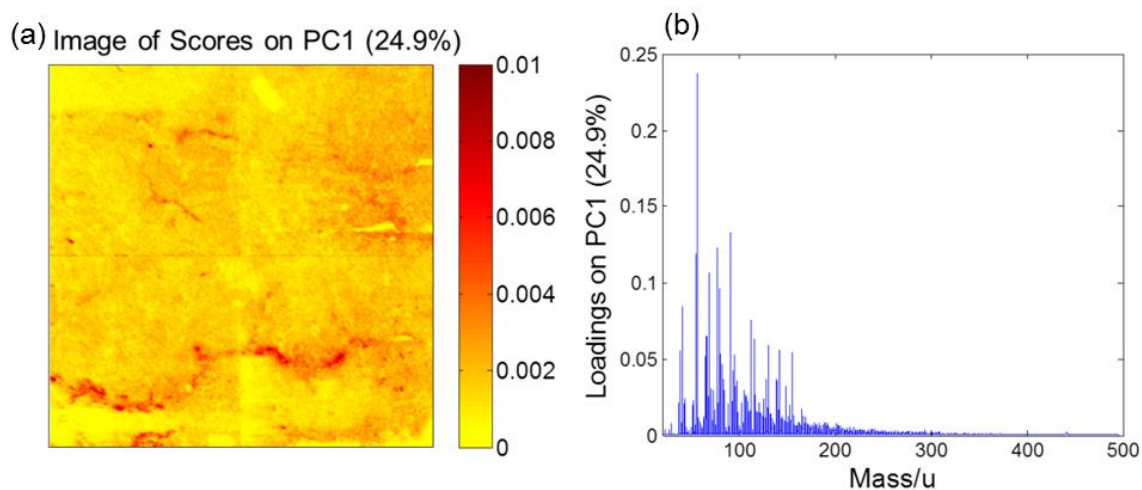
Fig. 5-8. *Score image (a) and loading plot (b) of PC1 (24.9%).*

Surprisingly, it was the second principal component (PC2) derived from 8.8% of the variance, which provided the best contrast between the areas (see Fig. 5-9; next page). Thus, PC2 most clearly highlighted the differences in the composition of the organic material in the analysis region. PC2 was able to distinguish two sets of organic compounds, those that were positively weighted and those that were negatively weighted. *Credit: AIP, see permissions (page ii).*

The positive values in the score plot of the PC2, corresponded to the matrix and glass shard areas, and both organic and inorganic fragments in the positive loadings were observed. The main organic fragments were assigned aromatic hydrocarbons such as $C_6H_5^+$, $C_7H_7^+$, $C_9H_7O^+$, and $C_{10}H_{13}O^+$. Also, some inorganic fragments assigned to K^+, Ca^+, Fe^+, Si^+ and Al^+ were also observed on the loadings plot, although the loading weights were not strong enough to be distinguished using the scales in the plot shown.

In contrast, the negatively weighted loadings co-located to regions that corresponded to fractures in the OJP_13 specimen. The negative loadings showed a greater number of fragments that correspond to nitrogenous organic compounds, for instance, CH_4N^+ (m/z 30); $C_5H_8N^+$ (m/z 82) and $C_8H_{16}N^+$ (m/z 126) were obtained. Furthermore, a greater number of alicyclic hydrocarbons, alkene or alkane could also be detected in the negative loadings,

149

such as $C_4H_7^+$ (m/z 55); $C_5H_9^+$ (m/z 69); $C_7H_{13}^+$ (m/z 97); $C_8H_{13}^+$ (m/z 109); $C_{11}H_{23}^+$ (m/z 155); $C_{12}H_{25}^+$ (m/z 169) and $C_{14}H_{19}^+$ (m/z 187).
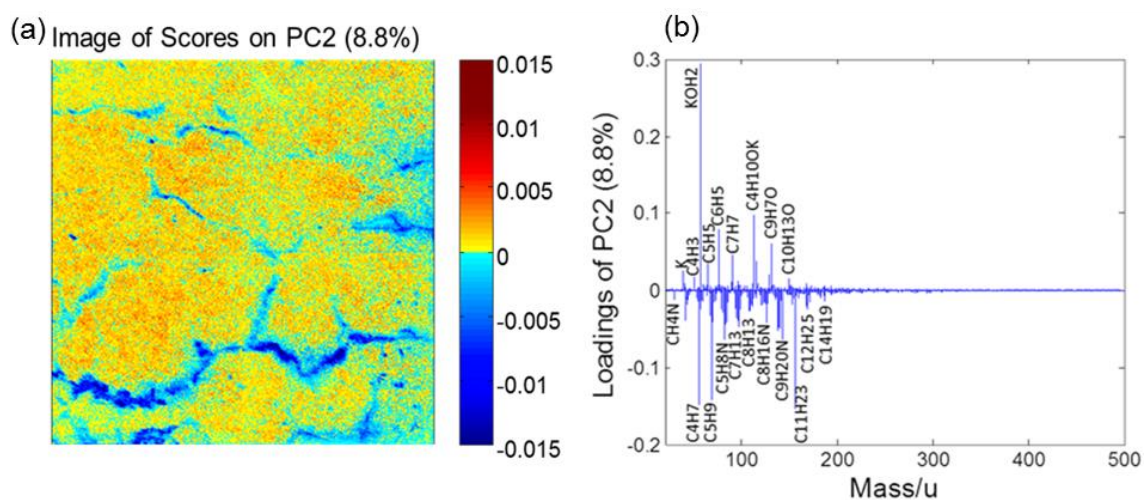
Fig. 5-9. *Core image (a) and loading plot (b) of PC2 (8.8%). Positive scores relate with the inside of the glass shard and the matrix, and negative scores correlate with the non-crystallised area and the fracture areas. Credit: AIP, see permissions (page ii).*

The results presented in Chapter 4 demonstrated that the molecular information obtained from THM-GC/MS were complementary to the surface analytical techniques, such as XPS. This suggested that other surface analytical techniques, such as the SIMS, could also be similarly comparable. This chapter demonstrated that the THM-GC/MS data was indeed complementary to the mass fragments that were obtained in the ToF-SIMS analysis described in this chapter.

Consequently, the molecular compounds that were detected by THM-GC/MS analysis (described in section 4.3.3) were compared to the identities of the J105 ToF SIMS mass fragments and these compounds are shown in Table 5-1. The assignments were used as supporting data for the identification of the mass fragments obtained from the PCA loadings (Fig. 5-8) of the ToF SIMS data. The suggested chemical structures of the SIMS fragments are presented in Table 5-2. For example, the fragments from the PCA loadings of the devitrified/weathered rind and the fracture areas are thought to be in the form of cyclo-octene (m/z 109, $C_8H_{13}^+$); indolizidine (m/z 126, $C_8H_{16}N^+$) and undecane (m/z 155, $C_{11}H_{23}^+$),

150

which were compounds that were identified based on the THM-GC/MS analysis and described in Chapter 4. It should be noted that C_7 and C_8 rings are not normally encountered in naturally occurring biochemical or geochemical samples. However, these rings can form during SIMS analysis when normal C_6 aromatic compounds are fragmented by the primary ion beam, which then recombines as artificially formed C_7 and C_8 rings. Thus, the presence of C_7 and C_8 ring compounds can indicate that aromatic compounds are present in the sample.
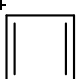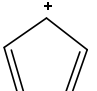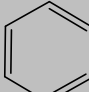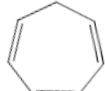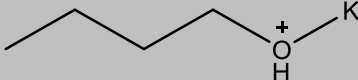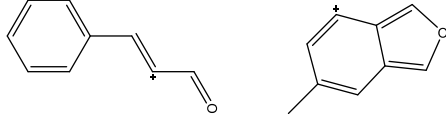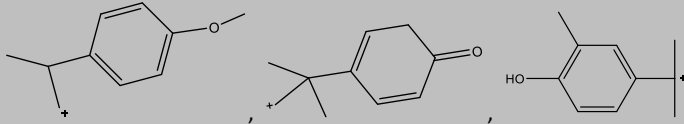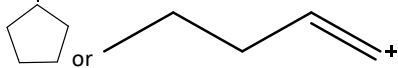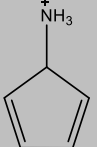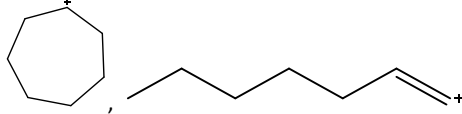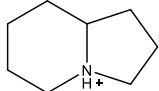
Although organic fragments were observed across the entire region under analysis, the composition of the suggested fragments on the matrix and glass shard areas were different from those on the devitrified glass and the microfracture areas. The data suggested that aromatic compounds and ethers were detected across the entire analysis area. Alicyclic hydrocarbons, alkanes and alkaloids were observed as dominant components on both the weathered rind/devitrified glass of the shard and within fractures of the surrounding lapilli matrix.

Table 5-1 *Candidate molecules and chemical formulae identified by THM-GC/MS analysis (see chapter 4)*

Molecular weight	Name	Chemical Formula
94.11	Phenol	C_6H_6O
108.14	Cresol	C_7H_8O
118.14	Benzofurans	C_8H_6O
120.20	Trimethylbenzene	C_9H_{12}
122.17	Xylenol	$C_8H_{10}O$
134.21	Durene	$C_{10}H_{14}$
137.22	Cyclopentenyl pyrrolidine	$C_9H_{15}N$
148.20	Dimethylphenyl ethanone	$C_{10}H_{12}O$
148.25	Pentamethyl benzene	$C_{11}H_{16}$
162.22	Methylphenyl propanal	$C_{11}H_{14}O$
256.33	Bisphenol C	$C_{17}H_{20}O_2$

Table 5-2 *Candidate chemical structures of characteristic positive fragment ions from the loadings of PC2 (8.8%). Credit: AIP, see permissions (page ii).*

	Mass	Empirical formula	Chemical structure
Positive loadings	41	K^+	K^+
	51	$C_4H_3^+$	
	57	KOH_2^+	K—$\overset{+}{OH_2}$
	65	$C_5H_5^+$	
	77	$C_6H_5^+$	
	91	$C_7H_7^+$	
	113	$C_4H_{10}OK^+$	
	131	$C_9H_7O^+$	
	149	$C_{10}H_{13}O^+$	
Negative loadings	30	CH_4N^+	H_2C—NH_2
	55	$C_4H_7^+$	H_2C
	69	$C_5H_9^+$	or
	82	$C_5H_8N^+$	$\overset{+}{NH_3}$
	97	$C_7H_{13}^+$	
	109	$C_8H_{13}^+$	
	126	$C_8H_{16}N^+$	
	155	$C_{11}H_{23}^+$	

5.3.3 Scanning Electron Microscopy with Electron Dispersive Spectroscopy

SEM microscopy was not conducted in the same region as the light microscope region since the high energy electron source of the SEM would potentially damage any organic material in the region of the OJP_13 that had been prepared for surface analysis. However, the SEM images presented in Fig. 5-10 demonstrated that the lapilli matrix contained a number of cracks and that the EDS analysis showed that these cracks were infilled with carbon. The region bounded by a green ellipse showed a false positive for carbon. This was the result of the build-up of an electrical charge on the surface of the sample caused by the X-ray irradiation.
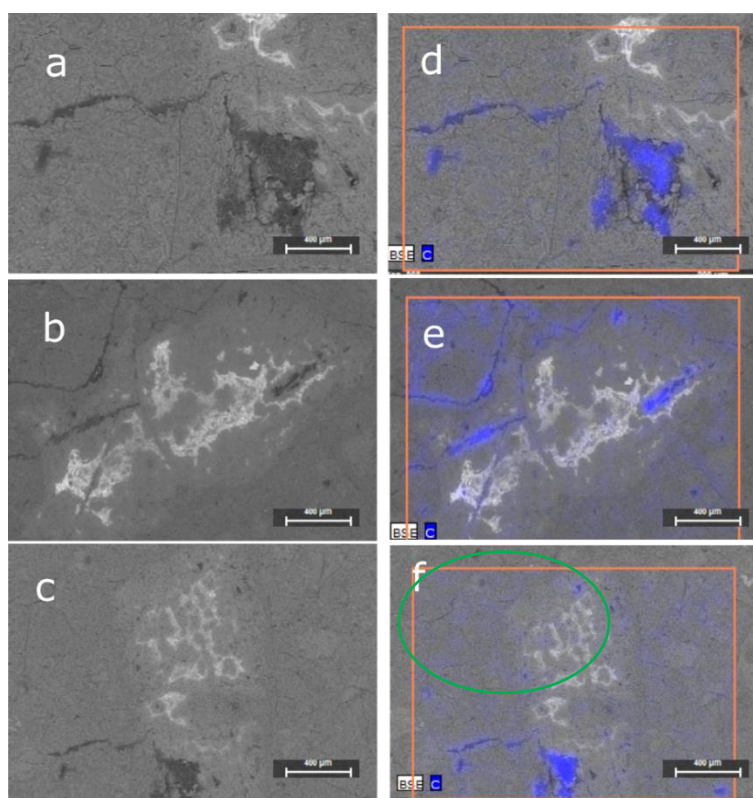
Figs 5-10 a-c. *Scanning electron micrographs (SEM) of OJP_13 sample (x50). The three sections were taken from different areas of the OJP-13 sample used in this investigation.* **Figs d-f:** *the distribution of carbon obtained by energy dispersive spectroscopy images (EDS). This distribution is superimposed upon the corresponding SEM image to its left.*

5.4 Discussion

By using several different analytical approaches, it was possible to assign specific compounds to particular regions of the glass shards, specifically to the tubule-rich, tubule-poor and lapilli matrix textures of the OJP_13. The data obtained in this chapter was able to differentiate between organic compounds in the weathered rinds of the glass shards of the OJP_13 sample. Aromatic hydrocarbons and inorganic elements were observed in the

surrounding lapilli matrix and the non-weathered interiors of the glass shards. The distribution of the different types of organic molecules indicated that a positive correlation existed between the presence of microtubule textures and the higher concentration of specific classes of organic molecules.

The centres of the basaltic glass shards have a vitric texture, which was formed through rapid quenching in either water or air. The surfaces of basaltic glasses are susceptible to weathering. The weathering results in the decomposition of the vitric texture and this process often has a microbial component, e.g. (Marshall, 1961; Smits, 2006a). It is speculated here, that the microbially assisted devitrification process could release a range of trace nutrients for any microorganisms that are associated with the rock. Therefore, it is perhaps unsurprising that organic material in the devitrified glass region was detected.

The increased concentration of organic material in the perimeter of the shard implies that the weathered textures are associated with prior microbial activity. However, whether this devitrification was the result of this putative microbial activity or whether the putative microorganisms opportunistically penetrated the eroded glass, was not clear.

The PCA processed data from the J105 SIMS with the Ar GCIB primary beam, indicated that aromatic hydrocarbons could be detected (Fig. 5-7). The source of this aromatic material was unclear but is considered in Chapter 8. In contrast, a complex range of carbon-nitrogen compounds was localised around the devitrified weathered perimeter of the glass shards and within fractures in the matrix. The presence of CH_4N^+ in the fractures observed using the PHI TRIFT V could not clearly be observed in the carbon and nitrogen elemental maps with XPS, due to the lower spatial resolution of this technique.

The scanning electron photomicrography with energy dispersive spectroscopy of other fragments of the OJP_13 demonstrated that micro-cracks or fractures were present in other regions of the sample used in this investigation, and by implication, these occur throughout the OJP_13 sample. The observed co-localisation of carbon with the micro-fractures within a sample of an unprepared OJP_13 indicated that the organic material observed using the XPS and both ToF SIMS analysis was not the result of an artefact of the sample preparation

process, or that the presence of carbon was not specific to the sample prepared for ToF SIMS analysis.

The morphology of the microtubular alteration textures observed in glass shards (see Fig. 4-1) has been proposed to be the result of the microbiological activity (Mcloughlin et al., 2007; Mcloughlin, 2010) and specifically the result of excavation by fungal hyphae (Smits, 2006b; see section 1.9.1). Therefore, it might be anticipated that any organic material that is collocated with these structures is potentially the diagenetic remnants of the organisms that produced these features, potentially providing supporting evidence that these features are the result of biological activity.

The investigation in this chapter had demonstrated that the organic material in the OJP_13 sample was indeed heterogeneously distributed and that the organic material is co-located to particular petrographic features of the sample. The carbon-nitrogen chemistry was concentrated in the devitrified rind that covers the glass shards. The XPS, ToF SIMS and EDS data also indicated that the carbon-nitrogen chemistry was predominantly located in the micro-fractures in the lapilli matrix surrounding the glass shards. By correlating this data with THM-GC/MS analysis, it was possible to provide an indication of the types of molecules that were present in the OJP_13 sample. This suggested that the C-N bond observed by XPS was a component of aromatic compounds with nitrogen substitutions, such as pyrroles and pyridines. The source of this nitrogenous organic material was not understood and therefore, was investigated in Chapters 6 and 7.

5.5.0 Conclusion

This chapter demonstrated that both XPS and ToF SIMS are capable of measuring the lateral distribution of organic material in the OJP and by implication in other geological samples at mm spatial scales with a resolution of 2 µm for ToF SIMS and 35 µm for the XPS. Further, these instruments, used along with GC/MS, can obtain the distribution of molecular information. The data showed that the nitrogenous organic material that was observed in the OJP_13 sample in Chapter 4 was heterogeneously distributed and was associated with microfractures and with the weathered rinds of the glass shards. This distribution implied that this organic material was chemically equivalent ,and therefore came from the same

source, which was potentially an endolithic organism that either (i) promotes the weathering process (see section 1.6.5) or (ii) exploits the weathering prosses and the observed microtubules are an inadvertent consequence of one of these processes. Further, this chapter demonstrated that ToF-SIMS with an Ar GCIB primary beam is effective at detecting and mapping organic molecules in geological samples, and also that the combination of XPS, ToF-SIMS and GC/MS analysis permits the simultaneous correlation of morphological and organo-geochemical evidence of fossilised biological activity.

CHAPTER 6: THE ORGANIC STRATIGRAPHY OF ONTONG JAVA PLATEAU TUFF CORRELATED WITH THE DEPTH RELATED PRESENCE AND ABSENCE OF PUTATIVE MICROBIAL ALTERATION STRUCTURES

Abstract

Chapter 4 indicated that functionalised aromatic compounds with nitrogen substitutions in the OJP_13 were detected with GC/MS and XPS. Chapter 5 showed that these were associated with the devitrified rind (weathered perimeter) of the glass OJP_13 sample. This chapter compares the composition of the organic material in the core samples containing microtubules, with other core samples from the Ontong Java Plateau that also contained glassy shards but where the microtubular features were absent. This analysis was conducted using thermal hydrolysis and methylation coupled to gas chromatography/mass spectrometry and X-ray photoelectron spectroscopy. The samples were from different depths of the OJP tuff, the overlying pelagic sediments. These were compared with pillow lava basalts from other geographical locations and Whin Sill Dolerite. Comparable nitrogen bearing aromatic compounds were detected in each of the deeper OJP tuff core samples but were not detected in either the overlying pelagic sediment or in the basalt samples from other locations or the Whin Sill dolerite. Thus, the results presented here make no direct link between the OJP core samples that contain extensive tubular alteration textures and the presence of nitrogenous organic compounds.

6.1 Introduction

The results in Chapter 5 suggested that C-N chemistry was detected in the microfractures in the lapilli matrix surrounding the glass shards and was concentrated in the weathered rind of the shards. However, a full range of controls was needed to verify the link between microtubular features and this organic material. The purpose of this chapter was to characterise the composition of the organic material in the OJP tuff occurring at different stratigraphic levels. This was carried out to compare the composition of the organic chemistry in the tuffs with microtubular alteration textures, and those without those textures. As a control, the OJP tuffs were compared with sub-marine basalts from other regions and with Whin Sill Dolerite (WSD).

Previously, Smits, (2006) suggested that the tubular alteration textures were the result of fungal excavation (also see section 1.9.2). The primary structural biopolymer of fungi is chitin (see section 1.10.2), which is composed of glucosamine residues (Bowman and Free, 2006) and is therefore rich in nitrogen in comparison to the other plant biopolymers, specifically cellulose and lignin. The chemical composition of the organic material associated with the microtubular features shown in Fig 4-1 is potentially an indication that it was derived from a fungus. Therefore, it was anticipated that elevated concentrations of nitrogen would be detected only in the samples with the alteration textures.

6.1.1 Geological Samples Used in this Chapter

In addition to OJP_13 investigation described in the Chapters 4 and 5, samples from Leg 192 Hole 1184A core 43R (OJP_43) and core 22R (OJP_22) were selected for analysis in this investigation (hereafter, these are collectively described as the OJP tuffs). These samples were selected because tubular alteration textures were reported to be rare in the other core samples from hole 1184A (Banerjee and Muehlenbachs, 2003; see section 1.10.2). In addition to these tuff samples, both the overlying pelagic ooze from core 8R from OJP hole 1184A (OJP_8) and a fragment of a charred fragment of higher plant material was also analysed (OJP_45).

OJP_8 is a pelagic Miocene nano-fossil foraminifera ooze (hereafter pelagic ooze; Fig. 6-1 Unit 1). It is a fine-grained sediment that accumulated as the result of the settling of

158

particles to the floor of the open ocean, and it is formed principally from either the calcareous or siliceous shells of phytoplankton or zooplankton.
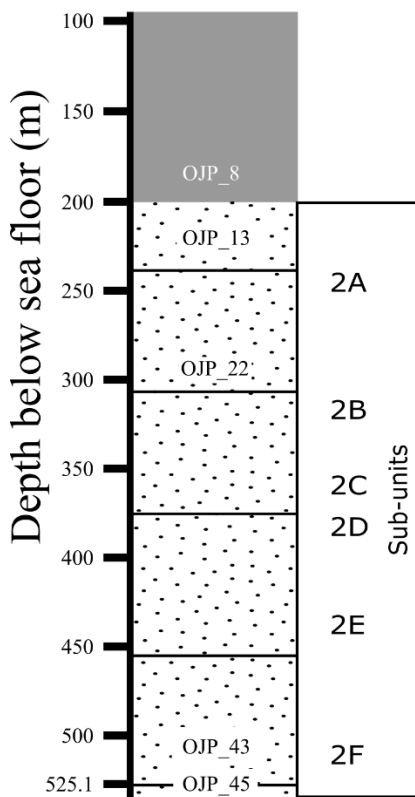
Fig 6-1. *Diagram of the of the Ontong Java Plateau drill hole 1184A site, and acquisition depths of the OJP core samples and the stratigraphic layer where the visible wood fragments were observed. Samples OJP_13, OJP_22 and OJP_43 are collectively described as OJP tuff. The OJP_8 sample is described as pelagic ooze and the OJP_47 is an example of one of the layers of charred woody fragments described here as wood remnants. © John Wiley & Sons Ltd 2018*

The formation of the Eastern lobe of the OJP by episodic volcanic activity permitted an intermittent colonisation of the surface by flora during the quiescent periods. The material resulting from this colonisation was subsequently buried in the tuff by each successive volcanic event. This resulted in 6-10 horizons in the 1184A hole that contain the remnants of woody material (see Fig. 6-1). Some of this woody material consists of visually identifiable fragments that are up to 6 cm long (Thordarson, 2003) and appear to have a char-like texture, presumably as a result of both the heating it experienced during the volcanic activity that caused the burial and then by the subsequent diagenesis (see Fig. 6-2).

Atlantic mid-ocean ridge (MAB) and Costa Rica flank (CRB) basalts were used to compare the organic composition in the OJP tuff and the submarine extrusive pillow lava basalts. Each of these has been reported to contain alteration textures (Staudigel et al., 2008). The MAB was basalt that was extruded 10 Ma ago and possessed glass shards, of which 60% to 95% contained granular textures and 5% to 40% contained tubular textures (Dilik, 1998). CRB was extruded 5 Ma ago, and 80% to 100% of the samples contained granular textures and 0% to 20% of the samples contained tubular textures (Furnes et al., 2001a). Additionally, dolerite from the Whin Sill complex was used to compare organic material in basalts without glass alteration textures (see section 3.1.1).
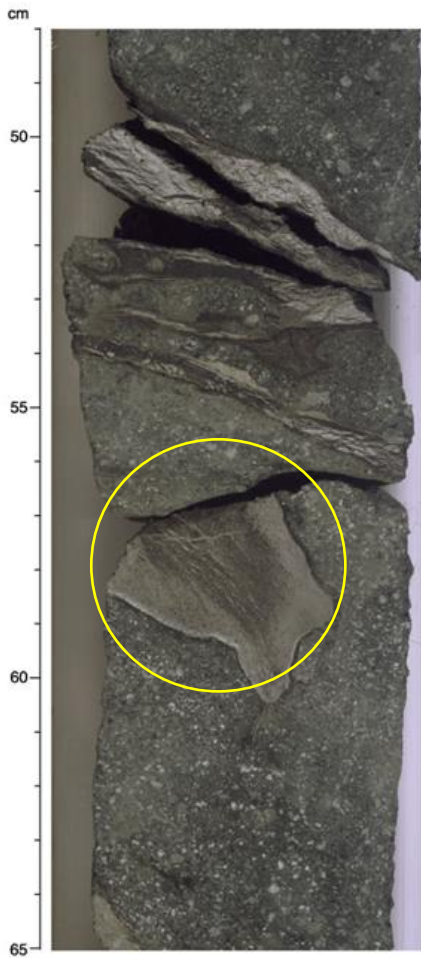
Fig 6-2. *Photograph of wood fragments (yellow circle) in tuff from 192-1184A-45R-7, 48-65 cm).*Credit: *www.odp.tamu.edu/publications/192_IR/.*

6.2 Methods

The analysis was conducted on the samples that are described in Chapter 2, Table 2-1, represented below for the reader's convenience. Sample handling was carried out according to the description in Chapter 2, Section 2.1.1. The optical petrography was conducted according to the protocol described in Section 2.5.1. Decontamination and analysis of samples were carried out according to the protocols described in Chapter 3 and Chapter 4. These chapters demonstrated that the optimal GC/MS analysis was conducted in the presence of TMAH, at a pyrolysis temperature of 610 °C and consequently these parameters were used in this chapter (see section 4.3.3). The THM-GC/MS analysis presented in Chapter 4 suggested that the ions with the five greatest intensities were sufficient to obtain a good match with the NIST05 mass spectra library. Therefore, only the 5 most intense ions are presented in the tables in this chapter, and the following chapter.

161

Re-presentation Table 2-1

Identifier	Description	Exp.	Site	Core	Sect.	interval(cm)*	Depth (m.b.s.f.)	Depth into basement (m.)	Glass Shards	Alteration Textures	Location	Ref
OJP_8	Pelagic Ooze	192	1184A	008R	04W	49-51	201.10	-	N/A	N/A	5°0.6653' S 164°13.9771'E	[1,2]
OJP_13	Oceanic tuff	192	1184A	013R	03W	145-148	224.55	23.45	Y	Y	5°0.6653' S 164°13.9771'E	[2,3]
OJP_22	Oceanic tuff	192	1184A	022R	03W	86.5-89	299.99	98.89	Y	N	5°0.6653' S 164°13.9771'E	[1,2,4]
OJP_43	Oceanic tuff	192	1184A	043R	03W	120-122	495.18	294.08	Y	N	5°0.6653' S 164°13.9771'E	[4]
OJP_45	Wood Fragment	192	1184A	045R	7	48-65	527.61	326.51	N	N	5°0.6653' S 164°13.9771'E	[4]
CRB	Oceanic Basalt	148	896A	011R	01W	111-115	287.10	91.9	Y	Y	1°13.0062'N 83°43.3920'W	[5]
MAB	Oceanic Basalt	46	396B	020R	4W	36-40	291.36	140.86	Y	Y	22°59.1420'N 43°30.9000'W	[6]
WSD	Terrestrial Basalt	-	-	-	-	-	0	-	N	N	N55° 28.427' 001 35. 577' W	[7]

The geological samples used for this chapter with acquisition location and depth and the Ocean Drilling Programme data and the codes for them used in this chapter. References **(**1*).*Thordarson (2004). (2) and (3) Ocean drilling programme (2004). (4) and (5) Dilick, (1998). (6). Banergee et al. (2003).

OJP= Ontong Java Plateau; CRB=costa Rica Basalt; MAB=Mid Atlantic Basalt; WSD=Whin Sill Dolerite.

6.3 Results

6.3.1 Visual Identification of tubular alteration textures in petrographic thin sections using Optical Petrography

Optical microscopy was able to verify that the microtubular features observed in earlier studies (Preston, 2011; Banerjee and Muehlenbachs, 2004) were present in the OJP_13 samples used for this study. Furthermore, those alteration textures were absent in each of the other OJP core samples, the pillow lava core samples (CRB and MAB), and the WSD samples (Fig 6-3 a-e). The petrography of the glass shards in the OJP tuff samples (OJP_13, _22 and _43) demonstrated that they were all of a similar size with the blocky sub-angular tektite morphology similar to those that have been reported previously (Thordarson, 2004). In contrast, the angular glass shards of the MAB and the CRB, which were the result of rapid aqueous quenching were observed (Heiken, 1972). The dark red/brown perimeter, previously observed in the glass shards of OJP_13 tuff sample (See Fig. 4-1), was also observed in the glass shards of the OJP _22 and OJP_45 tuff samples, which was indicative of weathering (devitrification) of the glass. Similarly, the glass shards in the OJP_22 and OJP_43 were also embedded in a matrix of lapilli sized shards that are characteristic of volcanishardic sediments. Visual inspection indicated the presence of microtubules only in OJP_13 (Fig. 4-2 a). In contrast, the tubule alteration textures were not identified in any of the glass shards the other OJP tuff samples (OJP_22 and OJP_43 or the glass shards of the CRB or MAB basalts. The WSD basalts obtained from the shoreline (see Table 2-1) did not possess glass shards. These differences permitted a comparison between the OJP samples with tubular textures and those without tubular textures.
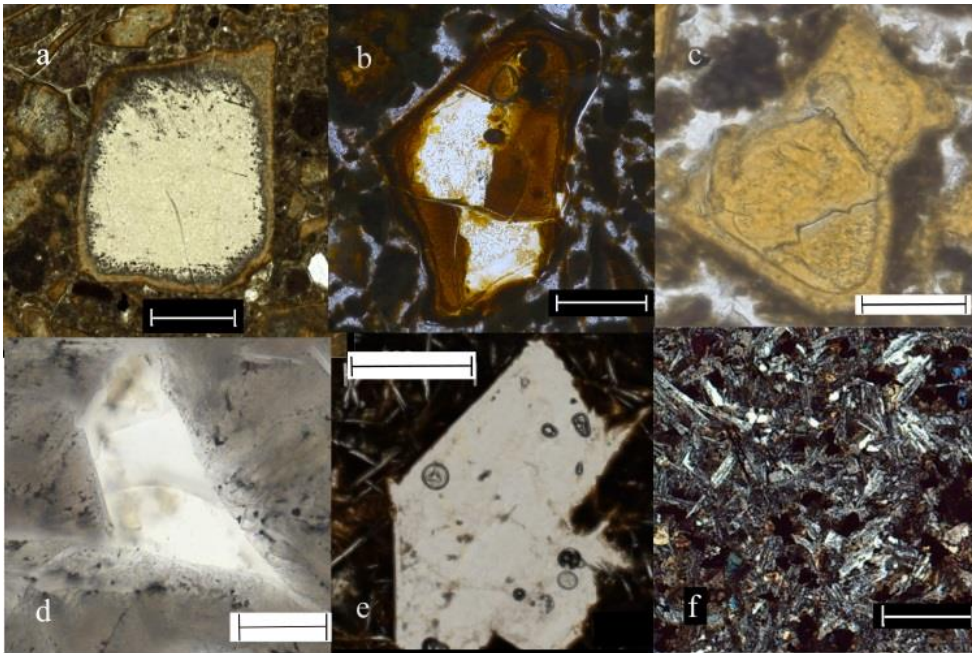
FIG 6-3 a-f. *Optical petrography of submarine basalts used in this investigation. Figs a-e show a glass shards embedded in a matrix. a. OJP_13, extensive tubular alteration textures are observable in the area around the perimeter of the shard and the orange/brown region is the devitrified rind. Figs: b. OJP_22, c. OJP_43, d. CRB e. MAB, The observed glass shards in figs b-e do not possess extensive alteration textures. f. WSD in which glass shards were absent. Scale bar= 100 µm.*

6.3.2 Analysis using X-ray Photoelectron Spectroscopy

High-resolution XPS spectra for carbon and nitrogen were obtained for the geological samples, and synthetic peak component fitting was conducted using the method described in section 4.2.5.

The high-resolution carbon XPS scans on OJP_13, OJP_22 and OJP_43, were conducted, and Fig. 6-2 a-c showed that these samples produced non-Gaussian spectra, which suggested that each of the samples contained a range of organic compounds. Seven synthetic components to be fitted were fitted to the high-resolution carbon spectra, and a single synthetic peak was fitted to the high-resolution nitrogen peak (Fig. 6-2 a-c inset). For convenience, the OJP_13 results are presented again from section 4.2.2. A comparison of the OJP_13 carbon and nitrogen spectra (Fig. 6-2a) with the OJP_22 and OJP_43 carbon and nitrogen spectra indicated that the composition of the chemical states in these samples was

comparable. This was contrary to expectations since the OJP_13 demonstrably contained microtubular textures that are suggested to be indicative of microbiological activity, whereas no microtubules could be visually identified in the OJP_22 or OJP_43 samples.
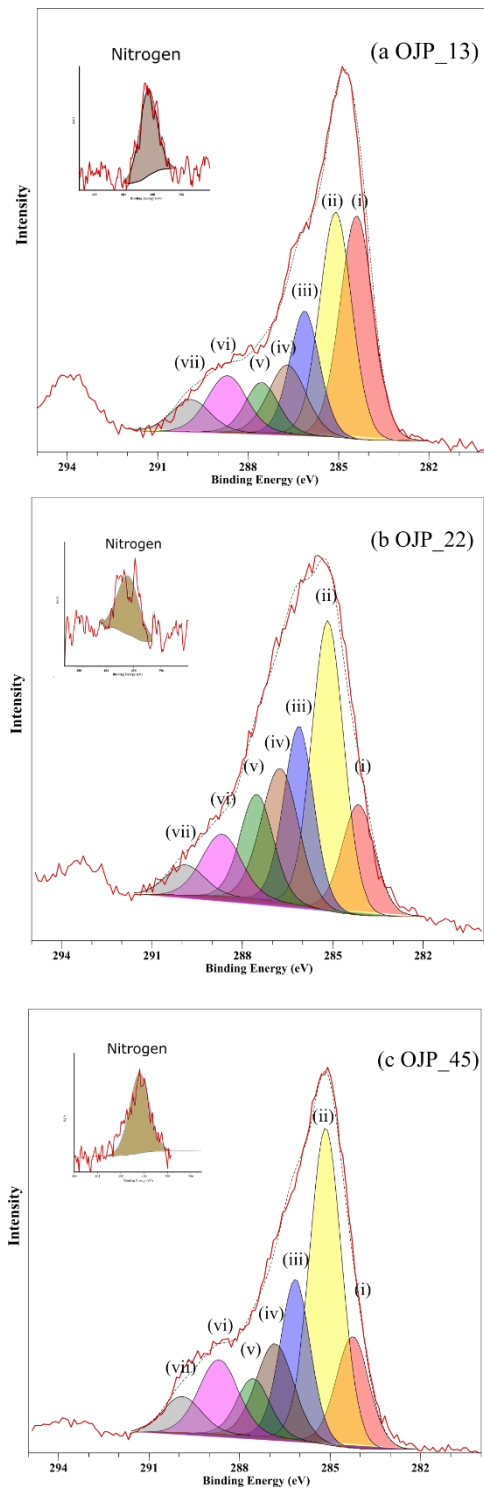
Fig 6-4. *(a) OJP_13 (b) OJP_22 (c) OJP_45. High-resolution XPS carbon spectra of the OJP tuffs, with synthetic component fitting. Key to the labelled components and the corresponding chemical state identities are presented in Table 6-1.* <u>*© John Wiley & Sons Ltd, 2018.*</u>

The carbon XPS high-resolution scans of the pelagic ooze (OJP_8) (Fig. 6-3 a) and buried remnant wood fragment (OJP_45) (Fig. 6-3 b) resulted in spectra that were closer to a Gaussian shape in profile. This analysis indicated that the range of the organic compounds in the OJP_8 sample was smaller than in the other OJP samples. The OJP_8 samples were dominated by the presence of inorganic carbonate in the form of $CaCO_3$. This is consistent with the calcareous material that is associated with the foraminifera origin of the sample (Rothwell, 2005). Additionally, the organic carbon component occurs at 284.9 eV, which is consistent with C=C chemistry, suggests the presence of polyaromatic hydrocarbons. Furthermore, a nitrogen peak in these samples was not detected.

C=C dominated the high-resolution carbon scans of the woody material (OJP_45), and crucially nitrogen was undetected in these samples (Fig. 6-5 b). These results were consistent with the XPS analysis of biochar (from Sani Mu'azu Makarfi, Newcastle University, Newcastle upon Tyne, UK, unpublished results), confirming the that OJP_45 consisted of the charred remnants of wood material. These results indicated that both the organic material in the pelagic ooze (OJP_8; Fig. 6-5a) and the woody material (OJP_45) were compositionally different to the organic material in the OJP tuff (OJP_13, OJP_22 and OJP_43).
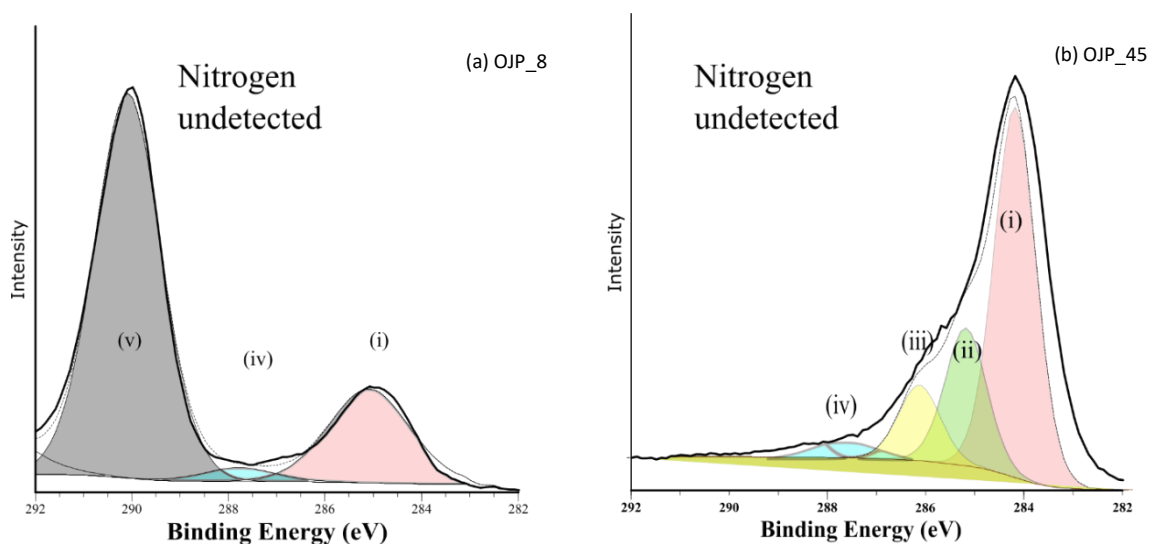
Fig. 6-5 a and b. *High-resolution XPS carbon spectra for (a) OJP_8 (foraminifera ooze) and (b) OJP_45 (charred remnant wood).* <u>*© John Wiley & Sons Ltd 2018.*</u>

XPS analysis was conducted on the submarine basalts that contained glass shards (CRB and MAB), where the presence of putative biogenic alteration textures was reported (Dilik et al.,

1998 and see section 1.9.2). In addition, the WSD results from section 4.3.2, were presented in this chapter with synthetic peak component fitting.

High-resolution carbon XPS scan of the other basalts and dolerite (CRB, MAB and WSD; 6-4 a-c), showed that a complex mixture of organic compounds could be detected. This indicated that the carbonaceous material in the CRB, MAB and WSD basalts was compositionally similar to the OJP tuffs (OJP_13, OJP_22 and OJP_43). However, in contrast to the OJP tuffs, nitrogen signal could not be detected the basalts. The data obtained by the peak component summarised in Table 6-1 on the following page.
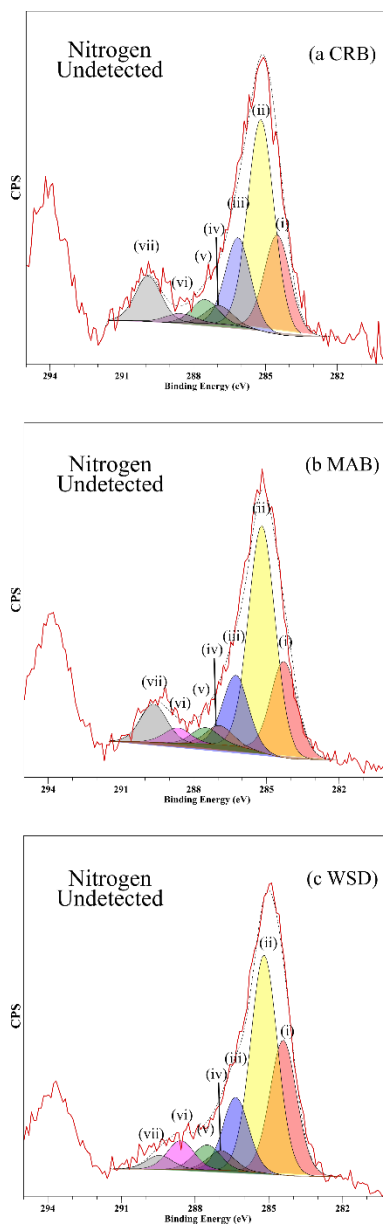
Fig 6-6 a-c. *XPS high-resolution carbon spectra of submarine basalts and dolerite retrieved from the shoreline. (a) CRB, (b) MAB and (c) WSD. © John Wiley & Sons Ltd 2018.*

Component	Binding Energy (eV)	Assignment	Moiety	% of the total synthetic component area							
				OJP_8	OJP_13	OJP_22	OJP_43	OJP_45	CRB	MAB	WSD
(i)	284.6	C=C	aromatic	15	22	10	9	74	22	20	27
(ii)	285	C-C	aliphatic	3	22	28	29	17	32	32	37
(iii)	286.4	C-OH	hydroxyl	0	16	20	21	7	17	17	16
(iv)	287	C-N	amide/furan	0	11	16	16	0	0	0	0
(v)	287.6	C=O	Carbonyl	0	7	12	8	3	8	8	12
(vi)	288.6	O-C=O	Carboxyl/Carbonyl	0	16	9	11	0	3	5	5
(vii)	290	CO3	Carbonate	82	6	5	6	0	18	18	3

Table 6-1. *The chemical states consistent with the peak component assignment and the assignment of the chemical bond to the component-binding energy contained a variation of ±0.1eV in positions to allow the best fit of each synthetic component. (Beamson 1992). The component areas expressed as a percentage of the total area and n/d = not detected.* <u>© **John Wiley & Sons Ltd 2018.**</u>

Peak component (i) and (ii) corresponds to C-C bonds. Component (i) is assigned to aromatic or alkene hydrocarbons, which corresponded to the aromatic compounds that were detected using THM-GC/MS. This suggested that each of the samples contained some aromatised hydrocarbon. Component (ii) which was indicative of aliphatic alkanes, corresponded to the side chains of the aromatic rings and the chain moiety of the fatty acids that were detected using THM-GC/MS. The results indicated that there was a variation in the aromatic and aliphatic concentrations between the different samples. The ratio of component (i) to component (ii) indicated that OJP_13, OJP_8 and WSD possessed a higher proportion of aromatic compounds, in comparison to the other samples used in this study.

The peak components (iii) and (iv) were a result of a combination of both C-N and C-O chemistry, respectively. However, the proximity of the binding energies of these components resulted in a considerable overlap. Therefore, both the survey spectra and the high-resolution nitrogen spectra, observed at 400.5 eV were used to confirm the identity of the C-N bonds in the high-resolution carbon spectra. The results showed that the components (iii) and (iv) were depleted in the samples where the nitrogen peaks at 400.5 eV, were not observed. This implied that the identity of component (iii) were indeed carbon-nitrogen bonds.

The carbon-nitrogen bonds corresponded to the amides that were detected using FTIR microscopy (Preston et al., 2011), and to the nitrogen substitutions within the aromatic rings that were identified using THM-GC/MS analysis (See section 4.3.3). This carbon-nitrogen signal was observed in each of the OJP tuff samples. In contrast, components (iii) were negligible, and the nitrogen signal could not be detected at 400.5 eV, in the pelagic ooze (OJP_8), the WSD, and in the submarine basalts (MAB and CRB). These results indicated that the detectable levels of nitrogen were specific to the OJP tuff but are not unique to the OJP_13 core sample. Component (v) was consistent with the presence of carbonates and was also observed in each of the marine basalts but was not observed in the WSD. Consequently, component (v) dominated the OJP_8 carbon high-resolution XPS spectra.

6.3.3 Analysis of organic compounds in basalt and sediments using THM-GC/MS analysis

THM-GC/MS analysis was conducted on the OJP tuffs to verify the data that was obtained with XPS. This is an extension of the analysis described in section 4.2.2 to include OJP_22 and OJP_43. The chromatograms for these were presented in Fig. 6-3a-c and the compounds identified are presented in Table 6-3.
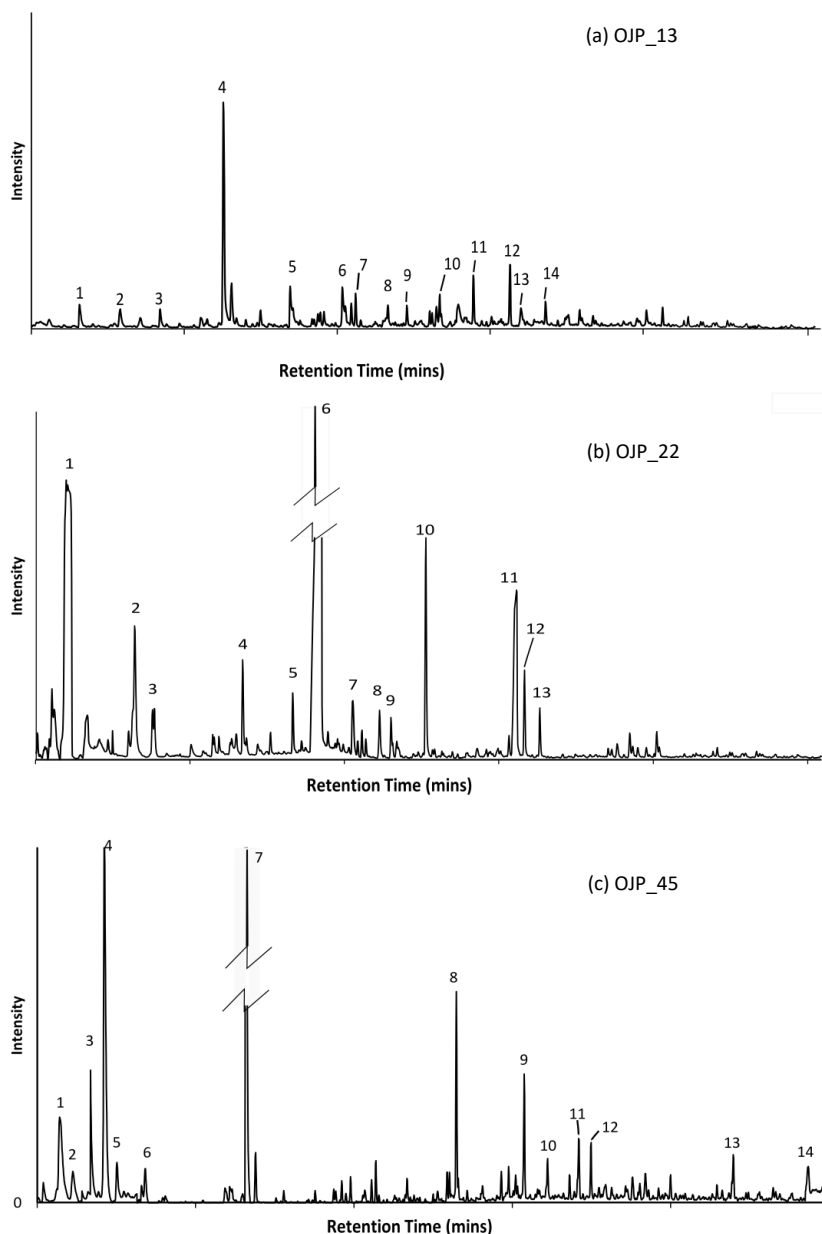
Fig 6-7 a-c. *THM-GC/MS analysis of OJP tuff (a)OJP_13 (b)OJP_22 and (c)OJP_43. The key the annotation is presented in Table 6-3.* <u>**© John Wiley & Sons Ltd 2018.**</u>

Table 6-2: Key to and Values Chromatogram in Fig. 6-7(a) *top 5 m/z values and Identified Peaks with match factors, for THM-GC/MS of OJP_13. Match= match factor with the NIST05 database. Nitrogenous compounds highlighted in bold. This table from chapter 4 is replicated for the reader's convenience.*

Peak	m/z	Ab.	m/z	Ab.	m/z	Ab.	m/z	Ab.	m/z	Ab.	peak assignment	match
1	54	1	55	1	56	2	57	4	58	100	**Butylamine**	0.8
2	51	11	63	9	65	11	77	14	78	8	**Ethylpyridine**	0.9
3	51	13	58	36	59	25	77	15	89	24	Ethylbenzene	0.85
4	50	12	51	16	63	13	65	69	77	21	Methoxybenzene	0.94
5	50	10	55	9	57	37	65	26	66	34	Triazine	0.71
6	77	13	86	9	91	12	94	11	103	10	Isopropylbenzene	0.88
7	55	11	57	32	77	16	79	11	91	23	**Butylpyridine**	0.86
8	51	17	53	12	77	41	78	11	79	40	4-Methylphenol	0.94
9	51	11	63	16	65	14	89	15	91	100	Meta Toluardehyde	0.9
10	51	12	65	15	77	12	91	42	92	16	1-Propenyl-Toluene	0.85
11	51	15	77	40	78	18	79	23	91	34	2,3-Dimethylphenol	0.9
12	65	5	77	8	91	16	115	9	117	9	Methylbenzene	0.93
13	77	13	91	22	107	10	115	11	117	11	Methylbenzene	0.86
14	77	6	91	12	105	8	115	10	117	8	Pentamethylbenzene	0.9

Table 6-3. Key to and Values Chromatogram in Fig. 6-7(b) *top 5 m/z values and Identified Peaks with match factors, for THM-GC/MS of OJP_22. Match= match factor with the NIST05 database. Nitrogenous compounds highlighted in bold.*

Peak	m/z	abund	m/z	abund	m/z	abund	m/z	abund	m/z	abund	peak assignment	match
1	92	28	91	46	70	66	69	100	53	5	phenylacetic acid	.77
2	106	54	105	24	93	38	92	20	91	100	1,3-dimethyl benzene	.81
3	104	100	103	47	78	33	77	18	51	11	styrene	.88
4	120	50	119	14	118	17	117	21	105	100	1,3,5-trimethyl-benzene, 1-ethynyl-4-methyl-	.84
5	117	9	116	99	115	100	108	13	89	10	benzene,	.76
6	109	67	108	100	83	53	82	28	67	36	TMAH	.82
7	123	11	109	8	108	100	97	6	67	9	**3-acetyl-1-methylpyrrole**	.86
8	123	10	109	6	108	100	95	3	67	9	**2,6-dimethyl-pyrazine,**	.65
9	130	100	129	80	128	39	127	18	115	85	benzene,	.77
10	129	11	128	100	127	12	126	7	102	7	naphthalene	.78
11	152	2	126	9	84	6	83	100	67	2	**1-methyl-1h-1,2,4-triazole**	.90
12	143	11	142	100	141	84	139	10	115	24	1-methyl-naphthalene	.97
13	143	12	142	100	141	88	139	11	115	26	1-methyl-naphthalene	.87

Table 6-4: Key to and Values Chromatogram in Fig. 6-7(b) *top 5 m/z values and Identified Peaks with match factors, for THM-GC/MS of OJP_43. Match= match factor with the NIST05 database. Nitrogenous compounds highlighted in bold.*

Peak	m/z	ab	m/z	ab	m/z	ab	m/z	ab	m/z	ab	peak assignment	match
1	**94**	100	**84**	12	**83**	18	**79**	48	**61**	10	dimethyl disulfide, 2-propenylidene	.88
2	**93**	5	**92**	60	**91**	100	**65**	9	**63**	6	cyclobutene,	.75
3	**74**	4	**73**	100	**72**	7	**58**	4	**56**	2	n,n-dimethyl-formamide,	.80
4	**61**	5	**59**	4	**58**	100	**57**	4	**56**	2	acetone	.88
5	**95**	62	**94**	100	**93**	8	**78**	6	**53**	9	**2,5-dimethyl-1h-pyrrole,**	.83
6	**106**	35	**105**	26	**103**	7	**93**	4	**91**	100	xylene	.71
7	**129**	31	**128**	100	**86**	96	**85**	11	**57**	31	TMAH	.82
8	**138**	5	**137**	57	**136**	100	**134**	3	**122**	38	phenol	.82
9	**148**	45	**147**	9	**134**	9	**133**	100	**115**	7	pentamethyl-benzene,	.85
10	**159**	14	**158**	63	**143**	100	**141**	24	**115**	19	1,2,3-trimethylindene 3,3-dimethyl-	.70
11	**165**	14	**162**	28	**148**	13	**147**	100	**136**	57	isobenzofuranone	.65
12	**162**	35	**148**	13	**147**	100	**133**	12	**115**	4	benzene, 6-methoxy-3-	.83
13	**163**	7	**162**	50	**161**	6	**148**	12	**147**	100	methylbenzofuran	.72
14	**170**	17	**159**	80	**158**	100	**155**	17	**144**	44	2,3,5-trimethyl-1h-indole,	.65

The THM-GC/MS analysis of OJP_13 had been conducted in chapter 4 (see section 4.2.2) but has been included here again for convenience. This chapter expands upon that investigation by conducting THM-GC/MS analysis on other OJP tuffs (OJP_22 and OJP_43). The compounds identified in these samples were comparable to the compounds identified in the OJP_13 and suggested that nitrogen was present as substitutions within the aromatic rings. This observation was consistent with the XPS data that demonstrated nitrogenous organic compounds were detected only in the OJP tuffs. The source nitrogenous organic compounds in the OJP was investigated by analysing the overlaying pelagic ooze (OJP_8) and a fragment of the charred plant remnant from the OJP (OJP_45) using THM-GC/MS and XPS (section 6.3.2).
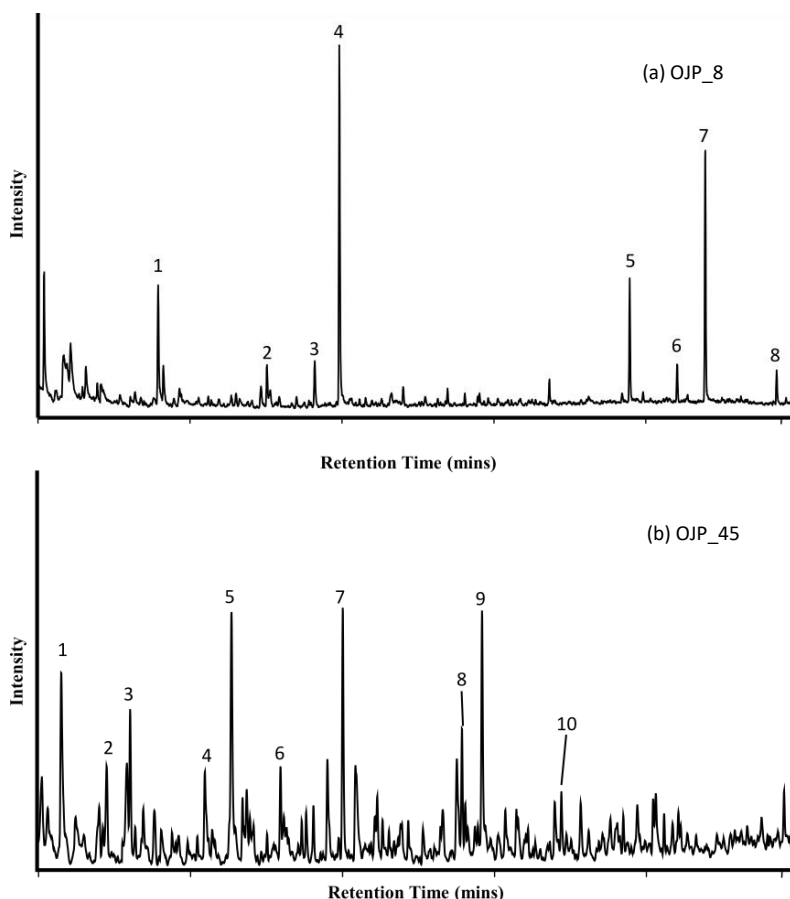
Fig. 6-8 (a-b). *THM-GC/MS of (a) OJP pelagic ooze OJP_8 and (b) OJP wood remnants OJP_45.* <u>© John Wiley & Sons Ltd 2018.</u>

174

Key to and Values Chromatogram in Fig. 6-4a (OJP_8)

Table 6-5: Key to and Values Chromatogram in Fig. 6-8(a): The *five most abundant m/z values and Identified peaks with match factors, for THM-GC/MS of OJP_8. Match= match factor with NIST05 mass spectra library. abund= ion abundance*

Peak	m/z	abund	m/z	abund	m/z	abund	m/z	abund	m/z	abund	peak assignment	match
1	104	100	103	47	78	36	77	17	51	19	styrene	.89
2	112	62	69	41	68	94	56	54	55	100	2 methyl cyclohexanone	.73
3	120	33	105	100	78	9	77	79	51	24	1-phenylethanone	.74
4	136	38	105	100	77	56	51	19	50	8	methyl ester benzoic acid	.95
5	138	92	129	100	97	73	74	84	69	83	dimethyl ester octanedioic acid,	.83
6	194	22	164	11	163	100	135	21	103	12	benzenedicarboxylic acid,	.75
7	185	56	152	100	83	60	74	69	55	83	dimethyl ester nonanedioic acid,	.87
8	199	100	125	94	98	64	74	94	55	63	decanoic acid,	.70

Table 6-6: Key to and Values Chromatogram in Fig. 6-8(b) *5most abundant m/z values and Identified peaks with match factors, for THM-GC/MS of OJP_45. Match= match factor with NIST05 mass spectra library.*

Peak	m/z	ab	m/z	ab.	m/z	ab	m/z	ab.	m/z	ab	Peak assignment	match
1	106.1	54	105.1	24	91.1	100	81.1	17	77.1	15	Xylene	84
2	108.1	100	79.1	19	78.1	57	77.1	20	65.1	54	methoxybenzene	66
3	106.1	100	105.1	98	77.1	89	51.1	31	50.1	19	Benzalderhyde	87
4	95.1	8	94.1	100	66.1	30	65.1	22	55.1	7	Phenol	87
5	120.1	49	105.1	100	95.1	31	79.1	19	67.1	23	trimethybenzene	69
6	122.1	100	121.1	46	107.1	30	91.1	34	77.1	41	Methoxybenzene	78
7	108.1	100	107.1	89	105.1	12	91.1	12	90.1	23	3 methyl phenol	90
8	108.1	84	107.1	100	79.1	21	77.1	25	51.1	9	4-methyl Phenol	74
											1-ethenyl-4-methoxy-	66
9	134.1	100	119.1	58	91.1	48	65.1	20	135.1	11	Benzene,	
10	129.1	14	128.1	100	127.1	14	121.1	8	102.1	7	Nepheline	78

THM-GC/MS analysis of the pelagic ooze (OJP_8) produced a range of aromatic and aliphatic compounds, which were consistent with the carbonaceous material identified in the XPS data. Furthermore, nitrogen was undetected; this supported the non-detection of nitrogen in the XPS analysis of the OJP_8. THM-GC/MS of the wood remnants (OJP_45) produced a complex chromatogram. Aromatic compounds dominated the peaks that were detected in these samples. However, nitrogenous compounds equivalent to those detected in the OJP tuffs samples were not detected.

To support the XPS data, THM-GC/MS analysis was conducted on the same submarine basalts that contained glass shards (CRB and MAB) that have been reported to possess the alteration textures that are proposed to be the result of microbiological activity (Staudigel et al., 2008; Staudigel et al., 2014; see section 1.9.2). In addition to the CRB and MAB samples, the WSD sample that was analysed previously using THM-GC/MS in Chapter 4, is presented here again.
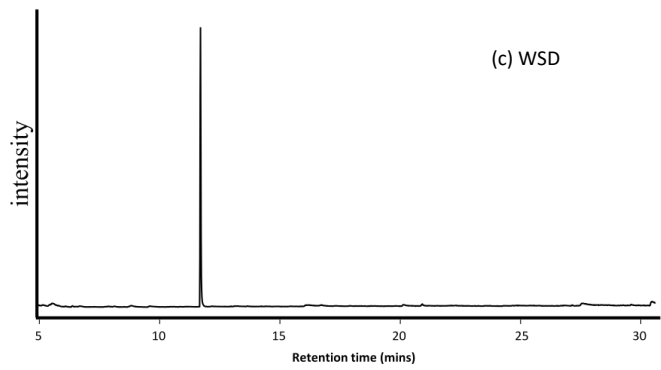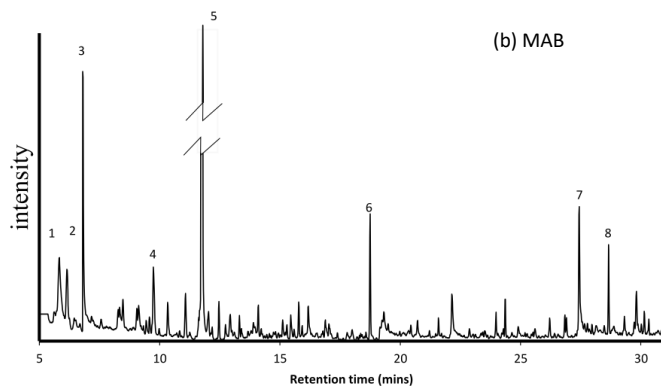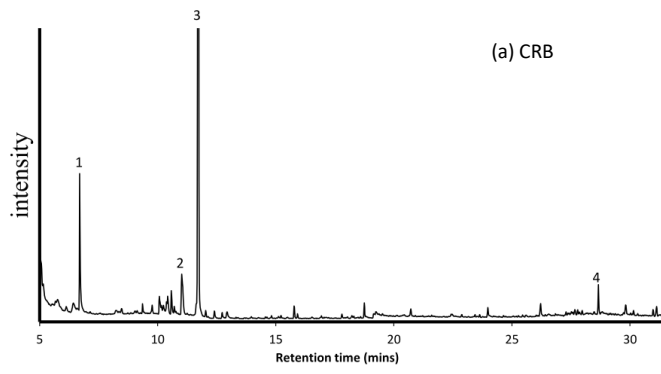
Fig 6-9. *Chromatograms of the THM-GC/MS analysis of submarine and terrestrial basalts(a) CRB, (b) MAB and (c) WSD.* <u>*© John Wiley & Sons Ltd 2018.*</u>

Table 6-7: Key to and Values Chromatogram in Fig. 6-6(a). *The five most abundant m/z values and Identified peaks with match factors, for THM-GC/MS of CRB. Match= match factor with NIST05 mass spectra library*

Peak	m/z	ab.	m/z	ab.	m/z	ab.	m/z	ab.	m/z	ab.	m/z	ab.		Match
1	56	2	56	2	58	8	72	8	73	100	74	51	Dimethyl-Formamide	.94
2	58	8	57	45	85	14	86	100	128	89	129	68	TMAH	.89
3	72	8	57	42	85	13	86	100	128	95	129	74	TMAH	.92
4	73	100	55	52	56	16	57	100	71	69	85	47	Hexadecane	.83

Table 6-8: Key to and Values Chromatogram in Fig. 6-6(b) showing the *five most abundant m/z values and Identified peaks with match factors, for THM-GC/MS of MAB. Match= match factor with NIST05 mass spectra library*

Peak #	m/z	ab.	m/z	ab.	m/z	ab.	m/z	ab.	m/z	ab.		match
1	52	15	58	96	79	25	83	100	84	56	Acetonitrile	71
2	58	30	65	11	83	16	91	100	92	60	Cyclobutene	94
3	56	2	58	9	72	8	73	100	74	4	Dimethyl-Formamide	94
4	65	64	77	20	78	62	79	17	108	100	Methoxybenzene	81
5	55	38	56	58	57	100	70	52	83	39	Chloro-octane	68
6	57	42	85	13	86	100	128	93	129	31	TMAH	91
7	55	21	59	13	74	100	87	46	141	11	Nonanoic acid, methyl ester	90
8	77	50	92	23	133	41	135	100	166	29	2-Methoxy benzoic acid	77
9	55	100	74	80	83	70	111	59	152	97	Nonanedioic acid, dimethyl ester	87
10	55	23	56	16	57	100	71	66	85	44	Hexadecane	86

No Peaks were detected in the WSD. Therefore, no table is presented.

The THM-GC/MS analysis of the submarine basalts indicated that a range of aromatic and aliphatic organic compounds was detected, which supported the identification of C-C and C=C component within the high-resolution carbon XPS spectra of the CRB and MAB. Crucially, no nitrogenous organic compounds were identified using THM-GC/MS, which supported the non-detection of nitrogen in these samples, using XPS. The preparation, decontamination and storage of each of the samples at Newcastle University were identical. Therefore, the negative result for the WSD indicates that the organic material detected in the sub-marine basalts and the OJP samples was indigenous.

6.4 Discussion

6.4.1 Verification that organic material is indigenous

The submarine samples were retrieved and stored by the Ocean Drilling Programme (ODP) repository in comparable conditions, prior to acquiring these samples for this study. Furthermore, the samples prepared for XPS analysis were decontaminated using gas cluster ion beam etching for 120 seconds at 4K eV (Purvis et al., 2017; see chapter 2). Therefore, the elevated concentrations of carbon in the OJP tuffs (OJP_13, OJP_22 and OJP_43) compared to the other basalts (WSD, MAB and CRB) were not the result of adventitious organic contaminants that had accrued during the extraction process or the subsequent storage by the ODP, or the preparation and storage during this study. Therefore, the higher concentrations of carbon measured in the OJP were the result of indigenous carbon.

The pelagic sediment (OJP_8; Unit 1, Fig. 6-1) that overlays the OJP tuff (Unit 2, Fig. 6-1) did not possess the elevated concentrations of nitrogen-bearing organic carbon that was observed in the OJP tuff. This suggests that the nitrogenous material that was observed in the OJP tuff was not the results of an adventitious contamination event that was specific to the procedure used to drill hole 1184A.

6.4.2 Obtaining a molecular identity of the organic material detected in the OJP tuffs

The organic compounds detected in the OJP_13 basalts in this study were comparable to those detected in earlier studies (Preston et al., 2011). However, the range of compounds that were identified by the NIST05 mass spectra library was highly complex and the major

compounds identified with match factors of < 0.7 (which indicated poor matches; see section 4.3.2). A simpler and broader interpretation based on the compound class of the parent moiety of the three closest matches obtained by the NIST library identification obviated this. This yielded a more confident assignment to general compound classes, rather than to a specific compound for each identified peak. Nevertheless, nitrogenous compounds were only detected in the OJP samples. These appear to consist of pyrrole and pyrazine based compounds. It is speculated in this chapter that the amine moiety of the glucosamine residue may have been incorporated into the aromatic ring during late diagenesis, and this was investigated in Chapter 7.

The detection of nitrogen is unsurprising since although 1-2% of the nitrogen may be preserved after early diagenesis (Schimmelmann and Lis, 2010; Ungerer et al., 2015), our results indicate 3.0-3.5% of the organic material detected by XPS in the OJP tuff was composed of nitrogen. The major structural biopolymer of fungus is chitin produced from chains of glucosamine monomers, which may have been the source of this material.

6.4.3 The distribution of organic material in the Eastern lobe of the OJP

In addition to carbonaceous material, also identified were nitrogenous organic compounds in the other OJP tuffs (OJP_22 and OJP_43) and crucially these core samples did not contain the tubular alteration textures. Although carbonaceous material in the other submarine pillow lava basalts (MAB, CRB), in the OJP pelagic ooze (OJP_8) and the wood remnants (OJP_45) was detected, nitrogen was undetected in these samples.

Banerjee and Muehlenbachs (2004) suggested that the overlying sediment was a repository and source of organic nutrients for any of the putative organisms that produced the alteration textures observed in the OJP_13. However, analysis of the OJP _8 foraminifera ooze indicated that it contained less carbonaceous material and no nitrogenous organic material, in comparison to the OJP tuff samples studied in this investigation (OJP_13, OJP_22 and OJP_43). It is anticipated that some organic nutrients would have been present in the OJP_8 pelagic ooze, based on this observation. This suggests that the overlying sediments were unlikely to be a source of substrates for any putative organotrophic endolithic bacteria.

The sedimentation of this volcanishardic tuff in this region of the OJP is layered with at least six horizons containing the visually observable remnants of higher plant material (Fig. 6-2) (Thordarson, 2003). The diagenesis of plant material results in compounds that primarily consist of aromatic compounds (Grew, 1974; Bernard and Papineau, 2014) and these were detected in the both the XPS and the THM-GC/MS analysis of the OJP_45. Potentially, the organic material observed in the OJP tuffs originated from one of these layers and may have then diffused throughout the entire unit. However, the OJP_45 did not possess the nitrogenous material observed in the OJP tuffs (OJP_13, OJP_22 and OJP_43) and no visible compacted plant material in the core samples was observed. These two observations argue against the possibility of the horizons of woody material as being the source of the organic material in the OJP tuffs.

6.4.4 Proposed Origin of the Organic Compounds Identified in OJP

Smits (2006b) suggested that tubular alteration textures are the result of excavation of geological material by fungal hyphae and therefore perhaps there is a link between the organic material with the elevated levels of nitrogenous compounds resulting from the presence of fungus and the presence of tubular alteration textures. The surface analysis investigation of OJP_13 described in Chapter 5 and published in Sano et al. (2016) supported this proposal by demonstrating that nitrogenous organic compounds were in the proximity of the microtubular features, specifically the perimeter of the glass shards in the OJP_13 sample.

However, contrary to expectations, the nitrogenous organics in the OJP_13 tuff were also detected in each of the other OJP tuffs (OJP_22 and OJP_43), and these did not possess the microtubules. Thus, each of the OJP tuff samples possessed a comparable nitrogenous organic composition, irrespective of the presence or absence of the microtubular textures. This indicated that there was no correlation between the presence of nitrogen-bearing aromatic compounds in the OJP tuffs and the presence of the microtubular alteration textures. Presuming the nitrogenous organic compounds were the remnants of chitin, and therefore, the organic material contained the remnants of fungi, then the remnant fungal material may be present throughout OJP tuff. This may also imply that either the physical or chemical geological conditions were different in the OJP_13 horizon or that another

unknown mechanism, rather than fungal excavation, may have been responsible for the formation of the microtubular structures observed in the OJP_13.

6.4.0 Conclusion

The study by Preston et al. (2011) and Sano et al. (2016) demonstrated that nitrogenous organic material was heterogeneously distributed at the µm scale and that this material was predominantly in micro-fissures and in the weathered perimeter of glass shards in the OJP_13. Of all the samples in this study, only the OJP tuffs showed elevated concentrations of nitrogenous organic material. In contrast, nitrogenous organic material was not detected in either the overlying sediment (OJP_8) or the charred woody material (OJP_45), indicating that neither of these horizons was the source of the nitrogen. Similarly, nitrogenous material in the basalt samples from other regions was not detected. This result implies that the composition of the organic material in the OJP tuff is different from the other geological samples investigated in this chapter. Furthermore, the nitrogen concentration in the OJP tuff is higher than in the other samples. This difference could potentially be the result of the presence the fungi that are found in the submarine crust, although further investigations to verify this are required. However, the evidence from our stratigraphic study indicates that the composition of the organic material is uncorrelated to the presence or absence of microtubular alteration textures in the glass shards of the OJP tuffs.

CHAPTER 7: A COMPARISON BETWEEN ARTIFICIALLY MATURED PLANT BIOPOLYMERS AND THE ORGANIC MATERIAL IN OJP

Abstract

Chapters 4 to 6 indicated that using THM-GC/MS and XPS, pyridine and pyrrole based compounds could be detected in the OJP tuffs, but not in the overlying pelagic ooze, the woody remnants or the other submarine or terrestrial basalts. Fungi play a key role in early diagenesis and are essential for the breakdown of plant structural biopolymers, which are relatively resistant to bacterially mediated decomposition. In these previous chapters, it was proposed that potentially the origin of this nitrogen was the diagenetic products of chitin, the key structural polymer of fungus, which could provide an indication of the taxonomic origin of the organic material in the OJP. To investigate this hypothesis, the same XPS and THM-GC/MS analytical methods used in Chapters 4-6 were applied to a range of plant and fungal structural biopolymers. These biopolymers were in both their original 'as received' condition and were also artificially decomposed using hydrous pyrolysis, in order to mimic late diagenesis. The compounds that were detected in the hydrous pyrolysed plant and fungus material were compared to the compounds detected in the OJP. Nitrogenous organic compounds were detected in the hydrous-pyrolysed products of chitin, the structural biopolymer of fungus. Additionally, to demonstrate that nitrogenous aromatics can be preserved in the fossil record during late diagenesis, chitin was heated at a range of temperatures up to 610 °C, to demonstrate that nitrogenous component in chitin was resistant to thermal decomposition and therefore had the potential to be preserved in the geosphere.

7.1 Introduction

It has been proposed that the microtubule structures studied in earlier chapters in this thesis and by other studies were formed by excavation by fungi (Banergee, 2007; Smits, 2013). The primary structural biopolymer of fungus is chitin, which is composed of glucosamine residues (Bowman and Free, 2006), and therefore it is rich in nitrogen, in comparison to the other plant biopolymers, specifically cellulose and lignin. Consequently,

the diagenetic remnants of fungus would be likely to possess elevated concentrations of nitrogenous organic chemistry (Schimmelmann et al., 1998). While taxonomically, fungus resides in a separate kingdom to plants, for simplicity, this chapter refers to the structural biopolymers collectively as 'plant' biopolymers.

XPS and ToF SIMS analysis demonstrated that nitrogenous organic material could be detected in the devitrified glass perimeter of a vitric shard and in microfractures and voids in the lithic matrix surrounding the shards in the OJP_13 sample (see Chapter 5). Chapter 6 demonstrated that this nitrogenous organic material could be detected in each of the OJP tuffs, but not in one of the fragments of charred of woody remnants buried in the eastern sea lobe of the OJP or in the other terrestrial and submarine basalts examined. The organic compounds that could be detected in the OJP tuffs were comparable to the nitrogenous aromatic compounds that were reported in the literature. These compounds were detected in the hydrous pyrolysis products of chitin standards (Monthioux and Landais, 1989; Gupta et al, 2007), and in chitinous arthropod fossils (Cody et al., 2011).

Hydrous pyrolysis (hy-py) can be used to artificially simulate the geochemical evolution of organic material (Tegelaar et al., 1989; Landais et al., 1995; Barth, 1999) and the hy-py of chitinous scorpion, arthropod and cockroach cuticles has resulted in the detection of pyrimidine and pyrrole compounds (Monthioux and Landais, 1989; Gupta et al., 2006). The presence of these compounds, associated with chitinous fossils, suggested that the nitrogen in chitin may be resistant to the anoxic combustion (e.g. Vulava et al., 2007; Cobb et al., 2012) that occurs during deep burial that is associated with late diagenetic processes (see sections 1.111.and 1.112) and therefore has the potential to be preserved in the fossil record.

Arthropod cuticles consist of chitin fibres embedded in a protein matrix, cross-linked by catechol, aspartate and histidyl functional groups (Schaefer et al., 1987). Similarly, fungal cell walls have been shown to be primarily composed of chitin, glucans, mannans and glycoproteins (Bowman and Free, 2006). The cuticles of fossil arthropods are thermally degraded in samples older than the Tertiary period >65 Ma and consequently show no trace of chitin or protein (Briggs et al., 2000) and the formation date of the Eastern lobe of the

Ontong Java Plateau (ODP Leg 192 Hole 1184A) is dated to ca. 93 Ma (see section 1.10.2 and Thordarson, 2001). Therefore, the organic material in the OJP would have comparable levels of diagenetic processing to that of the >65 Ma old material that is described by Briggs et al. (2000).

7.1.1 XPS Spectral Profiles of natural biopolymers that are commonly encountered in diagenetic environments

XPS carbon high-resolution spectral profiles can be used as 'fingerprints' for synthetic polymers (See section 1.12.3 and Briggs and Grant, 2003). However, no such database exists in the literature for naturally occurring polymers. Therefore, XPS high-resolution carbon spectra were evaluated as a method for distinguishing the taxonomic provenance of known plant structural biopolymers, that could then be used as references for the unknown provenance of the carbonaceous material in the OJP samples.

To investigate the taxonomic origin of the organic material in the OJP tuffs, plant structural biopolymers, cellulose, lignin and chitin, were subjected to hydrous pyrolysis to simulate late diagenesis. This was carried out in the presence of basalt to mimic any interaction between the mineral and the organic material. Chitin has been reported to be resistant to thermal decomposition (Schimmelmann et al., 1998). Therefore, the resistance of the nitrogenous component in chitin to thermal decomposition was evaluated. These treated and untreated materials were then characterised using the same methods that were employed in Chapter 6, with the intention of comparing the spectral profile of known biopolymers with the unknown organic compounds in the OJP samples.

7.2 Methods

7.2.1 Preparation of Plant Biopolymers

500 grams of Whin Sill dolerite (WSD) was ground in Tema ring rock pulveriser (Tema Machinery Ltd, Northants. UK), for 30 seconds then sieved to obtain particle 50μm to 150 μm sized particles (see section 2.1.1). This powder dry mixed with of either dry powdered chitin, cellulose or lignin (Analar grade, Sigma Aldrich, UK; hereafter collectively referred to as the biopolymers), in a ratio of 9:1 WSD:biopolymer,$^w/_w$. To prepare samples for XPS, ca. 1-2 grams of each of the standards were immobilised by compaction onto an aluminium disk using a manual hydraulic press (Specac Ltd. Orpington, London, UK), using 1.5 t.m^2 of pressure. This was necessary because fine rock particles can be drawn into the vacuum pump of the XPS, damaging them. Furthermore, the Al foil helped to mitigate the effects of surface charging that often occurs on the insulating rock surfaces during XPS analysis.

To hydrous pyrolyse the biopolymers, 10g of each of the WSD/biopolymer mixture was then added to Parr bomblets, and the remaining ⅓ of the total volume of each bomblet was made up with distilled water. These bomblet assemblages were then placed in a 1 litre Parr reactor (Parr Instrument Company, Moline, IL, US.A.). The reactor was then ⅓ filled with water. The reactor was run at 350 °C for 72 hrs. Following this, the cooled liquid from each of the bomblets was decanted, and the solids were freeze-dried for 48 hrs in a Thermo Modulyo D0230 (Sciquip ltd., Shropshire, UK). To assess the thermal stability of chitin, the samples were heated to 100°C, 200 °C, 300 °C and 610°C ±10% for 8 hours in a muffle furnace. All samples were stored in screw-top glass vials sealed with decontaminated Al foil.

7.2.3 Analysis of the plant biopolymers

The problem of a lack of a database of XPS spectral profiles for biopolymers was again resolved by preparing different biopolymer sample standards for XPS analysis, according to the description in section 7.2.1. The decontamination of the prepared samples prior to XPS and THM-GC/MS analysis was conducted according to the method described in Chapter 3. High-resolution carbon XPS scans were conducted according to the protocol described in section 2.4.1. THM-GC/MS analysis was conducted according to section 2.4.2 with a pyrolysis temperature of 610 °C; this is the Curie point for pyrolysis (Moldoveanu, 1998) and

was considered the optimal temperature for THM-GC/MS of geopolymers (see section 4.3.3). Peaks were identified the first derivative with signal:noise set to 10:1 and assignment were carried out with the NIST05 library using the Openchrom software package (See section 2.4.2).

7.3 Results

7.3.1 XPS analysis of Plant Biopolymers

XPS analysis of the untreated (as received; AR) plant structural biopolymers (Fig 7-1 a-c) indicated that each of their carbon spectral profiles was sufficiently dissimilar to each other, and may be used as a method for the identification plant and fungal biopolymers.
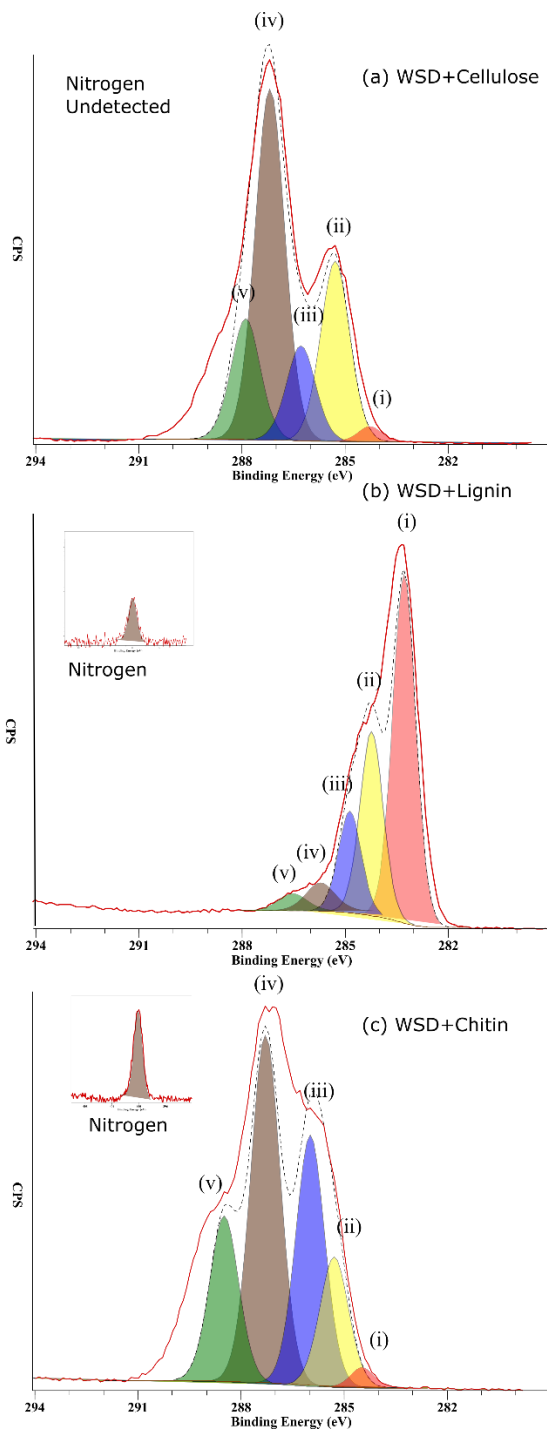
Fig. 7-1. *High-resolution XPS carbon spectra with high-resolution nitrogen spectra inset of WSD plus plant and fungal structural biopolymers_AR (a) Cellulose (b) Lignin (c) Chitin.*

190

Table 7-1. *Key to Fig. 7-1 (a-c) showing the component assignments.*

	Chemical State identified by XPS	Position (±0.1eV)	Compounds identified by GC/MS
(i)	C=C	284.6	Benzene/Naphthalene
(ii)	C-C	285.1	Lipids/Methyl side groups
(iii)	C-N C=O	285.6	Pyridine/Pyrrol
(iv)	C=O, CNO, C=OO	288	Lipids/amides
(v)	Ca/NaCO$_3$	289.5	N/D

The carbon spectra of the WSD spiked plant biopolymers produced different spectral profiles, as a function of the different chemical composition of the plant biopolymers. However, the spectral profile of these materials did not resemble the profile of the organic material in the OJP tuffs (Figs 6-2a-c) or OJP wood fragments (OJP_45) (Fig 6-3a) that are presented in chapter 6.
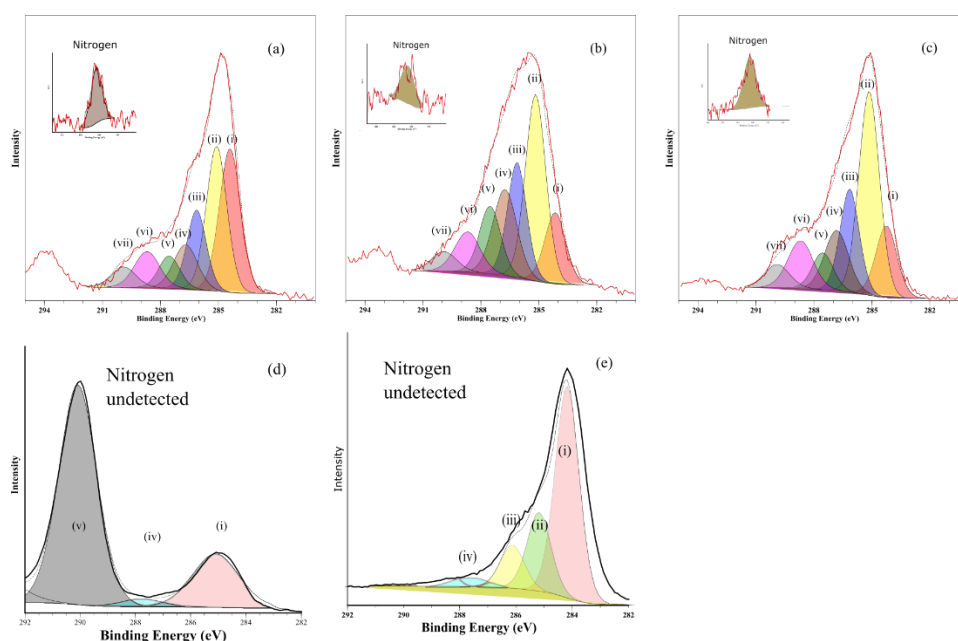
Replicated high-resolution XPS carbon and nitrogen scans of samples from Ontong Java Plateau from chapter 6: (a) OJP_13 (b) OJP_22 (c) OJP_43 (d) OJP_8 (e) OJP_45.

7.3.2 XPS analysis of Hydrous Pyrolysed products of Plant Biopolymers
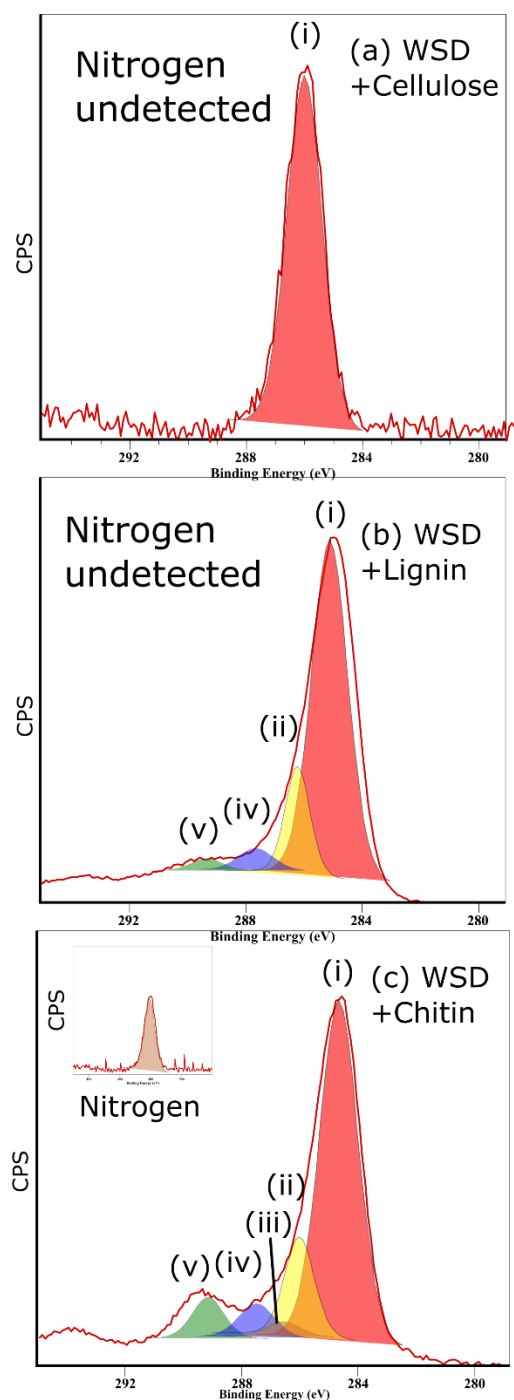
Fig. 7-2 a-c. *High-resolution carbon XPS spectra (nitrogen inset) showing hydrous pyrolysed WSD plus plant structural biopolymers (a) cellulose (b) lignin (c) chitin.*

Three XPS survey scans were also conducted on the WSD, and the WSD samples spiked with each of the plant biopolymers and subjected to hy-py. The C:N ratios for all the AR and hydrous pyrolysed (hy-py) samples were calculated from their peak areas (Table 7-2).

polymer	WSD only	Cellulose	Lignin	Chitin
C:N AR	N undetected	N undetected	58:1	10:1
C:N_hy-py	N undetected	N undetected	N undetected	12:1

Table7-2. *the C:N ratio of WSD samples spiked with plant biopolymers as received (AR) and following hydrous pyrolysis treatment (hy-py)*

Table 7-2   demonstrated that nitrogen could not be detected in the WSD or in the WSD plus cellulose, although it could be detected at trace levels in WSD plus lignin_AR but was undetected in the hy-py products of the WSD plus lignin. In contrast, nitrogen was detected at high concentrations in the WSD plus chitin, in both in the AR condition and in the samples following hy-py. XPS high-resolution spectra of the hy-py treated WSD plus plant biopolymers were obtained to measure the change in chemical composition.

A comparison of the XPS high-resolution carbon and nitrogen spectra of different biopolymers before (Fig. 7-1a-c) and after hydrous pyrolysis (Fig 7-2a-c) showed that the chemical states had been altered. The shape of carbon spectra of the hydrous pyrolysed biopolymers was close to a Gaussian profile, suggesting that the carbonaceous material was composed of a limited number of chemical states. Furthermore, the peak position of each of the hy-py biopolymers was at 284.9 eV ± 0.1 eV that indicated the organic material was dominated by C=C chemistry consistent with the formation of aromatic compounds. The hydrous pyrolysis of plant biopolymers resulted in carbon spectral profiles that were indistinguishable from each other. Therefore, synthetic peak component fitting did not yield significant information.

7.3.3 Measuring the resistance of chitin to thermal decomposition using XPS

Nitrogen could still be detected in the hydrous pyrolysis products of chitin. The resistance of chitin to thermal decomposition was tested further by dry thermal treatment of WSD plus chitin in a muffle furnace to a range of temperatures up to 610 °C. This analysis demonstrated that nitrogen could be still be detected in the samples that had been thermally treated up to 610°C (Fig. 7-5a-e). At temperatures >610 °C the chitin produced a hard residue that adhered to the surface of the crucible, and therefore could not be measured.
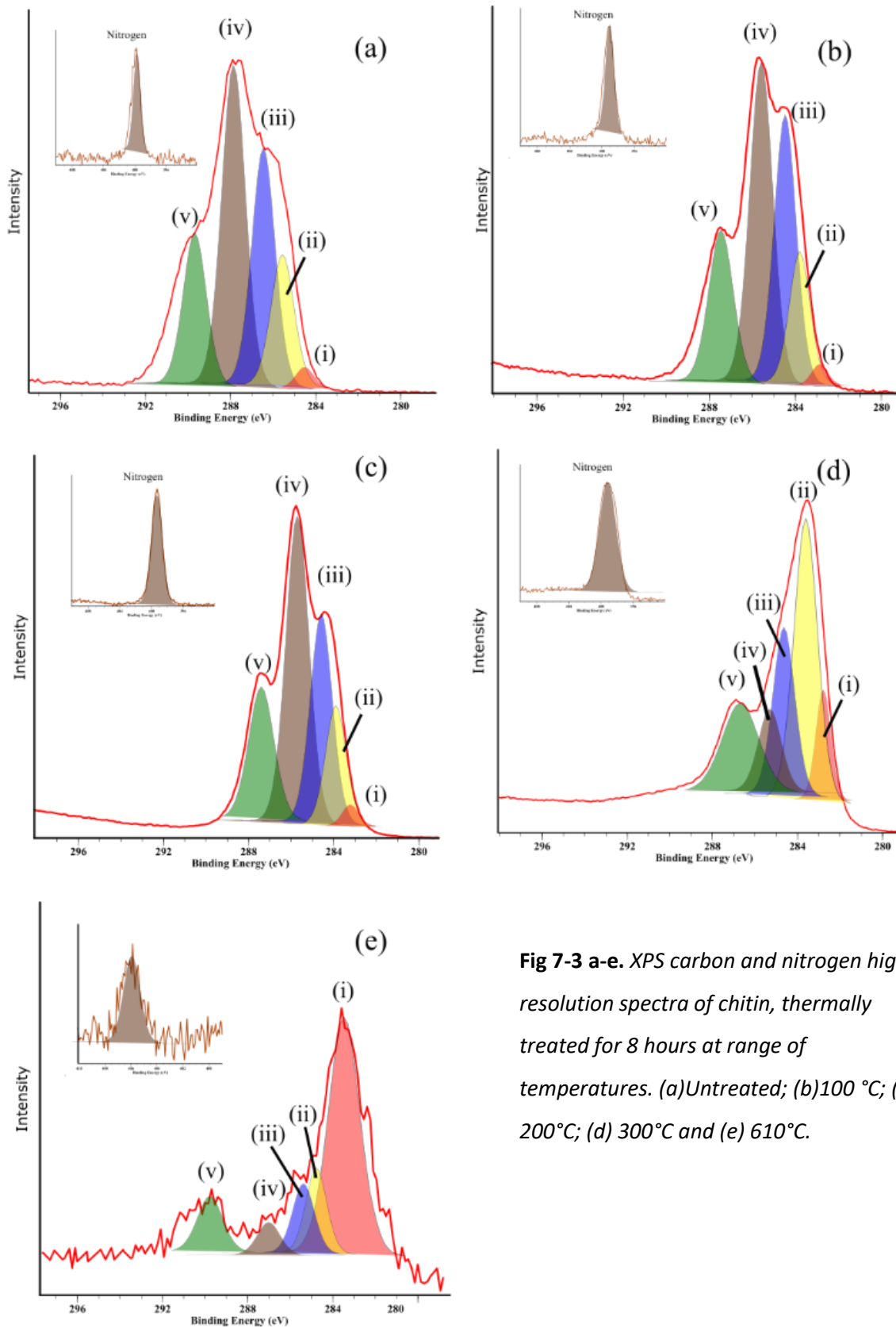
Fig 7-3 a-e. *XPS carbon and nitrogen high-resolution spectra of chitin, thermally treated for 8 hours at range of temperatures. (a)Untreated; (b)100 °C; (c) 200°C; (d) 300°C and (e) 610°C.*

Table 7-3. *Key to Fig. 7-1 a-c showing component assignments*

	Chemical State identified by XPS	Position (±0.1eV)	Compounds identified by GC/MS
(i)	C=C	284.6	Benzene/Naphthalene
(ii)	C-C	285.1	Lipids/Methyl side groups
(iii)	C-N C=O	285.6	Pyridine/Pyrrol
(iv)	C=O, CNO, C=OO	288	Lipids/amides
(v)	$CaCO_3$/$NaCO_3$	289.5	N/D

7.3.2 THM-GC/MS of Plant Biopolymers

The XPS data (Section 7.3.1) indicated that the nitrogenous organic compounds could only be detected in the WSD plus chitin (Fig. 7-2c). Therefore, to support this observation, THM-GC/MS analysis was conducted on WSD spiked with biopolymers that were untreated by hydrous pyrolysis.
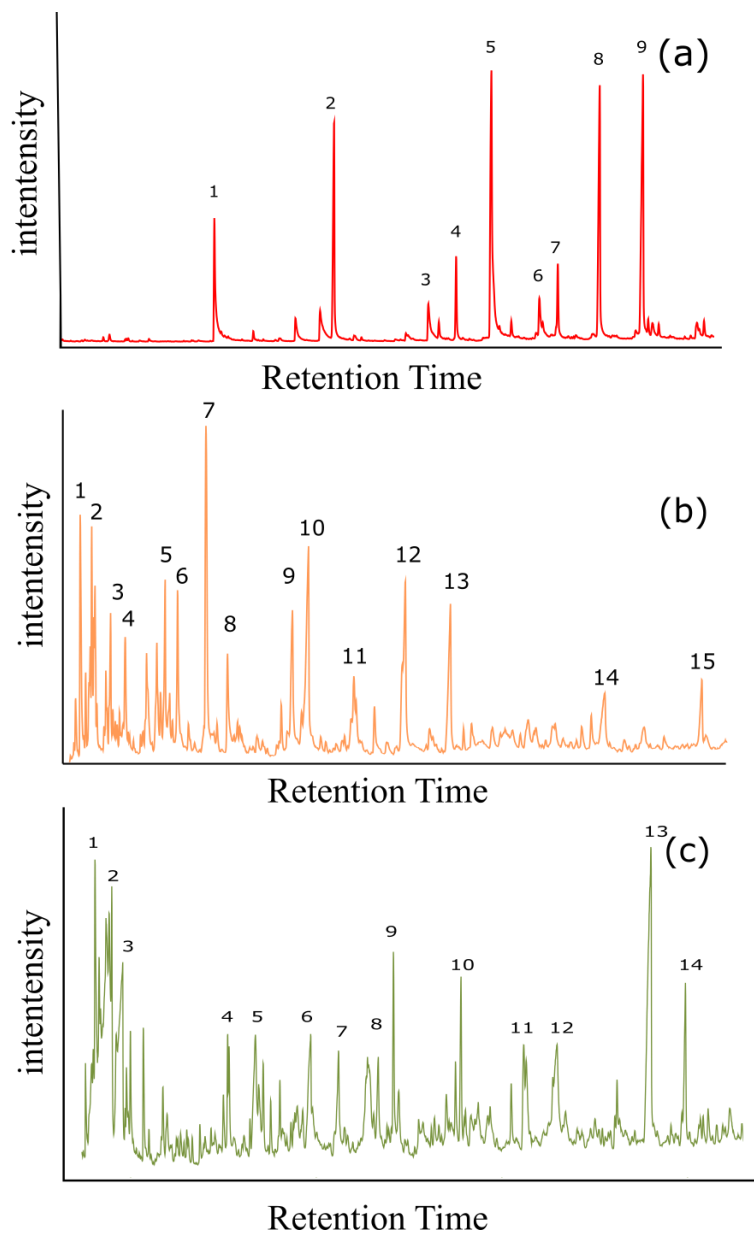
Fig 7-4. *Chromatograms produced by the THM-GC/MS analysis of WSB spiked with biopolymers(a) WSD plus cellulose, (b) WSD plus lignin and (c) WSD plus chitin.*

Table 7-4 : Key to and Values Chromatogram in Fig. 7-4(a). *5 most abundant m/z values and Identified peaks with match factors, for THM-GC/MS of WSD plus cellulose, as received. Match= match factor with NIST05 database*

Peak	m/z	ab.	m/z	ab.	m/z	ab.	m/z	ab.	m/z	ab.	Peak assignment	Match
1	96	24	95	20	86	100	81	9	74	9	Pentanoic acid	0.67
2	92	6	91	10	88	47	74	80	73	100	Ethylformamide	0.77
3	84.9	1	84	1	59.9	2	59	4	58	100	Acetamide	0.75
4	85	5	83.9	100	69	2	59.9	2	58	5	2-ethyl-5-methylPhenol	0.84
5	96.9	6	95.9	100	94.9	98	82	5	69	2	Octadecadiynoic acid	0.66
6	96.9	6	95.9	100	94.9	98	82	5	69	2	Acetic acid	0.65
7	98	86	97	36	83	25	81	35	72	100	1,4-dimethyl-Indole	0.67
8	110	3	109	2	84.9	3	83.9	61	69	1	5,7-dimethyl-Indazole	0.66
9	99	6	98	100	70	13	69	27	56	5	2,3,7-Trimethylindole	0.84

Table 7-5 : Key to and Values Chromatogram in Fig. 7-4(b). *5 most abundant m/z values and Identified peaks with match factors, for THM-GC/MS of WSD plus lignin, as received. Match= match factor with NIST05 database*

Peak	m/z	ab.	m/z	ab.	m/z	ab.	m/z	ab.	m/z	ab.	Peak assignment	match
1	56	22	55	100	72	15	58	14	53	17	Propenal	0.93
2	74	19	78	100	55	20	53	14	75	24	Acetamide	0.85
3	86	36	57	17	58	15	96	100	95	15	Pentanone	0.74
4	57	20	73	100	74	10	88	13	56	12	Butanoic acid,	0.75
5	58	11	57	17	55	13	59	100	53	31	Propanal	0.97
6	84	12	54	10	55	11	53	100	57	3	Furanone	0.82
7	96	12	94.9	32	67	11	97	21	82	17	Furfural	0.92
8	72	44	98	10	97	100	81	7	55	14	2-Furanmethanol	0.9
9	55	27	83.9	43	54	2	53	100	56	7	2(3H)-Furanone	0.92
10	98	32	55	8	69	21	70	20	99	100	5-methyl-Furanone	0.82
11	110	16	109	100	55	19	86	36	53	25	Furancarboxal	0.67
12	114	24	58	26	57	100	55	22	85	9	methyl-Oxazolidine	0.8
13	112	100	69	21	55	17	83	30	56	23	Cyclopentanedione,	0.9
14	114	100	56	13	83.9	53	85	32	55	17	Furandione	0.87
15	69	16	57	21	70	21	85	100	58	20	Pentanol	0.71

Table 7-6 : Key to and Values Chromatogram in Fig. 7-4(c). *5 most abundant m/z values and Identified peaks with match factors, for THM-GC/MS of WSD plus chitin, as received. Match= match factor with NIST05 database*

Peak	m/z	ab.	m/z	ab.	m/z	ab.	m/z	ab.	m/z	ab.	Peak assignment	Match
1	**93**	100	**59**	15	**66**	21	**92**	14	**78**	6	**3-methyl-Pyridine**	0.8
2	**59**	17	**109**	100	**81**	21	**80**	18	**54**	8	**3-amino- Phenol**	0.64
3	**73**	10	**17**	22	**59**	11	**74**	100	**54**	27	Acetaldehyde	0.91
4	**125**	100	**110**	30	**54**	18	**82**	20	**84**	15	**Pyrrolidinone**	0.73
5	**56**	10	**57**	100	**99**	28	**67**	12	**54**	18	**Piperidine**	0.73
6	**56**	10	**57**	16	**99**	100	**54**	19	**55.1**	3	**Acetamide**	0.7
7	**94**	38	**109**	20	**66**	24	**85**	18	**127**	100	**pyrroline**	0.66
8	**85**	16	**56**	22	**54**	30	**111**	100	**57**	17	Furanone	0.83
											2-methyl-	
9	**133**	22	**63**	12	**64**	17	**104**	100	**105**	10	Benzoxazole,	0.67
10	**97**	21	**139**	100	**54**	24	**96**	20	**68**	3	nonane	0.66
11	**109**	27	**95**	21	**137**	100	**81**	18	**68**	20	**1-pentyl-Pyrrole,**	0.69
12	**83**	21	**125**	100	**55**	17	**54**	16	**52**	24	**Pyrazole,**	0.69
13	**97**	21	**69**	23	**139**	100	**68**	29	**54**	13	**5-methyl- Imidazole**	0.69
14	**111**	28	**82**	21	**83**	25	**153**	100	**14**	20	acetyl-octane	0.82

The chromatograms resulting from the THM-GC/MS analysis of the WSD plus cellulose produced fewer peaks, which may have been a result of the complete thermal decomposition of the cellulose during the pyrolysis process. A lower pyrolysis temperature would perhaps have been more suitable, and this is the subject of further investigation.

7.3.4 THM-GC/MS Analysis of Hydrous-Pyrolysed products of Plant biopolymer standards
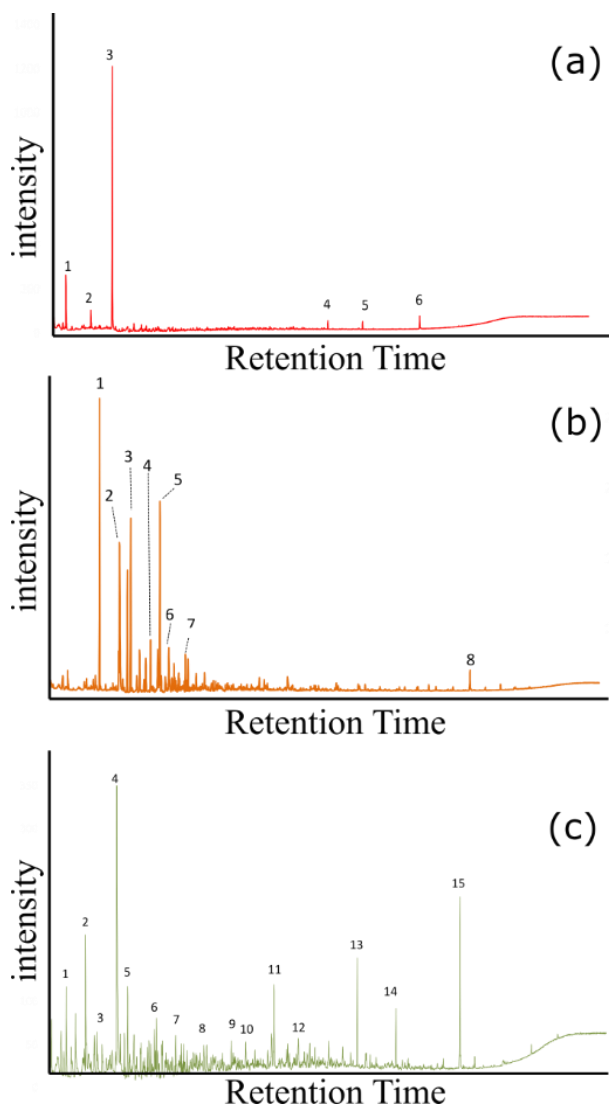
Fig 7-5. *THM-GC/MS chromatograms of hydrous pyrolysed (hy-py) plant biopolymers. WSD spiked with (a) cellulose (b) lignin and (c) chitin. The identifiable peaks are anotated and the mass to charge ratios (m/z) used to obtain the peak identity assignments.*

Table 7-7 : Key to and Values Chromatogram in Fig. 7-5(a). *5 most abundant m/z values and Identified peaks with match factors, for THM-GC/MS of WSD plus cellulose hydrous pyrolysed. Match= match factor with NIST05 database*

Peak	m/z	ab.	m/z	ab.	m/z	ab.	m/z	ab.	m/z	ab.	Peak assignment	Match
1	74.05	22	58.05	26	71.05	100	57.05	11	59.05	18	5-methyl-2-Heptanone	68
2	91.05	10	57.05	20	88.05	20	92.05	100	73.95	13	2,4-Difluorobenzene	60
3	86.05	17	128.05	100	57.05	14	129.05	10	85.05	16	1,3,5-Triazine,	92
4	74.05	8	87.05	10	55.05	16	75.05	17	143.05	100	Pentadecanoic acid	79
5	74.05	22	87.05	19	55.05	13	75.05	16	143.05	100	Heptadecanoic acid	83
6	55.05	13	69.05	15	83.05	15	97.05	18	122.05	11	Oleic acid	69

Table 7-8 : Key to and Values Chromatogram in Fig. 7-5(b). *5 most abundant m/z values and Identified peaks with match factors, for THM-GC/MS of WSD plus lignin hydrous pyrolysed. Match= match factor with NIST05 database*

Peak	m/z	ab.	m/z	ab.	m/z	ab.	m/z	ab.	m/z	ab.	Peak Assignment
1	73.05	100	72.05	17	58.05	25	74.05	30	56.05	11	dimethyl-Formamide
2	108.05	100	65.05	26	78.05	21	77.05	14	79.05	2	Methoxy-Benzene
3	86.05	17	128.05	100	57.05	14	129.05	10	85.05	16	1,3,5-Triazine
4	122.05	100	107.05	37	77.05	21	91.05	27	79.05	29	1-methoxy-2-methyl-Benzene
5	122.05	100	107.05	37	77.05	21	91.05	27	79.05	29	1-methoxy-4-methyl-Benzene
6	121.05	100	91.05	22	136.05	21	77.05	21	65.05	32	2,6-Dimethylanisole
7	121.05	10	136.05	18	77.05	22	91.05	21	122.05	100	1-ethyl-4-methoxy-Benzene
8	107.05	17	122.05	26	121.05	25	77.05	17	138.05	100	2,5-dimethyl-Phenol

Table 7-9 : Key to and Values Chromatogram in Fig. 7-5(c). *5 most abundant m/z values and Identified peaks with match factors, for THM-GC/MS of WSD plus chitin, hydrous pyrolysed. Match= match factor with the NIST05 database. Nitrogenous compounds in old*

Peak	m/z	ab.	m/z	ab.	m/z	ab.	m/z	ab.	m/z	ab.	Peak Assignment
1	73.05	100	72.05	10	58.05	17	74.05	8	56.05	16	Dimethyl-Formamide,
2	73.05	14	58.05	15	94.05	100	74.05	13	95.05	9	**Methyl-Acetamide**
3	87.05	100	72.05	22	88.05	7	56.05	14	58.05	2	**Dimethyl-Acetamide**
4	108.1	100	78.05	1	65.05	19	86.05	14	77.05	10	Methoxy-Benzene,
5	122.1	100	107.1	21	77.05	31	91.05	17	79.05	22	1-methoxy-2-methyl-Benzene
6	122.1	100	107.1	21	77.05	31	91.05	17	79.05	22	1-methoxy-4-methyl-Benzene
7	121.1	32	136.1	100	77.05	20	91.05	2	122.1	15	1-ethyl-4-methoxy-Benzene
8	133.1	10	135.1	8	148.1	100	91.05	7	147.1	1	Acetic acid
9	144.1	100	145.1	1	128.1	13	136.1	17	143.1	31	1,3-dimethyl-Indole,
10	144.1	19	145.1	21	161.1	100	156.1	34	115.1	18	1,3,5-Trimethyl-2-(2-**nitrovinyl benzene**
11	158.1	11	159.1	100	144.1	17	143.1	18	115.1	32	1,2,3-trimethyl-Indole,
12	172.1	100	173.1	6	158.1	15	159.1	16	174.1	1	1,2,3,7-Tetramethyl indole
13	74.05	4	87.05	8	55.05	3	75.05	22	143.1	100	Pentadecanoic acid
14	74.05	4	87.05	8	55.05	3	75.05	22	298.4	100	Heptadecanoic acid
15	55.05	15	69.05	29	83.05	27	97.05	16	122.1	100	Hexadecenoic acid

THM-GC/MS analysis of the WSD plus plant biopolymers indicated that their molecular composition was altered as a result of hy-py. Although, it would be anticipated that a fraction of this material would have adhered to the WSD surface, which would have been detectable using THM-GC/MS. The complete decomposition of the organic material during the hy-py of cellulose was possibly due to hydrolysis of the glycosidic link between the glucose residues, then the resulting glucose dissolved in the water used in the bomblets, which was not analysed. The THM-GC/MS analysis of hy-py residue of lignin (Fig. 7-5b) resulted in the detection of aromatic compounds. The THM-GC/MS analysis of hydrous pyrolysed chitin (Fig. 7-2c), suggested that chitin may have been the most resistant to thermal decomposition.

7.4.0 Discussion

7.4.1 Analysis of Plant Biopolymer Standards

It was reasoned that the spectral profiles of the OJP tuffs presented in Chapter 6 (OJP_13, OJP_22 and OJP_43; Fig 6-2a-c) might have provided an indication of the source taxonomic group. However, the carbon spectral profiles of the AR or the hy-py treated plant biopolymers, could not definitively demonstrate a diagnostic carbon spectral profile for interpretation of the taxonomic origin of the organic material in the OJP tuffs. Similarly, the supporting THM-GC/MS analysis of both plant biopolymers _AR and plant biopolymers_hy-py did not yield any specific compounds that permitted a definitive plant or fungal assignment. The implication is that neither the XPS carbon spectral profile nor a single compound identified in the THM-GC/MS can be used to specifically assign a plant or fungal origin to material that has undergone diagenesis.

However, the XPS analysis did show that the carbon spectral profile of each of the biopolymers had been altered as a result of thermal decomposition, using both hy-py and dry heating in the muffle furnace. The paucity of chemical states observed in these samples (Fig. 7-1a-c and 7-2a-c) may be as a result of the thermal decomposition of labile functional groups, particularly the hydroxyl and carboxyl groups, that are associated with the carbohydrate molecules of cellulose and chitin. This may also explain the loss of the nitrogen in the lignin, where organic nitrogen may have been decomposed and dissolved in

the water used during hy-py. This is unsurprising, as hydroxyl and carboxyl groups are the most thermally labile and are readily lost during diagenesis (see Section 1.11.2). The peak position at 284.9 eV in the carbon high-resolution XPS spectral profiles of the hy-py and the dry heated plant biopolymers suggested that they consisted of a greater proportion of aromatic compounds. This thermal decomposition mimicked the decomposition of biopolymers during late diagenesis, where organic matter is reduced to aromatic compounds by low-temperature anoxic combustion (Buseck and Beyssac, 2014; see sections 1.11.1 and 1.11.2). This suggested that the carbon spectral profiles provided evidence that the carbonaceous material in the OJP tuff had undergone late diagenetic processing and therefore implied that the carbonaceous material in the OJP is fossilised material, rather than an organic material derived from any extant organisms.

The carbon XPS spectral profiles could not provide data regarding a specific taxonomic assignment. However, nitrogen was detected in the untreated chitin (chitin_AR) and hydrous pyrolysed chitin (chitin_hy-py) samples, but not in either of the untreated and hydrous pyrolysed cellulose and lignin samples. This suggested that the presence of elevated concentrations of nitrogen in a fossil sample could have indicated a chitinous organism, rather than a higher plant provenance. Thus, the nitrogenous compounds that were detected in the OJP tuff (OJP_13, OJP_22 and OJP_43) were potentially the diagenetic remnants of a chitinous organism, of which the fungi were the most likely candidate taxonomic group.

The THM-GC/MS analysis of the samples resulted in a highly complex range of compounds, which confounded precise identification (see section 4.3.2). Nevertheless, the THM-GC/MS analysis also indicated that the compounds, which were detected in hydrous-pyrolysed chitin were comparable to the compounds that were detected in the OJP tuffs. In contrast, nitrogenous organic compounds were not detected in the cellulose or lignin. Although the compounds in the major peaks of the OJP tuff chromatograms could not be identified precisely. The peak reverse match factors of >70, provided confidence in the class of compounds that were identified; these were principally alkyl or ethyl functionalised aromatic compounds with nitrogen substituting carbon in some of the aromatic rings. This nitrogen could have originated from the amine group in chitin (see section 1.10.2). This

observation is consistent with Boudou et al. (2008), where it was demonstrated that nitrogen was incorporated into aromatic compounds to form pyridine and pyrrole compounds during diagenesis and catagenesis (see section 1.11.2). This is also supported by other investigations reported in the literature, where the hydrous pyrolysis of arthropod chitin resulted in the detection of pyrimidines and pyrrole compounds using pyrolysis GC/MS analysis (Monthioux and Landais, 1989; Gupta, 2006). Additionally, nitrogen-containing aromatic compounds have been detected using py-GC/MS in both fossilised scorpion exoskeletons (Stankiewicz et al., 1996), and in sediments that contain the fossils of chitinous insects (Flannery et al., 2001) and where the chemical states detected in the hy-py chitin were comparable to the chemistry detected in fossil chitinous arthropods using X-ray absorption near edge structure (XANES) analysis (Cody et al., 2011).

7.4.2 A Potential origin for the nitrogenous aromatic material in the OJP Tuff

The observations imply that the organic material in the OJP tuffs may contain the diagenetic products of chitin. The eastern lobe of the OJP was formed from a recurrent, intermittent, deposition of volcanishardic sediments (tuff). Between the volcanic events, the land surfaces were colonised by flora, that was then buried during the volcanic events, resulting in the deposition of several layers of plant material (see Fig. 6-1; Thordarson, 2001; ODP, 2005), which would have provided a suitable substrate for marine fungi, which are known to be the major decomposers of ligneous material in marine sediments, throughout the world's oceans (Hyde et al, 1998). Furthermore, the evidence for the presence of submarine endoliths in the oceanic crust (Bengtson et al., 2014; Ivarsson, 2011; Ivarsson et al., 2012a; Ivarsson et al., 2013a; Ivarsson et al., 2013b; Ivarsson et al., 2015a; Ivarsson et al., 2015b) suggests that this environment may be the Earth's largest habitat for fungi (Ivarsson et al., 2012b; Ivarsson et al., 2016). Perhaps this is unsurprising since the presence of fossilised and extant fungal communities, deep within sub-seafloor basalts has been previously reported (Ivarsson et al., 2012; Ivarsson et al., 2016) and these communities would certainly be capable of metabolising the plant material buried during the construction of this region of the OJP.

The geochemical remnants of this fungal community could have been preserved in the form of the nitrogenous aromatic compounds. Cody et al.(2011) and Ehrlich et al. (2013)

suggested that the diagenetic remnants of chitin, from other types of organisms, appear to persist in the geological record, in a time scale of millions of years. The investigation conducted here and showed that the nitrogenous chemistry of chitin is resistant to thermal decomposition at temperatures in excess of the ca. 350-400 °C, that are encountered in the upper 8 km of the lithosphere (Stacey, 1977). Thus, the remnants of a fungal endolithic organism, or fungal endolithic community in the OJP tuff, may have produced the observed elevated concentrations of nitrogen.

7.5 Conclusion

The carbon spectral profiles cannot be used to ascertain any taxonomic information in the OJP tuff samples. However, the untreated plant structural biopolymer high-resolution XPS spectral profiles were presented here, for the benefit of future studies. Analysis of plant biopolymer following hydrous pyrolysis (a process that mimicked late diagenesis), indicated that nitrogenous aromatic compounds were detected in chitin, but not in the other plant biopolymers, cellulose and lignin. This indicated that the nitrogenous organic material detected in the OJP tuff (OJP_13, OJP_22 and OJP_43) that were described in Chapters 4-6 could potentially have been the result of the diagenetic products of chitin, the key structural biopolymer of fungus. Heating the chitin to 610 °C demonstrated that the nitrogen component, in chitin, was resistant to thermal decomposition to that temperature and could therefore plausibly be resistant to thermal decomposition, at the temperatures experienced during the deep burial of organic material. The carbon XPS spectra profile of the plant biopolymers indicated that the organic material in the OJP tuff had undergone diagenesis. However, it did not provide any evidence to suggest a taxonomic source of the hydrous pyrolysed organic material, and therefore, the use of XPS carbon high-resolution profiles are insufficient for this purpose.

CHAPTER 8: THE DETECTION OF CARBONACEOUS FILMS ON MARS ANALOGUES AND ON THERMALLY TREATED GEOLOGICAL SAMPLES.

Abstract

The organic material present on the surface of Mars could be derived from any number of non-biological sources, such as geochemical and cosmochemical processes, or potentially organic material could be derived from an extinct or extant biosphere. Determining the differences between these two sources of organics will require instigation during the forthcoming astrobiological exploration of Mars. Ubiquitous layers of carbonaceous material described as 'adventitious carbon' (AC) can be found on all surfaces, and to date, the implications of this material in the context of the astrobiological exploration of Mars has received little consideration. This chapter considers the impact of AC in the explorations of Mars, by investigating the limitations of the pyrolysis instruments to thermally extract organic material prior to analysis by gas chromatography/mass spectrometry (py-GC/MS), which is a technique that is commonly employed in the characterisation of organic material in the exploration of the solar system and has been deployed on Mars. It is demonstrated that the surface localised aromatic hydrocarbons that are detected using X-ray photoelectron spectroscopy (XPS) are present on geological samples that were then subsequently undetectable using py-GC/MS. It is further demonstrated in this chapter that a portion of this organic matter is still present after treatment to 1000 °C. This may explain why it is undetectable by py-GC/MS. However, this hydrocarbon, which is potentially bound by the same interactions as those that form adventitious carbon, was in contrast, detectable by XPS. It is speculated that this organic matter/rock surface interaction may also drive otherwise unfavourable reactions such as polymerisation, resulting in the formation of high molecular weight organic compounds from low molecular weight organic compounds.

8.1 Introduction

Complex organic materials can be observed throughout the cosmos, e.g. (Henning and Salama, 1998; Botta and Bada, 2002; Pizzarello et al., 2006; Ehrenfreund and Cami, 2010, Pizzarello and Shock, 2010). Therefore, it is unsurprising that even if a biosphere had ever

been present on Mars, then its remnant organic material, should be detectable (Grotzinger et al. 2013; Eignenbrode et al., 2018; TenKate, 2018). This material could have been deposited by carbonaceous chondritic meteorites (Hayatsu and Anders 1981; Lancet and Anders 1970) and by interplanetary dust in fall (Llorca 2002; Pizzarello et al., 2006) onto the tectonically inactive surface of Mars for at least 4.0 billion years (Flynn, 1996). Additionally, this material could have originated from the Martian magma (Steele et al., 2012). Due to the reliability and robust designs, pyrolysis-gas chromatography/mass spectrometry (py-GC/MS) has been employed extensively in space exploration, for the characterisation of organic material (Johnson, 2012). Consequently, previous and current Mars missions have used both thermal extraction and pyrolysis (thermal cleavage) to extract organic material from the Martian rock. Here the term pyrolysis (py) is used to encompass each of these processes. This is coupled to gas chromatography/mass spectrometry (GC/MS) to detect and characterise organic material on Mars (Cabane, 2001; Rodier et al., 2005; Buch et al., 2009; also see section 1.7.1.)

Organic material has recently been detected on Mars by the Curiosity rover (Eigenbrode et al., 2018), using the SAM instruments, which includes a py-GC/MS (Cabane et al., 2001). However, earlier investigations had suggested that there may be limitations of the pyrolysis pre-step, which is used to thermally-desorb the traces of organic material from the host mineral matrix, in organic-poor Mars analogues, which may have explained the challenge in detecting such material on Mars (Navarro-Gonzalez et al., 2006; Navarro-González et al., 2009). Thus, not all carbonaceous may be accessible using py-GC/MS-based analysis, which may impair the complete characterisation of organic material on Mars, in the future.

8.1.1 The Ubiquity of Adventitious Carbon

Ubiquitous carbonaceous films, described as "adventitious carbon" (AC) have been reported since the instruments that are able to conduct their analysis at nano-scale depths, were first used (Siegbahn et al., 1967; Wagoner, 1980). These AC films are present on the surface of all materials, and it forms when any freshly exposed surface absorbs material from the immediate environment. It is a process that occurs essentially instantaneously, at atmospheric pressures, and occurs within 30 minutes at ultra-high vacuum conditions

(Briggs, 1983 and Seah, 1983; Barr and Seal, 1995; Miller et al., 2002; Piao and McIntyre, 2002; De Gregorio, 2011; Mangolini et al., 2014; Paul et al., 2016).

Until recently, the role of AC has been given little consideration in the context of organic cosmochemistry. However, the ubiquity of AC implies that it could be present even on geological samples that are thought be essentially devoid of organic material, including the desert rocks that are used as Mars analogues, which have previously been analysed using py-GC/MS, and indeed it should be present on the internal surfaces of rocks that are buried on Mars, which are not exposed to the harsh Martian radiological environment. Potentially, AC could be detected on Mars, which could provide an insight into Martian organic geochemistry and a context for its astrobiology.

In contrast to py-GC/MS, surface analytical techniques such as X-ray photoelectron spectroscopy (XPS) can directly measure the concentrations of all elements (other than H) and their chemical states, in the top 1-10nm on a sample surface (see section 1.12.4) without an extraction step. This direct measurement can mitigate the limitations imposed by thermal extraction prior to GC/MS analysis. In this chapter, XPS was used to measure AC on the surface of near barren desert samples that have been used as Mars analogues and compare these to the measurements of organic materials in these samples that could be obtained from GC/MS. Then expendable geological samples were heated to the temperatures typically used in the pyrolysis step of py-GC/MS to remove organic material prior to analysis and were then analysed with XPS and py-GC/MS. In this way, any limitations of pyrolysis apparatus used to extract organic material prior to GC/MS analysis thermally were evaluated, and the basis for any limitation was investigated. Finally, the potential implications for the presence of AC in the form of a hydrocarbon for the geochemical and the astrobiological exploration of Mars are considered.

8.1.3 Gas chromatography/Mass spectrometry and the Definition of Limits of Detection

Chapter 3 described how XPS analysis was able to quantify carbon, following decontamination with the gas cluster ion beam etching (Fig. 3-3a). However, py-GC/MS analysis of the organic material in Whin Sill dolerite (WSD) was described as being

'undetected' (Fig. 3-4 a-c and Purvis et al., 2017). Hence, GC/MS alone was not able to determine whether organic material was entirely absent from the WSD samples.

Detecting low concentrations of organic material in geological samples, such as in igneous rocks or regoliths, is problematic because the concentration of the organic material is close to the limits of detection (LOD) for GC/MS. The LOD for GC/MS is typically quoted by manufacturers in the low femtogram range using an octafluoronaphthalene (OFN) standard. However, GC/MS LOD for the different analytes that are encountered in real-world samples, are often orders of magnitude higher than the values quoted for OFNs and this has resulted in confusion and debate in the literature, about the correct definition of the terms "sensitivity", "measurement" and "LOD" (Ekins and Edwards, 1997; Pardue, 1997; Fialkov et al., 2007). Therefore, in situations where the concentrations of the analytes are equivalent or lower than the LOD, such as in the organic poor geological samples used in this investigation, any signal is often indistinguishable from background noise and any traces of procedural contamination. Hence, it is not always possible to say definitively whether organic material is present or absent in a sample, at concentrations close to or less than LOD. In the investigation here, this uncertainty is addressed by using the term 'trace' to describe the unmeasurable concentrations of organic material in the geological samples, which is a definition that has been used previously (Eigenbrde et al., 2009). Since the organic carbon that occurs at trace levels in geological samples is usually inaccessible by py-GC/MS measurements, it is usually unreported in the literature (Botta, 2007; Fristad, 2015).

The near-barren telluric regoliths that have been used as analogues for the organic-poor Martian regolith (Marlow et al., 2008) were analysed with GC/MS and XPS. In this thesis, organic-poor Polar Desert and Atacama Desert samples were analysed. These were comparable to some of the samples that were previously used to investigate the failure of py-GC/MS to detect low concentrations of organic material in desert rock specimens by Navarro-Gonzalez et al. (2006). These earlier experiments were conducted with py-GC/MS. Therefore, this method of analysis was the one selected for these investigations. However, the addition of TMAH during pyrolysis (thermal hydrolysis and methylation) increased the range and intensity of the organic compounds that were detected in the OJP_13 samples

(See section 1.12.3 and Fig. 4-2). Therefore THM-GC/MS was also conducted on these samples. Since the desert samples used in the first part of this investigation were rare and precious, it was necessary to use other geological samples that possessed low concentrations of organic material to conduct further investigations of the AC.

8.1.4 Mars Analogue JSC-1

The Mars JSC-1 analogue was selected as it is a near-barren regolith and because it is routinely used in the investigations of the Martian regolith (McCown et al., 2005; ten Kate et al., 2013). JSC-1 is a Hawaiian palogonised volcanic tephra, which possesses the same spectral signature as the bright regions on Mars (Allen, 1997). It is obtained from in between the cinder cones of Mauna Loa and Mauna Kea. These are mature lava fields, which are in the process of colonisation by higher plants (see Fig. 8-1). Consequently, these samples were from organic-rich soils, and the intention was to remove this material using thermal treatment.

Fig 8-1. *A panoramic view of the region located between the Mauna Loa and Mauna Kea where the JSC-1 was collected. Note: the colonisation of the lava field by vegetation in the foreground. Credit: Google maps. www.google.com/maps/place/Mauna+Loa/*

8.1.5 Thermal Treatment of Geological Samples

Pyrolysis is based on the volatilisation and thermal decomposition of organic compounds at temperatures up to 1000 °C (see section 1.12.2). The integration of peak areas in the GC/MS chromatograms can provide quantitative information on the analytes detected by these instruments. In addition to py-GC/MS, quantification of the total organic carbon (TOC) in the samples was conducted by thermally desorbing and thermally decomposing (pyrolysing) samples at 2700 °C in the presence of an oxidising agent, which is described as dry combustion analysis (Bernard, 1995). The thermal desorption and decomposition of organic material are routinely exploited to remove contamination from laboratory equipment by

heating the equipment in a bench top furnace (e.g. Eigenbrode, et al. 2009). It was anticipated that such thermal treatment would desorb any carbonaceous material from the WSD rock samples, thereby removing carbonaceous material from those samples. Therefore, the carbonaceous material in organic-poor, geological samples before and after thermal treatment to 1000 °C was measured using this procedure.

The samples selected for thermal treatments were: Whin Sill dolerite (WSD); sand that had been cleaned of organic material using Soxhlet extraction for 24 hours and allowed to dry (hereafter referred to as sand) and bentonite. WSD is an igneous rock, and its internal volume possessed no detectable levels of biological activity or organic material when examined using py-GC/MS. It contained none of the geological textures such as glass shards, seen in the other samples used in this thesis. Therefore, it was selected for the investigations as a procedural blank (see section 3.1.1; Purvis et al., 2017). Solvent cleaned sand is frequently used as a procedural blank for py-GC/MS investigations at Newcastle University. Bentonite was used to study the effect of thermal treatment on clay, since these have large surface areas that could potentially absorb proportionally high amounts of organic material that could be preserved on Mars (Ehlmann et al., 2008; McKeown et al., 2009; Bonaccorsi et al., 2010; Ehlmann et al., 2011) but have been reported to be unamenable to py-GC/MS (Milliken and Bish, 2010).

8.2 Methods

The Atacama and Polar Desert samples were obtained from the locations described in Table 8-1a, and samples used in thermal treatment experiments are described in Table 8-1b and were analysed with both py-GC/MS and XPS in either an untreated (hereafter described as 'As Received' or _AR) or thermally treated to 1000 °C for 8 hours in a 15 litre muffle furnace (Hereafter _1000).

Code	Description	Acquired from
At_ 01	Atacama Desert	23° 24' 27.38"S 69° 31' 3.78" W
PD_01	Polar Desert	Ref: 845/240
PD_02	Polar Desert	Ref: 856/123

Table 8-1(a). *The codes and descriptions of the near barren, desert samples equivalent to those samples used as Mars Analogues.*

Code	Description	Acquired from
JSC-1	Volcanic palagonite	Orbitec, Inc
WSD	Whin Sill dolerite	N55° 28.427' 001 35. 577' W
Sand	Soxhlet extracted Sand	Sigma Aldrich
Bent	Bentonite clay	Sigma Aldrich

Table 8-1(b). *The codes and descriptions of the samples that served as expendable analogues for the desert samples in table 8-1(a).*

Py-GC/MS, THM-GC/MS and XPS were conducted upon the samples according to the protocols in section 2.4.2. and 2.4.1, respectively. The quantification of the AC with XPS was carried out using survey spectra, utilising the non-carbon elements as an unchanging standard (see section 3.2.2).

The analysis of organic material using py-GC/MS was conducted according to the protocol described in section 2.4.2, with the following changes: 2 pmol androstane was added immediately prior to pyrolysis, as an internal standard peak and peak area integration was conducted using the OpenChrom software (www.openchrom.net) to measure the organic carbon concentration in the samples using GC/MS. The total organic carbon (TOC) concentration was obtained using dry combustion with a Leco 2300 Carbon Determinator according to the manufacturer's instructions (Leco, 2016).

8.3 Results

8.3.1 Analysis of Organic-Poor Desert Samples.

The first part of the investigation measured the levels of organic material in near-barren desert samples: Polar desert_1; Polar Desert_2 and Atacama desert_1 (PD_1, PD2 and At_01) with py-GC/MS, which was compared to measurements of carbon made with XPS. THM-GC/MS was also conducted on these desert samples, but this produced results that were identical to the py-GC/MS results, and therefore have not been presented here.
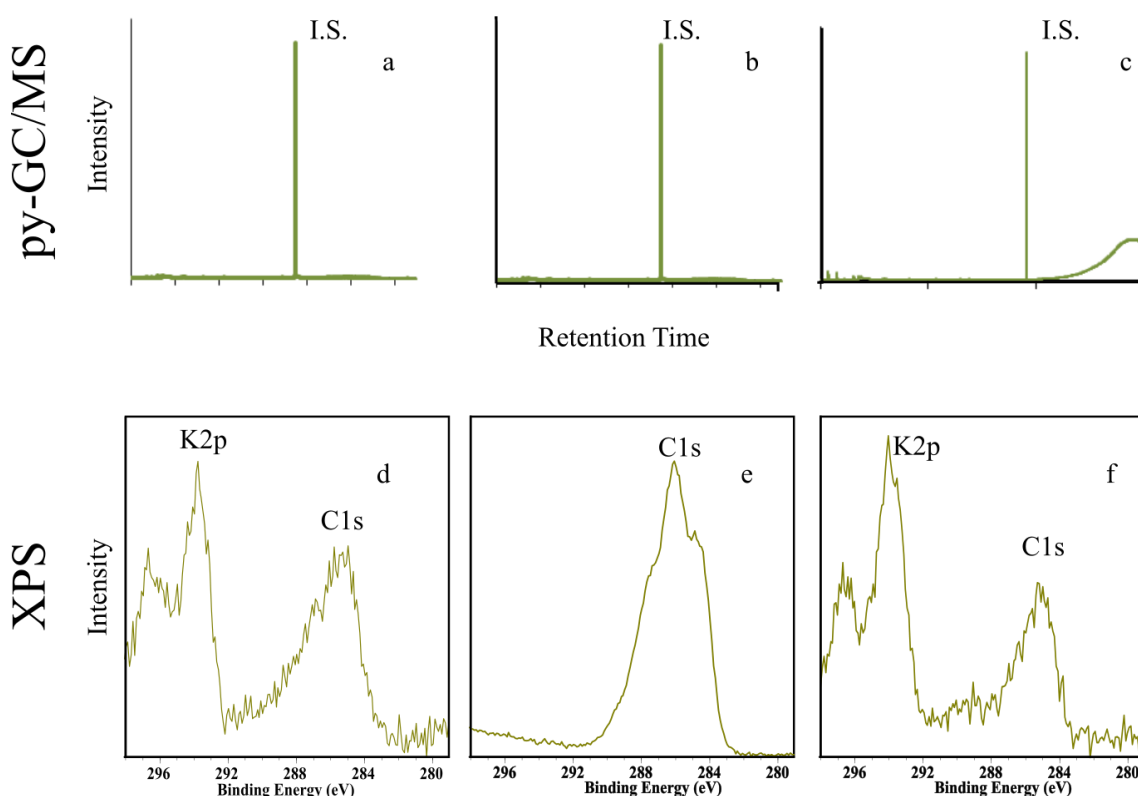
Fig. 8-2. *Py-GC/MS and XPS analysis of desert samples. I.S.=internal standard, this peak is produced by 2 pmol androstane. High-resolution of 297.0-279.0 eV region shows carbon and potassium peaks. Note: nitrogen was undetected.* **XPS:** (a) PD_1. (b) PD_ 2 (c) At_01. **py-GC/MS** (d) PD_1. (e) PD_ 2 (f) At_01. *See table 2-2 for key Carbon= carbon; K2p= potassium*

Fig 8-2a-c presented the THM-GC/MS analysis of the PD_1, PD_2 and At_01 desert samples. A comparison between the 2μl of 8 pM androstane internal standard (I.S.) intensity and the chromatograph signal intensity, suggested any organic material was detected at fmol concentrations. Thus, the organic concentration was below the LOD and was therefore

described as occurring at" trace" levels. These results were consistent with the results obtained by Navarro-Gonzalez (2006).

In contrast to the Py-GC/MS analysis, carbon was detected by XPS, in all the desert samples. The profile of the carbon spectra indicated the presence of a single component at a position of 284.8 eV, which was consistent with the presence of the C=C chemical state that was associated with aromatic compounds, implying that the carbonaceous films on the surfaces of the desert samples were in the form of PAHs. The surface concentration of carbon was quantified using the XPS survey spectra (spectra not shown), according to the methods described in Chapter 2. Additionally, the total organic carbon (TOC) concentration was obtained with dry combustion. However, the concentration was less than the LOD for the instrument used in this analysis. These results are summarised in Table 8-2. The TOC background noise level for dry combustion is ± 0.03% (Green 2015, personal communication). Therefore, the measured TOC values for the Polar and Atacama Desert regoliths, using dry combustion are effectively zero.

Sample	Dry Combustion TOC (% $^w/_w$)	GC/MS ug/g	XPS at %
At_01	0.016	Trace	6.2
PD_01	0.093	Trace	10.2
PD_02	0.006	Trace	12.7

Table 8-2. *a comparison between the quantification of carbon concentration measured by GC/MS, XPS and Dry Combustion (D.C.).*

8.3.2 Analysis of Heat treated JSC-1 Mars simulant

Given the plant material in the collection location (See fig 8-1), and the results obtained by Morisson (2017), it was anticipated that JSC-1 would have a high organic content. Thermal treatment is part of the protocol that is regularly used to remove organic material from geological samples, to facilitate the accurate measurement of the carbon content. It is also used to clean samples. Therefore, JSC-1 was heated to 1000 °C to remove the organic material from this sample.
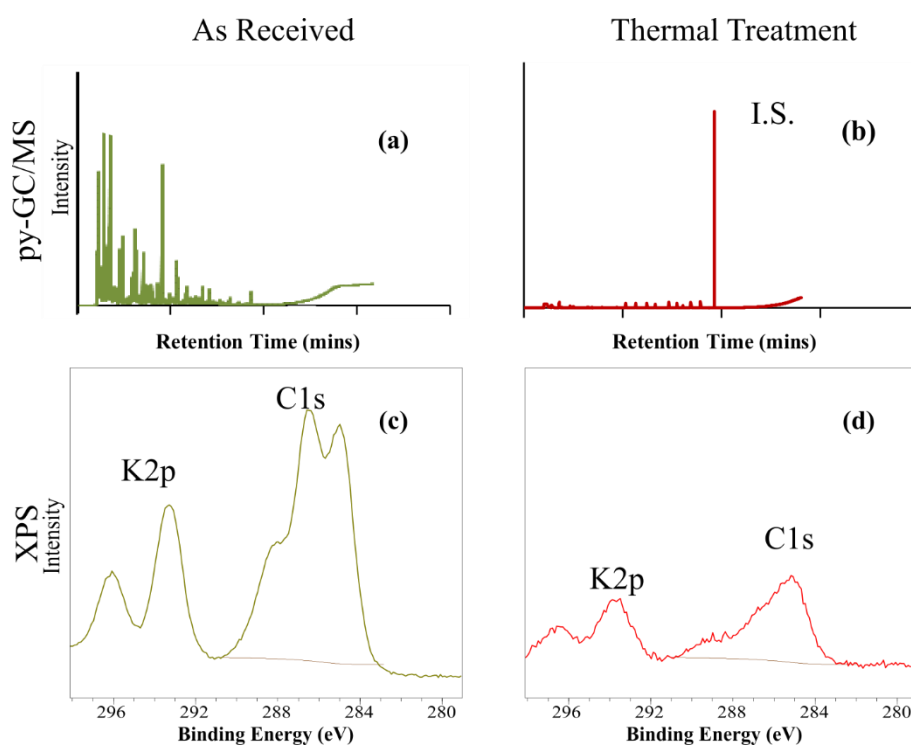
Fig. 8-3. *thermal treatment upon the JSC-1 soil sample. (a) and (c) untreated sample (JSC-1_AR) analysed with py-GC/MS and XPS, respectively. (b) and (d) sample analysed following the thermal treatment to 1000 °C (JSC-1_1000) with py-GC/MS and XPS respectively. For clarity, the binding energy for K2p at 294 eV was also labelled. I.S. Androstane internal standard. C1s= carbon; K2p= potassium.*

The py-GC/MS analysis of the untreated JSC-1 (Fig. 8-3 a) produced a range of high-intensity peaks demonstrating that the JSC-1 contained measurable levels of organic material. The peaks identified consisted of PAHs and their alkylated and alkynylated derivatives but also included N and O bearing heterocyclic compounds. The data was consistent with earlier investigations of JSC-1_AR using THM-GC/MS (Morrison et al., 2017). However, following thermal treatment, of the JSC-1 sample with py-GC/MS (Fig. 8-3 b), the chromatogram appeared to suggest that this organic material had been removed from the JSC-1_1000 sample.

As expected, XPS analysis of the JSC-1_AR sample (Fig. 8-3 c) indicated the presence of carbonaceous material, which corresponded to the organic material detected in the py-GC/MS analysis and the complex spectral profile, which suggested a complex suite of

216

chemical states that was consistent with the range of compounds that were identified using THM-GC/MS (Morisson, 2017). However, contrary to the predictions, a carbon peak was present in XPS analysis of the JSC-1 following thermal treatment to 1000 °C (JSC-1_1000). The spectral profile of JSC-1_1000 was transformed, which resulted in a spectral profile that was comparable to the AC observed in the desert samples (PD_1, PD2 and At_01).

Potentially, the organic material in the JSC-1_1000 sample has thermally decomposed and desorbed from the samples upon the thermal treatment, and the AC was reabsorbed following cooling. Py-GC/MS and dry combustion were used to measure the TOC of JSC-1 sample, before and after thermal treatment (see table 8-3) to test this possibility. This demonstrated that organic material was undetectable in the thermally treated JSC-1, using dry combustion or with py-GC/MS, but was detectable with XPS.

Sample	Dry Combustion TOC (%^{w}/$_w$)	GC/MS ug/g	XPS at %
JSC-1 AR	1.368	4.95	21.2
JSC-1_1000	0.000	Trace	4.35

Table 8-3. *the concentrations of organic material in the JSC-1 sample before and after thermal treatment.*

8.3.3 Thermal treatment of organic-poor rock samples

The results from Section 8.3.1 indicated that AC was detected in the desert samples (At_01, PD_1 and PD2) using XPS. The AC is undetectable with py-GC/MS, due to the failure of the pyrolysis step, to desorb the AC from the samples. Accordingly, it was hypothesised that thermal treatment would also not desorb the AC from the surface of the samples. Furthermore, the results from Section 8.3.2 suggested that the AC was not desorbed as a result of thermal treatment from the JSC-1 (AR and 1000) sample. Therefore, it was essential to investigate whether the AC was not desorbed from the organic-poor desert samples in a similar way. However, the At_01, PD_1 and PD2 desert samples could not be used due to their value and scarcity. Consequently, the second part of the investigation

217

studied the effect of thermal treatment of the organic material on low organic geological samples using the WSD, Sand and Bentonite samples with py-GC/MS, dry combustion and XPS analysis identical to the analysis that was conducted on the Mars analogue desert samples.
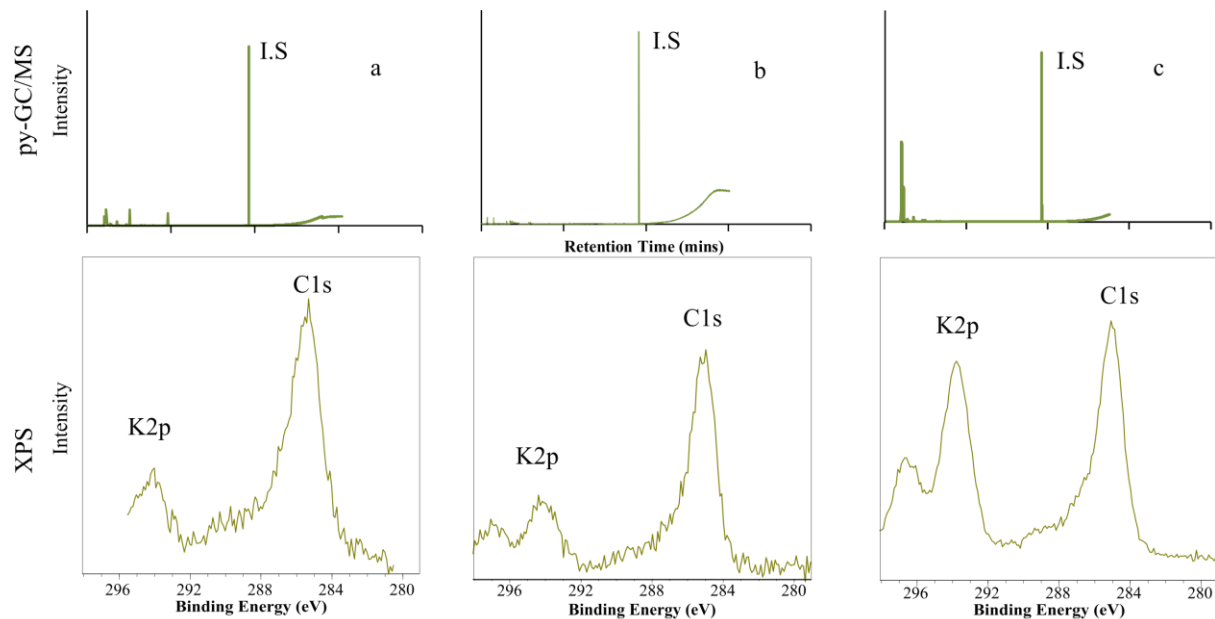
Fig. 8-4. *the py-GC/MS and XPS analysis of organic poor geological samples **(a) WSD_AR (b) Sand_AR (c) Bent_AR (d) WSD_AR (e) Sand_AR (f) Bent_AR** that were available for thermal treatment, in their As Received condition. Carbon= carbon; K2p= potassium*

Py-GC/MS analysis suggested that the organic poor, geological samples (WSD_AR, Sand_AR and Bent_AR) contained trace levels of organic material (Fig 8-4a-c), whereas, Fig 8-4d-f showed that AC could be detected in these samples using XPS. The peak position and spectral profiles of the WSD, Sand_Ar and Bent_AR peaks were comparable to those of the desert samples (PD_1, PD_2 and At_01). Suggesting that the chemical state of the AC in each of these samples were equivalent. Consequently, the low organic geological samples would serve as analogues for the desert samples. Accordingly, the low organic content geological samples were thermally treated to 1000 °C for 8 hours, before being analysed using the same py-GC/MS and XPS procedures as the desert samples.
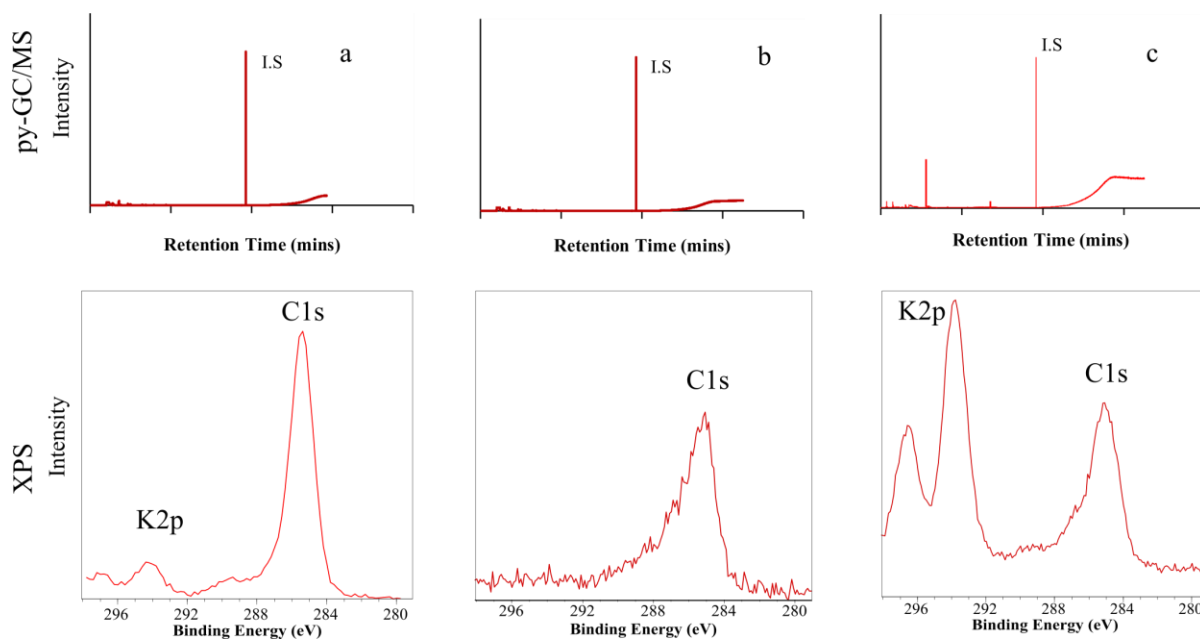
Fig. 8-5. *The py-GC/MS and XPS analysis of organic-poor geological samples following thermal treatment to 1000 °C. (a) WSD_1000 (b) Sand_1000 (c) Bent_1000, (d) WSD_1000 (e) Sand_1000 (f) Bent_1000 Carbon= carbon; K2p= potassium*

Fig 8-5a-c showed that organic material could not be detected using py-GC/MS and Fig 8-5e-f showed that AC could be detected in the organic-poor, geological samples (WSD_1000, sand_1000 and Bent_1000), following thermal treatment. These results matched those of the desert samples.

Organic material was not detectable in the organic-poor geological samples (WSD, Sand or Bent), using Py-GC/MS and dry combustion, whereas AC could be detected in these samples using XPS analysis. This suggested that the AC content of these samples was equivalent to the desert samples (PD_1, PD_2 and At-01). Therefore, they could serve as expendable analogues for the irreplaceable desert samples.

Additionally, dry combustion was used to measure any organic material that was released from the organic-poor geological samples (WSD_1000, sand_1000 and Bent_1000).

219

Sample	Dry Combustion TOC ($\%^w/_w$)	GC/MS ug/g	XPS at%
WSD_AR	0.041	Trace	4.1
WSD_1000	0.003	Trace	8.2
Sand_AR	0.005	Trace	3.4
Sand_1000	0.000	Trace	4.2
Bent_AR	0.942	Trace	2.6
Bent_1000	0.003	Trace	3.6

Table 8-4. *the quantification of the carbonaceous material in the organic-poor samples before (AR) and after (1000) thermal treatment.*

Table 8-5 shows that organic material was undetectable in the organic-poor samples with py-GC/MS. This demonstrates that organic material was undetected with dry combustion suggesting that organic material is not released from either the AR samples or the thermally treated samples.

8.4 Discussion

Organic matter was always detectable using XPS on the surfaces of the geological samples, regardless of whether the organic matter was also detected, or not detected, by py-GC/MS. The contrast between XPS and py-GC/MS in their ability to detect organic matter was most obvious in the organic-poor desert samples. The possibility of XPS instrument contamination could not be entirely excluded. However, several observations argue against this being the AC, originally described by Bar and Seal (1980).

(A) The samples were cleaned with argon GCIB sputter etching, then immediately analysed.

(B) Due to its reactivity, atmospheric O_2 the primary contaminant of any 'clean' surface, which interacts with the carbon resulting in the carbon peak of AC is 288.0 ±0.5 eV with a broad spectral profile reflecting a diverse range of C-O chemical states (Bar and Seal, 1980). In contrast, the peak position at 284.8 ±0.1 eV and the narrow spectral profile, observed in

this investigation, suggest the presence of a limited number of hydrocarbons consistent with aromatic or polyaromatic compounds.

(C) The sample analysis with GC/MS and dry combustion was conducted following XPS analysis. An estimate of the latter can be calculated based on the following values and assumptions. The particle size range of the JSC-1 samples was supplied in a grain size of 10-25 μm (www.orbitec.com).This was equivalent to a fine sand, which is reported to have a specific surface area of ca. 444.4 $cm^2.g^{-1}$, to 250 $cm^2.g^{-1}$ (Kuila et al., 2014), and assuming a 1-100 nm layer of hydrocarbon-like AC on the surface (De Gregorio et al., 2011), then a calculated value of between 0.03 and 5 $mg.g^{-1}$ AC per gram of sample could be present on the surface of the JSC-1 particles. Therefore, with regards to the 10 mg sample used in the py-GC/MS and the 2 g sample used in dry combustion and method, the calculated lower limit (0.03 $mg.g^{-1}$) should be within the detection limits of both GC/MS and dry combustion. This lower limit was computed on the assumption that every particle was the smallest surface area for a given weight of material (i.e. the largest particles) and possessed a 10 nm thick layer of AC, which is the thinnest film of AC that is reported by Gregorio et al., (2011), whereas in reality the particle sizes will have the Poisson distribution described by Kuila et al., (2014).

(D) The principal AC species are generally considered to be physically (physisorbed) rather than chemically involved with the fresh surface species, therefore at least some of the hydrocarbons from anthropogenic pollution or lubricants are amenable to thermal desorption and should be detectable by GC/MS, and dry combustion as these instruments are sensitive to traces of organic compounds in the ppb and 10 ppm range respectively.

The JSC-1_AR study demonstrated that organics were identifiable as a broad XPS spectrum, which was due to the structural and chemical diversity rather than its particular chemistry. Unsurprisingly, these were detected by py-GC/MS and were equivalent to the range and intensity of the compounds that were found in the same material, using py-GC/MS (Morisson, 2018). Additionally, the TOC value of the JSC-1_AR (1.3%) was equivalent to concentrations typically found in soils (Nelson and Sommers, 1982). The compounds detected are certainly consistent with plant matter that had been incorporated into the soils

in the JSC-1 collection site. This material was thermally labile and clearly represented the most dominant form of organic matter in JSC-1, since, as with the desert soils, no organic material could be detected in the JSC-1_1000, using py-GC/MS, demonstrating that thermal treatment removes a large proportion of organic material, associated with these soils. This result is, of course, consistent with the common use of thermal decomposition during soil organic matter quantification (Nelson and Sommers, 1982). In contrast, for soils with low levels of organic matter (i.e. regoliths), it appears that the thermally stabilised organic carbon will make a proportionally greater contribution to the overall TOC.

This salient difference between detection of organic material made by the XPS and the subsequent non-detection by py-GC/MS and the dry combustion method was due to both the limitations of the pyrolysis pre-step to thermally desorb organic material, that was described by Navarro-Gonzalez (2006). Other factors include the fact that the indigenous hydrocarbons were localised (and were therefore concentrated) on the surfaces of shards and micro-fractures in the geological samples and these were detected by XPS, beneath the GCIB cleaned top layer.

8.4.1 Implications of the presence of thermally stabilised organic matter either as biological or abiotic 'adventitious' carbon

Any fresh surface will physio-absorb material from its surroundings (Buckley, 1981) it is speculated here, that an unknown, but a significant proportion of organic material in the environment, will interact with the mineral surfaces. This interaction confers resistance to thermal volatilisation, rendering much of this material unamenable to detection, using the methods that are predicated on thermal extraction and coupled to GC/MS. This is despite the concentrations of AC being greater than the LOD of GC/MS in the organic poor geological samples, such as the regoliths that were used in this investigation, or indeed potentially on Mars. The organic material that is stabilised must be limited to the material that is in proximity to the mineral surfaces. Thus, this mechanism reasonably explains why there is a diminishing contribution of thermally stabilised carbon, as the levels of carbon increase to the level normally encountered in the organic-rich soils in the upper part of the Earth's crust. An alternative explanation is that this non-detection may be a consequence of

surface assisted reactions that are analogous to those described by Grill et al.   (2010) that may result in on-surface synthesis of macromolecular organic assemblies, through the molecular interaction or transformation of the constituent AC building blocks (Méndez et al., 2011) resulting in relatively high molecular weight PAHs, which may be more resistant to pyrolytic   fragmentation and therefore unamenable to detection by py-GC/MS.

Carbonaceous chondritic meteorites contain organic compounds consisting of a diverse range of 'kerogen-like' macromolecules and soluble compounds such as amino acids and polyols. Their transformation or synthesis from inorganic carbon occurs in response to thermodynamic drives, that are modulated by the kinetic properties of individual reactions (Pizzarello and Shock, 2010). Fischer-Tropsch type (FTT) reactions are commonly cited as a basis for prebiotic organic synthesis (De Gregorio et al., 2011; McCollum, 2013). FTT reactions are reported to result in the production of low molecular weight hydrocarbons (Proskurowski et al., 2008), whereas the synthesis mechanism of macromolecular compounds from low molecular weight organic compounds through the interaction of minerals (i.e. geopolymerisation) is less well understood (Johnson et al., 2015). However, the observed synthesis of polyaromatic hydrocarbons (PAHs) formed from carbon and hydrogen on quartz surfaces. This synthesis may occur in the protostellar object environment and has been proposed to explain the higher than predicted levels of PAHs that are observed throughout the cosmos (Merino et al., 2014).

What is also not understood is how such AC formation might proceed in the 98% CO_2 atmosphere of Mars. Fresh rock surfaces are continually created by aeolian driven grinding, on Mars (Jensen et al., 2014), which produce fresh surfaces that will inevitably absorb atmospheric gases, including any methane (see section1.6.3), explaining the adsorption of methane onto ground quartz surfaces by Jakobsen et al. (2016), which has been invoked to explain the higher than expected loss of methane from the Martian atmosphere (Lefevre and Forget, 2009). The possibility of what other additional reactions, this adsorbed methane could possibly undergo, such as geopolymerisation, is unknown. Therefore, such surface-assisted reactions have the potential to confound the identification of genuine telluric molecular fossils (De Gregorio et al., 2011) and by implication any molecular fossils

that may be detected on Mars. Furthermore, contamination of carbonaceous material in fossil specimens by modern AC, during sample preparation has been reported (Paul et al., 2017) and samples returned from Mars could also be contaminated, in a similar way.

8.5 Conclusion

The results in this chapter indicate that AC covers all surfaces, and this includes the surfaces of near barren rocks that serve as analogues for Mars. This material is undetectable with py-GC/MS and dry combustion, but it is detectable using surface analytical instruments such as XPS. We show here that hydrocarbons were also present on low organic content geological samples, including near barren rocks, such as those found in the Polar regions and the Atacama Desert and the precise mechanism for this non-detection remains elusive and should be the subject of further investigation. There are several problematic consequences of these observations. (i) GC/MS may not be the most efficient methods of detecting organic material on Mars. (ii) The possibility that apparatus and samples materials that were thought to be decontaminated by thermal treatments may still possess a layer of organic material, which increases the possibility of forward contamination, including those delivered to the surface of Mars. Samples returned to the Earth can be readily contaminated by terrestrial AC. However, observational evidence suggests that the interaction of AC with mineral surfaces has a role in the formation of high molecular weight compounds, and therefore may have an unknown role in organic geochemistry and cosmochemistry.

CHAPTER 9: SUMMARY

9.1 The key findings of each research chapter

Chapter 1 and 2 were a literature review and generic methods and therefore had no conclusions.

Chapter 3

The preparation and storage of geological samples will result in the accumulation of contamination on the surfaces of samples. The objective of this chapter was to fully evaluate the decontamination methods that would need to be applied to the samples prior to surface analysis. Decontamination of a geological sample using either gas cluster ion beam etching or ultra-violet/ozone cleaning was evaluated for the first time. This chapter demonstrated that:

- XPS was able to acquire quantitative elemental data from dolerite samples.

- The XPS non-carbonaceous elemental concentration measurements were accurate, as well as being precise, implying that the carbon concentrations measured by XPS were similarly accurate.

- Gas cluster ion beam etching was able to remove levels of contamination that was far in excess of that normally encountered in standard geological sample preparation.

- UV/O_3 was effective at cleaning the surfaces of samples.

- XPS was able to distinguish between adventitious and indigenous carbonaceous material.

- Indigenous, thermally stable carbon was detected in the WSD.

Chapter 4

Tuff from the Ontong Java Plateau was reported to contain organic material, the objective of this chapter was to characterise this material using GC/MS and XPS. Thermal extraction of

the organic material was carried using both conventional pyrolysis and pyrolysis in the presence of TMAH. High-resolution XPS spectra of carbon and nitrogen were obtained, and these were compared to the GC/MS data.

- A range of organic compounds could be detected in the OJP. However, no such compounds could be detected in the WSD, using GC/MS

- In comparison to conventional pyrolysis, conducting pyrolysis in the presence of TMAH increased the efficiency of the thermal extraction process, in terms of both the numbers of compounds that were detected and the peak intensity of each of the peaks.

- A range of aliphatic and aromatic compounds was detected in the OJP, nitrogen substitutions were observed within the aromatic rings.

- A number of peak components could be identified in the XPS high-resolution spectra of carbon in the OJP sample, whereas only a single component could be detected in the WSD.

- Nitrogen could be detected in the OJP, whereas it was not detected in the WSD.

- The organic compounds detected by GC/MS were consistent with the chemical states that could be assigned to the components in the XPS high-resolution carbon and nitrogen spectra.

- These compounds were consistent with the hydrous pyrolysis products of chitin.

- The hydrous pyrolysed compounds were consistent with the reported diagenetic products of organisms that use chitin as their structural biopolymer.

Chapter 5

The XPS measurements that were made on the organic material in OJP that had been presented in chapter 3 indicated that the organic material was heterogeneously distributed across the surface of the OJP sample. The objective of this chapter was to map the lateral distribution of organic material on the surface of the sample, with the OJP sample with microtubular features (OJP_13) using ToF SIMS and XPS.

- XPS and ToF SIMS was able to map the organic carbon and nitrogen on the OJP_13 sample.

- The data showed that the organic carbon and nitrogen on the OJP_13 was predominantly located in micro-cracks in the lapilli matrix and also in the devitrified part of the glass shards, which were embedded in the matrix.

- The XPS and ToF SIMS data also detected elevated concentrations of organic carbon and nitrogen in the weathered rinds of the glass shards.

- The GC/MS data that was obtained in the investigations described in Chapter 3 was used to assign molecular identities to the ToF SIMS mass fragments.

- Compounds consistent with hydrous pyrolysed chitin were identified by GC/MS and were located in the micro-fissures and the weathered rinds of the glass shards.

- The implication of the data obtained in the chapter was that the diagenetic products of chitin appear to have occurred predominantly in the micro-cracks and in the weathered rind of the glass shards.

Chapter 6

Chapter 3 and 4 indicated that the diagenetic products of chitin could be measured and located in micro-cracks and in the weathering textures of the OJP core sample that contained observable microtubular structures. The purpose of this chapter was to compare the composition of the organic material in OJP samples where these microtubules could be observed with other core samples from the same drill hole but were obtained from different horizons, this included the overlaying pelagic ooze, the charred woody fragments that were buried in the OJP tuff, and also with submarine basalt samples containing glass shards, but also without the microtubules.

- The composition of the organic carbon and nitrogen in each of the OJP tuff samples was comparable, which implied that the nitrogenous organic material occurred in the OJP tuff irrespective of whether the glass shards contained the microtubules, or not.

227

- The organic compounds that were observed in the OJP tuff were absent in the OJP pelagic ooze, implying that this was not the source of the organic material.

- The compounds that were detected in the OJP tuff were also absent in the submarine pillow basalts and in the terrestrial basalts from other regions implying that these nitrogenous organic compounds were not specific to the OJP tuffs containing microtubular features.

Chapter 7

The purpose of this chapter was to demonstrate how the pyrrole and pyridine compounds that had been detected in the OJP tuff was the result of the decomposition of chitin and the elevated levels of nitrogen from chitin could be preserved in the geological record.

- The nitrogenous organic material in chitin was resistant to decomposition through hydrous pyrolysis and thermal decomposition.

- A subset of the range of compounds detected in the OJP samples was comparable to those in the products of hydrous pyrolysis.

Chapter 8

The analysis conducted in chapters 3 to 7 demonstrated that carbonaceous material could be detected in the geological samples using XPS, whereas this material remained undetected using py-GC/MS and THM-GC/MS. Chapter 8, evaluated this observation, in the light of the non-detection of organic material on Mars, a possible mechanism for this, is considered. It concludes with some of the implications that this mechanism may have on the organo-geochemical and astrobiological exploration of Mars or elsewhere in the solar system.

- The carbonaceous films on the surface of minerals are thermally stable.

- This carbonaceous film may be a source of the complex organic compounds that form on the surfaces of minerals.

- These carbonaceous films are undetectable using methods that rely on thermal extraction to mobilise then measure organic material, such as py-GC/MS.

9.2 Overall Conclusions Regarding the Biogenicity of Microtubules in OJP Tuff and their value as a Mars analogue

The advocates for a biological origin for the alteration textures, which are seen in basaltic glasses, have been assertive in their opinion (Banerjee et al., 2003). In contrast, the study made here made no such pre-assumptions, since the origin of such features still remains contentious. Even the distinctive microtubular features observed in OJP_13 proved to be a difficult specimen to study and therefore did not provide any definitive proof for or against the biogenicity of the OJP alteration textures specifically or these types of alteration textures in general.

The investigation here showed that organic compounds, which are consistent with the diagenetic products of organisms that originally contained high levels of nitrogen and were predominantly located not only in the weathered rind of the glass tektites but also within fractures in the surrounding rocks. Whether this infilling by organic material was post-deposition or peri-depositional is not clear, however, the results in this study do suggest that this organic material could be the remnants of a chitinous organism, and this organism was either responsible for the weathering process or may have been exploiting a pre-existing geochemical process on the surfaces of the glass shards. Consequently, the microtubules that were observed ingressing from the surface to the interior of the shards may have been the result of an exploratory excavation for the resources contained in the shards by an organism with a filamentous morphology. Chitin is the key structural biopolymer of fungus, suggesting that the candidate organisms responsible for this excavation process, are in this taxonomic group and the crenelated tube-like morphology would certainly be consistent with an excavation carried out by fungal hyphae. However, since other parts of the OJP tuff did not possess the distinctive tubular structures, but contained a similar suite of organic compounds, then this pattern may argue against any direct correlation between these tubular features and the nitrogen-rich organic compounds.

229

The OJP tuff serving as an analogue for the types of investigations that might be carried out on samples returned to the Earth from Mars has proved useful for demonstrating the value of using surface analysis to complement other conventional analytical approaches. The investigations described here were able to use surface analytical approaches to obtain quantitative information on the elemental composition of geological samples and were able to characterise the organic composition of the endogenous material in geological samples.

Furthermore, it was demonstrated that the types of data that are obtained using the surface analytical techniques supported GC/MS analysis, which is the method that is commonly used for the analysis of organic material in geological samples. This supporting evidence also provided confidence in the mass spectral data that was obtained from the ToF SIMS, which was able to measure the distribution of the organic material in the OJP sample containing the putatively biogenic microtubular structures. In this way, two types of complementary data (morphological and chemical) were obtained, which is an approach that could be exploited in the organic geochemical exploration of Mars.

In conclusion, this investigation was able to determine the effectiveness of surface analytical techniques to measure the composition and distribution of organic material in geological samples, which served as analogues for the types of rock and the types of fossilised morphological biosignatures that might, one day, be encountered on Mars. However, further work is required to distinguish and clearly assign any organic material to a molecular biosignature.

9.3 Future investigations

The techniques that were developed in these investigations can be applied to more elaborate astrobiological investigations. This could be done by characterising the distribution of organic compounds in fossilised Precambrian microorganisms, at the macroscopic scale and upon structures with readily identifiable morphologies where specific molecular biomarker compounds could then be identified.

This analysis could be carried out on a range of fossils that have different ages to provide information on the effect of burial time on the biomarkers. Fossil samples that do not have a

readily identifiable morphology could then be analysed to detect the presence of biomarkers. At the microscopic scale, helium ion microscopy in conjunction with quadrupole mass spectrometry could be utilised to provide images and analyse structures that are putatively cellular fossils. This analysis could be conducted on meteorites that originated on Mars. This would provide the experience for the analysis of samples from Mars that may be returned to the Earth in the coming decades.

The application of surface analysis for *in situ* planetary exploration requires further investigation. The acquisition of XPS data requires the sample to be placed in an ultra-high vacuum ($< 10^{-7}$ Pa) to prevent the loss of kinetic energy through interactions between the emitted electrons and air molecules. Therefore, the current technology means that instruments are necessarily laboratory based. However, a current area of development is ambient-pressure XPS, in which samples are analysed at pressures of a few tens of Pascal, which would be capable of being operated in planetary exploration and is currently under evaluation for this purpose by NASA (Bryson, 2003; Bryson, 2007). Furthermore, the py-GC/MS and THM-GC/MS analysis on coalified fossil samples, conducted in this thesis will be replicated with laser desorption/mass spectrometry (Kevin Lepot, personal communication, kevin.lepot@univ-lille.fr)

Since the commencement of this study in 2012, further reports have been made regarding structures on Mars, in the vicinity of paleo-hydrothermal systems, which resemble structures around telluric hydrothermal systems that have a microbial component to their formation process have been reported (Ruff and Farmer, 2016). This observation suggests that the case for life on the surface of Mars is now more compelling. Therefore, the study of telluric analogues from hydrothermal systems that are more comparable to the one in these reports is the next step.

APPENDIX A: CHEMICAL AND MOLECULAR CHARACTERISATION BY GC/MS AND SURFACE ANALYSIS OF LOWER DEVONIAN COALIFIED FOSSIL SAMPLES

A 1.0 Introduction

Chapters 6 and 7 demonstrated that the assignment of taxonomic groups to specific fossil organisms was challenging based upon morphological and/or geochemical evidence alone. The task of determining a taxonomic origin to any fossil organism is particularly difficult when there is no extant counterpart to the fossil organism that would allow a direct morphological or molecular comparison. *Pachytheca* and *Prototaxites*, are one such example of enigmatic of fossil organisms that do not have any known contemporary plant or fungal counterparts. Therefore, whose taxonomic assignment has therefore remained elusive, and the subject of debate. This group of fossils include the organisms '*Nematothallus*', '*Parka*', and '*Nematoplexus*', which appeared in the fossil record, ca. 420 to 370 Ma ago (Hueber, 2001), which therefore makes their appearance in the geological record concurrent with the emergence of vascular land plants (Stein et al., 2007).

Morphologically *Prototaxites* appear to have possessed a large trunk-like structure up to 1 m in diameter, and up to 8 m high, which may have dominated the Silurian and Devonian landscape. In contrast, *Pachytheca* has a small glossy spherical morphology, measuring 1 to 6 mm in diameter and possess characteristic internal structure and are found in the Upper Silurian and the Lower Devonian sediments (Taylor, 2009). As a result, *Prototaxites* were initially assigned to the phylum that includes higher vascular plants, despite being anatomically distinct from contemporaneous tracheophytes and bryophytes. It has therefore been proposed that the observed fossil structure of *Prototaxites* was not the innate structure, but was, in fact, the result of physical and mechanical processes acting upon liverwort assemblages that resulted in the formation of roll-like secondary structures (Graham et al., 2010a; Graham et al., 2010b). However, the structure of both *Prototaxites* and *Pachytheca* have similarities to fungus, which has led to the proposal that these organisms are, in fact, fungal in origin.

Additionally, the geological context in which the samples were found, did not provide any supporting evidence for the habitat of these organisms, which could have provided an

indication of their taxonomic group. The fossil samples appear to have been typically preserved in freshwater sediments (Schmid, 1976) and in habitats that are occasionally identified in marine sediments. However, they have also been observed in association with land plant fossils that implied a terrestrial habitat (Hueber, 2001). Thus, given the ambiguous morphological and contextual evidence, the *Prototaxites* and *Pachytheca* taxonomy remains conjectural.

The characterisation of any associated organic material could provide evidence of the taxonomic provenance of these organisms. This proposal was supported by the large variation in the range of the ^{12}C:^{13}C isotope ratio values that have been observed in a number of *Prototaxites* specimens. These isotope values were inconsistent with the atmospheric carbon isotope ratios, which implied that *Prototaxites* might have possessed a heterotrophic rather than an autotrophic metabolism (Boyce et al., 2007).

The kerogenisation and subsequent mineralisation of biological material to inorganic 'coalified' carbon are characterised by the loss of functional groups and aromatisation (see section 1.10.1) that results in the progressive loss of molecular information regarding the original organism's taxonomy, as a function of the age of the sample. (Buseck and Beyssac, 2014). Nevertheless, it may be possible that molecular taxonomic information may still reside in mature organic fossil (coalified) samples.

Abbott et al. (1998) attempted to obtain a taxonomic assignment of *Prototaxites* and *Pachytheca*. The organic molecular characteristics were investigated using py-GC/MS analysis, which was supported by FTIR and ^{13}C nuclear magnetic resonance (NMR). This analysis was used to assess the effects of the host lithology on the insoluble organic composition of *Prototaxites* and *Pachytheca*. However, the results of the analysis were ambiguous, which led to the proposal that these organisms were composed of an unknown, extinct, structural biopolymer.

In addition to the *Pachytheca* and *Prototaxites*, a specimen of *Archaeopteris* was also studied. *Archaeopteris* is an extinct genus of a 'tree-like' plant (Beck, 1962) that had a global distribution and is also found in strata dating from the Upper Devonian to Lower

Carboniferous 383 to 323 Ma (Meyer-Berthaud et al., 1999). Since *Archaeopteris* is a well characterised vascular plant (Trivett, 1993) and of a similar geological age, the composition of the organic material in these specimens could be used as a 'reference standard' to compare with the composition of the organic material in the *Pachytheca* and *Prototaxites.*

Thus, the purpose of this supplementary investigation was to compare the relative nitrogen composition of the organic remnants of *Prototaxites* and *Pachytheca* with the fossilised remains known to be derived from higher plants to assist in determining the provenance of these organisms, using the THM-GC/MS, ToF SIMS and XPS techniques that had been developed in this thesis for the analysis of the OJP samples.

A 2.0 Methods

The samples were named after the location from where they were obtained. The names of the samples have been removed and replaced with Ax; Bx; Cx; Dx and Ex to anonymise these locations. Soxhlet thimbles were decontaminated by conducting a pre-extraction for 24 hours, using apparatus shown in Fig A-1 using a 93:7 ratio of dichloromethane to methanol. Samples were placed in the pre-extracted thimbles then Soxhlet extracted for 48 hours. The residues were dried and retained for analysis in precleaned vials. The cleaned sample residues were then analysed with py-GC/MS and THM-GC/MS, which was conducted according to the methods described in section 2.4.2 using a pyrolysis temperature of 610 ˚C

In addition to cleaning with Soxhlet extraction, the samples were also analysed by X-ray photoelectron spectroscopy (XPS). These were decontaminated using Ar GCIB sputter etching (Purvis et al., 2017; Chapter 3). XPS analysis was then carried out according to section 2.4.1. The Soxhlet decontaminated were analysed on Time of Flight Secondary Ion Mass Spectrometry using a Kore Surface Seer by Jesus Ojeda at the Institute of Material and Manufacturing, Brunel University, Middlesex.
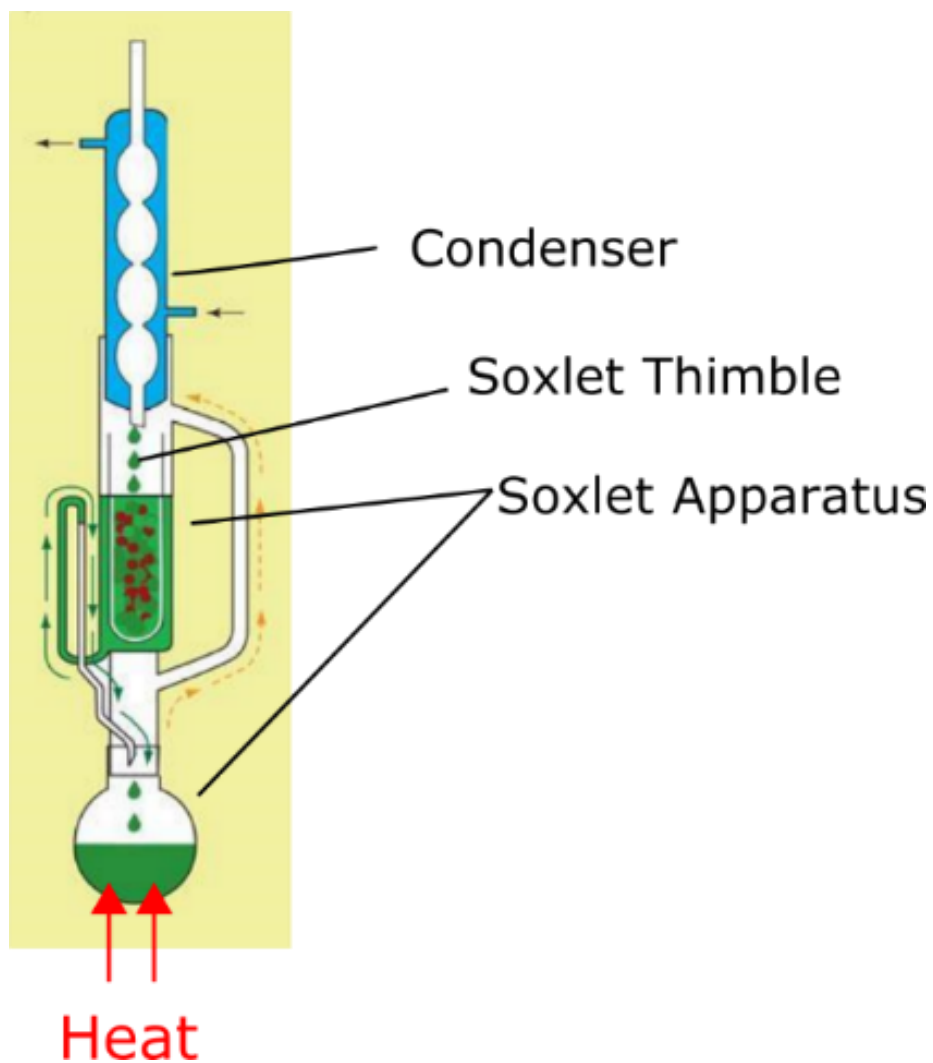
Fig A-1. *Illustration of Soxhlet extraction apparatus set-up. Adapted from: The Royal Society of Chemistry. https://www.chemistryworld.com/opinion/classic-kit-soxhlet-extractor/3004940.article*

A 3.0 Results

A.3.1.0 Pyrolysis-Gas Chromatography/Mass Spectrometry analysis of Prototaxites and
    Pachytheca.
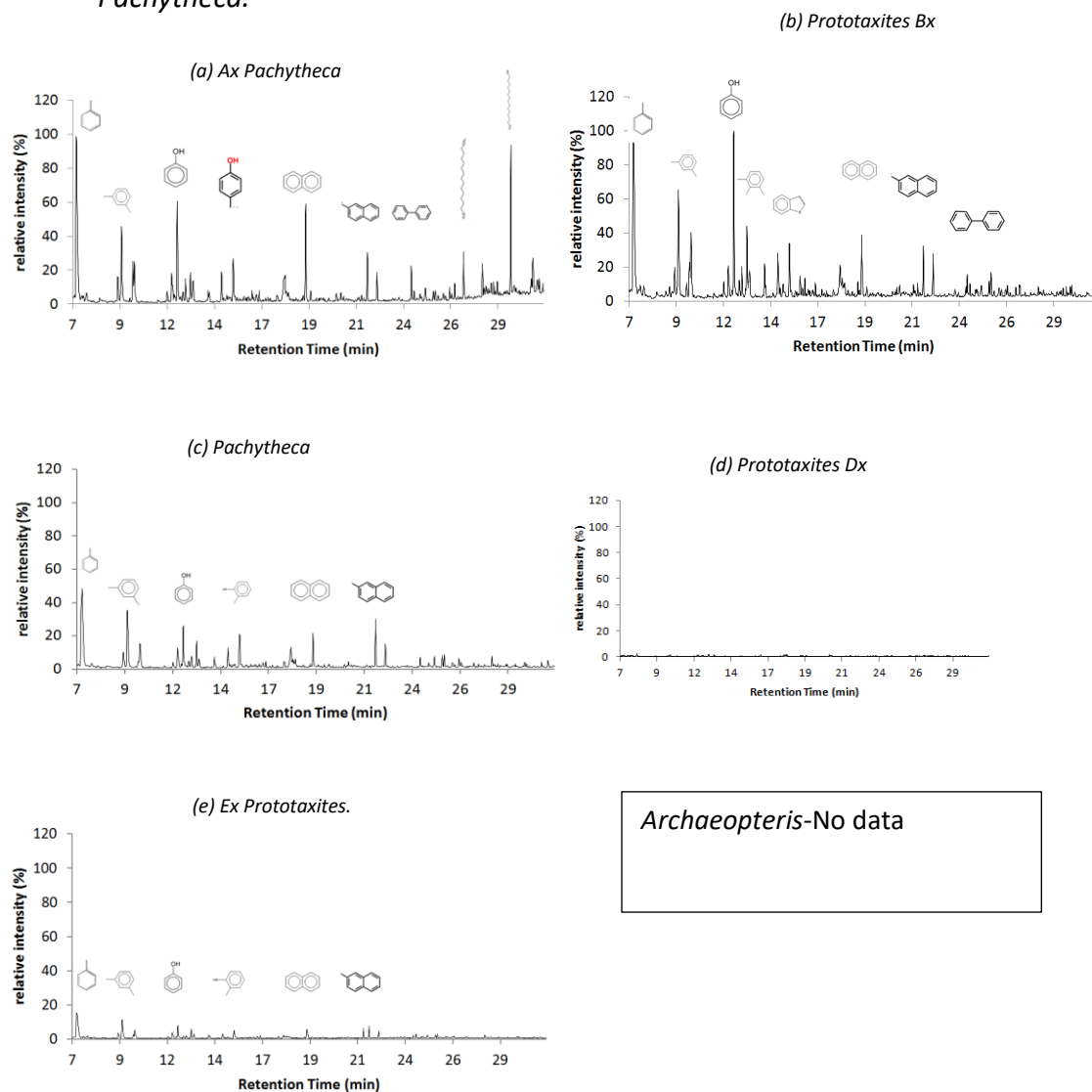
Fig. A-2. *Py-GC/MS chromatograms for (a) Ax Pachytheca (b) Prototaxites Bx (c) Pachytheca (d) Prototaxites Dx (e) Ex Prototaxites. Samples were normalised using the peak height of the androstane internal standard (not shown).*

Py-GC/MS spectra for the *Pachytheca* and *Prototaxites* are presented in Fig A-2. For simplicity, only the major peaks are labelled with diagrams of their compounds. There were variations in their response to the analysis. Ax *Pachytheca* and *Prototaxites* Bx yielded the strongest ion intensity and *Pachytheca* and *Ex Prototaxites* yielded ion intensities that were

lower but within the limits of analysis. However, the *Prototaxites Dx*, response to analysis was lower than the limits of detection, for the py-GC/MS instrument used in this investigation.

The same compounds were identified in the major peaks of each of the samples, with the exception of *Prototaxites Dx.* The spectra were dominated by a wide range of mono and bicyclic aromatic compounds, and a number of aliphatic compounds were identified in all samples other than *Prototaxites Dx.*

A 3.2 Thermal Hydrolysis and Methylation Gas Chromatograph/Mass Spectrometry analysis of Prototaxites and Pachytheca

Archaeopteris-No data

Fig A-3 *610˚ C THM-GC/MS spectra for (a) Ax Pachytheca (b) Prototaxites Bx (c) Pachytheca (d) Prototaxites Dx (e) Ex Prototaxites. Nitrogen atoms are highlighted in blue. This demonstrated that nitrogenous aromatic compounds could be detected.*
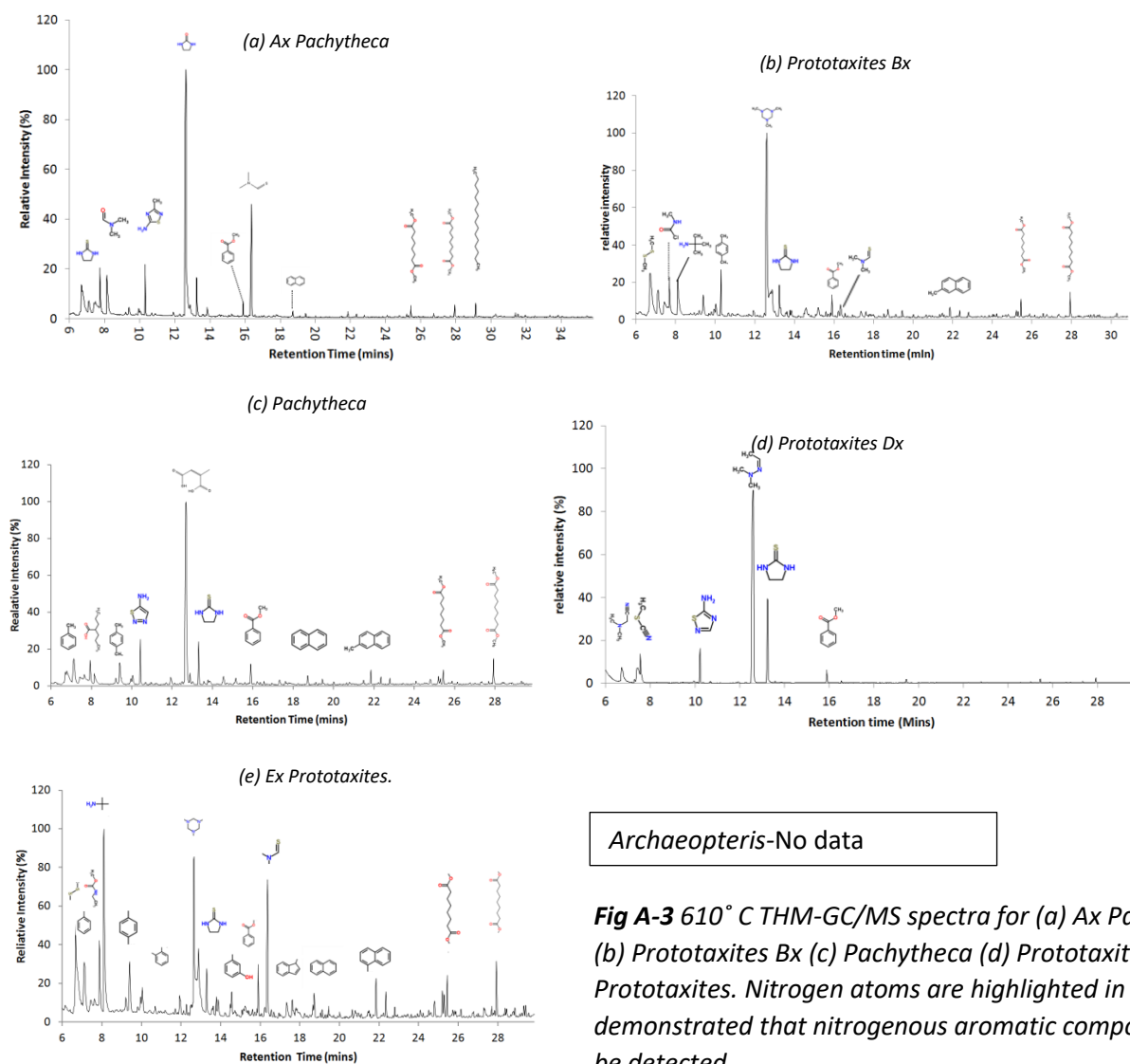
A 3.3.1 XPS Survey spectral analysis of Prototaxites, Pachytheca and Archaeopteris

Parent atom and Orbital	O 1s	C 1s	N 1s	F 1s	Ca 2p	Y 3p	S 2p	Si 2p	Al 2p	Dy 4d	Mg 1s	Na 1s	Sc 2p	Se 3p
XPS Peak Position (eV)	532.08	284.08	400.08	689.08	348.08	305.08	169.08	103.08	74.08	154.08	1305.08	1073.08	400.08	161.08
Ax *Pachytheca*	28.61	58.45	1.54	0.56	1.19	0.76	2.67	5.63	0.48	0.11	0	0	0	0
Prototaxites Bx	16.51	79.34	1.32	0.83	0	0	1.21	0.81	0	0	0	0	0	0
Pachytheca	43.47	29	1.11	0	2.18	0.65	2.9	13.57	7.54	0	0.4	0.14	0	0
Prototaxites Dx	54.21	8.05	0	0	0	0	0	35.41	2.32	0	0	0	0	0
Ex *Prototaxites*	18.17	66.82	2.01	7.72	0	0	1.42	0	2.68	0	0.4	0.52	0.26	0.01
Archaeopteris	38.9	42.82	0.39	0	0	0.84	4.87	7.13	5.02	0	0.01	0.02	0	0

Table A-1 *Major spectral peak identified using CASAXPS library with the corresponding peak positions and the surface concentration of elements, and values are in at %.*

Parent atom and Orbital	Y 3p	Dy 4d	Sc 2p	Se 3p
XPS Peak Position (eV)	305.08	154.08	400.08	161.08
Ax *Pachytheca*	+	+		
Prototaxites Bx				
Pachytheca	+			
Prototaxites Dx				
Ex *Prototaxites*			+	+
Archaeopteris				+

Table A-2: *XPS analysis of Pachytheca and Prototaxites**. (+) presence of metals in samples*

XPS analysis demonstrated that the elemental composition of the major mineral phases could be detected, on the surface of the samples. Oxygen and carbon were detected in all samples. Nitrogen and sulphur were also detected in all samples other than *Prototaxites* Dx. Additionally, this sample also contained the fewest number of other trace elements. Interestingly, both *Pachytheca* samples, which were from widely dispersed locations and geological settings, contained detectable levels of both calcium and yttrium, whereas these could not be detected in the *Prototaxites*.

Sample	C:N
Ax *Pachytheca*	37.9
Prototaxites Bx	60.3
Pachytheca	26.2
Prototaxites Dx	N/A
Ex *Prototaxites*	33.2
Archaeopteris	109.8
Hy-py Chitin	12.0
Hy-py Cellulose	N/D
Hy-py Lignin	N/D

Table A-3. *carbon: nitrogen ratios for fossil specimens. For convenience, the C:N ratios of the hydrous pyrolysed plant structural biopolymers are presented again here from table 7-1. N/D = nitrogen was not detected.*

Table A-3 presents the carbon:nitrogen ratio for the samples used in this chapter was obtained using XPS. These are compared to the hydrous-pyrolysed biopolymer samples that were obtained from the XPS survey spectra and described in Chapter 7 (see section 7.3.2). This indicates that the carbon:nitrogen ratio in the lower Devonian samples was

approximately 30% that of the carboniferous sample. This was a result of the proportionally higher nitrogen concentration in these samples, in comparison to the carboniferous samples. These are compared to the hydro-pyrolysed samples that demonstrated that nitrogen was observed only in the chitin sample.

A 3.3.2 XPS High-Resolution Carbon and Nitrogen Spectra
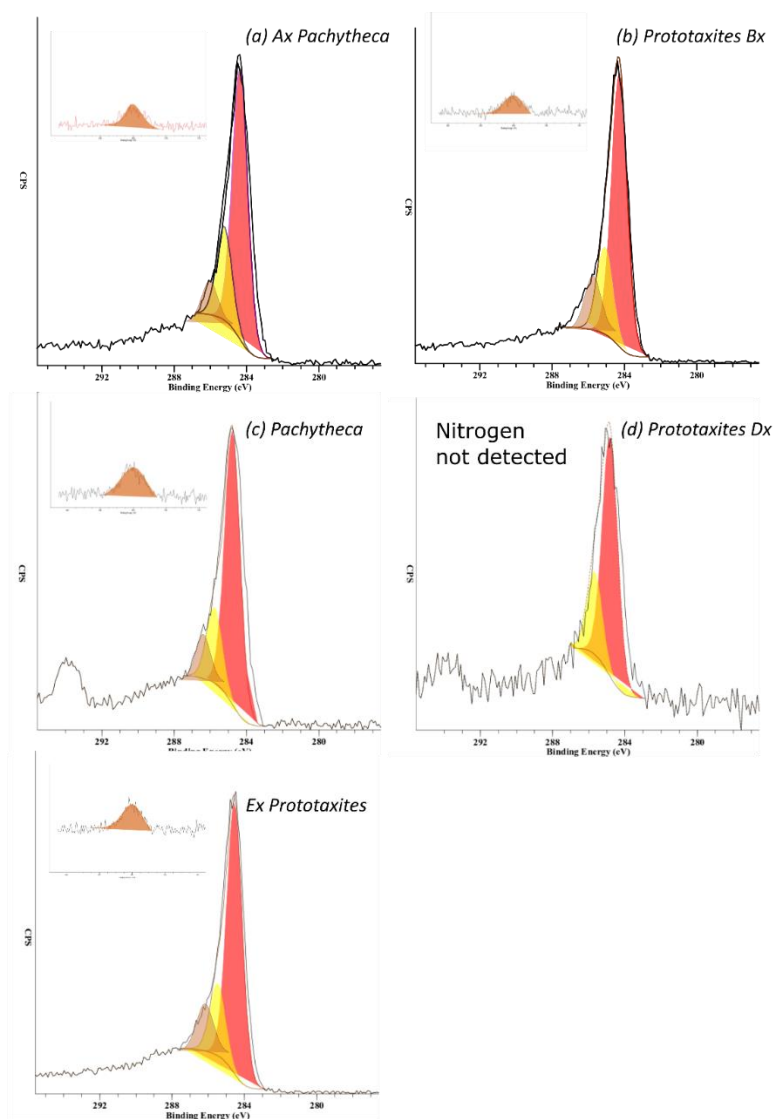
Fig. A-5. *High-resolution XPS carbon spectra (nitrogen inset). (a) Ax Pachytheca (b) Prototaxites Bx (c) Pachytheca (d) Prototaxites Dx (e) Ex Prototaxites.*
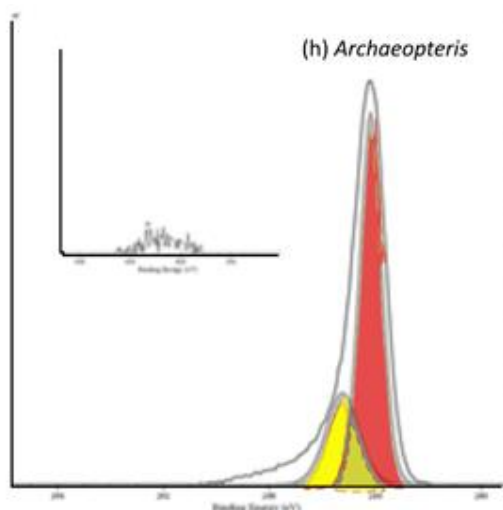
FIG A-6. *High-resolution XPS carbon spectra of coalified fossil identified as Archaeopteris.*

The XPS spectral profile of the lower Devonian fossils (*Prototaxites* and *Pachytheca*; Fig. A-5 a, b, c and e) indicates that three synthetic components can be fitted, in contrast, the narrower spectral profile of the *Archaeopteris* higher plant fossils (Figs S-6) indicated that two synthetic components could be confidently fitted. The difference in the spectral profiles was a result of the additional C-O and C-N bonds. This was illustrated by the additional fitted synthetic component at 287.0 eV in the Ax *Pachytheca, Prototaxites* Bx, *Pachytheca* and the Ex *Prototaxites*. This observation was consistent with the higher proportion of nitrogen detected in the survey spectra in those samples.

The presence of a synthetic peak carbon could be assigned to either C-O or C-N due to overlaps in these two components. However, the absence of a carbon component, concurrent with the absence of a detectable nitrogen peak in the Dx *Prototaxites*, suggests that the C-N is the most probable. This is supported by the nitrogen scan, that shows that although these spectra have a low signal to noise ratio, the component fitting indicated that the peak position appeared to occur at 400.5 eV, which is the binding energy consistent with the detection of N-C bonds. This is in contrast to the carbon component reported in Stoyka (2013) where this was assigned to C-O, where the O:C ratio was much lower.

The dominant component fitted in the carbon spectra was at 284.9 eV. The assignment of a component at peak this position indicates the presence of unsaturated C=C bonds, including

the delocalised electrons from the π system in aromatic compounds, however, a π-π* satellite peak was not observed at 291.0 eV. to support this observation.

A 3.3.3 ToF SIMS spectra
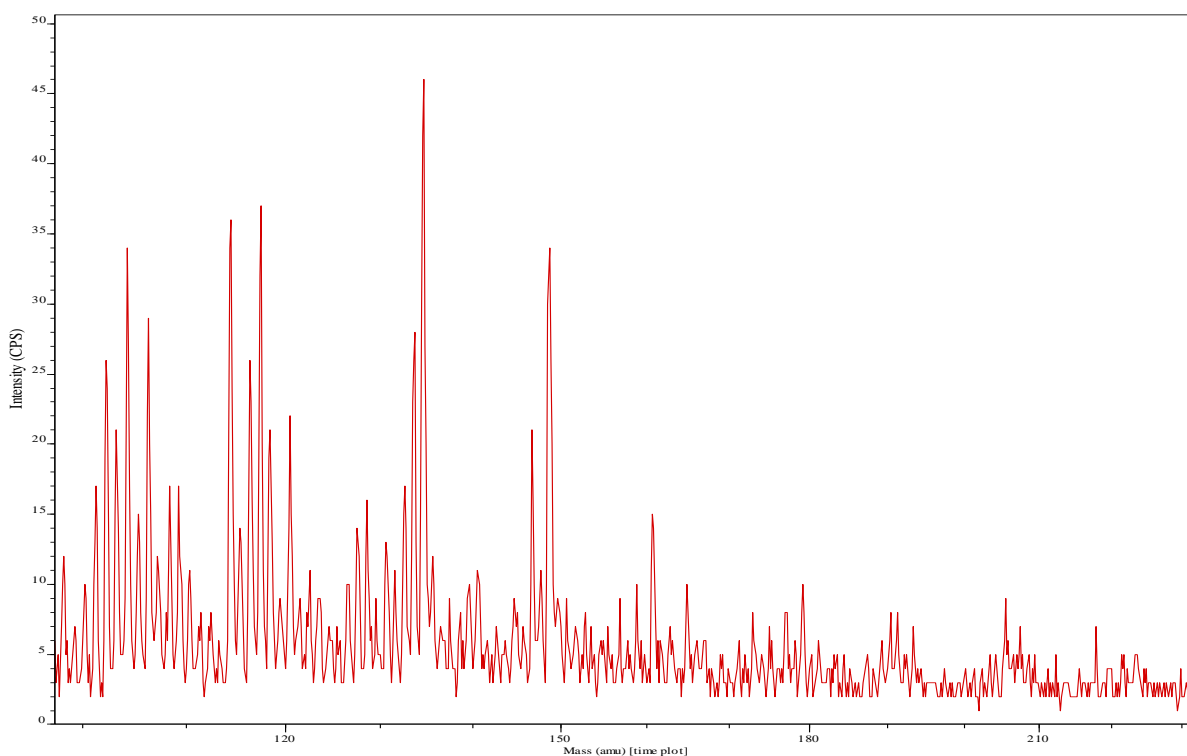
Fig. A-6. *positive spectra for a. Ax Pachytheca and b. Ex Prototaxites*

The positive ToF SIMS Spectra (Fig. A-7) produced an intense peak pattern at m/z <150 that became depleted at m/z <200. Interestingly a peak was observed at ca. 950 u in both Ax *Pachytheca* and b. Ex *Prototaxites* this indicated the peaks produced at m/z <200 might be the fragments of a high molecular weight organic compound. The lack of distribution clusters in the peaks indicated that this high molecular weight compound was not a polymer. ToF SIMs did not identify mass peak consistent with the presence of *N*-Acetyl glucosamine, or the glucosamine, or amide or long chain fatty acids or lipid biomarkers or cell membrane.

No unequivocal molecular assignments could be made, from the ToF SIMS mass spectra data. However, given some of the data obtained from the GC/MS and XPS, some inferences regarding the can be obtained from the spectra. Heterocyclic compounds could not be

242

observed. This is due to both high carbon:nitrogen ratios observed in the XPS spectra and the ionisation probability is higher in the homocyclic aromatic compounds. Thus, the analysis of heterocyclic compounds was excluded. A number of regularly spaced peaks were observed between m/z 100 and m/z 200 , which was consistent with aromatic compounds with different ring numbers (Stephan, 2003). These peaks could potentially have been assigned to aliphatic hydrocarbons. However, the non-detection of aliphatic compounds using py-GC/MS and THM-GC/MS excluded this possibility. The spread of the molecular weights suggested that the ring structures possessed short side chains in various numbers. This suggested that these may have been the fragments of the larger molecule detected at m/z 950 .

A 4.0 Discussion

The major peaks in the py-GC/MS chromatograms were dominated by alkylated aromatic compounds, principally hydroxyl and methyl moieties, furthermore, the presence of aliphatic chains was absent. These observations agree with the previous work (Abbott 1998), where an attempt at a taxonomic assignment, had been frustrated, at the time.

A mean C:N ratio of 39.2 for each of the samples, was obtained, with the exception of *Prototaxites* Dx, and *Archaeopteris*, using XPS. The C:N of 60.3 that was observed in the *Prototaxites* Cx may be a function of the thermal history of the geological sample. This was in contrast to the XPS data that was obtained from the *Archaeopteris*, which indicated that the carbon:nitrogen ratio was 2.5 times greater than that of the lower Devonian plant fossils (with the exception of the *Prototaxites* Dx). This decreased C:N ratio is a function of an increased surface concentration of nitrogen, which could the result of the increased number of n-alkylated pyrrole and pyridine compounds , which were observed in the THM chromatograms. The higher N:C ratios appear to suggest that the lower Devonian fossils contained elevated concentrations of nitrogen. This could be explained by the presence of the fossilised remnants of chitin in these samples (see section 6.4.4). Whether this chitin originated from the fossil structure themselves or originated from a fungus that had been involved in the decomposition of the higher plant material, is not known.

Surprisingly, the detection of the heavy metals yttrium, selenium, scandium and selenium in the samples at levels greater than might commonly be encountered in the elemental inventories in most modern rock types, and therefore would be anticipated that these were also equally unusual in the lower Devonian soil compositions. However, fungi are known to bioaccumulate heavy elements (Gadd, 2013), and therefore the transition elements enrichment that was observed within these samples may have been the product of fungal bioaccumulation *Prototaxites* and *Pachytheca*, which would support the conjecture, that the lower Devonian fossils were indeed taxonomically fungal in origin.

A 5.0 Conclusion

The analysis of the lower Devonian fossils, using a combination of py-GC/MS, THM-GC/MS, XPS and ToF SIMS demonstrated that it is possible to detect nitrogen in the *Prototaxites* samples, at greater levels than the Carboniferous higher plant fossil samples, which implied that there might be a difference in the taxonomy between the plants from these two eras. These elevated concentrations of nitrogen may be the result of n-alkylated pyrrole, and pyridine compounds the same classes of compounds that were detected in the OJP tuff. It was proposed that the compounds in the OJP tuff could be the products of the diagenesis of chitin. The compounds in the OJP tuff and in the lower Devonian fossil were comparable. This implies the presence of the diagenetically altered chitin in some of the lower Devonian fossils that could be could have originated from a fungal taxon in these samples.

APPENDIX B - CONTROL EXPERIMENTS

B 1.0 Pyrolysis Gas chromatography Mass Spectrometry Control experiments

A number of control experiments were carried out to exclude procedural artefacts that may have occurred in the experiments that were conducted for this thesis. First, it has been suggested that the detection of aromatic compounds is potentially the result of the aromatisation straight chain compounds during pyrolysis (Lewis et al., 2015). Therefore, WSD was intentionally spiked with the fatty acid, octadecanoic acid, to exclude the possibility that any of the aromatic compounds that were detected were the result of unknown interactions between long-chain organic compounds and the minerals in the rock samples. Second, the thermochemolytic agent TMAH contains nitrogen. To exclude the possibility that any of the nitrogen substitutions that were detected were the result of an unknown side reaction with the nitrogen atom in TMAH with the organic compounds in the OJP samples, in the presence of basalt minerals during pyrolysis, WSD was spiked with homoatomic aromatic compounds.

B 1.0 WSD spiked with Organic Compounds Control Investigation

As a control, the methods that were used to obtain and analyse organic material in the OJP tuff were compared to the WSD (see section 1.10.3). This was used because, in contrast to the OJP material, this basalt does not possess any of the glass shards or the putative microbial weathering textures that were observed in the OJP_13 sample (see section 3.1.1).

To demonstrate that the compounds that were detected in the THM-GC/MS analysis OJP_13 were not the result of a procedural artefact, resulting from pyrolysis, 10µg of either stearic acid or catechol (Analar grade, Sigma-Aldrich Ltd. Dorset, UK) was added and dispersed in 1 gram of WSD that had been milled and passed through a 150µm sieve (see section 2.1.1). Furthermore, 10 µl Xylene (Analar grade, Sigma-Aldrich Ltd. Dorset, UK) was added to an additional 1 g WSD sample, then allowed to dry. This was then analysed with either py-GC/MS or THM-GC/MS according to the description in section 2.4.2.
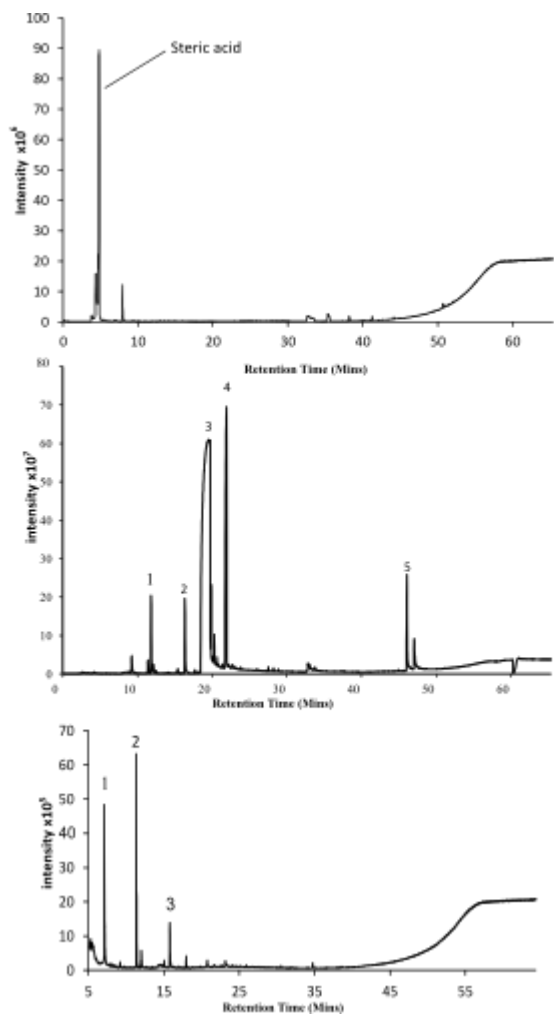
Fig B-1a-c: *py-GC/MS of WSD spiked with (a) steric acid and (b) Catechol*

Fig B-1b: 1. phenol, 2. 1,3-Benzodioxol-2-one, 3. Catechol, 4. 2,3-dihydro Indene, 5.1,3 Naphalene diol

Fig B-2: *THM-GC/MS of WSD spiked with Catechol.* 1. Formamide, 2. Triazene, 3. 1,2 dimethyl benzene

Fig. B-1a demonstrated that py-GC/MS analysis of the WSD spiked with 0.1% $^W/_W$ steric acid resulted in the detection of that compound, plus trace contaminants at a pyrolysis temperature of 610°C, importantly no aromatic compounds could be detected. The purpose of this analysis demonstrated that the aromatic compounds that had been detected in the OJP were not the result of thermally driven side reaction, in a similar reaction to the anoxic combustion described by Frenklach (1987).

Fig. B-1b and c demonstrated that heteroatomic nitrogen compounds, specifically the aromatic compounds with nitrogen substitutions (e.g. pyrrole and pyridine) were detected in the OJP_13, but were undetected in the WSD spiked with catechol with both py-GC/MS and THM-GC/MS at pyrolysis temperatures of 610 °C. This implies that the nitrogenous aromatic compounds that were observed in the OJP_13 were unlikely the result of an interaction between the TMAH and the aromatic compounds in OJP_13.

246

The intentionally added aliphatic and aromatic compounds were unaffected by either the py-GC/MS or the THM-GC/MS process. No additional aromatic compounds were observed in the WSD spiked with oleic acid, implying that the aromatic compounds detected in the OJP were not a result of an aromatisation of straight-chain compounds , during thermal extraction, conducted in the presence of TMAH. In addition, no nitrogen compounds were observed in the rings of the catechol that was added to WSD, demonstrating that the nitrogen bearing compounds that were detected in the OJP were not nitrogen substitution side-reactions that could have occurred during thermal extraction, Hence, the compounds detected in the OJP were unlikely to be artefacts of the thermal extraction in the presence of TMAH.

B 2.0 The effect of UV/O$_3$ cleaning on the organic chemistry of WSD spiked with organic compounds.

To investigate whether the UV/O$_3$ cleaning may have an affected the chemical states of the organic composition of the OJP_13, powdered WSD was spiked with a range of organic compounds then subjected to a time series of UV/O$_3$ cleaning.
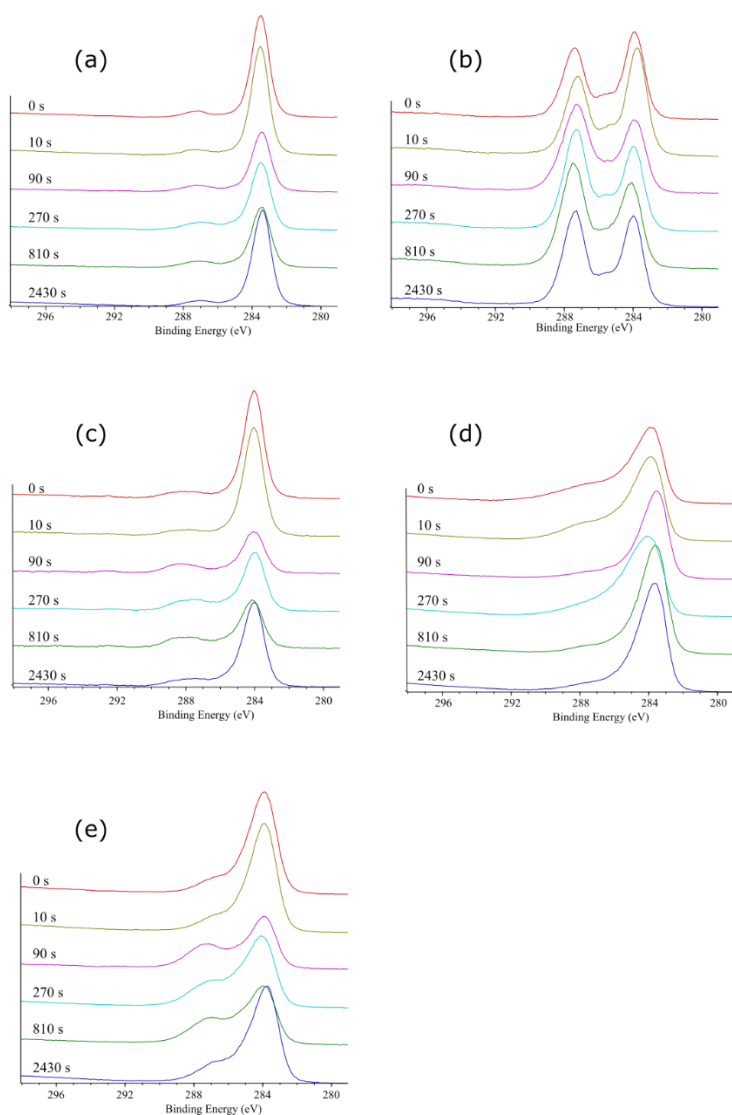
Fig. B-3 a-e. *High-resolution carbon spectra of organic compounds controls and of the OJP_13 sample. This shows the effect of UV/O$_3$ cleaning on their chemical composition. (a) hexadecenoic acid; (b) citric acid (c) Pyrene (d) Triazene (e) OJP_13. The values annotating each of the spectra are the time (seconds) of exposure to UV/O$_3$.*

248

	[C] at %				
	HDA	CA	Pyrene	Triazene	OJP_13
T= 0 s	30.5	40.2	35.6	12.0	12.0
T-810 s	10.7	15.3	10.4	7.1	3.5

Table B-1. *the carbon concentration before UV/O₃ cleaning and after 810 seconds of UV/O₃ cleaning. [C] = carbon concentration, HDA = Hexadecenoic acid; CA = Citric Acid.*

Fig B-2 demonstrated that the peak positions of the organic compounds standards in the XPS carbon spectral profiles were unchanged as a result of repeated exposure to UV/O$_3$ cleaning up to 2430 seconds. Thus, the chemical composition of the organic material in the OJP_13 samples was unaffected by UV/O$_3$ cleaning.

Table B-2 presents the carbon concentration of WSD deliberately spiked with different organic compounds. This demonstrated that the carbon concentration decreased as a result of UV/O$_3$ cleaning.

Figure 1-23 is replicated from the introduction section 1.11.4. The analysis of the XPS carbon spectral profiles indicated that exposure to UV/O$_3$ had no detectable effect on the chemical composition of the organic compounds analysed in this investigation (see below; fig 1-23). However, the carbon concentration was reduced in these samples, further demonstrating the efficacy of UV/O$_3$ to decontaminate the geological samples (see section 3.3.4). It should be noted that the hexadecenoic acid and triazene possessed a single peak at ca. 284.0 eV. This is assumed to be a result of vacuum boiling of these compounds. Furthermore, a C$_{35}$ alkane was also prepared as a standard. However, this resulted in damage to the X-ray source. Therefore, its use as a control standard should be avoided in future investigations.
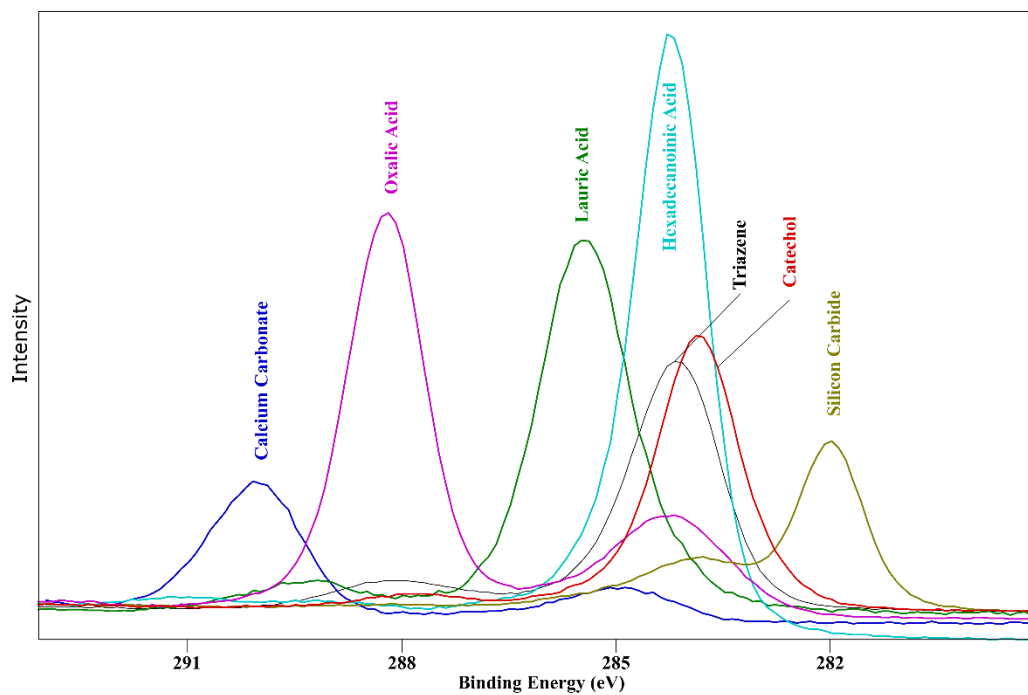
Replicate Fig. 1-23. *High-resolution XPS spectra of different carbon compounds these values are consistent with online databases (srdata.nist.gov/xps/; www.lasurface.com) Fig. 1-23 re-presented from* Purvis et al., under review. *CPS= counts per second.*

REFERENCES

A

Abbott, G.D., Swain, E.Y., Muhammad, A.B., Allton, K., Belyea, L.R., Laing, C.G. and Cowie, G.L. (2013) 'Effect of water-table fluctuations on the degradation of Sphagnum phenols in surficial peats', *Geochimica et Cosmochimica Acta*, 106, pp. 177-191.

Abramov, O. and Mojzsis, S.J. (2009) 'Microbial habitability of the Hadean Earth during the late heavy bombardment', *Nature*, 459(7245), pp. 419-22.

Acuna, M.H., Connerney, J.E.P., Wasilewski, P., Lin, R.P., Anderson, K.A., Carlson, C.W., McFadden, J., Curtis, D.W., Mitchell, D., Reme, H., Mazelle, C., Sauvaud, J.A., d'Uston, C., Cros, A., Medale, J.L., Bauer, S.J., Cloutier, P., Mayhew, M., Winterhalter, D. and Ness, N.F. (1998) 'Magnetic field and plasma observations at Mars: Initial results of the Mars global surveyor mission', *Science*, 279(5357), pp. 1676-1680.

Adeli, S., Hauber, E., Kleinhans, M., Le Deit, L., Platz, T., Fawdon, P. and Jaumann, R. (2016) 'Amazonian-aged fluvial system and associated ice-related features in Terra Cimmeria, Mars', *Icarus*, 277, pp. 286-299.

Allen, C.C., Gooding, J.L., Jercinovic, M. and Keil, K. (1981) 'Altered basaltic glass: A terrestrial analog to the soil of Mars', *Icarus*, 45(2), pp. 347-369.

Allen, C.C., Morris, R.V., Lindstrom, D.J., Lindstrom, M.M. and Lockwood, J.P., (1997), March. 'JSC Mars-1-Martian regolith simulant'. In *Lunar and Planetary Science Conference* (Vol. 28).

Alleon, J., Bernard, S., Le Guillou, C., Marin-Carbonne, J., Pont, S., Beyssac, O., McKeegan, K.D. and Robert, F. (2016) 'Molecular preservation of 1.88 Ga Gunflint organic microfossils as a function of temperature and mineralogy', *Nature Communications*, 7. p.11977

Allwood, A.C. (2016) 'Evidence of life in Earth's oldest rocks', *Nature*, 537,(7621), pp. 500-501.

Alt, J.C. and Mata, P. (2000) 'On the role of microbes in the alteration of submarine basaltic glass: a TEM study', *Earth and Planetary Science Letters*, 181(3), pp. 301-313.

Amend, J.P. and Teske, A. (2005) 'Expanding frontiers in deep subsurface microbiology', *Palaeogeography Palaeoclimatology Palaeoecology*, 219(1-2), pp. 131-155.

Anders, E. (1989) 'Pre-Biotic Organic-Matter from Comets and Asteroids', *Nature*, 342(6247), pp. 255-257.

Anderson, D.L. (1972) 'Internal Constitution of Mars', *Journal of Geophysical Research*, 77(5), p. 789.

Angerer, T.B., Blenkinsopp, P. and Fletcher, J.S., 2015. High energy gas cluster ions for organic and biological analysis by time-of-flight secondary ion mass spectrometry. *International Journal of Mass Spectrometry*, *377*, pp.591-598.

Arkani-Hamed, J. and Ghods, A. (2011) 'Could giant impacts cripple core dynamos of small terrestrial planets?', *Icarus*, 212(2), pp. 920-934.

Atreya, S.K., Mahaffy, P.R. and Wong, A.S. (2007) 'Methane and related trace species on Mars: Origin, loss, implications for life, and habitability', *Planetary and Space Science*, 55(3), pp. 358-369.

Attard, G., and Barnes, C. (1998). Chapter 3, *Surfaces* (Oxford science publications). Oxford: Oxford University Press.

Ausloos, P., Clifton, C.L., Lias, S.G., Mikaya, A.I., Stein, S.E., Tchekhovskoi, D.V., Sparkman, O.D., Zaikin, V. and Zhu, D. (1999) 'The critical evaluation of a comprehensive mass spectral library', *Journal of the American Society for Mass Spectrometry*, 10(4), pp. 287-299.

Awramik, S.M., Schopf, J.W. and Walter, M.R. (1983) 'Filamentous Fossil Bacteria from the Archean of Western Australia', *Precambrian Research*, 20(2-4), pp. 357-374.

Awramik, S.M. (1992) 'The Oldest Records of Photosynthesis', *Photosynthesis Research*, 33(2), pp. 75-89.

B

Bach, W. and Edwards, K.J. (2003) 'Iron and sulfide oxidation within the basaltic ocean crust: implications for chemolithoautotrophic microbial biomass production', *Geochimica et Cosmochimica Acta*, 67(20), pp. 3871-3887.

Bada, J.L. (2013) 'New insights into prebiotic chemistry from Stanley Miller's spark discharge experiments', *Chemical Society Reviews*, 42(5), pp. 2186-2196.

Baker, V.R., Milton,D.J. (1974) 'Erosion by catastrophic floods on Mars and Earth', *Icarus*, 23, pp. 27-41.

Ballou, E.V., Wood, P.C., Wydeven, T., Lehwalt, M.E. and Mack, R.E. (1978) 'Chemical Interpretation of Viking Lander 1 Life Detection Experiment', *Nature*, 271(5646), pp. 644-645.

Banerjee, D., Hirani, M. and Sanyal, S.K., (2000). Coal-quality deterioration in a coal stack of a power station. *Applied Energy*, *66*(3), pp.267-275.

Banerjee, N.R. and Muehlenbachs, K. (2003) 'Tuff life: Bioalteration in volcanishardic rocks from the Ontong Java Plateau', *Geochemistry Geophysics Geosystems*, 4(4).

Banerjee, N.R., Furnes, H., Muehlenbachs, K., Staudigel, H. and de Wit, M. (2006) 'Preservation of ca. 3.4–3.5 Ga microbial biomarkers in pillow lavas and hyaloshardites from the Barberton Greenstone Belt, South Africa', *Earth and Planetary Science Letters*, 241(3-4), pp. 707-722.

Banin, A., Ben-Shlomo, T., Margulies, L., Blake, D.F., Mancinelli, R.L. and Gehring, A.u. (1993) 'The Nanophase Iron Mineral(S) in Mars Soil', *Journal of Geophysical Research-Planets*, 98(E11), pp. 20831-20853.

Barghoorn, E.S.a.T., S.A. (1965) 'Microorganisms from the Gunflint chert', *Science*, 147(5658), pp. pp.563-575.

Barlow A. J., Portoles J. F., and Cumpson P. J. (2014). 'Observed damage during Argon gas cluster depth profiles of compound semiconductors'. *Journal of Applied Physics*, 116(5), 054908.

Barr, T.L. (1980) *Applied Surface Analysis: A Symposium*. ASTM International.

Barth, T. (1999). 'Similarities and differences in hydrous pyrolysis of biomass and source rocks'. *Organic Geochemistry*, *30*(12), pp.1495-1507.

Barr, T.L. and Seal, S. (1995) 'Nature of the Use of Adventitious Carbon as a Binding-Energy Standard', *Journal of Vacuum Science and Technology a-Vacuum Surfaces and Films*, 13(3), pp. 1239-1246.

Bateman M.D., Evans D.J.A. Buckland, P.C., Connell E.R., Friend R.J., Hartmann D., Moxon H., Fairburn W.A., Panagiotakopulu E. and Ashurst R.A., (2015). 'Last glacial dynamics of the Vale of York and North Sea lobes of the British and Irish Ice Sheet'. *Proceedings of the Geologists' Association*, *126*(6), pp.712-730.

BBC (2016) 'Newcastle University lab hopes to find life on Mars', [Online]. Available at: www.bbc.co.uk/news/uk-england-tyne-37637466.

Beamson, G., and Briggs, D. (1992) 'High-resolution XPS of organic polymers: the Scienta ESCA300 database', John Wiley and Sons Ltd, Chichester

Beck, C.B. (1962). Reconstructions of Archaeopteris, and further consideration of its phylogenetic position. *American Journal of Botany*, *49*(4), pp.373-382.

Behar, F. and Vandenbroucke, M. (1986) 'Chemical Modeling of the Structure of Kerogens and Asphaltenes as a Function of Their Origin and Evolution Stage', *Revue De L Institut Francais Du Petrole*, 41(2), pp. 173-188.

Bell, E.A., Boehnke, P., Harrison, T.M. and Mao, W.L. (2015) 'Potentially biogenic carbon preserved in a 4.1 billion-year-old zircon', *Proceedings of the National Academy of Sciences of the United States of America*, 112(47), pp. 14518-14521.

Bell, J.F., Mccord, T.B. and Owensby, P.D. (1990) 'Observational Evidence of Crystalline Iron-Oxides on Mars', *Journal of Geophysical Research-Solid Earth and Planets*, 95(B9), pp. 14447-14461.

Bengtson, S., Ivarsson, M., Astolfo, A., Belivanova, V., Broman, C., Marone, F. and Stampanoni, M. (2014) 'Deep-biosphere consortium of fungi and prokaryotes in Eocene subseafloor basalts', *Geobiology*, 12(6), pp. 489-496.

Benner, S.A. (2010) 'Defining Life', *Astrobiology*, 10(10), pp. 1021-1030.

Benner, S.A., Devine, K.G., Matveeva, L.N. and Powell, D.H., (2000). 'The missing organic molecules on Mars'. *Proceedings of the National Academy of Sciences*, *97*(6), pp.2425-2430. Benner, S.A., Ricardo, A. and Carrigan, M.A. (2004) 'Is there a common chemical model for life in the universe?', *Current Opinion in Chemical Biology*, 8(6), pp. 672-689.

Bennett, B., Chen, M., Brincat, D., Gelin, F.J.P. and Larter, S.R. (2002) 'Fractionation of benzocarbazoles between source rocks and petroleums', *Organic Geochemistry*, 33(5), pp. 545-559.

Benzerara, K., Menguy, N., Banerjee, N.R., Tyliszczak, T., Brown, G.E. and Guyot, F. (2007) 'Alteration of submarine basaltic glass from the Ontong Java Plateau: A STXM and TEM study', *Earth and Planetary Science Letters*, 260(1-2), pp. 187-200.

Bernard, S. and Papineau, D. (2014) 'Graphitic Carbons and Biosignatures', *Elements*, 10(6), pp. 435-440.

Berthelin, J. (1988). 'Microbial weathering processes in natural environments'. In *Physical and Chemical Weathering in Geochemical Cycles* (pp. 33-59). Springer, Dordrecht, Netherlands.

Bianciardi, G., Vincenzo Rizzo, Maria Eugenia Farias, and Nicola Cantasano. (2015) 'Microbialites at Gusev Crater, Mars', *Journal of astrobiology and outreach*, pp. 1-8.

Bibring, J.P., Langevin, Y., Mustard, J.F., Poulet, F., Arvidson, R., Gendrin, A., Gondet, B., Mangold, N., Pinet, P., Forget, F. and team, O. (2006) 'Global mineralogical and aqueous mars history derived from OMEGA/Mars express data', *Science*, 312(5772), pp. 400-404.

Biemann, K., Oro, J., Toulmin, P., Orgel, L.E., Nier, A.O., Anderson, D.M., Simmonds, P.G., Flory, D., Diaz, A.V., Rushneck, D.R. and Biller, J.A., (1976). Search for organic and volatile inorganic compounds in two surface samples from the Chryse Planitia region of Mars. *Science*, *194*(4260), pp.72-76.

Biemann, K., Oro, J.I.I.I.P.T., Toulmin, P., Orgel, L.E., Nier, A.O., Anderson, D.M., Simmonds, P.G., Flory, D., Diaz, A.V., Rushneck, D.R. and Biller, J.E. (1977) 'The search for organic substances and inorganic volatile compounds in the surface of Mars', *Journal of Geophysical Research*, 82(28), pp. 4641-4658.

Biemann, K. and Lavoie, J.M., (1979). 'Some final conclusions and supporting experiments related to the search for organic compounds on the surface of Mars'. *Journal of Geophysical Research: Solid Earth*, *84*(B14), pp.8385-8390.

Biemann, K. (2007) 'On the ability of the Viking gas chromatograph–mass spectrometer to detect organic matter', *Proceedings of the National Academy of Sciences*, 104(25), pp. 10310-10313.

Bland, P.A. and Smith, T.B. (2000) 'Meteorite accumulations on Mars', *Icarus*, 144(1), pp. 21-26.

Boldyreva, E.V. (1997) 'The concept of the 'reaction cavity': A link between solution and solid-state chemistry', *Solid State Ionics*, 101, pp. 843-849.

Bonaccorsi, R., McKay, C.P. and Chen, B. (2010) 'Biomass and habitability potential of clay minerals- and iron-rich environments: Testing novel analogs for Mars Science

Laboratory landing sites candidates', *Philosophical Magazine*, 90(17-18), pp. 2309-2327.

Boston, P.J., Ivanov, M.V. and P. McKay, C. (1992) 'On the possibility of chemosynthetic ecosystems in subsurface habitats on Mars', *Icarus*, 95(2), pp. 300-308.

Botta, O. and Bada, J.L. (2002) 'Extraterrestrial organic compounds in meteorites', *Surveys in Geophysics*, 23(5), pp. 411-467.

Botta, O., Fristad, K. E., Mahaffy, P. R., Eigenbrode, J., and Steele, A. (2007) 'Dolomite sample from Svalbard, Norway, analyzed using the pyrolysis protocol of the SAM Instrument.', *In Lunar and Planetary Institute Science Conference Abstracts*, 38.

Botta, O., Bada, J.L., Gomez-Elvira, J., Javaux, E., Selsis, F. and Summons, R. (2008) 'Strategies of Life Detection": Summary and Outlook', *Space Science Reviews*, 135(1-4), pp. 371-380.

Boudou, J.P., Schimmelmann, A., Ader, M., Mastalerz, M., Sebilo, M. and Gengembre, L. (2008) 'Organic nitrogen chemistry during low-grade metamorphism', *Geochimica Et Cosmochimica Acta*, 72(4), pp. 1199-1221.

Bowman, S.M. and Free, S.J. (2006) 'The structure and synthesis of the fungal cell wall', *Bioessays*, 28(8), pp. 799-808.

Boyce, C.K., Hotton, C.L., Fogel, M.L., Cody, G.D., Hazen, R.M., Knoll, A.H. and Hueber, F.M. (2007) 'Devonian landscape heterogeneity recorded by a giant fungus', *Geology*, 35(5), pp. 399-402

Boynton, W.V., Taylor, G.J., Evans, L.G., Reedy, R.C., Starr, R., Janes, D.M., Kerry, K.E., Drake, D.M., Kim, K.J., Williams, R.M.S., Crombie, M.K., Dohm, J.M., Baker, V., Metzger, A.E., Karunatillake, S., Keller, J.M., Newsom, H.E., Arnold, J.R., Bruckner, J., Englert, P.A.J., Gasnault, O., Sprague, A.L., Mitrofanov, I., Squyres, S.W., Trombka, J.I., d'Uston, L., Wanke, H. and Hamara, D.K. (2007) 'Concentration of H, Si, Cl, K, Fe, and Th in the low- and mid-latitude regions of Mars', *Journal of Geophysical Research-Planets*, 112(E12).

Bradley, J.P., Harvey, R.P. and McSween, H.Y. (1997) 'No 'nanofossils' in Martian meteorite', *Nature*, 390(6659), pp. 454-454.

Brain, D.A. and Jakosky, B.M. (1998) 'Atmospheric loss since the onset of the Martian geologic record: Combined role of impact erosion and sputtering', *Journal of Geophysical Research-Planets*, 103(E10), pp. 22689-22694.

Brantley, S.L., Liermann, L., Bau, M. and Wu, S., (2001). Uptake of trace metals and rare Earth elements from hornblende by a soil bacterium. *Geomicrobiology Journal*, *18*(1), pp.37-61.

Brasier, M., McLoughlin, N., Green, O. and Wacey, D. (2006) 'A fresh look at the fossil evidence for early Archaean cellular life', *Philosophical Transactions of the Royal Society B-Biological Sciences*, 361(1470), pp. 887-902.

Brasier, M.D., Antcliffe, J., Saunders, M. and Wacey, D. (2015) 'Changing the picture of Earth's earliest fossils (3.5-1.9 Ga) with new approaches and new discoveries', *Proceedings of the National Academy of Sciences of the United States of America*, 112(16), pp. 4859-4864.

Brearley, A.J. (2003). 'Magnetite in ALH 84001: An origin by shock-induced thermal decomposition of iron carbonate'. *Meteoritics and Planetary Science*, *38*(6), pp.849-870.

Briggs, D., and Seah, M. P. (Eds) (1983) *Practical Surface Analysis Volume 1 – Auger and X-ray Photon Spectroscopy*. John Wiley and Sons Ltd, Chichester.

Briggs, D.E.G., Evershed, R.P. and Lockheart, M.J. (2000) 'The biomolecular palaeontology of continental fossils', *Paleobiology*, 26(4), pp. 169-193.

Briggs, D.E.G. and Summons, R.E. (2014) 'Ancient biomolecules: Their origins, fossilization, and role in revealing the history of life', *Bioessays*, 36(5), pp. 482-490.

Briggs, D.E.G., and Grant J. T. (Eds.). (2003). 'Surface analysis by Auger and X-ray photoelectron spectroscopy'.p.53 IM publications.

Brock, T.D. (1967). 'Life at High Temperatures: Evolutionary, ecological, and biochemical significance of organisms living in hot springs is discussed'. *Science*, *158*(3804), pp.1012-1019.

Brock, J. and Banfield, J. (2007). 'Molecular fossils and early life'. In *Geochimica Et Cosmochimica Acta* Vol. **71**, No. 15, pp. A123-A123).

Brothers, T.C. and Holt, J.W. (2016) 'Three-dimensional structure and origin of a 1.8km thick ice dome within Korolev Crater, Mars', *Geophysical Research Letters*, 43(4), pp. 1443-1449.

Brown, A.J., Hook, S.J., Baldridge, A.M., Crowley, J.K., Bridges, N.T., Thomson, B.J., Marion, G.M., de Souza Filho, C.R. and Bishop, J.L. (2010) 'Hydrothermal formation of Clay-Carbonate alteration assemblages in the Nili Fossae region of Mars', *Earth and Planetary Science Letters*, 297(1-2), pp. 174-182.

Brown, D., Webster, G., Hoover,R. (2012) *NASA Rover's First Soil Studies Help Fingerprint Martian Minerals*. Available at: http://www.nasa.gov/home/hqnews/2012/oct/HQ_12-383_Curiosity_CheMin.html (Accessed: 25 September).

Bryson, C. (2003) 'A High Performance, Low Mass, XPS for Biosignature Detection'. https://www.sbir.gov/sbirsearch/detail/114710 (Accessed: 14 Jan 2019).

Bryson, C. (2007) Elemental and Chemical State Analysis, XPS, for In-Situ Materials Analysis on Mars https://www.sbir.gov/sbirsearch/detail/91912 (Accessed: 14 Jan 2019).

Buch, A., Glavin, D.P., Sternberg, R., Szopa, C., Rodier, C., Navarro-González, R., Raulin, F., Cabane, M. and Mahaffy, P.R. (2006) 'A new extraction technique for in situ analyses of amino and carboxylic acids on Mars by gas chromatography mass spectrometry', *Planetary and Space Science*, 54(15), pp. 1592-1599.

Buch, A. Sternberg, R., Szopa, C., Freissinet, C., Garnier, C., Bekri, E.J., Rodier, C., Navarro-González, R., Raulin, F., Cabane, M., Stambouli, M., Glavin, D.P. and Mahaffy, P.R. (2009) 'Development of a gas chromatography compatible Sample Processing System (SPS) for the in-situ analysis of refractory organic matter in Martian soil: preliminary results', *Advances in Space Research*, 43(1), pp. 143-151.

Buckley, D.H. (1981). 'Surface effects in adhesion, friction, wear, and lubrication' (Vol. 5). Elsevier.

Buseck, P.R. and Beyssac, O. (2014). 'From organic matter to graphite: Graphitization'. *Elements*, *10*(6), pp.421-426.

C

Cabane, M., Coll, P., Rodier, C., Israel, G., Raulin, F., Sternberg, R., and Rannou, P. (2001) 'In situ inorganic and organic analysis (Pyr/CD-GC/MS) of the Martian soil, on the Mars 2005 mission.', *Planetary and Space Science*, 49(5), pp. 523-531.

Cabane, M., Coll, P., Szopa, C., Israel, G., Raulin, F., Sternberg, R., Mahaffy, P., Person, A., Rodier, C., Navarro-Gonzalez, R., Niemann, H., Harpold, D. and Brinckerhoff, W. (2004) 'Did life exist on Mars? Search for organic and inorganic signatures, one of the goals for "SAM" (sample analysis at Mars)', *Mercury, Mars and Saturn*, 33(12), pp. 2240-2245.

Cabrol, N.A. and Grin, E.A. (1999) 'Distribution, classification, and ages of martian impact crater lakes', *Icarus*, 142(1), pp. 160-172.

Cady, S.L., Farmer, J.D., Grotzinger, J.P., Schopf, J.W. and Steele, A. (2003) 'Morphological biosignatures and the search for life on Mars', *Astrobiology*, 3(2), pp. 351-368.

Cady, S. and Noffke, N. (2009) 'Geobiology: Evidence for early life on Earth and the search for life on other planets', *GSA Today*, pp. 4-10.

Carleton, N. P., and W. A. Traub. 'Detection of molecular oxygen on Mars'." *Science* 177, no. 4053 (1972): 988-992.

Cannon, K. M., and Mustard, J. F. (2015). 'Preserved glass-rich impactites on Mars'. *Geology*, *43*(7), 635-638.

Carr, M.H. (1979) 'Formation of Martian flood features by release of water from confined aquifers', *Journal of Geophysical Research: Solid Earth*, 84((B6)), pp. 2995-3007.

Carr, M.H. (1986) 'Mars - a Water-Rich Planet', *Icarus*, 68(2), pp. 187-216.

Carr, M.H. and Wanke, H. (1992) 'Earth and Mars - Water Inventories as Clues to Accretional Histories', *Icarus*, 98(1), pp. 61-71.

Carr, M.H. (1999) 'Retention of an atmosphere on early Mars', *Journal of Geophysical Research-Planets*, 104(E9), pp. 21897-21909.

Carr, M.H. and Head, J.W. (2003) 'Oceans on Mars: An assessment of the observational evidence and possible fate', *Journal of Geophysical Research-Planets*, 108(E5).

Carr, M.H. (2006), 'The Surface of Mars'. Cambridge Planetary Science Series, Cambridge University Press

Carr, M.H. and Head, J.W. (2010) 'Geologic history of Mars', *Earth and Planetary Science Letters*, 294(3-4), pp. 185-203.

Carrier, B.L. and Kounaves, S.P. (2015) 'The origins of perchlorate in the Martian soil', *Geophysical Research Letters*, 42(10), pp. 3739-3745.

Cary, S.C., McDonald, I.R., Barrett, J.E. and Cowan, D.A. (2010) 'On the rocks: the microbiology of Antarctic Dry Valley soils', *Nature Reviews Microbiology*, 8(2), pp. 129-138.

Castenholz, R.W., and Ferran Garcia-Pichel. (2013) Ecology of Cyanobacteria II: Their Diversity in Space and Time. Springer, Dordrecht, Netherlands.

Challinor, J.M. (1989) 'A Pyrolysis Derivatization Gas-Chromatography Technique for the Structural Elucidation of Some Synthetic-Polymers', *Journal of Analytical and Applied Pyrolysis*, 16(4), pp. 323-333.

Chambers, L.M., Pringle, M. S., and Fitton, J. G.. (2002) 'Age and duration of magmatism on the Ontong Java Plateau: ^{40}Ar-^{39}Ar results from ODP Leg 192.', *In AGU Fall Meeting Abstracts*. p. p. 1271.

Chapelle, F.H., O'Neill, K., Bradley, P.M., Methe, B.A., Ciufo, S.A., Knobel, L.L. and Lovley, D.R. (2002) 'A hydrogen-based subsurface microbial community dominated by methanogens', *Nature*, 415(6869), pp. 312-315.

Chassefiere, E. and Leblanc, F. (2011) 'Methane release and the carbon cycle on Mars', *Planetary and Space Science*, 59(2-3), pp. 207-217.

Chassefiere, E., Dartois, E., Herri, J.M., Tian, F., Schmidt, F., Mousis, O. and Lakhlifi, A. (2013) 'CO2-SO2 clathrate hydrate formation on early Mars', *Icarus*, 223(2), pp. 878-891.

Chastain J., and King R. C. (Eds.). (1995) 'Handbook of X-ray photoelectron spectroscopy: a reference book of standard spectra for identification and interpretation of XPS data'. Eden Prairie, MN: Physical Electronics.

Chastain, B.K. and Chevrier, V. (2007) 'Methane clathrate hydrates as a potential source for Martian atmospheric methane', *Planetary and Space Science*, 55(10), pp. 1246-1256.

Chatzitheodoridis, E., Haigh, S. and Lyon, I. (2014) 'A Conspicuous Clay Ovoid in Nakhla: Evidence for Subsurface Hydrothermal Alteration on Mars with Implications for Astrobiology', *Astrobiology*, 14(8), pp. 651-693.

Cheng J., Wucher A. and Winograd N. (2006) 'Molecular depth profiling with cluster ion beams', *Journal of Physical Chemistry B*, **110**(16), pp. 8329-8336.

Chevrier, V. and Mathé, P.E. (2007) 'Mineralogy and evolution of the surface of Mars: A review', *Planetary and Space Science*, 55(3), pp. 289-314.

Choblet, G., Tobie G., Sotin, C., Běhounková, M., Čadek, O.,Frank Postberg4,5 and Souček, O. (2017) 'Powering prolonged hydrothermal activity inside Enceladus', *Nature Astronomy*, 1.

Christensen, P.R., Jakosky, B., Kieffer, H.H., Malin, M.C., McSween, H.Y., Nealson, K., Mehall, G.L., Silverman, S.H., Ferry, S., Caplinger, M. and Ravine, M. (2004) 'The Thermal Emission Imaging System (THEMIS) for the Mars 2001 Odyssey Mission', *Space Science Reviews*, 110(1-2), pp. 85-130.

Chyba, C.F., Thomas, P.J., Brookshaw, L. and Sagan, C. (1990). Cometary delivery of organic molecules to the early Earth. *Science*, *249*(4967), pp.366-373.

Chyba, C. and Sagan, C. (1992) 'Endogenous Production, Exogenous Delivery and Impact-Shock Synthesis of Organic-Molecules - an Inventory for the Origins of Life', *Nature*, 355(6356), pp. 125-132.

Clark, B.C., Baird, A.K., Rose , H.J., Toulmin, P., Keil, K., Castro, A.J., Kelliher, W.C., Rowe, C.D. and Evans, P.H. (1976) 'Inorganic analyses of Martian surface samples at the Viking landing sites', *Science*, 194(4271), pp. pp.1283-1288.

Clark, B.C. and Vanhart, D.C. (1981) 'The Salts of Mars', *Icarus*, 45(2), pp. 370-378.

Cleland, C.E. and Chyba, C.F. (2002) 'Defining 'life'', *Origins of Life and Evolution of the Biosphere*, 32(4), pp. 387-393.

Clifford, S.M., Lasue, J., Heggy, E., Boisson, J., McGovern, P. and Max, M.D. (2010) 'Depth of the Martian cryosphere: Revised estimates and implications for the existence and detection of subpermafrost groundwater', *Journal of Geophysical Research-Planets*, 115.

Cobb, A., Warms, M., Maurer, E.P. and Chiesa, S., (2012). 'Low-tech coconut shell activated charcoal production'. *International Journal for Service Learning in Engineering* Vol. 7, No. 1, pp. 93-104.

Coates, J.D. and Achenbach, L.A. (2004) 'Microbial perchlorate reduction: Rocket-fuelled metabolism', *Nature Reviews Microbiology*, 2(7), pp. 569-580.

Cockell, C. (2000) 'The Ultraviolet Environment of Mars: Biological Implications Past, Present, and Future', *Icarus*, 146(2), pp. 343-359.

Cockell, C.S., Lee, P., Osinski, G., Horneck, G. and Broady, P. (2002a) 'Impact-induced microbial endolithic habitats', *Meteoritics and Planetary Science*, 37(10), pp. 1287-1298.

Cockell, C.S., McKay, C.P. and Omelon, C. (2002b) 'Polar endoliths an anti-correlation of climatic extremes and microbial biodiversity', *International Journal of Astrobiology*, 1(4), pp. 305-310.

Cockell, C.S. and Herrera, A. (2008) 'Why are some microorganisms boring?', *Trends Microbiol*, 16(3), pp. 101-6.

Cockell, C.S., Olsson-Francis, K., Herrera, A. and Meunier, A. (2009) 'Alteration textures in terrestrial volcanic glass and the associated bacterial community', *Geobiology*, 7(1), pp. 50-65.

Cockell C.S. (2011) 'Life in the lithosphere, kinetics and the prospects for life elsewhere', *Philosophical Transactions of the Royal Society A: Mathematical, Physical and Engineering Sciences*, 369(1936), pp. 516-37.

Cockell, C.S., Kelly, L.C., Summers, S. and Marteinsson, V. (2011) 'Following the kinetics: iron-oxidizing microbial mats in cold Icelandic volcanic habitats and their rock-associated carbonaceous signature', *Astrobiology*, 11(7), pp. 679-94.

Cockell, C.S. (2014) 'Trajectories of Martian Habitability', *Astrobiology*, 14(2), pp. 182-203.

Cody, G.D. (2005) 'Geochemical connections to primitive metabolism', *Elements*, 1(3), pp. 139-143.

Cody, G.D., Gupta, N.S., Briggs, D.E.G., Kilcoyne, A.L.D., Summons, R.E., Kenig, F., Plotnick, R.E. and Scott, A.C. (2011) 'Molecular signature of chitin-protein complex in Paleozoic arthropods', *Geology*, 39(3), pp. 255-258.

Conway, S.J., Balme, M.R., Kreslavsky, M.A., Murray, J.B. and Towner, M.C. (2015) 'The comparison of topographic long profiles of gullies on Earth to gullies on Mars: A signal of water on Mars', *Icarus*, 253, pp. 189-204.

Conway, S.J.a.B., M.R. (2016) 'A novel topographic parameterization scheme indicates that martian gullies display the signature of liquid water', *Earth and Planetary Science Letters*, 454, pp. 36-45.

Cooper, G., Kimmich, N., Belisle, W., Sarinana, J., Brabham, K. and Garrel, L., 2001. Carbonaceous meteorites as a source of sugar-related organic compounds for the early Earth. *Nature*, *414*(6866), p.879.

Costard, F., Forget, F., Mangold, N. and Peulvast, J.P. (2002) 'Formation of recent Martian debris flows by melting of near-surface ground ice at high obliquity', *Science*, 295(5552), pp. 110-113.

Counsell J. D. P., Roberts, A. J., Boxford, W., Moffitt, C., and Takahashi, K. (2014). 'Reduced Preferential Sputtering of TiO$_2$ using Massive Argon Clusters'. *Journal of Surface Analysis*, **20**(3), 211-215.

Craddock, R.A. and Maxwell, T.A. (1990) 'Resurfacing of the Martian Highlands in the Amenthes and Tyrrhena Region', *Journal of Geophysical Research-Solid Earth and Planets*, 95(B9), pp. 14265-14278.

Craddock, R.A., Maxwell, T.A. and Howard, A.D. (1997) *In Early Mars: Geologic and Hydrologic Evolution Physical and Chemical Environments, and the Implications for Life* Houston, Texas. The Smithsonian/NASA Astrophysics Data System.

Craddock, R.A. and Greeley, R. (2009) 'Minimum estimates of the amount and timing of gases released into the Martian atmosphere from volcanic eruptions', *Icarus*, 204(2), pp. 512-526.

Cronin, J.R. and Moore, C.B., (1971). Amino acid analyses of the Murchison, Murray, and Allende carbonaceous chondrites. *Science*, *172*(3990), pp.1327-1329.

Crovisier, J. (2004) 'The molecular complexity of comets', *Astrobiology: Future Perspectives*, 305, pp. 179-203.

Cumpson P J and Seah M P (1996) 'Stability of reference masses. IV: Growth of carbonaceous contamination on platinum-iridium alloy surfaces, and cleaning by UV/ozone treatment', *Metrologia* 33 507

Cumpson P J. and Sano N. (2013) 'Stability of reference masses V: UV/ozone treatment of gold and platinum surfaces', *Metrologia*, **50**(1), pp. 27-36.

Cumpson P.J., Portoles, J.F., Sano, N., Barlow, A.J., and Birch, M. (2013a) Depth profiling organic/inorganic interfaces by argon gas cluster ion beams: sputter yield data for biomaterials, in-vitro diagnostic and implant applications, Surf. Int. Anal. **45**, 1859

263

Cumpson P. J., Portoles J. F., Barlow A. J., and Sano N. (2013b). Accurate argon cluster-ion sputter yields: Measured yields and effect of the sputter threshold in practical depth-profiling by X-ray photoelectron spectroscopy and secondary ion mass spectrometry. *Journal of Applied Physics*, **114**(12), 124313.

Cumpson, P.J., Sano, N., Fletcher, I.W., Portoles, J.F., Bravo-Sanchez, M. and Barlow, A.J., (2015). Multivariate analysis of extremely large ToFSIMS imaging datasets by a rapid PCA method. *Surface and Interface Analysis*, *47*(10), pp.986-993.).

Czanderna, A. W. (Ed.). (2012). *Methods of surface analysis* (Vol. 1). Elsevier.

D

Dartnell, L.R., Desorgher, L., Ward, J.M. and Coates, A.J. (2008) 'Modelling the surface and subsurface Martian radiation environment: implications for astrobiology', *International Journal of Astrobiology*, 7(1), pp. 64-64.

Davies, N.S., Liu, A.G., Gibling, M.R. and Miller, R.F. (2016) 'Resolving MISS conceptions and misconceptions: A geological approach to sedimentary surface textures generated by microbial and abiotic processes', *Earth-Science Reviews*, 154, pp. 210-246.

Davies, P. (2010) 'The eerie silence', *Physics World*, 23(3), pp. 28-33.

De Gregorio, B.T., Sharp, T. G., Rushdi, A. I., and Simoneit, B. R. (2011) 'Bugs or gunk? Nanoscale methods for assessing the biogenicity of ancient microfossils and organic matter', in *Earliest Life on Earth: Habitats, Environments and Methods of Detection.*, pp. 239-289. Springer, Dordrecht, Netherlands

Deamer, D. and Damer, B. (2017) 'Can Life Begin on Enceladus? A Perspective from Hydrothermal Chemistry', *Astrobiology*, 17(9), pp. 834-839.

Decho, A.W. (1990) 'Microbial Exopolymer Secretions in Ocean Environments - Their Role(S) in Food Webs and Marine Processes', *Oceanography and Marine Biology*, 28, pp. 73-153.

Di Achille, G. and Hynek, B.M., (2010). 'Ancient ocean on Mars supported by global distribution of deltas and valleys'. *Nature Geoscience*, *3*(7), p.459.

Dick, S.J. (2006) 'NASA and the search for life in the universe', *Endeavour*, 30(2), pp. 71-75.

Dilik, Y. (1998) *Structure and Tectonics of Intermediate-Spread Oceanic Crust Drilled at DSDP/ODP holes 504B and 896A, Costa Rica Rift*. London: Geological Society of London.

Dilek, Y. Furnes, H. And Muehlenbachs, K. (Eds): (2008) *Links Between Geological Processes, Microbial Activities and Evolution of Life*, (Springer Dordrecht,Netherlands).

Diniega, S., Byrne, S., Bridges, N.T., Dundas, C.M. and McEwen, A.S. (2010) 'Seasonality of present-day Martian dune-gully activity', *Geology*, 38(11), pp. 1047-1050.

Dodd, M.S., Papineau, D., Grenne, T., Slack, J.F., Rittner, M., Pirajno, F., O'Neil, J. and Little, C.T.S (2017) 'Evidence for early life in Earth's oldest hydrothermal vent precipitates', *Nature*, 543(7643), pp. 60-64.

Dolomatov, M.Y. and Zhuravleva, N.A. (2014) 'Thermodynamic models of the distribution of life-related organic molecules in the interstellar medium', *Astrophysics and Space Science*, 351(1), pp. 213-218.

Downs, R.T. and MSL Science Team, (2015). 'Determining mineralogy on Mars with the CheMin X-ray diffractometer'. *Elements*, *11*(1), pp.45-50.

Drake, M.J. (2005) 'Origin of water in the terrestrial planets', *Meteoritics and Planetary Science*, 40(4), pp. 519-527.

Drury, J. (2016). Reuters Video News. www.reuters.com/video/2016/12/13/uk-scientists-search-for-life-on-mars-ev?videoId=370706088andvideoChannel=6andchannelName=Technology.

Dundas, C.M., McEwen, A.S., Diniega, S., Byrne, S. and Martinez-Alonso, S. (2010) 'New and recent gully activity on Mars as seen by HiRISE', *Geophysical Research Letters*, 37.

Dundas, C.M., Diniega, S., Hansen, C.J., Byrne, S. and McEwen, A.S. (2012) 'Seasonal activity and morphological changes in Martian gullies', *Icarus*, 220(1), pp. 124-143.

Dundas, C.M. and Keszthelyi, L.P. (2014) 'Emplacement and erosive effects of lava in south Kasei Valles, Mars', *Journal of Volcanology and Geothermal Research*, 282, pp. 92-102.

E

Edwards, C.S. and Piqueux, S. (2016) 'The water content of recurring slope lineae on Mars', *Geophysical Research Letters*, 43(17), pp. 8912-8919.

Eglinton G. (1964) 'Hydrocarbons of biological origin from a one-billion-year-old sediment', *Science*, **145**.3629 pp. 263-264.

Ehlmann, B.L., Mustard, J.F., Fassett, C.I., Schon, S.C., Head Iii, J.W., Des Marais, D.J., Grant, J.A. and Murchie, S.L. (2008) 'Clay minerals in delta deposits and organic preservation potential on Mars', *Nature Geoscience*, 1(6), pp. 355-358.

Ehlmann, B.L., Mustard, J.F., Murchie, S.L., Bibring, J.P., Meunier, A., Fraeman, A.A. and Langevin, Y. (2011) 'Subsurface water and clay mineral formation during the early history of Mars', *Nature*, 479(7371), pp. 53-60.

Ehrenfreund, P. and Charnley, S.B., (2000). Organic molecules in the interstellar medium, comets, and meteorites: a voyage from dark clouds to the early Earth. *Annual Review of Astronomy and Astrophysics*, *38*(1), pp.427-483.

Ehrenfreund, P. and Cami, J. (2010) 'Cosmic Carbon Chemistry: From the Interstellar Medium to the Early Earth', *Cold Spring Harbor Perspectives in Biology*, 2(12).

Ehrlich, H., Rigby, J.K., Botting, J.P., Tsurkan, M.V., Werner, C., Schwille, P., Petrasek, Z., Pisera, A., Simon, P., Sivkov, V.N., Vyalikh, D.V., Molodtsov, S.L., Kurek, D., Kammer, M., Hunoldt, S., Born, R., Stawski, D., Steinhof, A., Bazhenov, V.V. and Geisler, T. (2013) 'Discovery of 505-million-year old chitin in the basal demosponge Vauxia gracilenta', *Scientific Reports*, 3.

Eigenbrode, J.L. (2007) 'Fossil Lipids for Life-Detection: A Case Study from the Early Earth Record', *Space Science Reviews*, 135(1-4), pp. 161-185.

Eigenbrode J., Benning L.G., Maule J., Wainwright N., Steele A., Amundsen H.E.F. and Team A. (2009) 'A Field-Based Cleaning Protocol for Sampling Devices Used in Life-Detection Studies', *Astrobiology*, **9**(5), pp. 455-465.

Eigenbrode, J., Glavin, D., Dworkin, J., Conrad, P., and Mahaffy, P. (2011) 'Thermochemolysis-A New Sample Preparation Approach for the Detection of Organic Components of Complex Macromolecules in Mars Rocks Via Gas Chromatography Mass Spectrometry in SAM on MSL',. *In Lunar and Planetary Institute Science Conference Abstracts*, 42, p. 1460.

Eigenbrode, J.L., Summons, R.E., Steele, A., Freissinet, C., Millan, M., Navarro-González, R., Sutter, B., McAdam, A.C., Franz, H.B., Glavin, D.P. and Archer, P.D., (2018). Organic

matter preserved in 3-billion-year-old mudstones at Gale crater, Mars. *Science*, *360*(6393), pp.1096-1101.

Ekins, R. and Edwards, P. (1997) 'On the meaning of '"sensitivity", *Clinical Chemistry*, 43(10), pp. 1824-1831.

Engel, M. and Macko, S.A. (eds.) (2013) 'Organic geochemistry: principles and applications' *Springer Science and Business Media*.

Etienne, S. and Dupont, J. (2002) 'Fungal weathering of basaltic rocks in a cold oceanic environment (Iceland): Comparison between experimental and field observations', *Earth Surface Processes and Landforms*, 27(7), pp. 737-748.

Etiope, G. and Lollar, B.S. (2013) 'Abiotic Methane on Earth', *Reviews of Geophysics*, 51(2), pp. 276-299.

Evens, E.D. Grinsell, L.V. Piggott, S. and Wallis, F.S. (1962) 'Fourth report of the sub-committee of the south-western group of museums and art galleries on the petrological identification of stone axes'. *Proceedings of the Prehistoric Society* **28** 209–266.

F

Fairley, N. (2009). 'CasaXPS Manual 2.3.15: Introduction to XPS and AES'. *Casa Software.* www.casaxps.com. accessed 8th May 2017

Fanale, F.P. (1976) 'Martian volatiles: Their degassing history and geochemical fate', *Icarus*, 28(2), pp. 179-202.

Farquhar, J., Savarino, J., Jackson, T.L. and Thiemens, M.H. (2000) 'Evidence of atmospheric sulphur in the Martian regolith from sulphur isotopes in meteorites', *Nature*, 404(6773), pp. 50-52.

Fearn, S. (2015) 'An Introduction to Time-of-Flight Secondary Ion Mass Spectrometry (ToF-SIMS) and its Application to Materials Science'. *Morgan and Claypool Publishers*.

Fedorova, R.I. (1972) 'Possibilities of Gas Exchange Method for Detection of Extraterrestrial Life', *Izvestiya Akademii Nauk Sssr Seriya Biologicheskaya*, (5), pp. 717.

Fedorova, R.I., Milekhin.Ei and Ilyukhin.Ni (1973) 'Possibilities of Gas-Exchange Method for Detection of Extraterrestrial Life-Identification of Nitrogen-Fixing Microorganisms', *Izvestiya Akademii Nauk Sssr Seriya Biologicheskaya*, (6), pp. 797-806.

Feldman, W.C. (2004) 'Global distribution of near-surface hydrogen on Mars', *Journal of Geophysical Research*, 109(E9).

Fialkov, A.B., Steiner, u., Lehotay, S.J. and Amirav, A. (2007) 'Sensitivity and noise in GC/MS: Achieving low limits of detection for difficult analytes', *International Journal of Mass Spectrometry*, 260(1), pp. 31-48.

Fischer, F. and Tropsch, H. (1926) 'The synthesis of petroleum at atmospheric pressures from gasification products of coal', *Brennstoff-Chemie*, 7, pp. 97-104.

Fisher, G.L. (2014). 'Simplified, High-Throughput TOF-SIMS Analysis via HR 2 and Uniform Molecular Imaging of Rough Surfaces'. *Microscopy and Microanalysis*, *20*(S3), pp.2046-2047.Fisk, M.R., Crovisier, J.L. and Honnorez, J. (2013) 'Experimental abiotic alteration of igneous and manufactured glasses', *Comptes Rendus Geoscience*, 345(4), pp. 176-184.

Fisk, M.R., Giovannoni, S.J. and Thorseth, I.H. (1998) 'Alteration of oceanic volcanic glass: Textural evidence of microbial activity', *Science*, 281(5379), pp. 978-980.

Fitch, F.J.and Miller, J. A. (1967) 'The age of the Whin Sill', *Geological Journal*, 5(2), pp. 233–250.

Fitton, J.G., Godard, M., Mahoney, J.J. and Herzberg, C. (2004a) 'Origin of the Ontong Java Plateau', *Geochimica Et Cosmochimica Acta*, 68(11), pp. A581-A581.

Fitton, J.G., Mahoney, J.J., Wallace, P.J. and Saunders, A.D., (2004b). 'Origin and evolution of the Ontong Java Plateau: introduction'. *Geological Society, London, Special Publications*, *229*(1), pp.1-8.

Flannery, M.B., Stott, A.W., Briggs, D.E.G. and Evershed, R.P. (2001) 'Chitin in the fossil record: identification and quantification of D-glucosamine', *Organic Geochemistry*, 32(5), pp. 745-754.

Flynn, G.J. (1996) 'The delivery of organic matter from asteroids and comets to the early surface of Mars.', *Earth, Moon, and Planets*, 72(1-3), pp. 469-474.

Formisano, V., Atreya, S., Encrenaz, T., Ignatiev, N. and Giuranna, M. (2004) 'Detection of methane in the atmosphere of Mars', *Science*, 306(5702), pp. 1758-1761.

Frenklach, M. and Warnatz, J. (1987) 'Detailed Modeling of Pah Profiles in a Sooting Low-Pressure Acetylene Flame', *Combustion Science and Technology*, 51(4-6), pp. 265-283.

Freissinet, C., Glavin, D.P., Mahaffy, P.R., Miller, K.E., Eigenbrode, J.L., Summons, R.E., Brunner, A.E., Buch, A., Szopa, C., Archer, P.D., Franz, H.B., Atreya, S.K., Brinckerhoff, W.B., Cabane, M., Coll, P., Conrad, P.G., Des Marais, D.J., Dworkin, J.P., Fairen, A.G., Francois, P., Grotzinger, J.P., Kashyap, S., ten Kate, I.L., Leshin, L.A., Malespin, C.A., Martin, M.G., Martin-Torres, F.J., McAdam, A.C., Ming, D.W., Navarro-Gonzalez, R., Pavlov, A.A., Prats, B.D., Squyres, S.W., Steele, A., Stern, J.C., Sumner, D.Y., Sutter, B., Zorzano, M.P. and Team, M.S. (2015) 'Organic molecules in the Sheepbed Mudstone, Gale Crater, Mars', *Journal of Geophysical Research-Planets*, 120(3), pp. 495-514.

French, J.E. and Blake, D.F. (2016) 'Discovery of Naturally Etched Fission Tracks and Alpha-Recoil Tracks in Submarine Glasses: Reevaluation of a Putative Biosignature for Earth and Mars', *International Journal of Geophysics*.

Friedmann, E.I. and Weed, R. (1987) 'Microbial Trace-Fossil Formation, Biogenous, and Abiotic Weathering in the Antarctic Cold Desert', *Science*, 236(4802), pp. 703-705.

Fries, M., Christou, A., Archer, D., Conrad, P., Cooke, W., Eigenbrode, J., ten Kate, I.L., Matney, M., Niles, P., Sykes, M., Steele, A. and Treiman, A. (2015) 'A Meteor Shower Origin for Martian Methane.', *Meteoritics and Planetary Science*, 50.

Fristad, K. (2015) Personal communication Kirsten.Fristad@wwu.edu.

Furnes H. and Staudigel H. (1999) 'Biological mediation in ocean crust alteration: how deep is the deep biosphere?', *Earth and Planetary Science Letters*, **166**(3-4), pp. 97-103.

Furnes, H., Muehlenbachs, K., Torsvik, T., Thorseth, I.H. and Tumyr, O. (2001a) 'Microbial fractionation of carbon isotopes in altered basaltic glass from the Atlantic Ocean, Lau Basin and Costa Rica Rift', *Chemical Geology*, 173(4), pp. 313-330.

Furnes, H., Muehlenbachs, K., Tumyr, O., Torsvik, T. and Xenophontos, C. (2001b) 'Biogenic alteration of volcanic glass from the Troodos ophiolite, Cyprus', *Journal of the Geological Society*, 158, pp. 75-82.

G

Gadd, G.M. (2013) 'Geomycology: Fungi as Agents of Biogeochemical Change', *Biology and Environment-Proceedings of the Royal Irish Academy*, 113b(2), pp. 139-153.

Gaillard, F. and Scaillet, B. (2009) 'The sulfur content of volcanic gases on Mars', *Earth and Planetary Science Letters*, 279(1-2), pp. 34-43.

Garrison, B.J.a.P., Z. (2013) 'Molecular dynamics simulations, the theoretical partner to dynamic cluster SIMS experiments', in Vickerman, J.C., and Briggs, D. (ed.) ToF-SIMS: surface analysis by mass spectrometry. *2nd edn. I.M. Publications*.

Geffroy-Rodier, C., Grasset, L., Sternberg, R., Buch, A. and Amblès, A. (2009) 'Thermochemolysis in search for organics in extraterrestrial environments', *Journal of Analytical and Applied Pyrolysis*, 85(1-2), pp. 454-459.

Geminale, A., Formisano, V. and Giuranna, M. (2008) 'Methane in Martian atmosphere: Average spatial, diurnal, and seasonal behaviour', *Planetary and Space Science*, 56(9), pp. 1194-1203.

Glavin, D.P., Malespin, C., ten Kate, I. L., Getty, S. A., Holmes, V. E., Mumm, E., and Mahaffy, P. R. (2012) 'Volatile Analysis by Pyrolysis of Regolith for planetary resource exploration', *In Aerospace Conference,* pp. 1-11.

Glavin, D.P., Freissinet, C., Miller, K.E., Eigenbrode, J.L., Brunner, A.E., Buch, A., Sutter, B., Douglas Archer, P., Atreya, S.K. and Brinckerhoff, W.B. (2013) 'Evidence for perchlorates and the origin of chlorinated hydrocarbons detected by SAM at the Rocknest aeolian deposit in Gale Crater', *Journal of Geophysical Research: Planets*.

Goesmann, F., Raulin, F., Becker, L., Ehrenfreund, R. and Hilchenbach, M. (2007) 'MOMA, the Martian Organic Molecule Analyser; current Developments and Capabilities of a combined GC/MS and LD-MS Instrument".*Geophysical Research Abstracts*.

Goudge, T.A., Head, J.W., Mustard, J.F. and Fassett, C.I. (2012) 'An analysis of open-basin lake deposits on Mars: Evidence for the nature of associated lacustrine deposits and post-lacustrine modification processes', *Icarus*, 219(1), pp. 211-229.

Goulty N.R. (2005). Emplacement mechanism of the Great Whin and Midland Valley dolerite sills. *Journal of the Geological Society* 162(6): 1047-1056.

Graham, D.J. and Castner, D.G., (2012). 'Multivariate analysis of ToF-SIMS data from multicomponent systems: the why, when, and how'. *Biointerphases*, *7*(1), p.49.Graham, L.E., Cook, M.E., Hanson, D.T., Pigg, K.B. and Graham, J.M. (2010a) 'Rolled Liverwort Mats Explain Major *Prototaxites* Features: Response to Commentaries', *American Journal of Botany*, 97(7), pp. 1079-1086.

Graham, L.E., Cook, M.E., Hanson, D.T., Pigg, K.B. and Graham, J.M. (2010b) 'Structural, Physiological, and Stable Carbon Isotopic Evidence That the Enigmatic Paleozoic

Fossil *Prototaxites* Formed from Rolled Liverwort Mats', *American Journal of Botany*, 97(2), pp. 268-275

Grew, E.S. (1974) 'Carbonaceous Material in Some Metamorphic Rocks of New-England and Other Areas', *Journal of Geology*, 82(1), pp. 50-73.

Griffith, J.D., Willcox, S., Powers, D.W., Nelson, R. and Baxter, B.K., (2008). 'Discovery of abundant cellulose microfibers encased in 250 Ma Permian halite: a macromolecular target in the search for life on other planets'. *Astrobiology*, 8(2), pp.215-228.

Grill, L., Dyer, M., Lafferentz, L., Persson, M., Peters, M.V. and Hecht, S., (2007). 'Nano-architectures by covalent assembly of molecular building blocks'. *Nature Nanotechnology*, 2(11), p.687.

Grotzinger, J.P. and Rothman, D.H. (1996) 'An abiotic model for stromatolite morphogenesis', *Nature*, 383(6599), pp. 423-425.

Grotzinger, J.P., Sumner, D.Y., Kah, L.C., Stack, K., Gupta, S., Edgar, L., Rubin, D., Lewis, K., Schieber, J., Mangold, N. and Milliken, R., (2014). A habitable fluvio-lacustrine environment at Yellowknife Bay, Gale Crater, Mars. *Science*, 343(6169), p.1242777.

Grotzinger, J.P., Sumner, D.Y., Kah, L.C., Stack, K., Gupta, S., Edgar, L., Rubin, D., Lewis, K., Schieber, J., Mangold, N., Milliken, R., Conrad, P.G., DesMarais, D., Farmer, J., Siebach, K., Calef, F., Hurowitz, J., McLennan, S.M., Ming, D., Vaniman, D., Crisp, J., Vasavada, A., Edgett, K.S., Malin, M., Blake, D., Gellert, R., Mahaffy, P., Wiens, R.C., Maurice, S., Grant, J.A., Wilson, S., Anderson, R.C., Beegle, L., Arvidson, R., Hallet, B., Sletten, R.S., Rice, M., Bell, J., Griffes, J., Ehlmann, B., Anderson, R.B., Bristow, T.F., Dietrich, W.E., Dromart, G., Eigenbrode, J., Fraeman, A., Hardgrove, C., Herkenhoff, K., Jandura, L., Kocurek, G., Lee, S., Leshin, L.A., Leveille, R., Limonadi, D., Maki, J., McCloskey, S., Meyer, M., Minitti, M., Newsom, H., Oehler, D., Okon, A., Palucis, M., Parker, T., Rowland, S., Schmidt, M., Squyres, S., Steele, A., Stolper, E., Summons, R., Treiman, A., Williams, R., Yingst, A. and Team, M.S. (2014) 'A Habitable Fluvio-Lacustrine Environment at Yellowknife Bay, Gale Crater, Mars', *Science*, 343(6169).

Grotzinger, J.P., Crisp, J.A., Vasavada, A.R. and Team, M.S. (2015) 'Curiosity's Mission of Exploration at Gale Crater, Mars', *Elements*, 11(1), pp. 19-26.

Gupta, N.S., Michels, R., Briggs, D.E.G., Evershed, R.P. and Pancost, R.D. (2006) 'The organic preservation of fossil arthropods: an experimental study', *Proceedings of the Royal Society B-Biological Sciences*, 273(1602), pp. 2777-2783.

H

Halevy, I., Zuber, M.T. and Schrag, D.P. (2007) 'A sulfur dioxide climate feedback on early Mars', *Science*, 318(5858), pp. 1903-1907.

Harrison, K.P. and Grimm, R.E. (2004) 'Tharsis recharge: A source of groundwater for Martian outflow channels', *Geophysical Research Letters*, 31(14).

Harrison, K.R. and Chapman, M.G. (2008) 'Evidence for ponding and catastrophic floods in central Valles Marineris, Mars', *Icarus*, 198(2), pp. 351-364.

Hartmann, W.K.a.N., G. (2001) 'Cratering chronology and the evolution of Mars', in *In Chronology and evolution of Mars*. Springer, Dordrecht, Netherlands: pp. 165-194.

Hartgers, W.A., Damste, J.S.S. and Deleeuw, J.W. (1991) 'Mechanisms of Hydrocarbon Formation during Flash Pyrolysis of Kerogen', *Abstracts of Papers of the American Chemical Society*, 201, pp. 107-FUEL.

Hasegawa, M., Kimata, M. and Kobayashi, S.I. (2001) 'Mechanochemical polymerization of styrene initiated by the grinding of quartz', *Journal of Applied Polymer Science*, 82(11), pp. 2849-2855.

Hasegawa, M., Kimata, M. and Takahashi, I. (2007) 'Mechanochemical polymerization of styrene initiated by the grinding of layered clay minerals', *Advanced Powder Technology*, 18(5), pp. 541-554.

Hausrath E.M., Treiman A.H., Vicenzi E., Bish D.L., Blake D., Sarrazin P., Hoehler T., Midtkandal I., Steele A. and Brantley S.L., (2008). Short-and long-term olivine weathering in Svalbard: implications for Mars. *Astrobiology*, **8**(6), pp.1079-1092.

Hayes, J.M., (1967). Organic constituents of meteorites—a review. *Geochimica et Cosmochimica Acta*, *31*(9), pp.1395-1440.Head, J.W.; Wilson, L. (2011). The Noachian-Hesperian Transition on Mars: Geological Evidence for a Punctuated Phase of Global Volcanism as a Key Driver in Climate and Atmospheric Evolution. 42nd Lunar and Planetary Science Conference (2011), Abstract #1214.

Hecht, M.H., Kounaves, S.P., Quinn, R.C., West, S.J., Young, S.M.M., Ming, D.W., Catling, D.C., Clark, B.C., Boynton, W.V., Hoffman, J., DeFlores, L.P., Gospodinova, K., Kapit, J. and Smith, P.H. (2009) 'Detection of Perchlorate and the Soluble Chemistry of Martian Soil at the Phoenix Lander Site', *Science*, 325(5936), pp. 64-67.

Hedges, S.B., Blair, J.E., Venturi, M.L. and Shoe, J.L., (2004). A molecular timescale of eukaryote evolution and the rise of complex multicellular life. *BMC evolutionary biology*, *4*(1), p.2.

Heiken, G. (1972). Morphology and petrography of volcanic ashes. *Geological Society of America Bulletin*, *83*(7), pp.1961-1988.

Helz, R. T. D. A. Clague, T. W. Sisson, and C. R. Thornber, in *Characteristics of Hawaiian Volcanoes,* Eds: M. P. Poland, T. J. Takahashi, and C. M. Landowski, (u.S. Geological Survey Professional Paper 1801, US, 2014), Chapter 6.

Henning, T. and Salama, F. (1998) 'Carbon-Carbon in the Universe', *Science*, 282(5397), pp. 2204-2210.

Herrera, A., Cockell, C. S., Self, S., Blaxter, M., Reitner, J., Thorsteinsson, T.,and Tindle, A. (2009) 'A cryptoendolithic community in volcanic glass', *Astrobiology*, 9(4), pp. 369-381.

Hickenboth, C.R., Moore, J.S., White, S.R., Sottos, N.R., Baudry, J. and Wilson, S.R. (2007) 'Biasing reaction pathways with mechanical force', *Nature*, 446(7134), pp. 423-427.

Hiebert, F.K. and Bennett, P.C., (1992). Microbial control of silicate weathering in organic-rich groundwater. *Science*, *258*(5080), pp.278-281.

Hiscox, J.A. (1999) 'An overview of the origin of life: the case for biological prospecting on Mars', *Earth, Moon, and Planets*, 87(3), pp. 191-212.

Hobley, D.E.J., Howard, A.D. and Moore, J.M. (2014) 'Fresh shallow valleys in the Martian mid-latitudes as features formed by meltwater flow beneath ice', *Journal of Geophysical Research-Planets*, 119(1), pp. 128-153.

Hoehler, T.M., Amend, J.P. and Shock, E.L. (2007) 'A "follow the energy" approach for astrobiology', *Astrobiology*, 7(6), pp. 819-23.

Hofmann, B.A. (2007) 'Morphological Biosignatures from Subsurface Environments: Recognition on Planetary Missions', *Space Science Reviews*, 135(1-4), pp. 245-254.

Hoke, M.R.T., Hynek, B.M. and Tucker, G.E. (2011) 'Formation timescales of large Martian valley networks', *Earth and Planetary Science Letters*, 312(1-2), pp. 1-12.

Holm, N.G. and Charlou, J.L. (2001) 'Initial indications of abiotic formation of hydrocarbons in the Rainbow ultramafic hydrothermal system, Mid-Atlantic Ridge', *Earth and Planetary Science Letters*, 191(1-2), pp. 1-8.

Horita, J. and Berndt, M.E. (1999) 'Abiogenic methane formation and isotopic fractionation under hydrothermal conditions', *Science*, 285(5430), pp. 1055-1057.

Horowitz, N.H., Hubbard, J.S. and Hobby, G.L. (1972) 'The carbon-assimilation experiment: the Viking Mars lander.', *Icarus*, 16(1), pp. 147-152.

Horowitz, N.H., Hobby, G.L. and Hubbard, J.S. (1977) 'Viking on Mars: the carbon assimilation experiments', *Journal of Geophysical Research*, 82(28), pp. 4659-4662.

Houtkooper, J.M. and Schulze-Makuch, D. (2007) 'A possible biogenic origin for hydrogen peroxide on Mars: the Viking results reinterpreted', *International Journal of Astrobiology*, 6(2), pp. 147-152.

Howard, A.D., Moore, J.M. and Irwin, R.P. (2005) 'An intense terminal epoch of widespread fluvial activity on early Mars: 1. Valley network incision and associated deposits', *Journal of Geophysical Research-Planets*, 110(E12).

Hubbard, G.S., Naderi, F.M. and Garvin, J.B. (2002) 'Following the water, the new program for Mars exploration', *Acta Astronautica*, 51(1-9), pp. 337-350.

Hueber, F.M. (2001) 'Rotted wood-alga-fungus: the history and life of *Prototaxites* Dawson 1859', *Review of Palaeobotany and Palynology*, 116(1-2), pp. 123-158.

Hugenholtz, C.H. (2008). Frosted granular flow: A new hypothesis for mass wasting in Martian gullies. *Icarus*, *197*(1), pp.65-72.

Hyde, K.D., Jones, E.B.G., Leano, E., Pointing, S.B., Poonyth, A.D. and Vrijmoed, L.L.P. (1998) 'Role of fungi in marine ecosystems', *Biodiversity and Conservation*, 7(9), pp. 1147-1161.

Hynek, B.M., Osterloo, M.K. and Kierein-Young, K.S. (2015) 'Late-stage formation of Martian chloride salts through ponding and evaporation', *Geology*, 43(9), pp. 787-790.

I

Irwin, L.N. and Schulze-Makuch, D. (2002) 'Origin and evolution of life on other worlds: Lessons from the history of life on Earth', *Proceedings of the Second European Workshop on Exo-Astrobiology*, 518, pp. 463-464.

Irwin, R.P., Howard, A.D., Craddock, R.A. and Moore, J.M. (2005) 'An intense terminal epoch of widespread fluvial activity on early Mars: 2. Increased runoff and paleolake development', *Journal of Geophysical Research-Planets*, 110(E12).

Irwin, R.P., Tanaka, K.L., and Robbins, S.J., (2013), 'Distribution of Early, Middle, and Late Noachian cratered surfaces in the Martian highlands: Implications for resurfacing events and processes' *Journal of Geophysical Research*, 118, p. 278–291.

Ivarsson, M., Broman, C., Holmstrom, S.J.M., Ahlbom, M., Lindblom, S. and Holm, N.G. (2011) 'Putative Fossilized Fungi from the Lithified Volcanishardic Apron of Gran Canaria, Spain', *Astrobiology*, 11(7), pp. 633-650.

Ivarsson, M. (2012) 'Subseafloor basalts as fungal habitats', *Biogeosciences*, 9(9), pp. 3625-3635.

Ivarsson, M., Bengtson, S., and Neubeck, A. (2016). The igneous oceanic crust–Earth's largest fungal habitat?. *Fungal Ecology*, *20*, 249-255.

Ivarsson, M., Bengtson, S., Belivanova, V., Stampanoni, M., Marone, F. and Tehler, A. (2012a) 'Fossilized fungi in subseafloor Eocene basalts', *Geology*, 40(2), pp. 163-166.

Ivarsson, M., Broman, C., Sturkell, E., Ormo, J., Siljestrom, S., van Zuilen, M. and Bengtson, S. (2013a) 'Fungal colonization of an Ordovician impact-induced hydrothermal system', *Scientific Reports*, 3.

Ivarsson, M., Bengtson, S., Skogby, H., Belivanova, V. and Marone, F. (2013b) 'Fungal colonies in open fractures of subseafloor basalt', *Geo-Marine Letters*, 33(4), pp. 233-243.

Ivarsson, M., Bengtson, S., Skogby, H., Lazor, P., Broman, C., Belivanova, V. and Marone, F. (2015a) 'A Fungal-Prokaryotic Consortium at the Basalt-Zeolite Interface in Subseafloor Igneous Crust', *Plos One*, 10(10).

Ivarsson, M., Peckmann, J., Tehler, A., Broman, C., Bach, W., Behrens, K., Reitner, J., Bottcher, M.E. and Ivarsson, L.N. (2015b) 'Zygomycetes in Vesicular Basanites from

Vesteris Seamount, Greenland Basin - A New Type of Cryptoendolithic Fungi', *Plos One*, 10(7).

Izawa, M.R.M., Banerjee, N.R., Flemming, R.L., Bridge, N.J. and Schultz, C. (2010) 'Basaltic glass as a habitat for microbial life: Implications for astrobiology and planetary exploration', *Planetary and Space Science*, 58(4), pp. 583-591.

J

Jakobsen, H.J., Song, L., Gan, Z., Hung, I., Bildsøe, H., Skibsted, J., Bak, E.N., Finster, K., Nørnberg, P. and Jensen, S.J.K., (2016). NMR and EPR Studies of Free-Radical Intermediates from Experiments Mimicking the Winds on Mars: A Sink for Methane and Other Gases. *The Journal of Physical Chemistry C*, *120*(45), pp.26138-26149.

Jakosky, B.M., Henderson, B.G. and Mellon, M.T., (1995). Chaotic obliquity and the nature of the Martian climate. *Journal of Geophysical Research: Planets*, 100(E1), pp.1579-1584.

Jakosky, B.M. and Shock, E.L. (1998) 'The biological potential of Mars, the early Earth, and Europa', *Journal of Geophysical Research-Planets*, 103(E8), pp. 19359-19364.

Jakosky, B.M., Grebowsky, J.M., Luhmann, J.G., Connerney, J., Eparvier, F., Ergun, R., Halekas, J., Larson, D., Mahaffy, P., McFadden, J., Mitchell, D.F., Schneider, N., Zurek, R., Bougher, S., Brain, D., Ma, Y.J., Mazelle, C., Andersson, L., Andrews, D., Baird, D., Baker, D., Bell, J.M., Benna, M., Chaffin, M., Chamberlin, P., Chaufray, Y.Y., Clarke, J., Collinson, G., Combi, M., Crary, F., Cravens, T., Crismani, M., Curry, S., Curtis, D., Deighan, J., Delory, G., Dewey, R., DiBraccio, G., Dong, C., Dong, Y., Dunn, P., Elrod, M., England, S., Eriksson, A., Espley, J., Evans, S., Fang, X., Fillingim, M., Fortier, K., Fowler, C.M., Fox, J., Groller, H., Guzewich, S., Hara, T., Harada, Y., Holsclaw, G., Jain, S.K., Jolitz, R., Leblanc, F., Lee, C.O., Lee, Y., Lefevre, F., Lillis, R., Livi, R., Lo, D., Mayyasi, M., McClintock, W., McEnulty, T., Modolo, R., Montmessin, F., Morooka, M., Nagy, A., Olsen, K., Peterson, W., Rahmati, A., Ruhunusiri, S., Russell, C.T., Sakai, S., Sauvaud, J.A., Seki, K., Steckiewicz, M., Stevens, M., Stewart, A.I.F., Stiepen, A., Stone, S., Tenishev, V., Thiemann, E., Tolson, R., Toublanc, D., Vogt, M., Weber, T.,

Withers, P., Woods, T. and Yelle, R. (2015) 'MAVEN observations of the response of Mars to an interplanetary coronal mass ejection', *Science*, 350(6261).

James, A.T.and.Martin., A.J.P. (1952) 'Gas-liquid partition chromatography: the separation and micro-estimation of volatile fatty acids from formic acid to dodecanoic acid', *Biochemical Journal*, 50(5).

Jensen, S.J.K., Skibsted, J., Jakobsen, H.J., ten Kate, I.L., Guimlaugsson, H.P., Merrison, J.P., Finster, K., Bak, E., Iversen, J.J., Kondrup, J.C. and Nornberg, P. (2014) 'A sink for methane on Mars? The answer is blowing in the wind', *Icarus*, 236, pp. 24-27.

Jepsen, S.M., Priscu, J.C., Grimm, R.E. and Bullock, M.A. (2007) 'The potential for lithoautotrophic life on Mars: application to shallow interfacial water environments', *Astrobiology*, 7(2), pp. 342-54.

Jerolmack, D.J. (2013) 'Pebbles on Mars', *Science*, 340(6136), pp. 1055-1056.

Johnson, F.S. (1965). 'Atmosphere of Mars. *Science'*, *150*(3702), pp.1445-1448.

Johnson, K., Purvis, G., Lopez-Capel, E., Peacock, C., Gray, N., Wagner, T., März, C., Bowen, L., Ojeda, J., Finlay, N. and Robertson, S., (2015). 'Towards a mechanistic understanding of carbon stabilization in manganese oxides'. *Nature communications*, *6*.

Johnson, P.V., Beegle, L. W., and Kanik, I. (2012) 'Chapter 17 Mass Spectrometry in Solar System Exploratio' 7th edn. *New Jersey: John Wiley and Sons.*

K

Kaal, E., de Koning, S., Brudin, S. and Janssen, H.G. (2008) 'Fully automated system for the gas chromatographic characterization of polar biopolymers based on thermally assisted hydrolysis and methylation', *Journal of Chromatography A*, 1201(2), pp. 169-175.

Kasting, J.F. (1993). 'Earth's early atmosphere' *Science*, *259*(5097), pp.920-926.

Kayser, S. D. Rading, R. Moellers, F. Kollmer, and E. Niehuis (2013) 'Surface spectrometry using large argon clusters' *Surface Interface and Analysis*. **45**, 131

Kelley, D.S., Karson, J.A., Fruh-Green, G.L., Yoerger, D.R., Shank, T.M., Butterfield, D.A., Hayes, J.M., Schrenk, M.O., Olson, E.J., Proskurowski, G., Jakuba, M., Bradley, A., Larson, B., Ludwig, K., Glickson, D., Buckman, K., Bradley, A.S., Brazelton, W.J., Roe,

277

K., Elend, M.J., Delacour, A., Bernasconi, S.M., Lilley, M.D., Baross, J.A., Summons, R.T. and Sylva, S.P. (2005) 'A serpentinite-hosted ecosystem: The lost city hydrothermal field', *Science*, 307(5714), pp. 1428-1434.

Kelly, L.C., Cockell, C.S., Piceno, Y.M., Andersen, G.L., Thorsteinsson, T. and Marteinsson, V. (2010) 'Bacterial diversity of weathered terrestrial Icelandic volcanic glasses', *Microbial Ecology*, 60(4), pp. 740-52.

Kelly, L.C., Cockell, C.S., Herrera-Belaroussi, A., Piceno, Y., Andersen, G., DeSantis, T., Brodie, E., Thorsteinsson, T., Marteinsson, V., Poly, F. and LeRoux, X. (2011) 'Bacterial diversity of terrestrial crystalline volcanic rocks, Iceland', *Microbial Ecology*, 62(1), pp. 69-79.

Keppler, F., Vigano, I., McLeod, A., Ott, u., Fruchtl, M. and Rockmann, T. (2012) 'Ultraviolet-radiation-induced methane emissions from meteorites and the Martian atmosphere', *Nature*, 486(7401), pp. 93-96.

Kerridge, J.F. (1983) 'Isotopic Composition of Carbonaceous-Chondrite Kerogen - Evidence for an Interstellar Origin of Organic-Matter in Meteorites', *Earth and Planetary Science Letters*, 64(2), pp. 186-200.

Kerridge, J.F., Chang, S. and Shipp, R. (1987) 'Isotopic Characterization of Kerogen-Like Material in the Murchison Carbonaceous Chondrite', *Geochimica Et Cosmochimica Acta*, 51(9), pp. 2527-2540.

Keske, A.L., Hamilton, C.W., McEwen, A.S. and Daubar, I.J. (2015) 'Episodes of fluvial and volcanic activity in Mangala Valles, Mars', *Icarus*, 245, pp. 333-347.

Killops, S.D., and Killops, V. J. (2013) *'Introduction to organic geochemistry'* John Wiley and Sons ltd, Cirencester.

Kim, C.D., Min, B.K. and Jung, W.S. (2009) 'Preparation of graphene sheets by the reduction of carbon monoxide', *Carbon*, 47(6), pp. 1610-1612.

Kite, E.S., Sneed, J., Mayer, D.P. and Wilson, S.A. (2017) 'Persistent or repeated surface habitability on Mars during the Late Hesperian-Amazonian', *Geophysical Research Letters*.

Kitson, F.G., Larsen, B.S. and McEwen, C.N., (1996). *Gas chromatography and mass spectrometry: a practical guide*. Academic Press Ltd, London.

Klein, H.P. (1978) 'The Viking biological experiments on Mars', *Icarus*, 34(3), pp. 666-674.

278

Klein, H.P. (1991) 'The Viking Biology Experiments - Epilogue and Prologue', *Origins of Life and Evolution of the Biosphere*, 21(4), pp. 255-261.

Kobayashi, K. and Ponnamperuma, C., 1985. 'Trace elements in chemical evolution' *Origins of Life and Evolution of the Biosphere*, *16*(1), pp.41-55.

Kounaves, S.P., Carrier, B.L., O'Neil, G.D., Stroble, S.T. and Claire, M.W. (2014) 'Evidence of martian perchlorate, chlorate, and nitrate in Mars meteorite EETA79001: Implications for oxidants and organics', *Icarus*, 229, pp. 206-213.

Krasnopolsky, V.A. and Parshev, V.A. (1981) 'Chemical-Composition of the Atmosphere of Venus', *Nature*, 292(5824), pp. 610-613.

Krasnopolsky, V.A., Maillard, J.P. and Owen, T.C. (2004) 'Detection of methane in the martian atmosphere: evidence for life?', *Icarus*, 172(2), pp. 537-547.

Kuila, u., Berend, I. and Prasad, M. (2013) 'Specific surface area and pore-size distribution in clays and shales (', *Geophysical Prospecting*, 61(2), pp.341-362.

L

Lakdawalla E. (2013) www.planetary.org/blogs/emily-lakdawalla/2013/10251246-noachian-hesperian-amazonian.html.Accessed 17th October 2017

Lammer, H., Kasting, J.F., Chassefiere, E., Johnson, R.E., Kulikov, Y.N. and Tian, F. (2008) 'Atmospheric Escape and Evolution of Terrestrial Planets and Satellites', *Space Science Reviews*, 139(1-4), pp. 399-436.

Landais, P., Michels, R. and Elie, M. (1994). 'Are time and temperature the only constraints to the simulation of organic matter maturation?' *Organic Geochemistry*, *22*(3-5), pp.617-630.

Lazcano, A. (2007) 'Towards a Definition of Life: The Impossible Quest?', *Space Science Reviews*, 135(1-4), pp. 5-10.

Leco Corporation, Instruction Manual CS 230 BS7755, Section 3.8, 1995; ISO 10694, 1995; Soil Quality, Part 3, Chemical Methods, Section 3.8, Determination of organic carbon and total carbon after dry combustion (elementary analysis) retrieved from uk.leco-europe.com/analytical-elemental-analysis-page/approved-methods/ August 2016.

Lefevre, F. and Forget, F. (2009) Observed variations of methane on Mars unexplained by known atmospheric chemistry and physics. Nature 460:720–723.

Leray, C. *Introduction to Lipidomics: From Bacteria to Man*, (CRC Press, Florida, US, 2013), Chapter 1.

Lever, M.A. (2013a) 'Functional gene surveys from ocean drilling expeditions a review and perspective', *Fems Microbiology Ecology*, 84(1), pp. 1-23.

Lever, M.A., Rouxel, O., Alt, J.C., Shimizu, N., Ono, S.H., Coggon, R.M., Shanks, W.C., Lapham, L., Elvert, M., Prieto-Mollar, X., Hinrichs, K.u., Inagaki, F. and Teske, A. (2013b) 'Evidence for Microbial Carbon and Sulfur Cycling in Deeply Buried Ridge Flank Basalt', *Science*, 339(6125), pp. 1305-1308.

Levin, G.V. (1972) 'Detection of metabolically produced labelled gas: The Viking Mars Lander', *Icarus*, 16(1), pp. 153-166.

Levin, G.V. and Straat, P.A. (1979) 'Laboratory Simulations of the Viking Labeled Release Experiment - Kinetics Following 2nd Nutrient Injection and the Nature of the Gaseous End Product', *Journal of Molecular Evolution*, 14(1-3), pp. 185-197.

Levin, G.V. (2007) 'The revival of life on Mars'. Invited paper. SPIE -*The International Society for Optical Engineering.* pp6694

Lewis, J.M.T., Watson, J.S., Najorka, J., Luong, D. and Sephton, M.A. (2015) 'Sulfate Minerals: A Problem for the Detection of Organic Compounds on Mars?', *Astrobiology*, 15(3), pp. 247-258.

Lewis, K.W., Aharonson, O., Grotzinger, J.P., Kirk, R.L., McEwen, A.S. and Suer, T.A., (2008). Quasi-periodic bedding in the sedimentary rock record of Mars. *science*, *322*(5907), pp.1532-1535.

Lewis, N.G. and Yamamoto, E. (1990) 'Lignin - Occurrence, Biogenesis and Biodegradation', *Annual Review of Plant Physiology and Plant Molecular Biology*, 41, pp. 455-496.

Lillis, R.J., Robbins, S., Manga, M., Halekas, J.S. and Frey, H.V. (2013) 'Time history of the Martian dynamo from crater magnetic field analysis', *Journal of Geophysical Research-Planets*, 118(7), pp. 1488-1511.

Lim, D.S., and Cockell, C. S. (2002) 'Paleolimnology in the High Arctic-implications for the exploration of Mars.', *International Journal of Astrobiology*, 1(04), pp. 381-386.

Liss D., Owens W.H. and Hutton D.H.W. (2004) 'New palaeomagnetic results from the Whin Sill complex: evidence for a multiple intrusion event and revised virtual geomagnetic

poles for the late Carboniferous for the British Isles', *Journal of the Geological Society*, 161, pp. 927-938.

Lovley, Derek R., and Phillips, E. (1988) 'Novel mode of microbial energy metabolism: organic carbon oxidation coupled to dissimilatory reduction of iron or manganese' *Applied and environmental microbiology* 54, no. 6 1472-1480.

Lovley, D.R. and Chapelle, F.H. (1995) 'Deep subsurface microbial processes', *Reviews Of Geophysics-Richmond Virginia Then Washington-*, 33, pp. 365-365.

Lovley, D.R., Holmes, D.E. and Nevin, K.P. (2004) 'Dissimilatory Fe(III) and Mn(IV) reduction', *Advances in Microbial Physiology, Vol. 49*, 49, pp. 219-286.

Lowe, D.R. and Tice, M.M. (2007) 'Tectonic controls on atmospheric, climatic, and biological evolution 3.5-2.4 Ga', *Precambrian Research*, 158(3-4), pp. 177-197.

Lubert, S., John, L.T. and Jeremy, M.B. (2015) *Biochemistry*. W H Freeman, New York 5th edn.

Lundin, R., Lammer, H. and Ribas, I. (2007) 'Planetary Magnetic Fields and Solar Forcing: Implications for Atmospheric Evolution', *Space Science Reviews*, 129(1-3), pp. 245-278.

M

Madden, M.E.E., Bodnar, R.J. and Rimstidt, J.D. (2004) 'Jarosite as an indicator of water-limited chemical weathering on Mars', *Nature*, 431(7010), pp. 821-823.

Madigan, M.T., Martinko, J.M., Dunlap, P.V. and Clark, D.P. (2008) '*Brock Biology of microorganisms'*. **Pearson Prentice Hall, Inc** 12th edn.

Mahaffy, P. (2008) 'Exploration of the habitability of Mars: Development of analytical protocols for measurement of organic carbon on the 2009 Mars science laboratory', *Space Science Reviews*, 135(1-4), pp. 255-268.

Mahoney, J.J., Storey, M., Duncan, R. A., Spencer, K. J., and Pringle, M. (1993) 'Geochemistry and age of the Ontong Java Plateau.', *The Mesozoic Pacific: Geology, Tectonics, and Volcanism, Geophysical Monogram. Series*, 77, pp. 233-261.

Mahoney, J.J., Fitton, J.G. and Wallace, J., (2001) 'Leg 192 Summary', *Shipboard Scientific Party, In Proceedings of the Ocean Drilling Program, Initial Reports* 192, pp. 1-75.

Mahoney C. M. (2010). 'Cluster secondary ion mass spectrometry of polymers and related materials'. *Mass spectrometry reviews*, 29(2), 247-293.

Miller, D.J., Biesinger, M.C. and McIntyre, N.S. (2002) 'Interactions of CO_2 and CO at fractional atmosphere pressures with iron and iron oxide surfaces: one possible mechanism for surface contamination?', *Surface and Interface Analysis*, 33(4), pp. 299-305.

Mangold, N., Adeli, S., Conway, S., Ansan, V. and Langlais, B. (2012) 'A chronology of early Mars climatic evolution from impact crater degradation', *Journal of Geophysical Research-Planets*, 117.

Mangolini, F., McClimon, J.B., Rose, F. and Carpick, R.W. (2014) 'Accounting for Nanometer-Thick Adventitious Carbon Contamination in X-ray Absorption Spectra of Carbon-Based Materials', *Analytical Chemistry*, 86(24), pp. 12258-12265.

Marbot, R., (1997). 'The selection of pyrolysis temperatures for the analysis of humic substances and related materials 1. Cellulose and chitin'. *Journal of analytical and applied pyrolysis*, *39*(2), pp.97-104.

Marlow, J.J., Martins, Z. and Sephton, M.A. (2008) 'Mars on Earth: Soil analogues for future Mars missions', *Astronomy and Geophysics*, 49(2), pp. 20-23.

Marshall, C.P., Love, G.D., Snape, C.E., Hill, A.C., Allwood, A.C., Walter, M.R., Van Kranendonk, M.J., Bowden, S.A., Sylva, S.P. and Summons, R.E. (2007) 'Structural characterization of kerogen in 3.4Ga Archaean cherts from the Pilbara Craton, Western Australia', *Precambrian Research*, 155(1-2), pp. 1-23.

Marshall, R.R. (1961) 'Devitrification of natural glass', *Geological Society of America Bulletin*, 72(10), pp. 1493-1520.

Martel, J., Young, D., Peng, H.H., Wu, C.Y. and Young, J.D. (2012) 'Biomimetic Properties of Minerals and the Search for Life in the Martian Meteorite ALH84001', *Annual Review of Earth and Planetary Sciences, Vol 40*, 40, pp. 167-193.

Martin, W. and Russell, M.J. (2007) 'On the origin of biochemistry at an alkaline hydrothermal vent', *Philosophical Transactions of the Royal Society B-Biological Sciences*, 362(1486), pp. 1887-1925.

Martins, Z., Botta, O., Fogel, M.L., Sephton, M.A., Glavin, D.P., Watson, J.S., Dworkin, J.P., Schwartz, A.W. and Ehrenfreund, P., (2008). Extraterrestrial nucleobases in the Murchison meteorite. Earth and planetary science Letters, 270(1-2), pp.130-136.

Martin-Torres, F.J., Zorzano, M.P., Valentin-Serrano, P., Harri, A.M., Genzer, M., Kemppinen, O., Rivera-Valentin, E.G., Jun, I., Wray, J., Madsen, M.B., Goetz, W., McEwen, A.S., Hardgrove, C., Renno, N., Chevrier, V.F., Mischna, M., Navarro-Gonzalez, R., Martinez-Frias, J., Conrad, P., McConnochie, T., Cockell, C., Berger, G., Vasavada, A.R., Sumner, D. and Vaniman, D. (2015) 'Transient liquid water and water activity at Gale crater on Mars', *Nature Geoscience*, 8(5), pp. 357-361.

Mason S.L., Filley, T.R. and Abbott G.D. (2009). 'The effect of afforestation on the soil organic carbon (SOC) of a peaty gley soil using on-line thermally assisted hydrolysis and methylation (THM) in the presence of ^{13}C-labelled tetramethylammonium hydroxide (TMAH)' *Journal of Analytical and Applied Pyrolysis,* **85**(1), 417-425.

Mason, O.u., Stingl, u., Wilhelm, L.J., Moeseneder, M.M., Di Meo-Savoie, C.A., Fisk, M.R. and Giovannoni, S.J. (2007) 'The phylogeny of endolithic microbes associated with marine basalts', *Environ Microbiol*, 9(10), pp. 2539-50.

Mathez, E.A. (1987) 'Carbonaceous Matter in Mantle Xenoliths - Composition and Relevance to the Isotopes', *Geochimica Et Cosmochimica Acta*, 51(9), pp. 2339-2347.

Mattey, D.P., Carr, R.H., Wright, I.P. and Pillinger, C.T. (1984) 'Carbon Isotopes in Submarine Basalts', *Earth and Planetary Science Letters*, 70(2), pp. 196-206.

Mattingly, R. S. Matousek, and F. Jordan, (2004), Aerospace. ConferenceProceedingd. 1, 477.

Mayer, L.M. (2004) 'The inertness of being organic', *Marine Chemistry*, 92(1-4), pp. 135-140.

McBride N. and Gilmour I. (2004), Chapter 2, *An introduction to the solar system*. Cambridge University Press, Cambridge.

McCollom, T.M., Ritter, G. and Simoneit, B.R., (1999). Lipid synthesis under hydrothermal conditions by Fischer-Tropsch-type reactions. *Origins of Life and Evolution of the Biosphere*, *29*(2), pp.153-166.

McCollom, T.M. (2003) 'Formation of meteorite hydrocarbons from thermal decomposition of siderite (FeCO$_3$)', *Geochimica Et Cosmochimica Acta*, 67(2), pp. 311-317.

McCollom, T.M. and Seewald, J.S. (2006) 'Carbon isotope composition of organic compounds produced by abiotic synthesis under hydrothermal conditions', *Earth and Planetary Science Letters*, 243(1-2), pp. 74-84.

McCollom, T.M. and Seewald, J.S. (2007) 'Abiotic synthesis of organic compounds in deep-sea hydrothermal environments', *Chemical Reviews*, 107(2), pp. 382-401.

McCollom, T.M. (2013) 'Laboratory Simulations of Abiotic Hydrocarbon Formation in Earth's Deep Subsurface', *Carbon in Earth*, 75, pp. 467-494.

McCown, R., Gross, F.B. and Calle, C.I. (2005) 'Comparison of two particle charging experiments for testing the JSC Mars-1 Martian regolith simulant against man-made materials', *Ieee Transactions on Dielectrics and Electrical Insulation*, 12(4), pp. 821-826.

McEwen, A.S., Malin, M.C., Carr, M.H. and Hartmann, W.K. (1999) 'Voluminous volcanism on early Mars revealed in Valles Marineris', *Nature*, 397(6720), pp. 584-586.

McKay, D.S., Gibson, E.K., ThomasKeprta, K.L., Vali, H., Romanek, C.S., Clemett, S.J., Chillier, X.D.F., Maechling, C.R. and Zare, R.N. (1996) 'Search for past life on Mars: Possible relic biogenic activity in Martian meteorite ALH84001', *Science*, 273(5277), pp. 924-930.

McKay, C.P., Friedmann, E.I., Frankel, R.B. and Bazylinski, D.A. (2003) 'Magnetotactic bacteria on Earth and on Mars', *Astrobiology*, 3(2), pp. 263-270.

McKay, C. (2010) 'The Eerie Silence: Renewing Our Search for Alien Intelligence/Are We Alone In The Universe?', *Nature*, 464(7285), pp. 34-34.

McKeown, N.K., Bishop, J.L., Noe Dobrea, E.Z., Ehlmann, B.L., Parente, M., Mustard, J.F., Murchie, S.L., Swayze, G.A., Bibring, J.-P. and Silver, E.A. (2009) 'Characterization of phyllosilicates observed in the central Mawrth Vallis region, Mars, their potential formational processes, and implications for past climate', *Journal of Geophysical Research*, 114.

McKinley, J.P., Stevens, T.O. and Westall, F. (2000) 'Microfossils and paleoenvironments in deep subsurface basalt samples', *Geomicrobiology Journal*, 17(1), pp. 43-54.

McLoughlin, N., Brasier, M.D., Wacey, D., Green, O.R. and Perry, R.S. (2007) 'On biogenicity criteria for endolithic microborings on early Earth and beyond', *Astrobiology*, 7(1), pp. 10-26.

Mcloughlin, N., Staudigel, H., Furnes, H., Eickmann, B. and Ivarsson, M. (2010) 'Mechanisms of microtunneling in rock substrates: distinguishing endolithic biosignatures from abiotic microtunnels', *Geobiology*, 8(4), pp. 245-255.

McMahon, S. (2013) 'Deep Biospheres On Earth, Mars And Beyond', in *ESA Special Publication*. p. 32.

McMahon, S., Parnell, J., Ponicka, J., Hole, M. and Boyce, A., (2013). 'The habitability of vesicles in Martian basalt'. *Astronomy & Geophysics*, *54*(1), pp.1-17.

Méndez, J., López, M.F. and Martín-Gago, J.A., (2011). 'On-surface synthesis of cyclic organic molecules'. *Chemical Society Reviews*, *40*(9), pp.4578-4590.

Meinert, C., de Marcellus, P., d'Hendecourt, L.L., Nahon, L., Jones, N.C., Hoffmann, S.V., Bredehoft, J.H. and Meierhenrich, u.J. (2011) 'Photochirogenesis: Photochemical models on the absolute asymmetric formation of amino acids in interstellar space', *Physics of Life Reviews*, 8(3), pp. 307-330.

Melosh, H.J. and Vickery, A.M. (1989) 'Impact Erosion of the Primordial Atmosphere of Mars', *Nature*, 338(6215), pp. 487-489.

Merino, P., Svec, M., Martinez, J.I., Jelinek, P., Lacovig, P., Dalmiglio, M., Lizzit, S., Soukiassian, P., Cernicharo, J. and Martin-Gago, J.A. (2014) 'Graphene etching on SiC grains as a path to interstellar polycyclic aromatic hydrocarbons formation', *Nature Communications*, 5.

Meyer-Berthaud, B., Scheckler, S.E. and Wendt, J., (1999). Archaeopteris is the earliest known modern tree. *Nature*, *398*(6729), p.700.

Michael, J. P. (2007). 'Indolizidines and quinolizidines: natural products and beyond'.*Beilstein Journal of Organic Chemistry* . 3, No.27

Mickol, R.L., and T. A. Kral. (2016) 'Low-Pressure Tolerance by Methanogens in an Aqueous Environment: Implications for Subsurface Life on Mars', *Origins of Life and Evolution of Biospheres*, pp. 1-22.

Millar, T.J. (2004) 'Organic molecules in the interstellar medium', *Astrobiology: Future Perspectives*, 305, pp. 17-31.

Miller, D.J., Biesinger, M.C. and McIntyre, N.S. (2002) 'Interactions of CO_2 and CO at fractional atmosphere pressures with iron and iron oxide surfaces: one possible

mechanism for surface contamination?', *Surface and Interface Analysis*, 33(4), pp. 299-305.

Miller, K.E., Eigenbrode, J.L., Freissinet, C., Glavin, D.P., Kotrc, B., Francois, P. and Summons, R.E. (2016) 'Potential precursor compounds for chlorohydrocarbons detected in Gale Crater, Mars, by the SAM instrument suite on the Curiosity Rover', *Journal of Geophysical Research-Planets*, 121(3), pp. 296-308.

Miller, S.L. (1953). A production of amino acids under possible primitive Earth conditions. *Science*, *117*(3046), pp.528-529.

Milliken, R.E., Mustard, J.F. and Goldsby, D.L. (2003) 'Viscous flow features on the surface of Mars: Observations from high-resolution Mars Orbiter Camera (MOC) images', *Journal of Geophysical Research-Planets*, 108(E6).

Milliken, R.E. and Bish, D.L. (2010) 'Sources and sinks of clay minerals on Mars', *Philosophical Magazine*, 90(17-18), pp. 2293-2308.

Ming, D.W., H. V. Lauer, P. D. Archer, B. Sutter, D. C. Golden, R. V. Morris, P. B. Niles, and W. V. Boynton. (2009) *In Lunar and Planetary Science Conference*.

Miot, J., Benzerara, K., Banerjee, N.R., Menguy, N., Tyliszczak, T., Brown, G.E. and Guyot, F. (2007) 'Study at the nanoscale of the alteration of submarine basaltic glass from the Ontong Java Plateau', *Geochimica Et Cosmochimica Acta*, 71(15), pp. A671-A671.

Miyayama, T., Sanada, N., Bryan, S.R., Hammond, J.S. and Suzuki, M. (2010) 'Removal of Ar$^+$ beam-induced damaged layers from polyimide surfaces with argon gas cluster ion beams', *Surface and Interface Analysis*, 42(9), pp. 1453-1457.

Mojzsis, S.J., Arrhenius, G., McKeegan, K.D., Harrison, T.M., Nutman, A.P. and Friend, C.R.L. (1996) 'Evidence for life on Earth before 3,800 million years ago', *Nature*, 384(6604), pp. 55-59.

Moldoveanu, S.C. (1998) *Analytical Pyrolysis of Natural Organic Polymers*. Elsevier SA, Amsterdam, Netherlands.

Molina-Cuberos, G.J., Stumptner, W., Lammer, H. and Komle, N.I. (2001) 'Cosmic ray and UV radiation models on the ancient Martian surface', *Icarus*, 154(1), pp. 216-222.

Monthioux, M. and Landais, P. (1989) 'Natural and Artificial Maturation of Coal - Non-Hopanoid Biomarkers', *Chemical Geology*, 77(1), pp. 71-85.

Moran, M. A., Pomeroy, L. R., Sheppard, E. S., Atkinson, L. P., and Hodson, R. E. (1991). Distribution of terrestrially derived dissolved organic matter on the southeastern US continental shelf. *Limnology and Oceanography*, *36*(6), 1134-1149.

Morisson, M.A.Buch., A and Szopa, C and Raulin, F and Stambouli, M (2017) 'TMAH Thermochemolysis of a Martian Regolith Simulant: Optimization of an Analytical Method for the Detection of Trace Organic Matter by the MOMA-Pyr-GC/MS Experiment Onboard the ExoMars-2020 Rover', *Lunar and Planetary Science XLVIII*. Heterocycles. Available at: https://www.hou.usra.edu/meetings/lpsc2017/pdf/1079.pdf.

Mumma, M.J., Villanueva, G.L., Novak, R.E., Hewagama, T., Bonev, B.P., DiSanti, M.A., Mandell, A.M. and Smith, M.D. (2009) 'Strong Release of Methane on Mars in Northern Summer 2003', *Science*, 323(5917), pp. 1041-1045.

Muntener, O. (2010) 'Serpentine and serpentinization: A link between planet formation and life', *Geology*, 38(10), pp. 959-960.

Murchie, S.L., Mustard, J.F., Ehlmann, B.L., Milliken, R.E., Bishop, J.L., McKeown, N.K., Noe Dobrea, E.Z., Seelos, F.P., Buczkowski, D.L., Wiseman, S.M., Arvidson, R.E., Wray, J.J., Swayze, G., Clark, R.N., Des Marais, D.J., McEwen, A.S. and Bibring, J.-P. (2009) 'A synthesis of Martian aqueous mineralogy after 1 Mars year of observations from the Mars Reconnaissance Orbiter', *Journal of Geophysical Research*, 114.

Muromtsev, G.S., Voblikova, V.D., Kobrina, N.S., Koreneva, V.M., Krasnopolskaya, L.M. and Sadovskaya, V.L., (1994). 'Occurrence of fusicoccanes in plants and fungi'. *Journal of Plant Growth Regulation*, *13*(1), p.39.

N

Nair, H., Allen, M., Anbar, A.D., Yung, Y.L. and Clancy, R.T. (1994) 'A Photochemical Model of the Martian Atmosphere', *Icarus*, 111(1), pp. 124-150.

Naraoka H., Shimoyama A. and Harada K. (2000) 'Isotopic evidence from an Antarctic carbonaceous chondrite for two reaction pathways of extraterrestrial PAH formation', *Earth and Planetary Science Letters*, 184(1), pp. 1-7.

NASA (2018) nssdc.gsfc.nasa.gov/planetary/factsheet/marsfact.html. Retrieved 21 March 2019

Navarro-González, R., Rainey, F.A., Molina, P., Bagaley, D.R., Hollen, B.J., de la Rosa, J., Small, A.M., Quinn, R.C., Grunthaner, F.J., Cáceres, L. and Gomez-Silva, B., (2003). 'Mars-like soils in the Atacama Desert, Chile, and the dry limit of microbial life'. *Science*, *302*(5647), pp.1018-1021.Navarro-Gonzalez, R., Navarro, K.F., de la Rosa, J., Iniguez, E., Molina, P., Miranda, L.D., Morales, P., Cienfuegos, E., Coll, P., Raulin, F., Amils, R. and McKay, C.P. (2006) 'The limitations on organic detection in Mars-like soils by thermal volatilization-gas chromatography-MS and their implications for the Viking results', *Proceedings of the National Academy of Sciences of the United States of America*, 103(44), pp. 16089-16094.

Navarro-González, R., Iñiguez, E., Rosa, J. D. L., and McKay, C. P. (2009) 'Characterization of Organics, Microorganisms, Desert Soils, and Mars-like Soils by Thermal Volatilization Coupled to Mass Spectrometry and Their Implications for the Search for Organics on Mars by Phoenix and Future Space Missions', *Astrobiology*, 9(8), pp. 703-715.

Navarro-González, R., Vargas, E., de La Rosa, J., Raga, A.C. and McKay, C.P. (2010) 'Reanalysis of the Viking results suggests perchlorate and organics at midlatitudes on Mars', *Journal of Geophysical Research*, 115(E12), p. E12010.

Nealson, K.H., and Popa, R. (1999) *Metabolic diversity in the microbial world: relevance to exobiology*. Cambridge: Cambridge University Press.

Nealson, K.H. and Cox, B.L. (2002) 'Microbial metal-ion reduction and Mars: extraterrestrial expectations?', *Current Opinion in Microbiology*, 5(3), pp. 296-300.

Nelson, D.and.Sommers., L.E. (1982) 'Total carbon, organic carbon, and organic matter', in *Methods of soil analysis. Part 2.* Chemical and microbiological properties. American Society of Agronomy, Soil Science Society of America, pp. 539-579.

Neukum, G., Jaumann, R., Hoffmann, H., Hauber, E., Head, J.W., Basilevsky, A.T., Ivanov, B.A., Werner, S.C., van Gasselt, S., Murray, J.B., McCord, T. and Team, H.C.-i. (2004) 'Recent and episodic volcanic and glacial activity on Mars revealed by the High-resolution Stereo Camera', *Nature*, 432(7020), pp. 971-979.

Niemann, H.B., Atreya, S.K., Bauer, S.J., Carignan, G.R., Demick, J.E., Frost, R.L., Gautier, D., Haberman, J.A., Harpold, D.N., Hunten, D.M., Israel, G., Lunine, J.I., Kasprzak, W.T., Owen, T.C., Paulkovich, M., Raulin, F., Raaen, E. and Way, S.H. (2005) 'The

abundances of constituents of Titan's atmosphere from the GC/MS instrument on the Huygens probe', *Nature*, 438(7069), pp. 779-784.

Nimmo, F. (2005) 'Tectonic consequences of Martian dichotomy modification by lower-crustal flow and erosion', *Geology*, 33(7), p. 533.

Ninomiya, S., Nakata, Y., Ichiki, K., Seki, T., Aoki, T. and Matsuo, J., (2007). 'Measurements of secondary ions emitted from organic compounds bombarded with large gas cluster ions'. *Nuclear Instruments and Methods in Physics Research Section B: Beam Interactions with Materials and Atoms*, *256*(1), pp.493-496.Nixon, S.L., Cockell, C.S. and Tranter, M. (2012) 'Limitations to a microbial iron cycle on Mars', *Planetary and Space Science*. *72*(1), pp.116-128.

Noffke, N., and S. M. Awramik (2013a) 'Stromatolites and MISS-differences between relatives', *GSA Today*, 23(No 9), pp. 4-9.

Noffke, N., Decho, A.W. and Stoodley, P. (2013b) 'Slime through Time: The Fossil Record of Prokaryote Evolution', *Palaios*, 28(1-2), pp. 1-5.

Noffke, N. (2015) 'Ancient Sedimentary Structures in the < 3.7 Ga Gillespie Lake Member, Mars, That Resemble Macroscopic Morphology, Spatial Associations, and Temporal Succession in Terrestrial Microbialites', *Astrobiology*, 15(2), pp. 169-192.

Nugent M.A., Brantley S.L., Pantano C.G. and Maurice P.A., (1998). 'The influence of natural mineral coatings on feldspar weathering'. *Nature*, **395**(6702), pp.588-591.

Nutman, A.P., Bennett, V.C., Friend, C.R.L., Van Kranendonk, M.J. and Chivas, A.R. (2016) 'Rapid emergence of life shown by discovery of 3,700-million-year-old microbial structures', *Nature*, 537(7621), p. 535.

Nyquist, L.E., Bogard, D.D., Shih, C.Y., Greshake, A., Stöffler, D. and Eugster, O., (2001). Ages and geologic histories of Martian meteorites. In *Chronology and evolution of Mars* (pp. 105-164). Springer, Dordrecht, Netherlands.

O

Ocean Drilling Program (2005): Archive of Core and Site/Hole Data and Photographs from the Ocean Drilling Program (ODP). National Geophysical Data Center, NOAA. doi:10.7289/V5W37T8C,

www.odp.tamu.edu/publications/prelim/192_prel/192pr84.html [accessed: 15 September 2015]

Ohara, Y., Reagan, M.K., Fujikura, K., Watanabe, H., Michibayashi, K., Ishii, T., Stern, R.J., Pujana, I., Martinez, F., Girard, G., Ribeiro, J., Brounce, M., Komori, N. and Kino, M. (2012) 'A serpentinite-hosted ecosystem in the Southern Mariana Forearc', *Proceedings of the National Academy of Sciences of the United States of America*, 109(8), pp. 2831-2835.

Ojha, L., Wilhelm, M.B., Murchie, S.L., McEwen, A.S., Wray, J.J., Hanley, J., Masse, M. and Chojnacki, M. (2015) 'Spectral evidence for hydrated salts in recurring slope lineae on Mars', *Nature Geoscience*, 8(11), pp. 829-+.

Ojha, L., Wilhelm, M.B., Murchie, S.L., McEwen, A.S., Wray, J.J., Hanley, J., Massé, M. and Chojnacki, M. (2015). Spectral evidence for hydrated salts in recurring slope lineae on Mars. *Nature Geoscience*, *8*(11), p.829.

Onstott, T.C., Phelps, T.J., Colwell, F.S., Ringelberg, D., White, D.C., Boone, D.R., McKinley, J.P., Stevens, T.O., Long, P.E., Balkwill, D.L., Griffin, W.T. and Kieft, T. (1998) 'Observations pertaining to the origin and ecology of microorganisms recovered from the deep subsurface of Taylorsville Basin, Virginia', *Geomicrobiology Journal*, 15(4), pp. 353-385.

Onstott, T.C., McGown, D., Kessler, J., Lollar, B.S., Lehmann, K.K. and Clifford, S.M. (2006) 'Martian CH_4: Sources, flux, and detection', *Astrobiology*, 6(2), pp. 377-395.

Oren, A., Bardavid, R.E. and Mana, L. (2014) 'Perchlorate and halophilic prokaryotes: implications for possible halophilic life on Mars' *Extremophiles*, *18*(1), pp.75-80.

Orosei, R., Jordan, R.L., Morgan, D.D., Cartacci, M., Cicchetti, A., Duru, F., Gurnett, D.A., Heggy, E., Kirchner, D.L., Noschese, R., Kofman, W., Masdea, A., Plaut, J.J., Seu, R., Watters, T.R. and Picardi, G. (2015) 'Mars Advanced Radar for Subsurface and Ionospheric Sounding (MARSIS) after nine years of operation: A summary', *Planetary and Space Science*, 112, pp. 98-114.

Osinski, G.R., Tornabene, L.L., Banerjee, N.R., Cockell, C.S., Flemming, R., Izawa, M.R.M., McCutcheon, J., Parnell, J., Preston, L.J., Pickersgill, A.E., Pontefract, A., Sapers, H.M. and Southam, G. (2013) 'Impact-generated hydrothermal systems on Earth and Mars', *Icarus*, 224(2), pp. 347-363.

Owen, T., Biemann, K., Rushneck, D.R., Biller, J.E., Howarth, D.W. and Lafleur, A.L., (1977). The composition of the atmosphere at the surface of Mars. *Journal of Geophysical Research*, *82*(28), pp.4635-4639.

Oyama, V.I. (1972) 'The gas exchange experiment for life detection: the Viking Mars lander', *Icarus*, 16(1), pp. 167-184.

Oyama, V.I.a.B., B.J. (1977) 'The Viking gas exchange experiment results from Chryse and Utopia surface samples', *Journal of Geophysical Research*, 82(28), pp. 4669-4676.

Oze, C. and Sharma, M. (2005) 'Have olivine, will gas: Serpentinization and the abiogenic production of methane on Mars', *Geophysical Research Letters*, 32(10).

Oze, C. and Sharma, M. (2007) 'Serpentinization and the inorganic synthesis of H-2 in planetary surfaces', *Icarus*, 186(2), pp. 557-561.

Oze, C., L. Camille Jones, Jonas I. Goldsmith, and Robert J. Rosenbauer. (2012) 'Differentiating biotic from abiotic methane genesis in hydrothermally active planetary surfaces.', *Proceedings of the National Academy of Sciences*, 109(25), pp. 9750-9754.

P

Pardue, H.L. (1997) 'The inseparable triad: analytical sensitivity, measurement uncertainty, and quantitative resolution', *Clinical Chemistry*, 43(10), pp. 1831-1837.

Pasteris, Jill D and Wopenka, B. (2002) *Geological Society of America*. Denver.

Pavlov, A.K., Blinov, A.V. and Konstantinov, A.N. (2002) 'Sterilization of Martian surface by cosmic radiation', *Planetary and Space Science*, 50(7-8), pp. 669-673.

Paul, D., Been, H.A., Aerts-Bijma, A.T. and Meijer, H.A.J. (2016) 'Contamination on Ams Sample Targets by Modern Carbon Is Inevitable', *Radiocarbon*, 58(2), pp. 407-418.

Pepin, R.O. (1994) 'Evolution of the Martian atmosphere', *Icarus*, 111(2), pp. 289-304.

Peters, K.E., Walters, C.C. and Moldowan, J.M. (2005) *'The biomarker guide'* Cambridge University Press, Cambridge, UK.

Pilorget, C.a.F., F. (2015) *AAS/Division for Planetary Sciences Meeting Abstracts*.

Piao, H. and McIntyre, N.S. (2002) 'Adventitious carbon growth on aluminium and gold-aluminium alloy surfaces', *Surface and Interface Analysis*, 33(7), pp. 591-594.

Pizzarello, S., (2004). Chemical evolution and meteorites: an update. *Origins of Life and Evolution of the Biosphere*, *34*(1-2), pp.25-34.

Pizzarello S., Cooper G. W. and Flynn G. J. (2006) 'The nature and distribution of the organic material in carbonaceous chondrites and interplanetary dust particles', in *Meteorites and the early solar system II*. 1. University of Arizona Press, pp. 625-651.

Pizzarello, S. and Shock, E. (2010). The organic composition of carbonaceous meteorites: the evolutionary story ahead of biochemistry. *Cold Spring Harbor perspectives in biology*, *2*(3), p.a002105.

Pollack, J.B., Kasting, J.F., Richardson, S.M. and Poliakoff, K. (1987) 'The Case for a Wet, Warm Climate on Early Mars', *Icarus*, 71(2), pp. 203-224.

Postawa Z. (2004). Sputtering simulations of organic overlayers on metal substrates by monoatomic and clusters projectiles. *Applied surface science*, **231**, 22-28.

Poulet, F., Bibring, J.P., Mustard, J.F., Gendrin, A., Mangold, N., Langevin, Y., Arvidson, R.E., Gondet, B., Gomez, C. and Team, O. (2005) 'Phyllosilicates on Mars and implications for early Martian climate', *Nature*, 438(7068), pp. 623-627.

Preston L.J., Izawa M.R. and Banerjee N.R. (2011) 'Infrared spectroscopic characterization of organic matter associated with microbial bioalteration textures in basaltic glass', *Astrobiology*, **11**(7), 585-99.

Preston, L. J. and L. R. Dartnell, Int. J. Astrobiology. **13**; 81 (2014).

Pretsch, E., Bühlmann, P., Affolter, C., Pretsch, E., Bhuhlmann, P. and Affolter, C., (2009) 'Mass Spectrometry', in *Structure determination of organic compounds*. Berlin: Springer, Dordrecht, Netherlands.

Proskurowski, G., Lilley, M.D., Seewald, J.S., Fruh-Green, G.L., Olson, E.J., Lupton, J.E., Sylva, S.P. and Kelley, D.S. (2008) 'Abiogenic hydrocarbon production at Lost City hydrothermal field', *Science*, 319(5863), pp. 604-607.

Purvis, G., Gray, N., Sano, N., Barlow, A., Cockell, C., Abbott, G.D., van der Land, C. and Cumpson, P. (2017) 'Decontamination of geological samples by gas cluster ion beam etching or ultraviolet/ozone', *Chemical Geology*, 466, pp. 256-262.

Purvis under review a The Molecular Identities of the Organic Compounds in Ontong Java Plateau Tuff

Purvis, G., Sano, N., Barlow, A., Cockell, C., van der Land, C., Lopez-Capel, E., Cumpson P. and Gray N. (2018) 'A stratigraphic comparison of the Organic Material in Submarine Basalts containing Microtubular Alteration Textures.' *Geobiology*, *17*(3), pp.281-293

Q

Quinn, R. and Orenberg, J. (1993) 'Simulations of the Viking Gas-Exchange Experiment Using Palagonite and Fe-Rich Montmorillonite as Terrestrial Analogs - Implications for the Surface-Composition of Mars', *Geochimica Et Cosmochimica Acta*, 57(19), pp. 4611-4618.

Quinn, R.C., Martucci, H.F.H., Miller, S.R., Bryson, C.E., Grunthaner, F.J. and Grunthaner, P.J. (2013) 'Perchlorate Radiolysis on Mars and the Origin of Martian Soil Reactivity', *Astrobiology*, 13(6), pp. 515-520.

R

Rabbani, S., Barber, A.M., Fletcher, J.S., Lockyer, N.P. and Vickerman, J.C. (2011) 'TOF-SIMS with Argon Gas Cluster Ion Beams: A Comparison with C-60(+)', *Analytical Chemistry*, 83(10), pp. 3793-3800.

Rahmati, A., Larson, D.E., Cravens, T.E., Lillis, R.J., Halekas, J.S., McFadden, J.P., Dunn, P.A., Mitchell, D.L., Thiemann, E.M.B., Eparvier, F.G. and DiBraccio, G.A., (2017). 'MAVEN measured oxygen and hydrogen pickup ions: Probing the Martian exosphere and neutral escape'. *Journal of Geophysical Research: Space Physics*, *122*(3), pp.3689-3706.

Randall, B. A. O. (1989) Dolerite-pegmatites from the Whin Sill near Barrasford, Northumberland. *Proceedings of the Yorkshire Geological Society* 47, 249-265

Reid, I.N., Sparks, W.B., Lubow, S., McGrath, M., Livio, M., Valenti, J., Sowers, K.R., Shukla, H.D., MacAuley, S., Miller, T., Suvanasuthi, R., Belas, R., Colman, A., Robb, F.T., DasSarma, P., Muller, J.A., Coker, J.A., Cavicchioli, R., Chen, F. and DasSarma, S. (2006) 'Terrestrial models for extraterrestrial life: methanogens and halophiles at Martian temperatures', *International Journal of Astrobiology*, 5(2), pp. 89-97.

Richardson, J.A., Bleacher, J.E. and Glaze, L.S. (2013) 'The volcanic history of Syria Planum, Mars', *Journal of Volcanology and Geothermal Research*, 252, pp. 1-13.

Riding, R. (2011). 'Microbialites, stromatolites, and thrombolites'. *Encyclopedia of Geobiology* (pp. 635-654). Springer, Dordrecht, Netherlands.

Riding, R. (2012) 'A Hard Life for Cyanobacteria', *Science*, 336(6080), pp. 427-428.

Ringwood, A.E. and Clark, S.P. (1971) 'Internal Constitution of Mars', *Nature*, 234(5324), pp. 89-and.

Roberts, J.H., Lillis, R.J. and Manga, M. (2009) 'Giant impacts on early Mars and the cessation of the Martian dynamo', *Journal of Geophysical Research-Planets*, 114.

Robertson, S.A., Mason, S.L., Hack, E. and Abbott, G.D. (2008) 'A comparison of lignin oxidation, enzymatic activity and fungal growth during white-rot decay of wheat straw (vol 39, pg 945, 2008)', *Organic Geochemistry*, 39(12), pp. 1816-1816.

Rodier, C., Sternberg, R., Szopa, C., Buch, A., Cabane, M. and Raulin, F. (2005) 'Search for organics in extraterrestrial environments by in situ gas chromatography analysis', *Space Life Sciences: Astrobiology: Steps toward Origin of Life and Titan before Cassini*, 36(2), pp. 195-200.

Rodriguez, J.A.P., Platz, T., Gulick, V., Baker, V.R., Fairen, A.G., Kargel, J., Yan, J.G., Miyamoto, H. and Glines, N. (2015) 'Did the Martian outflow channels mostly form during the Amazonian Period?', *Icarus*, 257, pp. 387-395.

Rogers, J.R., Bennett, P.C. and Choi, W.J., (1998). Feldspars as a source of nutrients for microorganisms. *American Mineralogist*, *83*(11-12_Part_2), pp.1532-1540.

Rubie, D.C., Gessmann, C.K. and Frost, D.J. (2004) 'Partitioning of oxygen during core formation on the Earth and Mars', *Nature*, 429(6987), pp. 58-61.

Rubin, A.B. (1973) 'Detection of Extraterrestrial Life Forms and Criteria for Existence of Biological-Systems', *Kosmicheskaya Biologiya I Meditsina*, 7(5), pp. 3-7.

Rüdiger, G.a.H., R. (2006) *The magnetic universe: geophysical and astrophysical dynamo theory*. John Wiley and Sons Ltd, Cirencester.

Ruff, S.W. and Farmer, J.D. (2016) 'Silica deposits on Mars with features resembling hot spring biosignatures at El Tatio in Chile', *Nature Communications*, 7.

Ruiz, J.M.G., Canerup, A., Christy, A.G., Welham, N.J. and Hyde, S.T. (2002) 'Morphology: An ambiguous indicator of biogenicity', *Astrobiology*, 2(3), pp. 353-369.

Rushdi, A.I. and Simoneit, B.R.T. (2001) 'Lipid formation by aqueous Fischer-Tropsch-type synthesis over a temperature range of 100 to 400 degrees C', *Origins of Life and Evolution of the Biosphere*, 31(1-2), pp. 103-118.

Russell, M.J. (2009) 'The Alkaline Solution to the Emergence of Life: Energy, Entropy and Early Evolution (vol 55, pg 133, 2007)', *Acta Biotheoretica*, 57(3), pp. 389-394.

S

Saccone, L., Gazze, S.A., Duran, A.L., Leake, J.R., Banwart, S.A., Ragnarsdottir, K.V., Smits, M.M. and McMaster, T.J. (2012) 'High-resolution characterization of ectomycorrhizal fungal-mineral interactions in axenic microcosm experiments', *Biogeochemistry*, 111(1-3), pp. 411-425.

Sáiz-Jiménez, C. (1994). Analytical pyrolysis of humic substances: pitfalls, limitations, and possible solutions. *Environmental science and technology*, *28*(11), pp.1773-1780.

Salese, F., Di Achille, G., Neesemann, A., Ori, G.G. and Hauber, E. (2016) 'Hydrological and sedimentary analyses of well-preserved paleofluvial-paleolacustrine systems at Moa Valles, Mars', *Journal of Geophysical Research-Planets*, 121(2), pp. 194-232.

Salisbury, F.B. (1962) 'Martian biology', *Science*, 136 (3510), pp. 17-26.Sano N., Purvis G.W., Barlow A.J., Abbott G.D., Gray N.N. and Cumpson P.J., 2016. Gas cluster ion beam for the characterization of organic materials in submarine basalts as Mars analogs. *Journal of Vacuum Science and Technology A*, *34*(4), p.041405.

Schaefer, J., Kramer, K.J., Garbow, J.R., Jacob, G.S., Stejskal, E.O., Hopkins, T.L. and Speirs, R.D. (1987) 'Aromatic Cross-Links in Insect Cuticle - Detection by Solid-State C-13 and N-15 Nmr', *Science*, 235(4793), pp. 1200-1204.

Schmid, R. (1976). 'Septal pores in *Prototaxites*, an enigmatic Devonian Plant' *Science*, *191*(4224), pp.287-288.

Schmitter, J.M., Ignatiadis, I. and Arpino, P.J. (1983) 'Distribution of Diaromatic Nitrogen Bases in Crude Oils', *Geochimica Et Cosmochimica Acta*, 47(11), pp. 1975-1984.

Schimmelmann, A., Wintsch, R.P., Lewan, M.D. and DeNiro, M.J. (1998) 'Chitin: 'Forgotten' source of nitrogen - From modern chitin to thermally mature kerogen: Lessons from nitrogen isotope ratios', *Nitrogen-Containing Macromolecules in the Bio- and Geosphere*, 707, pp. 226-242.

Schimmelmann, A. and Lis, G.P. (2010) 'Nitrogen isotopic exchange during maturation of organic matter', *Organic Geochemistry*, 41(1), pp. 63-70.

Schnitzer, M. (1991) 'Soil Organic-Matter - the Next 75 Years', *Soil Science*, 151(1), pp. 41-58.

Schon, S.C. and Head, J.W. (2011) 'Keys to gully formation processes on Mars: Relation to climate cycles and sources of meltwater', *Icarus*, 213(1), pp. 428-432.

Schopf, J.W. (2006) 'Fossil evidence of Archaean life', *Philosophical Transactions of the Royal Society B-Biological Sciences*, 361(1470), pp. 869-885.

Schulze-Makuch, D., and Irwin, L. N. (2008) *Life in the universe: expectations and constraints*. Springer Dordrecht, Netherlands.

Schulze-Makuch, D., Irwin, L.N., Lipps, J.H., LeMone, D., Dohm, J.M. and Fairén, A.G. (2005) 'Scenarios for the evolution of life on Mars', *Journal of Geophysical Research*, 110(E12).

Schummer, C., Delhomme, O., Appenzeller, B.M.R., Wennig, R. and Millet, M. (2009) 'Comparison of MTBSTFA and BSTFA in derivatization reactions of polar compounds prior to GC/MS analysis', *Talanta*, 77(4), pp. 1473-1482.

Scott, E.R., Krot, A.N. and Yamaguchi, A., (1998). Carbonates in fractures of Martian meteorite Allan Hills 84001: Petrologic evidence for impact origin. *Meteoritics and Planetary Science*, *33*(4), pp.709-719.

Segura, T.L., Toon, O.B., Colaprete, A. and Zahnle, K. (2002) 'Environmental effects of large impacts on Mars', *Science*, 298(5600), pp. 1977-1980.

Sephton, M.A. and Gilmour, I. (2001). Pyrolysis–gas chromatography–isotope ratio mass spectrometry of macromolecular material in meteorites. *Planetary and Space Science*, *49*(5), pp.465-471.

Sephton, M.A. (2002) 'Organic compounds in carbonaceous meteorites', *Natural Product Reports*, 19(3), pp. 292-311.

Sephton, M.A. and Botta, O. (2007) 'Extraterrestrial Organic Matter and the Detection of Life', *Space Science Reviews*, 135(1-4), pp. 25-35.

Shard A. G., Havelund R., Spencer S. J., Gilmore I. S., Alexander M. R., Angerer T. B. and Zhu Z. (2015). Measuring Compositions in Organic Depth Profiling: Results from a VAMAS Interlaboratory Study. *The Journal of Physical Chemistry B*, **119**(33), 10784-10797.

Sherman L.S., Waldbauer J.R. and Summons R.E. (2007) 'Improved methods for isolating and validating indigenous biomarkers in Precambrian rocks', *Organic Geochemistry*, 38(12), pp. 1987-2000.

Shock, E.L. (1996) 'Hydrothermal systems as environments for the emergence of life', *Evolution of Hydrothermal Ecosystems on Earth (and Mars?)*, 202, pp. 40-60.

Shock, E.L. (2002) 'Astrobiology - Seeds of life?', *Nature*, 416(6879), pp. 380-381.

Siegbahn, K., Nordling, C., Fahlman, A., Nordberg, R., Hamrin, K., Hedman, J., Johansson, G., Bergmark, T., Karlsson, S.E., Lindgren, I. and Lindberg, B., (1967*). Nova Acata Regiae* Soc. *Sci. Upsal. IV*, *20*, p.59.

Siljestrom, S., Lausmaa, J., Sjovall, P., Broman, C., Thiel, V. and Hode, T. (2010) 'Analysis of hopanes and steranes in single oil-bearing fluid inclusions using time-of-flight secondary ion mass spectrometry (ToF-SIMS)', *Geobiology*, 8(1), pp. 37-44.

Simmonds, P.G. (1970) 'Whole Microorganisms Studied by Pyrolysis-Gas Chromatography-Mass Spectrometry - Significance for Extraterrestrial Life Detection Experiments', *Applied Microbiology*, 20(4), pp. 567-and.

Simmonds, P.G., Shulman, G. P., and Stembridge, C. H. (1969) ' Organic Analysis by Pyrolysis-Gas Chromatography-Mass Spectrometry A Candidate Experiment for the Biological Exploration of Mars', *Journal of Chromatographic Science*, 36-41.

Sjovall, P., Thiel, V., Siljestrom, S., Heim, C., Hode, T. and Lausmaa, J. (2008) 'Organic geochemical microanalysis by time-of-flight secondary ion mass spectrometry (ToF-SIMS)', *Geostandards and Geoanalytical Research*, 32(3), pp. 267-277.

Smith J.W. and Kaplan I.R. (1970). Indigenous carbon in carbonaceous meteorites. *Science*, 167(3923), pp.1367-1370.

Smith, P.H., Tamppari, L., Arvidson, R.E., Bass, D., Blaney, D., Boynton, W., Carswell, A., Catling, D., Clark, B., Duck, T., DeJong, E., Fisher, D., Goetz, W., Gunnlaugsson, P., Hecht, M., Hipkin, V., Hoffman, J., Hviid, S., Keller, H., Kounaves, S., Lange, C.F., Lemmon, M., Madsen, M., Malin, M., Markiewicz, W., Marshall, J., McKay, C., Mellon, M., Michelangeli, D., Ming, D., Morris, R., Renno, N., Pike, W.T., Staufer, u., Stoker, C., Taylor, P., Whiteway, J., Young, S. and Zent, A. (2008) 'Introduction to special section on the Phoenix Mission: Landing Site Characterization Experiments, Mission Overviews, and Expected Science', *Journal of Geophysical Research*, 113.

Smits, M. M. in *Fungi in Biogeochemical Cycles*, Ed: Gadd, G.M.E., (2006a), (Cambridge University Press, Cambridge, England pp. 681, 717.

Smits, M.M. (2006b) ' Mineral Tunnelling by Fungi.', in Gadd, G.M.E. (ed.) *Fungi in Biogeochemical Cycles.* Cambridge: Cambridge University Press, pp. 681–717.

Simoneit, B.R., Schnoes, H.K., Haug, P. and Burlinga, A.l. (1971) 'High-resolution Mass Spectrometry in Molecular Structure Studies.34. High-Resolution Mass Spectrometry of Nitrogenous Compounds of Colorado Green River Formation Oil Shale', *Chemical Geology*, 7(2), pp. 123

Soare, R.J., Conway, S.J., Gallagher, C. and Dohm, J.M. (2016) 'Sorted (shardic) polygons in the Argyre region, Mars, and possible evidence of pre- and post-glacial periglaciation in the Late Amazonian Epoch', *Icarus*, 264, pp. 184-197.

Soffen, G.A.a.Y., A.T. (1972) 'The Viking missions to Mars', *Icarus*, 16(1), pp. 1-16.

Solomon, S.C., Aharonson, O., Aurnou, J.M., Banerdt, W.B., Carr, M.H., Dombard, A.J., Frey, H.V., Golombek, M.P., Hauck, S.A., 2nd, Head, J.W., 3rd, Jakosky, B.M., Johnson, C.L., McGovern, P.J., Neumann, G.A., Phillips, R.J., Smith, D.E. and Zuber, M.T. (2005) 'New perspectives on ancient Mars', *Science*, 307(5713), pp. 1214-20.

Southam, G. and Westall, F., (2007). Geology, life and habitability. pp 421-437.

Space.com (2015), www.space.com/16907-what-is-the-temperature-of-mars.html. Retrieved. 1 March 2019

Spool, A.M. (2004) 'Interpretation of static secondary ion spectra', *Surface and Interface Analysis*, 36(3), pp. 264-274.

Spool, A.M. (2016) *The Practice of TOF-SIMS: Time of Flight Secondary Ion Mass Spectrometry*. Momentum Press Inc., New York

Squyres, S.W. and Carr, M.H. (1986) 'Geomorphic Evidence for the Distribution of Ground Ice on Mars', *Science*, 231(4735), pp. 249-252.

Squyres, S.W. and Kasting, J.F. (1994) 'Early Mars - How Warm and How Wet', *Science*, 265(5173), pp. 744-749.

Stalport, F., Coll, P., Szopa, C. and Raulin, F. (2008) 'Search for organic molecules at the Mars surface: The 'Martian Organic Material Irradiation and Evolution' (MOMIE) project', *Advances in Space Research*, 42(12), pp. 2014-2018.

Stalport, F., Glavin, D.P., Eigenbrode, J.L., Bish, D., Blake, D., Coll, P., Szopa, C., Buch, A., McAdam, A., Dworkin, J.P. and Mahaffy, P.R. (2012) 'The influence of mineralogy on recovering organic acids from Mars analogue materials using the "one-pot" derivatization experiment on the Sample Analysis at Mars (SAM) instrument suite', *Planetary and Space Science*, 67(1), pp. 1-13.

Stankiewicz, B.A., Briggs, D.E.G., Evershed, R.P., Duncan, I.J., van Bergen, P.F. and Hof, C.H.J. (1996) 'In research of chitin: Pyrolysis-GC/MS studies of modern, decayed and fossil arthropod cuticles.', *Abstracts of Papers of the American Chemical Society*, 212, pp. 11-Geoc.

Stankiewicz, B.A., van Bergen, P.F., Smith, M.B., Carter, J.F., Briggs, D.E.G. and Evershed, R.P. (1998) 'Comparison of the analytical performance of filament and Curie-point pyrolysis devices', *Journal of Analytical and Applied Pyrolysis*, 45(2), pp. 133-151.

Staudigel H., Furnes H. and Smits M. (2014) 'Deep Biosphere Record of In Situ Oceanic Lithosphere and Ophiolites', *Elements*, 10(2), pp. 121-126.

Staudigel, H., Banergee,N.,Dilek,Y.,and Muehlenbachs,K. (2006) 'Microbes and volcanoes: A tale from the oceans, ophiolites, and greenstone belts', *GSA Today*, 16(10).

Staudigel, H., Furnes, H., McLoughlin, N., Banerjee, N.R., Connell, L.B. and Templeton, A. (2008) '3.5 billion years of glass bioalteration: Volcanic rocks as a basis for microbial life?', *Earth-Science Reviews*, 89(3-4), pp. 156-176.

Staudigel, H., Furnes, H. and Smits, M. (2014) 'Deep Biosphere Record of In Situ Oceanic Lithosphere and Ophiolites', *Elements*, 10(2), pp. 121-126.

Steele, A., McCubbin, F.M., Fries, M., Kater, L., Boctor, N.Z., Fogel, M.L., Conrad, P.G., Glamoclija, M., Spencer, M., Morrow, A.L. and Hammond, M.R. (2012). 'A reduced organic carbon component in martian basalts'. *Science*, *337*(6091), pp.212-215.

Stein, S.E. (1994) 'Estimating Probabilities of Correct Identification from Results of Mass-Spectral Library Searches', *Journal of the American Society for Mass Spectrometry*, 5(4), pp. 316-323.

Stein, S.E. (2008). NIST standard reference database 1A. *National Institute of Standards and Technology, Gaithersburg*.

Stein, W.E., Mannolini, F., Hernick, L.V., Landing, E. and Berry, C.M., (2007). Giant *cladoxylopsid* trees resolve the enigma of the Earth's earliest forest stumps at Gilboa. *Nature*, *446*(7138), p.904.

Stephan, T. (2001) 'TOF-SIMS in cosmochemistry', *Planetary and Space Science*, 49(9), pp. 859-906.

Stephan, T. (2005) 'TOF-SIMS - A tool for sub-micrometre analysis in geo- and cosmochemistry', *Geochimica Et Cosmochimica Acta*, 69(10), pp. A525-A525.

Stevens, T.O. and Mckinley, J.P. (1995) 'Lithoautotrophic Microbial Ecosystems in Deep Basalt Aquifers', *Science*, 270(5235), pp. 450-454.

Stevens, T.O. (1997) 'Subsurface lithoautotrophic microbial ecosystems (SLMEs) in igneous rocks: Prospects for detection', *Instruments, Methods, and Missions for the Investigation of Extraterrestrial Microorganisms*, 3111, pp. 358-365.

Stevenson, D.J. (2001) 'Mars' core and magnetism', *Nature*, 412(6843), pp. 214-219.

Straub, K.L., Benz, M., Schink, B. and Widdel, F. (1996) 'Anaerobic, nitrate-dependent microbial oxidation of ferrous iron', *Applied and Environmental Microbiology*, 62(4), pp. 1458-1460.

Strughold, H. (1967). Synopsis of Martian life theories. In *Advances in space science and technology* (Vol. 9, pp. 105-122). Elsevier, Amsterdam, Netherlands.

Summers, M.E., Lieb, B.J., Chapman, E. and Yung, Y.L. (2002) 'Atmospheric biomarkers of subsurface life on Mars', *Geophysical Research Letters*, 29(24).

Summons, R.E., Albrecht, P., McDonald, G. and Moldowan, J.M. (2007) 'Molecular Biosignatures', *Space Science Reviews*, 135(1-4), pp. 133-159.

Summons, R.E., Amend, J. P., Bish, D., Buick, R., Cody, G. D., Des Marais, D. J. and Sumner, D. Y. (2011) 'Preservation of Martian Organic and Environmental Records: Final Report of the Mars Biosignature Working Group', *Astrobiology*, 11(2).

Sutter, B., Ming, D.W., Boynton, W.V., Niles, P.B., Hoffman, J., Lauer, H.V. and Golden, D.C. (2009) *Summary of results from the Mars Phoenix lander's thermal evolved gas analyzer*. www.ntrs.nasa.gov.

Szabo, T., Domokos, G., Grotzinger, J.P. and Jerolmack, D.J. (2015) 'Reconstructing the transport history of pebbles on Mars', *Nature Communications*, 6, p.8366.

T

Taborelli, M. (2007). 'Cleaning and surface properties'.
http://cds.cern.ch/record/1047073/files/p321.pdf. Accessed 3rd May 2017

Tamppari, L.K.a.L., M.T., (2014) Mars Atmosphere: Modelling and Observation, *5th International Workshop*.

Tarduno, J.A., Sliter, W.V., Kroenke, L., Leckie, M., Mayer, H., Mahoney, J.J., Musgrave, R., Storey, M. and Winterer, E.L. (1991) 'Rapid Formation of Ontong Java Plateau by Aptian Mantle Plume Volcanism', *Science*, 254(5030), pp. 399-403.

Taylor, S. R. *Planetary Science: A Lunar Perspective*, (Lunar and Planetary Institute, Houston, US, 1982), Chapter 6.

Taylor, T.N., Taylor, E.L., Krings, M. (2009) 'The biology and evolution of fossil plants', *Palaeobotany*. Academic Press.

ten Kate, I.L., Ruiterkamp, R., Botta, O., Lehmann, B., Hernandez, C.G., Boudin, N., Foing, B.H. and Ehrenfreund, P. (2002) 'Investigating complex organic compounds in a simulated Mars environment', *International Journal of Astrobiology*, 1(4), pp. 387-399.

Tegelaar, E.W., De Leeuw, J.W., Derenne, S. and Largeau, C. (1989). A reappraisal of kerogen formation. *Geochimica et Cosmochimica Acta*, *53*(11), pp.3103-3106.

ten Kate, I.L. (2010) 'Organics on Mars?', *Astrobiology*, 10(6), pp. 589-603.

ten Kate, I.L., Armstrong, R., Bernhardt, B., Blumers, M., Craft, J., Boucher, D., Caillibot, E., Captain, J., Deleuterio, G., Farmer, J.D., Glavin, D.P., Graff, T., Hamilton, J.C., Klingelhofer, G., Morris, R.V., Nunez, J.I., Quinn, J.W., Sanders, G.B., Sellar, R.G., Sigurdson, L., Taylor, R. and Zacny, K. (2013) 'Mauna Kea, Hawaii, as an Analog Site for Future Planetary Resource Exploration: Results from the 2010 ILSO-ISRU Field-Testing Campaign', *Journal of Aerospace Engineering*, 26(1), pp. 183-196.

ten Kate, I.L., (2018) 'Organic molecules on Mars' *Science*, *360*(6393), pp.1068-1069.

Theil E. C. and Raymond, K. N.(1994) 'Transition-Metal Storage, Transport, and Biomineralization', chapter 1 , *in Bioinorganic Chemistry*, Bertini, I., Gray, H. B., Lippard, S. J. and Valentine, J.S. (eds). University Science Books ISBN 0-935702-57-1

Thiel, V. and Sjovall, P. (2011) Using Time-of-Flight Secondary Ion Mass Spectrometry to Study Biomarkers, *Annual Review of Earth and Planetary Sciences, Vol 39*, 39, pp. 125-156.

Thiemann, W.H.P. and Meierhenrich, U. (2001) 'ESA mission ROSETTA will probe for chirality of cometary amino acids', *Origins of Life and Evolution of Biospheres*, 31(1-2), pp. 199-210.

Thomas, H . H . (1927). Pp. 110-112 in Carruthers, R. G., Dinham, C. H., Burnett, G. A. and Maden, J. 'The geology of Belford, Holy Island and the Fame Islands' (2nd edn). *Memoir of the Geological Survey of Great Britain, New Series* Sheet 4.

Thomas, M., Clarke, J.D.A. and Pain, C.F. (2005) 'Weathering, erosion and landscape processes on Mars identified from recent rover imagery, and possible Earth analogues', *Australian Journal of Earth Sciences*, 52(3), pp. 365-378.

Thomas-Keprta, K.L., Clemett, S.J., Bazylinski, D.A., Kirschvink, J.L., McKay, D.S., Wentworth, S.J., Vali, H., Gibson Jr, E.K. and Romanek, C.S., 2002. Magnetofossils from ancient Mars: a robust biosignature in the Martian meteorite ALH84001. *Applied and Environmental Microbiology*, *68*(8), pp.3663-3672.

Thordarson, T. (2004) 'Accretionary-lapilli-bearing pyroshardic rocks at ODP Leg 192 Site 1184: A record of subaerial phreatomagmatic eruptions on the Ontong Java Plateau', *Geological Society, London, Special Publications*, 229(1), pp. 275-306.

Thorpe, R.S. and Macdonald, R. (1985) 'Geochemical Evidence for the Emplacement of the Whin Sill Complex of Northern England', *Geological Magazine*, 122(4), pp. 389-396.

Tielens, A.G.G.M. and Charnley, S.B. (1997) 'Circumstellar and interstellar synthesis of organic molecules', *Origins of Life and Evolution of Biospheres*, 27(1-3), pp. 23-51.

Tielens, A.G.G.M. (2013) 'The molecular universe', *Reviews of Modern Physics*, 85(3), pp. 1021-1081.

Tingle, T.N., Mathez, E.A. and Hochella, M.F. (1991) 'Carbonaceous Matter in Peridotites and Basalts Studied by Xps, Sali, and Leed', *Geochimica Et Cosmochimica Acta*, 55(5), pp. 1345-1352.

Tingle, T.N. and Hochella, M.F. (1993) 'Formation of Reduced Carbonaceous Matter in Basalts and Xenoliths - Reaction of C-O-H Gases on Olivine Crack Surfaces', *Geochimica Et Cosmochimica Acta*, 57(14), pp. 3245-3249.

Tissot, B.P.a.W., D.H. (1984) 'From Kerogen to Petroleum', in *In Petroleum Formation and Occurrence*. Springer Heidelberg, Berlin: pp. pp. 160-198.

Tonge, G. M. and Higgins, I. J. J. Gen. Microbiol. **81**, 521 (1974).

Tosca, N.J., McLennan, S.M., Clark, B.C., Grotzinger, J.P., Hurowitz, J.A., Jolliff, B.L., Knoll, A.H., Schröder, C. and Squyres, S.W. (2005) March. Geochemical modelling of evaporites on Mars: Insight from Meridiani Planum. In *36th Annual Lunar and Planetary Science Conference* (Vol. 36).

Touma, J. and Wisdom, J. (1993) 'The Chaotic Obliquity of Mars', *Science*, 259(5099), pp. 1294-1296.

Trivett, M.L. (1993). An architectural analysis of Archaeopteris, a fossil tree with pseudomonopodial and opportunistic adventitious growth. *Botanical Journal of the Linnean Society*, *111*(3), pp.301-329.

Tung, H.C., Bramall, N.E. and Price, P.B. (2005) 'Microbial origin of excess methane in glacial ice and implications for life on Mars', *Proceedings of the National Academy of Sciences of the United States of America*, 102(51), pp. 18292-18296.

u

Ungerer, P., Collell, J. and Yiannourakou, M. (2015) 'Molecular Modeling of the Volumetric and Thermodynamic Properties of Kerogen: Influence of Organic Type and Maturity', *Energy and Fuels*, 29(1), pp. 91-105.

V

Valeille, A., Bougher, S.W., Tenishev, V., Combi, M.R. and Nagy, A.F. (2010) 'Water loss and evolution of the upper atmosphere and exosphere over martian history', *Icarus*, 206(1), pp. 28-39.

Vandenbroucke, M. (2003) 'Kerogen: from types to models of chemical structure', *Oil and Gas Science and Technology-Revue D Ifp Energies Nouvelles*, 58(2), pp. 243-269.

Vandenbroucke, M. and Largeau, C. (2007) 'Kerogen origin, evolution and structure', *Organic Geochemistry*, 38(5), pp. 719-833.

Vig J.R. (1985) 'UV Ozone Cleaning of Surfaces', *Journal of Vacuum Science and Technology a-Vacuum Surfaces and Films*, **3**(3), pp. 1027-1034.

Vincendon, M. (2015) 'Identification of Mars gully activity types associated with ice composition', *Journal of Geophysical Research-Planets*, 120(11), pp. 1859-1879.

Vulava, V.M., McKay, L.D., Driese, S.G., Menn, F.M. and Sayler, G.S., 2007. Distribution and transport of coal tar-derived PAHs in fine-grained residuum. *Chemosphere*, *68*(3), pp.554-563.

W

Wacey, D., McLoughlin, N., Saunders, M., and Kong, C. (2014) 'The nano-scale anatomy of a complex carbon-lined microtube in volcanic glass from the ca. 92Ma Troodos Ophiolite, Cyprus. ', *Chemical Geology*, 363, pp. 1-12.

Walter, M.R., Buick, R. and Dunlop, J.S.R. (1980) 'Stromatolites 3,400-3,500 Myr Old from the North-Pole Area, Western-Australia', *Nature*, 284(5755), pp. 443-445.

Ward, W.R. (1973). Large-scale variations in the obliquity of Mars. Science, 181(4096), pp.260-262.

Ward, W.R. and Rudy, D.J. (1991) 'Resonant Obliquity of Mars', *Icarus*, 94(1), pp. 160-164.

Watts, J.F., and Wolstenholme, J. (2003) *An Introduction to surface analysis by XPS and AES*. Wiley Chichester.

Weber, K.A., Achenbach, L. A., and Coates, J. D. (2006) 'Microorganisms pumping iron: anaerobic microbial iron oxidation and reduction', *Nature Reviews Microbiology*, 4(10), pp. 752-764.

Webster, C.R., Mahaffy, P.R., Atreya, S.K., Flesch, G.J., Mischna, M.A., Meslin, P.Y., Farley, K.A., Conrad, P.G., Christensen, L.E., Pavlov, A.A., Martin-Torres, J., Zorzano, M.P., McConnochie, T.H., Owen, T., Eigenbrode, J.L., Glavin, D.P., Steele, A., Malespin, C.A., Archer, P.D., Sutter, B., Coll, P., Freissinet, C., McKay, C.P., Moores, J.E., Schwenzer, S.P., Bridges, J.C., Navarro-Gonzalez, R., Gellert, R., Lemmon, M.T. and Team, M.S. (2015) 'Mars methane detection and variability at Gale crater', *Science*, 347(6220), pp. 415-417.

Weiss, B.P., Yung, Y.L. and Nealson, K.H. (2000) 'Atmospheric energy for subsurface life on Mars?', *Proceedings of the National Academy of Sciences of the United States of America*, 97(4), pp. 1395-1399.

Werner, S.C. (2008) 'The early martian evolution - Constraints from basin formation ages', *Icarus*, 195(1), pp. 45-60.

Werner, S. C., and Tanaka K. L. (2011) 'Redefinition of the crater-density and absolute-age boundaries for the chronostratigraphic system of Mars', *Icarus*, 215(2), 603–607, doi:10.1016/j.icarus.2011.07.024.

Westall, F., de Wit, M.J., Dann, J., van der Gaast, S., de Ronde, C.E.J. and Gerneke, D. (2001) 'Early Archean fossil bacteria and biofilms in hydrothermally-influenced sediments from the Barberton greenstone belt, South Africa', *Precambrian Research*, 106(1-2), pp. 93-116.

Westall, F. (2008) 'Morphological Biosignatures in Early Terrestrial and Extraterrestrial Materials', *Space Science Reviews*, 135(1-4), pp. 95-114.

Westall, F., Loizeau, D., Foucher, F., Bost, N., Betrand, M., Vago, J. and Kminek, G. (2013) 'Habitability on Mars from a Microbial Point of View', *Astrobiology*, 13(9), pp. 887-897.

Westall, F., Foucher, F., Bost, N., Bertrand, M., Loizeau, D., Vago, J.L., Kminek, G., Gaboyer, F., Campbell, K.A., Breheret, J.G., Gautret, P. and Cockell, C.S. (2015) 'Biosignatures on Mars: What, Where, and How? Implications for the Search for Martian Life', *Astrobiology*, 15(11), pp. 998-1029.

Whitman, W.B., Coleman, D.C. and Wiebe, W.J. (1998) 'Prokaryotes: The unseen majority', *Proceedings of the National Academy of Sciences of the United States of America*, 95(12), pp. 6578-6583.

Wierzchos, J. B. Camara, A. de Los Rios, A. F. Davila, I. M. Sanchez Almazo, O. Artieda, K. Wierzchos, B. Gomez-Silva, C. McKay, and C. Ascaso, Geobiology. 9, 44 (2011).

Williams, J.P. and Nimmo, F. (2004) 'Thermal evolution of the Martian core: Implications for an early dynamo', *Geology*, 32(2), pp. 97-100.

Wilson, L. (2009). 'Volcanism in the solar system'. *Nature Geoscience*, *2*(6), p.389.Winograd N., Postawa Z., Cheng J., Szakal C., Kozole J., and Garrison B. J. (2006). 'Improvements in SIMS continue: Is the end in sight?'. *Applied surface science*, 252(19), 6836-6843.

Wood, B.E., Muller, H.R., Zank, G.P., Linsky, J.L. and Redfield, S. (2005) 'New mass-loss measurements from astrospheric Ly-alpha absorption', *Astrophysical Journal*, 628(2), pp. L143-L146.

Wordsworth, R.D., Kerber, L., Pierrehumbert, R.T., Forget, F. and Head, J.W. (2015) 'Comparison of "warm and wet" and "cold and icy" scenarios for early Mars in a 3-D climate model', *Journal of Geophysical Research-Planets*, 120(6), pp. 1201-1219.

Wordsworth, R.D. (2016) 'The Climate of Early Mars', *Annual Review of Earth and Planetary Sciences, Vol 44*, 44, pp. 381-408.

Wray, J.J., Murchie, S.L., Bishop, J.L., Ehlmann, B.L., Milliken, R.E., Wilhelm, M.B., Seelos, K.D. and Chojnacki, M. (2016) 'Orbital evidence for more widespread carbonate-bearing rocks on Mars', *Journal of Geophysical Research-Planets*, 121(4), pp. 652-677.

Y

Yamada I., Matsuo J., Toyoda N., and Kirkpatrick A. (2001). 'Materials processing by gas cluster ion beams'. *Materials Science and Engineering: R: Reports*, 34(6), 231-295

Yoshida, T.a.N., Kenichi and Tabata, Masahiro and Abe, Hiroshi and Kodama, Tatsuya and Tsuji, Masamichi and Tamaura, Yutaka 'Methanation of CO2 with H2-reduced magnetite', *Journal of Materials Science Letters*, 28(5), pp. 1220-1226.

Yung, Y.L., Russell, M. J., and Parkinson, C. D. (2010) 'The search for life on Mars', *Journal of Cosmology*, 5, pp. 1121-1130.

 Z

Zolotov, M.Y. and Shock, E.L. (2000). 'An abiotic origin for hydrocarbons in the Allan Hills 84001 martian meteorite through cooling of magmatic and impact-generated gases'. *Meteoritics and Planetary Science*, *35*(3), pp.629-638.

Zolotov, M.Y., Seewald, J.S. and McCollom, T.M. (2003) 'Dissolved carbon monoxide in hydrothermal fluids on solar system bodies: Experimental study of reactivity and organic synthesis', *Meteoritics and Planetary Science Supplement*, 38